

SCHOOL OF MEDICINE

Regulation of Human Heterochromatin Protein 1 Binding Protein 3 (HP1BP3, also known as HP1BP74) in Response to the DNA Damage

Makhliyo Normatova

(B.Sc., M.Sc.)

Thesis submitted to the University of Nottingham
for the degree of Doctor of Philosophy

June, 2016

Declaration

I hereby declare that this thesis is my own work except where otherwise indicated in the text. This thesis is based on research that was undertaken by me in Cancer Genetics & Stem Cell Group, under the supervision of Dr. Abdolrahman Shams Nateri at the School of Medicine, Faculty of Medicine and Health Sciences, University of Nottingham.

Makhliyo Normatova

Student ID: 4178034

Date: 28/06/2016

Abstract

DNA damage can result from exposure to exogenous agents such as ionizing radiation (IR), ultraviolet radiation (UV), environmental toxins and drugs or from endogenous sources such as reactive oxygen species or errors during DNA replication. DNA repair involves both post-translational modification of nucleosomes and concentration of DNA repair proteins at the damaged site(s). Therefore, the nucleosome rearrangement and chromatin disassembly with histones and other non-histone proteins upon damage must be in a dynamic balance with chromatin reestablishment following repair. Any impediment of this regulation process may cause extensive damage and trigger the growth of tumours. However, most studies have mainly focused on the core histones, whereas the heterochromatin proteins and their partners' identity remained unknown.

Recent studies in Dr Nateri's laboratory identified the heterochromatin protein HP1 binding protein 3 (HP1B3, also known HP1-BP74) as one of the FBXW7 (F-box and WD repeat domain containing 7, E3 ubiquitin protein ligase, also known Fbw7, CDC4, sel10) interacting proteins, using a modified yeast 2-hybrid reverse Ras-recruitment system (rRRS).

HP1BP3 is a predicted nuclear protein consisting of 553 amino acids with distinct protein interaction domains. At the start of this study, apart from a single publication (Hayashihara et al., 2010) very little was known about the HP1BP3 protein. HP1BP3 is a chromosomal protein that exists as a component of heterochromatin and is involved in chromatin function and structure. Our recent

laboratory analysis also indicate that HP1BP3 degradation by the E3 ubiquitin ligase Fbxw7 regulates mouse hematopoietic stem cell (HSC) cycle entry and the transcriptional "signature" that is associated with the quiescent, self-renewing of HSC phenotype and leukemic status (Abuzinadah et al., submitted). To this end, our laboratory and more recent data from other groups suggest that the regulation of HP1BP3 may play a key role in many types of biological events occurring in normal and cancer cells.

To investigate the molecular mechanisms underpinning HP1BP3 protein activity regulation that signal into biological response, we initially investigated structural features and phosphorylation sites of the HP1BP3 protein using various web-based computational and bioinformatics analyses. We determined the distribution of several clusters of amino acid residues surrounding the DNA damage-regulated phospho-SQ (S: Ser & Q: Gln), a consensus ATM and ATR phosphorylation motif on the HP1BP3. This is consistent with the notion that E (Glu) or D (Asp) is often found around SQ or TQ sequences phosphorylated by ATM or ATR kinases *in vitro*. We have therefore hypothesized that HP1BP3 protein could be a potential target of ATM/ATR in cells treated with DNA-damaging agents.

Herein, experimental evidence is presented on a wide range of cell and molecular biology tools and biochemical approaches to analyze the HP1BP3 regulation in response to DNA-damaging agents. This allows us to conclude a possible cross talk between HP1BP3 protein and activation of ATM and possibly ATR kinases via:

1) Identification of nuclear localization signals within the HP1BP3 protein (chapter 3)

2) ATM/ATR kinases coordinate the expression of HP1BP3 protein level and phosphorylation in response to DNA-damaging agents, such as UV light, ionizing radiation and chemotherapeutic drug in human fibroblasts (chapter 4)
3) FBXW7-mediated degradation of HP1BP3 protein is antagonized by ATM/ATR activation in human colorectal cancer (CRC) cells (chapter 5)
4) Knockout of HP1BP3 generated using CRISPR/Cas9 system, caused p53 accumulation in HCT116 CRC cells lacking FBXW7 after exposure to ionizing radiation (chapter 6).

From these data it was concluded that further research is required to explore the biological significance of HP1BP3 phosphorylation events modulated by ATM/ATR; to study mechanistic changes occurred on patterns of histone modifications as a result of HP1BP3 phosphorylation and the influence of nucleosome packing degree on the integration of DNA repair signaling and the complexity of the chromatin architecture. In addition, another challenge is to identify the direct target genes that are regulated via HP1BP3/ATM signaling axis, and to show how they contribute to cancer development, which could be critical for designing therapies to compensate mutation(s) of upstream regulators such as the FBXW7 tumour suppressor gene in human cancers.

Publications in collaboration with others

LI, N., LORENZI, F., KALAKOUTI, E., **NORMATOVA, M**., BABAEI-JADIDI, R., TOMLINSON, I. & NATERI, A.S. 2015. FBXW7-mutated colorectal cancer cells exhibit aberrant expression of phosphorylated-p53 at Serine-15. *Oncotarget*, 6.

Acknowledgments

"*Praise be to God, Lord of the Universe*"

This study presents the most challenging part of my life. I would not be able to walk through this path without the support of people who were beside me and to whom I am endlessly grateful. I would first like to thank my supervisor, Dr Nateri, for patiently guiding me throughout the course of study, for his invaluable discussion and professional support. I am also indebted to Dr Babaei-Jadidi, my second supervisor, for her encouragement, help and advice. Many thanks and gratitude goes to my very good friends and colleagues in cancer genetics and stem cell laboratory who volunteered their time and efforts to help me, and gave me moral and kind support. Thanks also directed to the Islamic Development Bank (IDB) for funding my PhD studentship.

Finally, and most importantly I wish to express my heartfelt and deepest thanks to the members of my family. My special thank-you and remembrance to my late wonderful and amazing mother whose sincere love and warm support was the source of inspiration for me, who believed in me, who was proud of me for all my achievements. She will be always in my heart. Also, my deepest gratitude and respect for my father, whose wise advice and peaceful mind made me overcome all difficulties. A very warm thank you to my younger sister Maftuna for being such a wonderful person and lifting my spirits in difficult times. Loving thanks to my blessed children (Farrukh and Kamilla) and nephew Sudays for making this whole adventure possible and by whom I am always inspired. Finally, I must thank "ALLAH" for HIS generosity for giving me the opportunity and ability to finish my PhD.

Table of contents

CHAPTER 1 21
General Introduction 21
1.1 Human Colorectal Cancer (CRC) 22
1.1.1 Colorectal cancer as consequence of genetic mutations 22
1.1.2 Protein degradation system 25
1.2 FBXW7 25
1.2.1 FBXW7 localization and isoforms 29
1.3 Role of epigenetics in the development of CRC 30
1.3.1 Chromatin structure 32
_Toc4541032351.3.2 States of chromatin structure 34
1.3.3 Nucleosome and posttranslational histone modifications 38
1.4 Chromosomal proteins 40
1.4.1 Heterochromatin Protein (HP1) and HP1 homologues 41
1.4.2 HP1 structure 43
1.5 DNA damage signalling pathway 45
1.5.1 Impact of chromatin structure on DNA damage response 53
1.6 Heterochromatin protein 1 binding protein 3 (HP1BP3, also known as HP1BP74) 57
1.6.1 HP1BP3 protein structure and localisation 58
1.6.2 HP1BP3 functions 61
1.7 Rational and objectives of this study 66
1.7.1 Rational 66
1.7.2 Objectives & Aims 68
CHAPTER 2 69
General Materials and Methods 69
2.1 Materials 70
2.1.1 Cell lines 70
2.1.2 DNA Plasmids 70
2.1.3 Antibodies 71
2.2 General Methods 73

2.2.1 Tissue culture techniques 73
2.2.1.1 Recovering the cells 73
2.2.1.2 Culturing and splitting the cells 73
2.2.1.3 Counting the cells 74
2.2.1.4 Transient transfection 75
2.2.1.5 Establishment of HP1BP3 stable cell lines 76
2.2.2 Gene cloning techniques 79
2.2.2.1 Standard Polymerase Chain Reaction (PCR) 79
2.2.2.2 Primer design 80
2.2.2.3 Restriction enzyme digestion 81
2.2.2.4 Agarose gel electrophoresis 81
2.2.2.5 DNA extraction from agarose gel and soluble reactions 82
2.2.2.6 DNA ligation 83
2.2.3 DNA preparation and manipulation 84
2.2.3.1 Bacterial transformation 84
2.2.3.2 Chemical preparation of bacterial competent cells 87
2.2.3.3 DNA isolation by Miniprep 87
2.2.3.4 DNA isolation by Midiprep 89
2.2.3.5 DNA quantification 91
2.2.4 Protein extraction and analysis 92
2.2.4.1 Protein extraction and quantification 92
2.2.4.2 SDS-PAGE electrophoresis and Western blotting analysis 93
2.2.4.3 Immunoprecipitation analysis 95
2.2.5 Immunofluorescence (IF) 96
2.2.5.1 Cell preparation 97
2.2.5.2 Fixation and permeabilization 97
2.2.5.3 Blocking and immunostaining 98
CHAPTER 3 99
Characterization of Functional Regions for Nuclear Localization of HP1BP3 99
3.1 BRIEF INTRODUCTION 100
3.2 RESULTS 103
3.2.1 Cloning of EGFP-fused HP1BP3 and its mutant constructs 103

3.2.1.1 Cloning of D1, D2 and D4 mutants using HP1BP3 short isoform cDNA construct 103

3.2.1.2 Cloning of HP1BP3-D0 and HP1BP3-Long recombinant constructs 109

*The restriction site for BstXI is located within the HP1BP3 cDNA sequence (518nt and 529nt) and presented by CCAGAAGAGTGG. 110

3.2.2 Expression analysis of human HP1BP3 recombinant proteins in HEK-293T cells 114

3.2.3 Sub-cellular localization of the EGFP-tagged HP1BP3 wild-type protein and its mutants 118

3.3 DISCUSSION 126

CHAPTER 4 130

DNA Damaging Agents Modulate the HP1BP3 Protein Expression via the ATM and ATR Protein Kinases in Human Fibroblasts 130

4.1 BRIEF INTRODUCTION 131

4.2 RESULTS 133

4.2.1 UV-irradiation elicits simultaneous induction of HP1BP3 and hallmark DDR proteins (γH2AX and p53) in human fibroblasts 133

4.2.2 Generation of stably-transfected human fibroblasts for the functional analysis of HP1BP3 137

4.2.2.1 Cloning of HP1BP3-Long cDNA into pLVX-EGFP 138

4.2.3 ATM/ATR-dependent induction of HP1BP3 caused by ionizing radiation 146

4.2.4 Oxaliplatin-induced phosphorylation of p53 positively correlated with HP1BP3 overexpression in human fibroblasts 149

4.2.5 HP1BP3 is phosphorylated within S/T residues 151

4.2.6 HP1BP3 co-localized with ATM foci in the nucleus 153

4.2.7 A potential interaction between ATM and HP1BP3 proteins in the cells treated with Oxaliplatin 156

4.2.8 Site-directed mutagenesis for replacement of Ser-Gln (SQ) with Ala-Ala (AA) in human HP1BP3 protein 157

4.2.9 Effect of site-directed mutagenesis on functional behaviour of HP1BP3 164

4.3 DISCUSSION 165

CHAPTER 5 169

FBXW7-Mediated Degradation of HP1BP3 is antagonized by ATM/ATR Activation in Human HCT116 Colon Carcinoma Cells 169

5.1 BRIEF INTRODUCTION 170
5.2 RESULTS 172
5.2.1 Negative correlation of HP1BP3 protein expression and ATM/ATR kinase activation in HCT116FBXW7 (-/-) CRC cell line 172
5.2.2 FBXW7 deficiency induces HP1BP3 expression in HCT116 CRC cells after Oxaliplatin treatment 176
5.2.3 ATM/ATR inhibitor induces HP1BP3 protein expression in wild type HCT116 CRC cells 180
5.2.4 The S-Q motif position on 142-143 a.a. of HP1BP3 protein is phosphorylated by ATM in vivo 185
5.2.5 Impact of HP1BP3-AA mutation on ATM and p53 protein expression levels 187
5.2.6 Effect of HP1BP3 inhibition on p53 protein expression 193
5.2.6.1 Successful shRNA-mediated knockdown of HP1BP3 in HCT116FBXW7(+/+) and HCT116FBXW7(-/-) cell lines 193
5.2.6.2 Loss of HP1BP3 led to accumulation of total p53 in HCT116 CRC cells after ionizing irradiation 195
5.2.6.3 Downregulation of HP1BP3 reduced the level of total p53 in HCT116 CRC lacking FBXW7 following Oxaliplatin treatment 198
5.3 DISCUSSION 200
CHAPTER 6 203
Generation of HP1BP3-Deficient CRC Cell Lines by Using the CRISPR/Cas9 Technology 203
6.1 BRIEF INTRODUCTION 204
6.2 RESULTS 206
6.2.1 Cloning of HP1BP3 sgRNA into pX459 expression plasmid 206
6.2.2 DNA sequence analysis of genomic PCR products illustrates alterations of HP1BP3 gene sequence in HCT116 cell lines 217
6.2.3 Loss of HP1BP3 led to accumulation of total p53 in HCT116 CRC lacking FBXW7 after ionizing irradiation 225
6.3 DISCUSSION 226
CHAPTER 7 228
General Discussion 228
7.1 Introduction 229
7.2 HP1BP3 expression in fibroblasts and CRC cell lines 229
7.3 HP1BP3 is a potential substrate of ATM/ATR kinases 233

7.4 The interplay between HP1BP3 and FBXW7 235
7.5 Experimental Limitations 237
7.5 Conclusions & Perspectives 238
References..... 241

List of Figures

Figure 1-1: The adenoma-carcinoma model. 23

Figure 1-2: Schematic presentation of SCF complex compromising 4 components: SKP1, CUL1, RBX and F-box protein. 26

Figure 1-3: Schematic illustration of FBXW7 interactions. 28

Figure 1-4: Contribution of genetics and epigenetics into development of CRC.

Figure 1-5: Schematic presentation of the compaction process of DNA into chromatin fibers. 32

Figure 1-6: Schematic illustration of euchromatin and heterochromatin structure and involvement of the posttranslational modifications. 35

Figure 1-7: A schematic interpretation of heterochromatin regions. 36

Figure 1-8: A simple model of spreading heterochromatin and a schematic representation of HP1α protein expressed by Su (var) 2-5 protein from *Drosophila melanogaster*. 44

Figure 1-9: Schematic presentation of domain architecture of PIKK family members. 48

Figure 1-10: Alterations in heterochromatin architecture as a result of DNA DSBs. 54

Figure 1-11: The schematic composition of human proteins involved in the formation and/or maintenance of metaphase chromosomes. 57

Figure 2-1: Top and side views of haemocytometer and its dimensions. 76

Figure 2-2: The proceeding steps of MiniPrep protocol. 90

Figure 2-3: Extraction of high copy number of recombinant DNA, carrying the gene of interest from bacterial culture using Midiprep kit. 91

Figure 3-1: Schematic representation of human HP1BP3 domains and defined NLS sequences. 103

Figure 3-2: Schematic representation of *HP1BP3-Short* construction. 104

Figure 3-3: Visualization of the *HP1BP3* deletion mutant constructs on a 1% agarose gel. 106

Figure 3-4: Validation of *HP1BP3* mutant clones through restriction enzyme digestion analysis. 107

Figure 3-5: Further confirmation of *HP1BP3* recombinant DNAs derived from HP1BP3-short isoform by distinct restriction enzymes. 109

Figure 3-6: The plasmid map of successfully generated recombinant EGFP-tagged HP1BP3 clones. 109

Figure 3-7: Validation of generated RT-PCR products by gel electrophoresis.

Figure 3-8: An overview of *HP1BP3* constructs cloning strategy. 113

Figure 3-9: The restriction enzyme digestion analysis of HP1BP3-D0 clones.

Figure 3-10: The restriction enzyme digestion analysis of HP1BP3-Long clones. 115

Figure 3-11: Validation assay for HP1BP3 recombinant constructs. 116

Figure 3-12: Frame – shift mutation led to formation of *HP1BP3-D1* truncation caused by formation of stop-codon "*TAG*". 117

Figure 3-13: HP1BP3 constructs. 119

Figure 3-14: Subcellular distribution of HP1BP3 recombinant constructs in HEK-293T cells. 120

Figure 3-15: Co-localization of endogenous HP1BP3 and exogenously expressed mutant HP1BP3 proteins in HCT116 cells. 122

Figure 3-16: Further observation of HP1BP3 protein expression in human fibroblasts. 124

Figure 3-17: Nucleolar localization signal detection by Nucleolar localization sequence Detector (NoD). 125

Figure 3-18: Schematic representation of joint NLS-NTS motifs of HP1BP3 protein. 126

Figure 4-1: A schematic representation of the HP1BP3 protein and its putative ATM/ATR phosphorylation sites. 133

Figure 4-2: γH2AX used as a positive control for UV irradiation. 135

Figure 4-3: UV irradiation induced HP1BP3 expression in human fibroblasts.

Figure 4-4: γH2AX induction (ATM/ATR activation) positively correlates with HP1BP3 expression. 137

Figure 4-5: The expression plasmid pLVX-EGFP. 139

Figure 4-6: Cloning strategy for pLVX-EGFP-HP1BP3-Long DNA clone. 141

Figure 4-7: Restriction enzyme digestion analysis of pLVX-EGFP-HP1BP3-Long cDNAs. 142
Figure 4-8: Restriction enzyme digestion analysis of Lentiviral constructs containing EGFP and EGFP-HP1BP3-Long cDNAs. 143
Figure 4-9: Confirmation of the stable expression of EGFP-HP1BP3 in human fibroblasts by fluorescent microscopy. 144
Figure 4-10: Nuclear localization pattern of stably expressed EGFP-HP1BP3.
Figure 4-11: Generation of stable cell lines in human fibroblasts. 146
Figure 4-12: Schematic representation of possible random integration of EGFP-HP1BP3 into the genome of human fibroblasts. 147
Figure 4-13: IR-induced HP1BP3 protein level in human fibroblasts stably overexpressing EGFP-HP1BP3. 149
Figure 4-14: Oxaliplatin-induced HP1BP3 protein level in human fibroblasts.
Figure 4-15: Detection of possible phospho-S/T for HP1BP3 protein by immunoprecipiation assay using anti-Serine/Threonine antibody. 154
Figure 4-16: Impact of ATM/ATR kinase inhibitor on HP1BP3/ATM colocalisation. 156
Figure 4-17: A potential interaction between ATM and HP1BP3 in Oxaliplatin treated fibroblasts. 158
Figure 4-18: Schematic representation of cloning strategy for pEGFP-C2-HP1BP3-D0-AA plasmid. 160
Figure 4-19: Validation of pEGFP-C2-HP1BP3-D0-AA by enzymatic digestion analysis. 161
Figure 4-20: Alignment of D0 and D0-AA sequences. 161
Figure 4-21: Restriction enzyme digestion to generate pEGFP-C2-HP1BP3-L-AA cDNA. 162
Figure 4-22: Cloning strategy for pEGFP-C2-HP1BP3-L-AA plasmid. 163
Figure 4-23: Validation of pEGFP-C2-HP1BP3-L-AA by enzymatic digestion analysis. 164
Figure 4-24: DNA sequencing result of pEGFP-C2-HP1BP3-L-AA. 164
Figure 4-25: Detection of HP1BP3-AA in response to Oxaliplatin DNA-damaging agent. 165

Figure 5-1: Expression of γH2AX and HP1BP3 protein levels in HCT116$^{FBXW7\ (+/+)}$ and HCT116$^{FBXW7\ (-/-)}$ cells before and after UV treatment and ionizing irradiation. 178

Figure 5-2: The effect of Oxaliplatin on HP1BP3 protein expression in HCT116 CRC cells with wild-type and deficient FBXW7. 180

Figure 5-3: The schematic representation of FBXW-dependent recruitment of HP1BP3 in DNA damage response in HCT116 cancer cell lines. 181

Figure 5-4: The effect of ATM/ATR inhibitor on HP1BP3 expression in HCT116 CRC cells. 183

Figure 5-5: The schematic representation of HP1BP3 response the presence of ATM/ATR pharmacological inhibitor in HCT116 cancer cell lines. 185

Figure 5-6: Impact of ATM/ATR kinase inhibitor on HP1BP3/ATM colocalisation in HCT116 CRC cells. 186

Figure 5-7: The mutated clone of HP1BP3 (AA) lost its physical interaction with ATM kinase due to lack of SQ phosphorylation. 188

Figure 5-8: HP1BP3-AA dependent expression of ATM and p53 in HCT116 CRC cells. 189

Figure 5-9: Dependence of expression levels of p53 and ATM proteins upon S-Q phosphorylation motif. 191

Figure 5-10: HP1BP3-AA dependent expression of ATM and p53 in HCT116 CRC cells. 192

Figure 5-11: ATM and p53 expression levels in response to Inhibition of ATM/ATR in the presence of mutated S-Q phosphorylation site. 193

Figure 5-12: Schematic presentation of pGIPZ backbone vector and inserted HP1BP3 shRNA into pGIPZ plasmid. 195

Figure 5-13: Successful shRNA-mediated knockdown of HP1BP3 in HCT116 CRC cells. 196

Figure 5-14: The response of HP1BP3-knockdown HCT116 CRC cells to ionizing radiation. 198

Figure 5-15: Schematic representation of the DNA damage effect on the expression levels of ATM, p53 and γH2AX proteins in HP1BP3-knockout HCT116 cell lines. 199

Figure 5-16: The response of HP1BP3-knockdown HCT116 CRC cells to Oxaliplatin exposure. 201

Figure 6-1: The schematic design for generation HP1BP3-knockout HCT116 CRC cell lines by application CRISPR/Cas9 technology. 207

Figure 6-2: The construction of pX459 expression plasmid for HP1BP3sgRNA.

Figure 6-3: The restriction enzyme digestion analysis of pX459 expression plasmid. 212

Figure 6-4: Schematic representation for cloning steps of the guide sequence oligos into a plasmid containing Cas9 and the sgRNA scaffold (pSpCas9 (BB)).

Figure 6-5: Validation of successful cloning of annealed HP1BP3 sgRNA into px459 expression vector by agarose gel electrophoresis. 216

Figure 6-6: DNA sequencing result for the generated HP1BP3/CRISPR plasmid.

Figure 6-7: Protein expression analysis of isolated clones derived from HCT116$^{FBXW7\ (+/+):HP1BP3\ (-/-)}$ and HCT116$^{FBXW7\ (-/-):HP1BP3\ (-/-)}$ cell pool. 218

Figure 6-8: The DNA sequencing result for sample 1 of HCT116$^{FBXW7\ (+/+):\ HP1BP3\ (-/-)}$. 223

Figure 6-9: The DNA sequencing result for sample 4 of HCT116$^{FBXW7\ (+/+):\ HP1BP3\ (-/-)}$. 224

Figure 6-10: The DNA sequencing result for sample 5 of HCT116$^{FBXW7\ (-/-):\ HP1BP3\ (-/-)}$. 225

Figure 6-11: The DNA sequencing result for sample 6 of HCT116$^{FBXW7\ (-/-):\ HP1BP3\ (-/-)}$. 226

Figure 6-12: The response of HP1BP3-knockout HCT116 CRC cells; [HCT116$^{FBXW7\ (+/+):HP1BP3\ (-/-)}$] vs. [HCT116$^{FBXW7\ (-/-):HP1BP3\ (-/-)}$] to ionizing radiation. 228

Figure 7-1: Schematic presentation of FBXW7-dependent expression of HP1BP3 in response to ATM/ATR activation. 238

Figure 7-2: Schematic presentation of possible cellular outcomes of HP1BP3-dependent chromatin modulation. 241

List of Tables

Table 2-1: List of DNA plasmids used throughout the thesis 72
Table 2-2: List of primary and secondary antibodies used for Western blotting and immunostaining analysis 73
Table 2-3: General cycling parameters and conditions used for standard PCR reaction. 81
Table 2-4: Brief outline of the processing steps of the extraction protocol. 84
Table 2-5: Composition of common solutions and buffers applied in this study.
Table 2-6: Solutions for preparing 6-10% resolving gels for SDS-PAGE. 95
Table 2-7: Solution for preparing 5% Stacking Gels for Tris-glycine SDS-PAGE. 96
Table 3-1: List of the restriction enzymes used for digestion and cloning of *HP1BP3* recombinant constructs. 105
Table 3-2: Primers used to amplify EGFP-fusion compatible fragments of human *HP1BP3* cDNA. 111
Table 3-3: Applied restriction enzymes for generation of *HP1BP3-D0* and *HP1BP3-Long* isoform from PCR products. 113
Table 3-4: The expected molecular weight of HP1BP3-recombinant cDNAs and protein molecules. 118
Table 4-1: Primer sequences used to amplify human HP1BP3-D0-AA cDNA.
Table 6-1: Two sets of guide sequence oligos attempted to be applied to engineer pX459 expression plasmid for HP1BP3sgRNA. 211
Table 6-2: Preparation of the HP1BP3 sgRNA oligos inserts. 213
Table 6-3: Set up of PCR mixture for further validation. 215
Table 6-4: Set up of the mixture for cDNA production. 220
Table 6-5: Conditions required for process of reverse transcription. 220
Table 6-6: Primers used for PCR to amplify HP1BP3 mutated region. 221

Abbreviations

3’ UTR	3’ Untranslated Region
5’ UTR	5’ Untranslated Region
ATM	Ataxia Telangiectasia Mutated
ATR	ATM and Rad3-related
CAF1	Chromatin-Assembly factor-1
CK2	Casein Kinase 2
CD	Chromo-Domain
cDNA	Complementary Deoxyribonucleic Acid
CHD	Chromo-Shadow Domain
CIN	Chromosomal Instability
CMV	Cytomegalovirus
Co-IP	Co-Immunoprecipitation
CRC	Colorectal Cancer
CTD	C-Terminal Domain
DDR	DNA Damage Response
DMEM	Dulbecco Modified Eagle Medium
DNA-PK	DNA-Dependent Protein Kinase
DSBs	Double-Strand Breaks
eGFP	Enhanced Green Fluorescence Protein
FBXW7	F-box and WD repeat domain-containing 7
GD	Globular Domain
HDACs	Histone Deacetylases
H3K9me3	HP1α/tri-methylated H3
HMTases	Histone Methyltransferases
HSC	Hematopoietic Stem Cells
HP1	Heterochromatin Protein
HP1BP3	Heterochromatin Protein 1Binding Protein 3

HR	Homologous Repair
IP	Immunoprecipitation
IF	Immunofluorescence
KAP1	KRAB-Associated Protein
Kb	Kilo Base Pair
kDa	Kilo Dalton
KRAS	Kristen Rat Sarcoma Viral Oncogene
MCS	Multiple Cloning Site
MSI	Microsatellite Instability
NTD	N-Terminal Domain
NHEJ	Non-Homologous End Joining
NLS	Nuclear Localization Signal
NTS	Nucleolar Target Sequence
ORF	Open Reading Frame
PCR	Polymerase Chain Reaction
PEI	Ployethylenimine
PHDs	Plant Homeodomains
PEV	Position Effect Variegation
PTM	Posttranslational Modifications
RNA	Ribonucleic Acid
RPMI	Roswell Park Memorial Institute
SMC	Structure Maintenance Chromosome
ssDNA	Single Stranded DNA
TALENs	Transcription Activator-like Effector Nucleases
TP53	Tumour Protein 53
UBA	Ubiquitin-Activating Protein Enzyme
UBC	Ubiquitin-Conjugating Protein Enzyme
UPS	Ubiquitin-Proteasome System
UV	Ultraviolet Radiation
WB	Western Blotting
ZFNs	Zinc-Finger Nucleases

CHAPTER 1

General Introduction

1.1 Human Colorectal Cancer (CRC)

CRC is the 2nd highest death-causing cancer in the world within the last few decades (Ricci-Vitiani et al., 2007). According to the statistics, the scale of incidence of CRC is higher in the developed countries with better living standards rather than in countries with low economic level (Hermsen et al., 2002, Douglas et al., 2004, Martin et al., 2007). Colorectal neoplasm can be induced by two factors. Approximately 5% of colorectal malignancy occurs due to genetic alterations inherited in an autosomal dominant mode whereas majority of CRC cases develops sporadically (Hermsen et al., 2002, Douglas et al., 2004, Martin et al., 2007).

1.1.1 Colorectal cancer as consequence of genetic mutations

CRC represents a multistage process with various clinical manifestations and histological alterations. CRC initiation and progression occurs as a result of sequential aggressive gene mutations and epigenetic alterations (Grady and Carethers, 2008). It has been documented that there are approximately 80 genes with amino acid-altering mutations which encountered in individual colorectal cancers. However, many of these mutations are probably harmless nature; and according to the following reviewers, only around 15 of them may contribute to the CRC pathogenesis (Sjoeblom et al., 2006, Wood et al., 2007).

These driver mutations lead to the disturbance in the intracellular signaling pathways involved in the processes such as proliferation, differentiation, cell adhesion and migration, apoptosis, DNA stability and repair (Sjoeblom et al., 2006). In addition, it is well known that the accumulation of oncogenes and down regulation of tumour suppressor genes, arising as consequence of the impact of

various factors, lead to the initiation of tumorigenesis (Powell et al., 1992). Moreover, it was determined that CRC develops according to the adenoma-carcinoma model with involvement of various gene mutations contributing at the specific stage of malignant transformation in colon **(Figure 1-1)**.

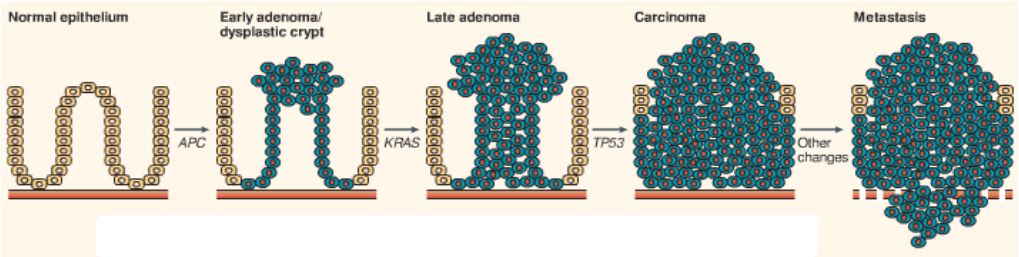


Figure 1-1: The adenoma-carcinoma model. The schematic chain of events involving various genes contributing to the CRC carcinogenesis at different stages starting with normal epithelium through adenoma to malignant process with spread to distal systems [Adapted from (Davies et al., 2005)].

As it has already been reported, mutations of tumour suppressor gene *APC* (Adenomatous polyposis coli) is associated with CRC development (Wang et al., 2012b). Likewise, there is a range of other somatic gene mutations which are encountered in CRC pathogenesis. Thus, mutant Kristen rat sarcoma viral oncogene (KRAS) is identified in approximately 50% of CRC cases whereas mutant tumour protein 53 (TP53) is found in 60% and transformed growth factor/bone morphogenic protein/SMAD4 in 10-20% (Hermsen et al., 2002, Douglas et al., 2004, Martin et al., 2007). Another causative factor of CRC is E3 ubiquitin ligase FBXW7, a member of F-box family proteins that regulates diverse cellular processes via interaction with various proteins, including c-Myc, cyclin-E, C-Jun, Notch, and Mcl-1. It has been reported that loss of function and mutation of FBXW7 occur in a wide range of human malignancies including

CRC where mutation of FBXW7 occur in 9-15% of CRC cases (Babaei-Jadidi et al., 2011, Cheng and Li, 2012). Furthermore, recent studies have implicated FBXW7 in causing chromosomal instability (CIN) (Rajagopalan et al., 2004) which is considered one of the contributing carcinogenetic factors and refers to one of the types of genomic instability. Indeed, the prevalent role in the development and progression of CRC belongs to genomic instability which is subdivided into chromosomal instability (CIN) and microsatellite instability (MSI). According to the recent studies, occurrence of aberrations is significantly higher in CIN^+ samples compared with MSI^+ samples in human CRC. In addition, most of CRC cases (≈85%) are caused by CIN and characterized by an elevated number of chromosomal losses and gains (Hermsen et al., 2002, Douglas et al., 2004, Martin et al., 2007).

This condition of abnormal chromosomal content within cancer cells is termed as aneuploidy. It has been suggested that alterations in proteins responsible for double-strand break repair, kinetochore function, and chromatid segregation may lead to aneuploidy.

Arising out of this, it has been proposed that CIN arise on a genetic basis, and occurrence of somatic mutations in cancer CIN genes are encountered in approximately 10% of CIN cancers (Wang et al., 2004). Indeed, recent results have demonstrated that mutational inactivation of tumour suppressor FBXW7 provokes upregulation of cyclin E and hence determines CIN (Rajagopalan et al., 2004). These data support the hypothesis that chromosomal instability in tumour cells is a consequence of genetic alterations (Rajagopalan et al., 2004).

Specifically, that mutation of FBXW7 as a component of the ubiquitin proteasome system underlies process of tumorigenesis through aberrant protein degradation.

1.1.2 Protein degradation system

The majority of intracellular proteins in all tissues undergo destruction by regulation of ubiquitin (UB)-proteasome system (UPS) which consists of three main constituents: 1. three enzymatic components; 2. a highly conserved 76-amino-acid polypeptide chain of ubiquitin molecules and 3. machinery for protein degradation presented by 26S proteasome (Lecker et al., 2006). A cascade of three consecutive enzymatic components of UPS such as E1 (Ub-Activating protein, termed UBA), E2s (Ub-Conjugating proteins, termed UBCs) and E3 (Ub-protein ligase) are implicated in the conjugation of the chain of ubiquitin moieties onto a protein substrate that is tagged for degradation. Firstly, activation of ubiquitin molecule occurs through the formation of a thioester bond with the ubiquitin-activating enzyme, E1. In the second stage, the activated E1 ubiquitin binds to the ubiquitin-conjugating enzyme, E2. And in the final step, transference of the ubiquitin from E2 to the lysine residue of the target protein substrate takes place (Lecker et al., 2006).

1.2 FBXW7

The key role in three step-chain reaction belongs to the E3 (Ub-protein ligase) as it possesses the ability to identify specific protein substrate and to bind the activated ubiquitin molecule to it in a highly regulated manner. Mammalian cells enclose hundreds of E3 ubiquitin ligases with features for specific selection of

the proteins (Wang et al., 2012b). There are two main classes of E3 ubiquitin ligases such as single RING type, homologous to E6-AP C terminus (HECT) type and RING/Cullin Ligase (RCL) type of E3 ligases which are structurally similar. Each is constructed of common subunits and variable components; however the protein target for degradation is different (SKP2 labels negative regulators of the cell cycle, such as p27, p21 and p57 for degradation, whereas FBXW7 promotes the degradation of positive regulators of the cell cycle, such as MYC, JUN, cyclin E and Notch) (Wang et al., 2012b, Babaei-Jadidi et al., 2011). Among the E3 ubiquitin ligases Skp1-Cullin1-F-box (SCF) E3 ligase complex is the best characterized **(Figure1-2)**. It contains three invariable subunits-RBX1 (RING-finger protein), CUL1 (scaffold protein), and SKP1 (adaptor protein) and bears an interchangeable substrate-recognition subunit, denoted as F-box.

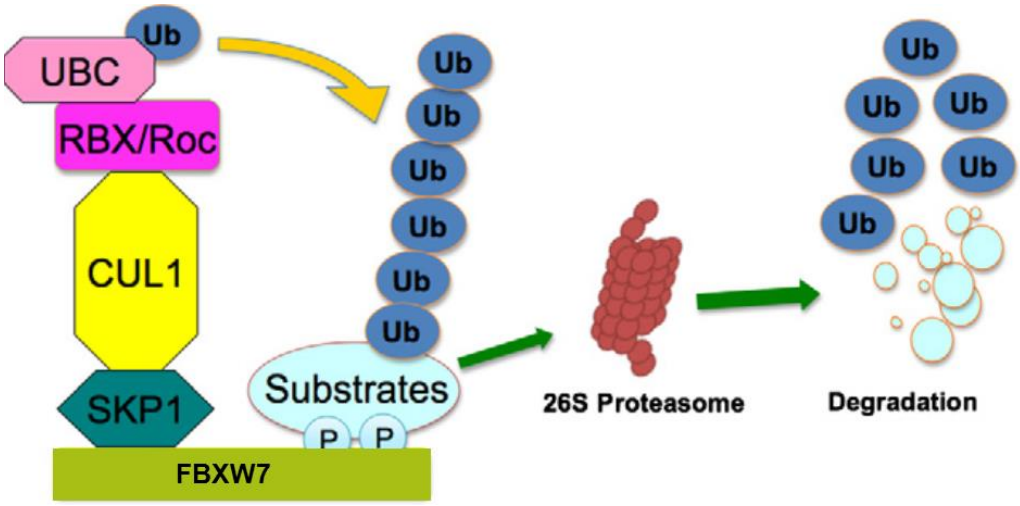


Figure 1-2: Schematic presentation of SCF complex compromising 4 components: SKP1, CUL1, RBX and F-box protein. Ubiquitin serves as the marker for recognition of the targeted proteins by the 26S proteasome system,

and attachment of a polyubiquitin chain to the protein substrates is essential step for initiation the UPP [(Adapted from(Wang et al., 2012b)].

FBXW7 (F-box and WD repeat domain-containing 7, also known hCDC4, FBW7, Sel10, Ago) is a variable protein substrate of evolutionary conserved SCF (complex of SKP1, CUL1 and F-box)-type ubiquitin ligases which is implicated in a wide range of diverse cellular functions such as cell cycle progression, cell growth, cellular metabolism, differentiation and apoptosis**.** FBXW7 (FBW7) orthologues have been identified in other living creatures. The first member of the FBXW7 gene family Cdc4 was discovered in budding yeast. Further studies revealed Cdc4 orthologues in the nematode (SEL-10) and in the Drosophila melanogaster (AGO) (Wang et al., 2012b).

FBXW7 protein consists of three main domains (Wang et al., 2012a). The first one is the F-box motif, the protein substrate of 40 amino acids which serves as the binding site for SKP1 (S-phase kinase associated protein 1), whereas SKP1 in its own turn promotes interlink between FBXW7 and E2 conjugating enzyme. The second FBXW7 domain is the conglomerate of eight WD40 repeats with multiple binding sites characterizing distinct functions. Interaction of FBXW7 with its downstream substrates occurs through arginine residues of 3^{rd} and 4^{th} WD repeats, whereas other phosphor-degron binding pockets facilitate substrate connection. And the last constitutive of FBXW7, determined as D domain, is considered to play a crucial role in FBXW7 dimerization (Wang et al., 2012b).

It has been determined that SCF^{FBXW7} possesses tumour suppressor properties due to its negative regulation of a wide range of oncoproteins **(Figure 1-3)** (Wang et al., 2012b, Wang et al., 2012a).

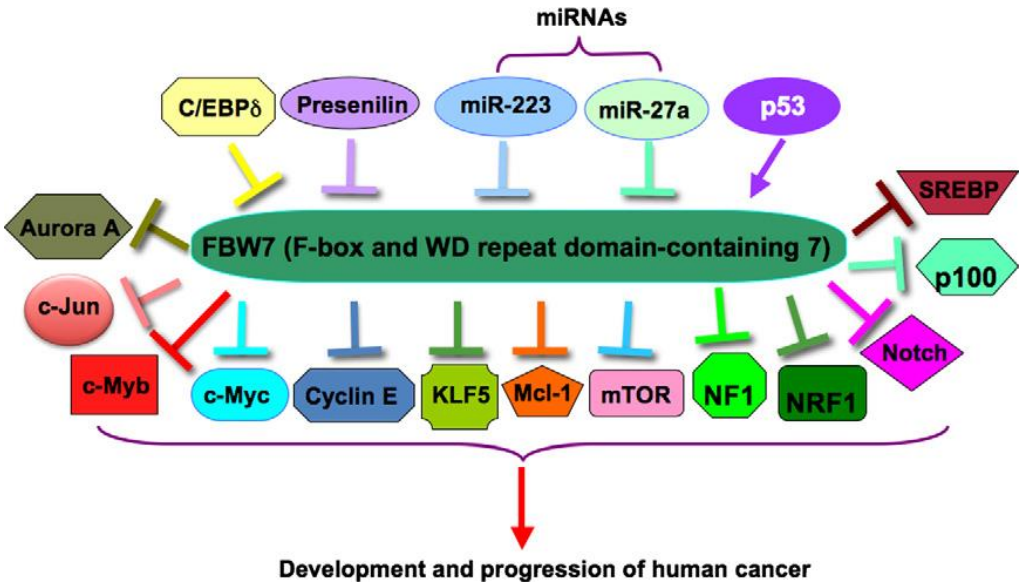


Figure 1-3: Schematic illustration of FBXW7 interactions. Upstream FBXW7 substrates regulate its expression and downstream substrates of are targeted for degradation by FBXW7 [(Adapted from(Wang et al., 2012b)].

Loss of FBXW7 function or its mutation impedes the rapid degradation of FBXW7 downstream substrates resulting in their excessive expression and further promotion of tumour development. Thus, FBXW7 plays a suppressive role in human tumorigenesis and mutation has been identified in many cancers (Wang et al., 2012a). Statistics shows that FBXW7 mutations have been revealed in approximately 6% cases of overall amount of primary human malignancies. It was reported that FBXW7 mutations predominantly encounter in the cholangiocarcinoma (35%), T-ALL (31%), endometrium (16%) and colorectal cancer (10-15%). Furthermore, it was determined that genetic alterations of FBXW7 contribute to the poor prognosis of patients with cancer (Wang et al., 2012b).

1.2.1 FBXW7 localization and isoforms

The human FBXW7 gene is located on the 4th chromosome on locus 32q, and its size comprises 200kb (Wang et al., 2012a). As a result of alternative splicing it encodes three different transcripts (FBXW7α, FBXW7β and FBXW7γ). Each of the protein isoforms is translated from an FBXW7 mRNA with distinct N-termini but share rest 10 exons represented by the three identical, functional domains of protein-protein interaction (F-box and WD40 repeating domains). Unique 5' exons of the generated three protein isoforms determines their isoform-specific transcription; however physiological explanation of this specificity still remains unclear. Difference in this first exon establish distinct subcellular localization and various tissue distributions of FBXW7 isoforms. Cis – acting signals of NH2-terminus point out the direction of specific localization of each protein isoforms. Gene products of FBXW7α, FBXW7β and FBXW7γ occupy the nuclear, cytoplasm and nucleolar cellular compartments, respectively.

Transcription of FBXW7α mRNA occurs at a higher level compared with the other two isoforms and can be observed almost in all human cell lines and primary cells. Accumulation of FBXW7β products is restricted to brain tissue, whereas FBXW7γ translation is detected in muscle fibrils including the heart and skeletal muscle.

Expression level of FBXW7γ is considered to be regulated in a p53-dependent manner; thus the radiation induced up-regulated expression of p53 promotes FBXW7γ production. This could be explained by existence of p53 binding site at exon 1b of FBXW7 gene. Despite this fact, regulation mechanisms of FBXW7 are not still completely understood. Isoform specific transcription of three

distinct protein substrates of FBXW7 might underlie the precise regulation of FBXW7 isoforms determined by different regulatory pathways (Wang et al., 2012b).

1.3 Role of epigenetics in the development of CRC

In early studies, CRC has predominantly been determined as a genetic pathological process which arises due to sequential accumulation of genetic abnormalities. However, with recent evidences, it is considered that histological progression of CRC is presented by possibly a combination of both genetic and epigenetic alterations (van Engeland et al., 2011). Epigenetic alterations are presented by inheritable changes in gene expression that do not induce the interruption in DNA sequence structure. However, it is well established that disturbance in epigenetic regulations underlies alterations in every stage of gene regulation, including DNA methylation, loss of imprinting, posttranslational histone modifications, nucleosome positioning, chromatin looping, and small non-coding RNA (van Engeland et al., 2011). The assembly of gene mutations and epigenetic alterations involves signaling pathways which regulate the hallmark behavior of cancer. This creates the fertile ground for the development of benign adenomas and further promotion and progression of the malignant process. In order to elucidate the background of epigenetic alterations in cancer it is essential to understand normal structure of chromatin and physiological functions in which chromatin is involved.

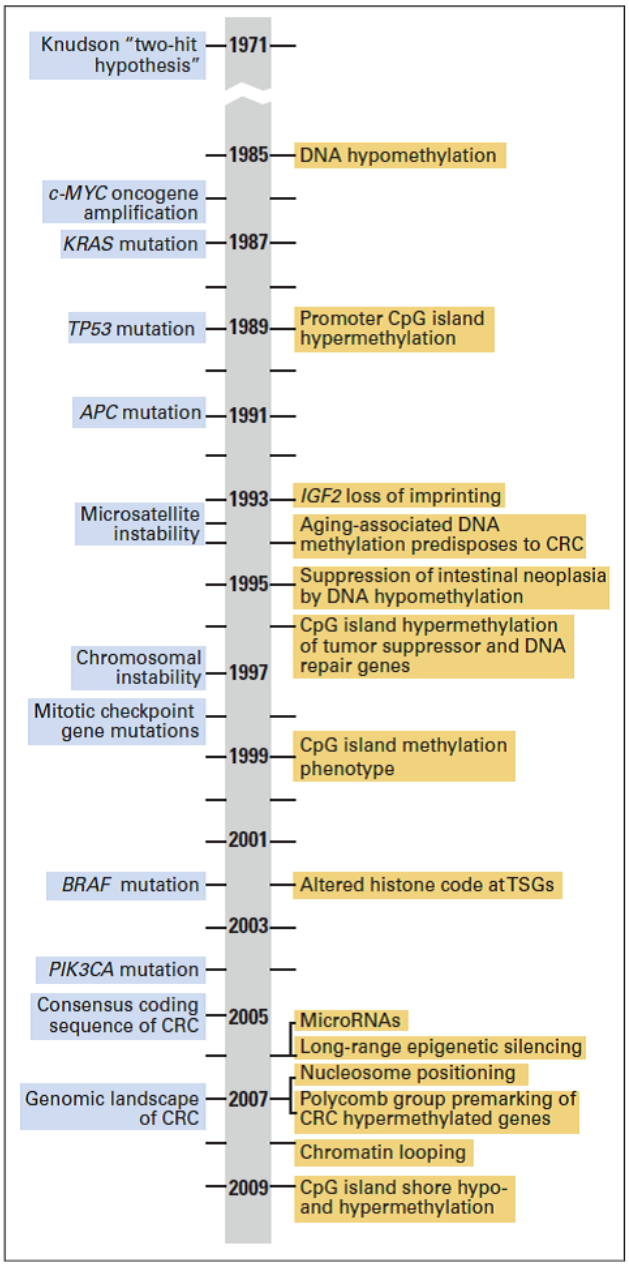


Figure 1-4: Contribution of genetics and epigenetics into development of CRC. Schematic demonstrates a chronological arrangement of discoveries depicting on the nature of CRC causes where genetic alterations marked as blue and epigenetic ones as yellow [Adapted from (van Engeland et al., 2011)].

1.3.1 Chromatin structure

Chromatin of the higher eukaryotic cells comprises the nucleo-protein complex, whereas chromosome represents condensed form of chromatin in metaphase during mitosis in order to provide equal and appropriate segregation of the genetic information to daughter cells. Higher-order chromatin organisation governs the transcriptional process through a series of diverse posttranslational modifications taking place at the amino-terminal tails of chromatin proteins (Luger et al., 1997, Rice and Allis, 2001, Jenuwein and Allis, 2001).

An assembly of polypeptide substrates such as histone and non-histone proteins are involved in the chromatin organisation and play a significant role in the formation of the condensed structure of the nucleo-protein complex. Such compaction process makes it possible to pack DNA molecules which constitute 6.4 billion base pairs and which is equivalent to 2 meters in length within the

boundaries of a tiny nucleus of human cell with a diameter of 10µm (Dillon and Festenstein, 2002) **(Figure 1-5)**.

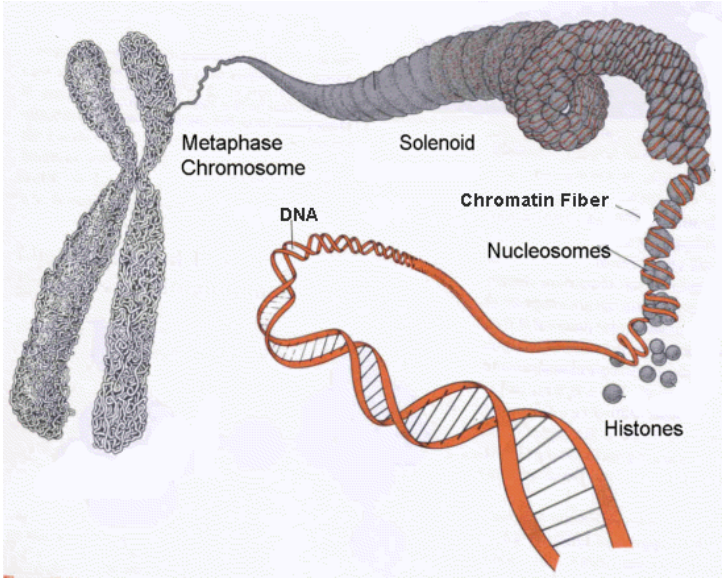


Figure 1-5: Schematic presentation of the compaction process of DNA into chromatin fibers. Nucleosome presents the building unit. Metaphase chromosomes present most condensed form of the chromatin fibers (adapted from **www.biology.westfield.ma.edu**).

Moreover, the collaboration of DNA-packaging proteins (histones) and associated covalent modifications impacts on the structure of chromatin template, thereby leading to the inherited differences in transcriptional states which underlie the "on" or "off" states of dynamic chromatin polymer (Maison and Almouzni, 2004). In addition, epigenetic alterations may lead to the stable states of gene silencing or accelerated transcription which occurs as result of specific hyper-methylation or hypo-methylation of genes, respectively. Thus, the altered patterns of histone modifications may underlie processes responsible for initiation and progression of cancer. Cancer cell genomes simultaneously

demonstrate global hypo-methylation and gene-promoter-specific-hyper-methylation action (Wood et al., 2007).

1.3.2 States of chromatin structure

The level of compaction in the interphase result in two distinct shapes of chromatin such as euchromatin and heterochromatin, which reflect different aspects of chromatin behavior such as transcription, recombination and DNA repair (Maison and Almouzni, 2004). The degree of chromatin condensation is determined by participation of epigenetic mechanisms such as posttranslational modifications, which occur on the protruding through nucleosome charged tails of core histones. Hence, the formation of compacted chromatin architecture as well as the storage and regulation of genetic information are governed by covalent modifications which also known as "histone code". Despite the fact that every single cell carries the same genetic code, pattern of gene expression varies from cell to cell, which is believed to be influenced by histone modifications (Schafer and Jung, 2005). On account of this, the condensed state of DNA macromolecule has to obtain more relaxed structure in order to be more accessible for transcriptional factors, and this process is regulated by covalent modifications (Schafer and Jung, 2005).

Heterochromatin represents tightly condensed, inaccessible and highly ordered modification of nuclei-protein complex, whereas euchromatin is less condensed, more accessible and more easily transcribed chromosome state (Grewal and Elgin, 2002) **(Figure 1-6).**

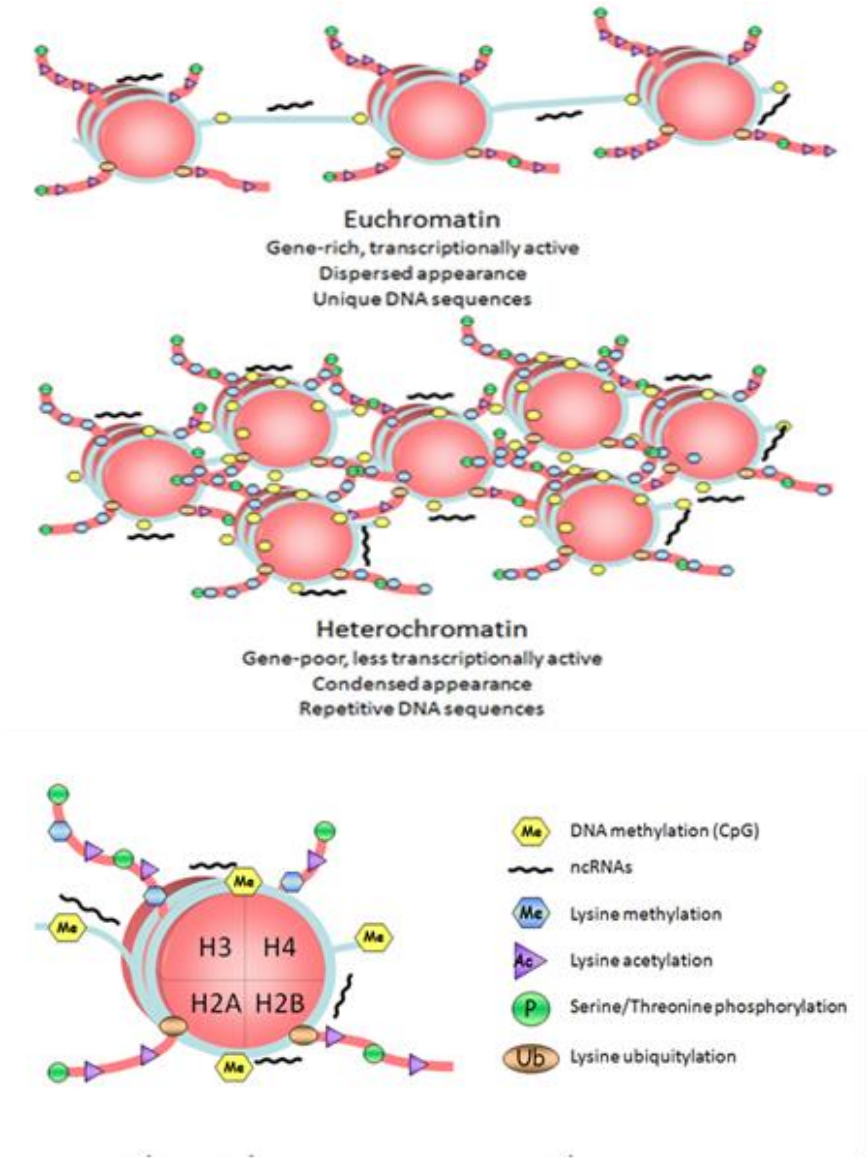


Figure 1-6: Schematic illustration of euchromatin and heterochromatin structure and involvement of the posttranslational modifications (adapted from www.biochem.slu.edu).

Heterochromatin that is maintained condensed throughout cell cycle is denoted as constitutive heterochromatin (Hediger and Gasser, 2006). However, some regions of heterochromatin state can experience alterations dictated by cellular signals and gene activities; this type of heterochromatin state refers to the facultative heterochromatin. Arising out of this, it is considered that architecture of constitutive heterochromatin is constructed at pericentromeric regions and is

organized in centromeres and telomeres, which are composed of stretches of multiple repetitive non-coding DNA sequences, called satellites (Dillon and Festenstein, 2002). Despite the fact that satellites of heterochromatin are considered as "parasitic regions" of DNA as they do not transcribe, they contribute as significant architectural components **(Figure 1-7)** (Henikoff et al., 2001).

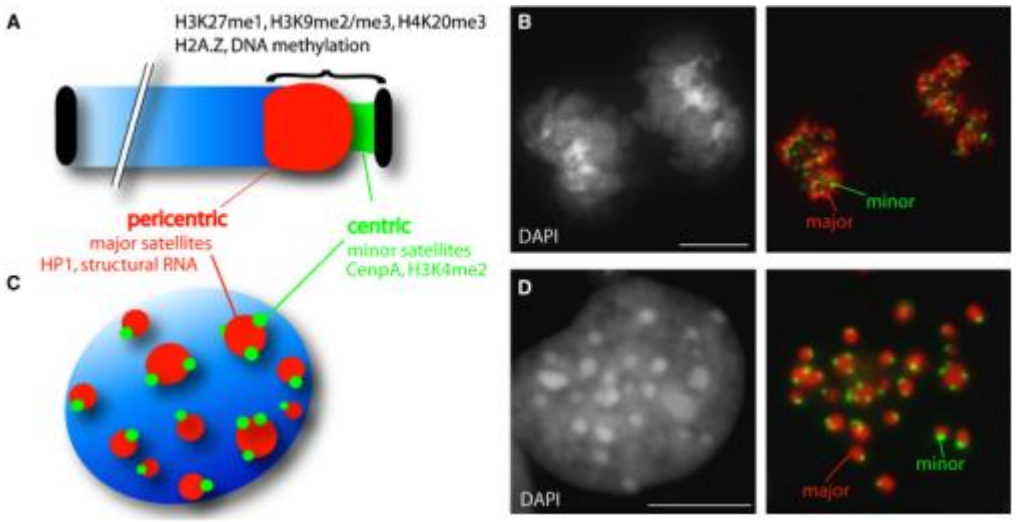


Figure 1-7: A schematic interpretation of heterochromatin regions [Adapted from (Probst and Almouzni, 2008)]. Centric and pericentric regions which comprise heterochromatin centromere are presented by minor (green) and major (red) satellite repeats, respectively. Both centric and pericentric domains serve as enriched methylation sites.

The length of satellite repeats is variable in different species. It comprises 5-7-bp repeats in *Drosophila* and 1950-bp in *Arabidopsis*, whereas the predominant satellite in human constitutes 171-bp α-satellite repeat and in mouse is 234-bp γ-

satellite repeat (Dillon and Festenstein, 2002). Heterochromatin governs a range of diverse nuclear processes including centromere function, gene silencing and nuclear organization. It has been identified that a high number of satellite repeats is required for proper centromere function in humans (Dillon and Festenstein, 2002).The centromere is the region of well-defined domains which is divided into centric and pericentric heterochromatin that are occupied by minor satellite repeats (≈600kb of 120bp units) and major satellite repeats (6 megabases of 234bp units), respectively (Henikoff et al., 2001).

Major satellites are organized into centromeric heterochromatin clusters (“chromocenters”) interacting with chromatin-associated proteins. They provide correct chromosome segregation and ensure proper sister chromatid cohesion, whereas minor satellites associated with centromeric proteins are responsible for kinetochore formation (Guenatri et al., 2004, Probst and Almouzni, 2008). Moreover, accurate chromosome segregation depends on the maintenance of prolonged sister chromatids. Methylated H3 (Me-K9H3) which exists in both centric and pericentric parts of heterochromatin determines the durable cohesion in major satellites whereas suppressor of variegation (*Suv39h*) attributes to sustainable holding of sister chromatids together (Peters et al., 2001). It is clearly known, that chromosome condensation is a vitally important process which provides an accurate segregation of genetic material equally between daughter cells, and failure in proper function of structures responsible for delivery may lead to undesirable outcomes (Maresca et al., 2005). Alongside contribution to centromere function, the accumulation of heterochromatin-forming satellite repeats is involved in transcriptional silencing (Dillon and Festenstein, 2002). The silencing effect of heterochromatin is well described as Position Effect

Variegation (PEV), the phenomenon that determines inheritable silencing of gene expression which remains stable through successive cell divisions. PEV results in abnormally gene location close to the heterochromatin region and as consequence lead to the silencing of the trans-located gene which in usual conditions is transcribed (Dillon and Festenstein, 2002).

There are more than 30 protein substrates that have been identified in human which are involved in the modification of PEV. They possess antagonistic properties and determine the level of accessibility of genomic DNA. Furthermore, the genetic studies of PEV modifiers have discovered methyltransferase Su (var) 3-9 and heterochromatin protein HP1 which significantly contribute to heterochromatin formation (Dillon and Festenstein, 2002).

Gene silencing has become the recent focus of investigations as it significantly contributes to tumour biology. Promoter hypermethylation has been recognized as mediator of tumorogenesis as it has become apparent that many tumour-suppressor genes were inactivated epigenetically as well as genetically in cancer cells. Consequently, studies have demonstrated that epigenetic alteration as gene silencing, which occurs due to abnormal methylation of CpG islands located in promoter regions of the genes, is substantial for tumour progression.

1.3.3 Nucleosome and posttranslational histone modifications

The very initial step of chromatin compacting process belongs to histones, basic highly conserved proteins; integral and dynamic components of machinery responsible for regulating of gene transcription. Histones are the proteins with the role of building blocks by compacting the DNA chain and folding it into

high-order chromatin structure. Complex of core histones, called octamer, and 146 base pairs of DNA sequence, wrapped in two superhelical turns around an octamer are the constituents of nucleosome (Luger et al., 1997). Nucleosomes are fundamental building blocks of chromatin where histone protein is the heart of this complex Strahl and Allis, 2000).

Depending on the difference in arginine/lysine ratio there are 5 distinguishable types of histones: H2A, H2B, H3, and H4 that function as core histones. Octamer of nucleosome is composed of a H3-H4 tetramer and two H2A-H2B dimers (Arents and Moudrianakis, 1993). Protruding histone tails serve as covalent histone marks which possess the properties for potential interaction with other non-histone proteins or protein modules which analyse genetic information encoded on these tail domains (Strahl and Allis, 2000).

The amino-terminal tails of core histone variants undergo a range of diverse posttranslational modifications (PTM) such as methylation, phosphorylation, acetylation, ubiquitination and sumoylation which have significant impact on chromatin status and able to alter the pattern of gene expression. These modifications are implicated not only in the transcription but also have great influence on all DNA-templated processes such as proliferation, differentiation and apoptosis (Kouzarides, 2007).

Moreover, the great diversity in histone modifications determines their distinct functions. For instance, in terms of transcription some of coexisting histone modifications participate in gene activation, some of them are involved in transcriptional repression. Posttranslational modifications (PTM) provide regulatory information on the amino tails of specific histones which is determined as a “histone code” that is read by the attachment of accessory

proteins. These accessory proteins, denoted as “readers” interact with specialized histone-PTM-binding domains such as bromo-domains, chromo-domains and plant homeodomains (PHDs).

H1 is the protein that contributes as a linker histone, whereas its globular domain (GD) interacts with linker DNA at the entry/exit site of nucleosomal DNA. Construction made by association of H1 and nucleosome is determined as a chromatosome, which is considered to be basic repeat unit of chromatin fibres (Hayashihara et al., 2010). Therefore, H1 promotes further folding of DNA into more high-order condensed structure. Moreover, recently the experiments on Xenopus laevis egg extracts have demonstrated that H1 is essential for condensation and segregation of vertebrate mitotic chromosomes as well. Indeed, H1-depleted chromosomes result in an elongated conformation and failure to align during metaphase and segregate during anaphase (Maresca et al., 2005).

1.4 Chromosomal proteins

Recently, (Hayashihara et al., 2010) have conducted the study to reveal the complete protein composition of human metaphase chromosomes, and as a result of the experiment, over 200 chromosomal proteins have been identified. However, the mechanisms involved in the chromatin condensation and the structure of metaphase chromosome are still unclear. Existing chromosomal proteins can be classified according to their location and biochemical properties into chromosome structural proteins, chromosome peripheral proteins, chromosome fibrous proteins and chromosome coating proteins.

The proteins contributing to the formation of chromatin organization can be further divided into structural proteins, participating in the scaffold formation of chromatin macromolecule, and regulatory proteins, maintaining the structure of the chromatin (Uchiyama et al., 2005). One of the well-known representatives of regulatory proteins is condensin encompassing the complex of two SMC (structure maintenance chromosome) subunits and three non-SMC subunits. It is considered to play a crucial role in maintaining chromatin integrity and proper segregation (Hirano and Mitchison, 1994). However, several studies have published controversial data regarding the importance of condensin by demonstrating that lack of condensin in mitotic chromosomes did not show significant impact on the condensation process of chromosomes (Hudson et al., 2003). The similar data have been shown that another regulatory condensation factor protein topoisomerase II α, which occupies the axial region of mitotic chromosomes, does not completely destroy the entirety of the chromatin structure. Thus, topoisomerase knockdown caused the partial chromosome segregation failure but did not lead to considerable condensation defects (Chang et al., 2003, Carpenter and Porter, 2004).

1.4.1 Heterochromatin Protein (HP1) and HP1 homologues

The compartmentalisation of chromatin in the nuclei of high eukaryotic cells can be observed at the cytological and biochemical levels. Proper condensation and individualisation of chromosomes on the onset of mitosis are provided by accurate package of DNA in nucleosomes (Eissenberg and Elgin, 2000). The compacted status of chromatin is maintained by the interaction of nucleosomes with non-histone proteins, which can influence the function of transcriptionary machinery. HP1 is the non-histone protein directly interacting with

heterochromatin (Chevillard et al., 1993, Mateescu et al., 2008). HP1 proteins represent small protein substrates (15-35 kDa) and refer to a highly conserved, through evolution, family of chromatin proteins that has originally been discovered in *Drosophila Melanogaster* (James et al., 1989, Vermaak et al., 2005).

HP1 homologues are encountered in nature from fission yeast (Swi6, Chp2 and Chp1) to humans (HP1α, HP1β, and HP1γ). All 3 isoforms of HP1 in mammals have similarities in their amino-acid sequences and structural organization but possess distinct functions and occupy different localizations. They are generally associated with more condensed parts of chromatin such as centromeres and telomeres; however HP1γ may occupy both heterochromatin as well as euchromatin (Fanti et al., 2003). As a consequence, different localization determines distinct functions. HP1γ due to its distribution in euchromatic regions is associated with actively transcribed gene regions, and serves as a marker to transcription elongation. Recent data have demonstrated that microsatellite repeat sequence D4Z4 comprises regions of euchromatic (H3K4me2 and H3Ac) as well as heterochromatic (H3K9me3 and H3K27me3) domains, whereas HP1γ have showed its relation to the D4Z4. It has documented that HP1γ and cohesin bind to D4Z4 in H3K9me3-dependent manner. These results depict the contribution of HP1γ together with cohesin to chromatin interaction and organization in the nucleus. With regard to the functions of HP1β, it has been demonstrated that its knockout led to genome instability in mouse (Zeng et al., 2010).

1.4.2 HP1 structure

The structure of the HP1 family members consists of two conserved domains: an N-terminal chromo-domain (CD) and a C-terminal chromo-shadow domain (CHD) interlinked by hinge, the variable-length region of HP1 **(Figure 1-8)** (Lomberk et al., 2006). CD implication was observed in the direct H3K9me interaction which serves as a hallmark histone modification for transcriptionally silenced heterochromatin, while the CHD contributes to various protein-protein chain reactions and functions as the dimerization module. These two domains, conserved from yeast to human, possess three-dimensional structure and form hydrophobic pockets which can function as protein-binding motif. The linker domain of HP1α possesses DNA and RNA-binding properties, and promotes specific targeting and accumulation of HP1α at pericentric heterochromatin (Muchardt et al., 2002).

Every domain is characterized by specific interacting partners. Thus, the CHD of HP1α possesses a consensus peptide pentomer which serves as recognition site and mediates protein-protein interaction. Moreover, this domain might provide heterochromatin compaction as a result of self-association with either HP1β or HP1α itself. In addition to these properties, chromo shadow domain CSD of HP1 interacts with DNA methyl-transferases Dnmt1 and Dnmt3a which provide CpG methylation. Another interacting partner of CSD is p150, the large subunit of chromatin-assembly factor-1 (CAF1) which plays significant role in DNA replication and DNA repair. It has been shown, that the essential partner for CD is H3K9me3, and communication between them mainly contributes to the heterochromatin stability. Direct interaction of CD with H3K9me is the histone modification pattern, which determines the condensed state of chromatin

and serves as critical marker of epigenetic silencing (Bannister et al., 2001). H3K9me in mammals interacts with multiple histone methyltransferases (HMTases) such as SUV39h (SUV39 h1 and SUV39 h2), SETDB1 and G9a which are encoded by homologues of the *D. melanogaster Suppressor of variegation 3-9 gene* **(Figure 1-8)**.

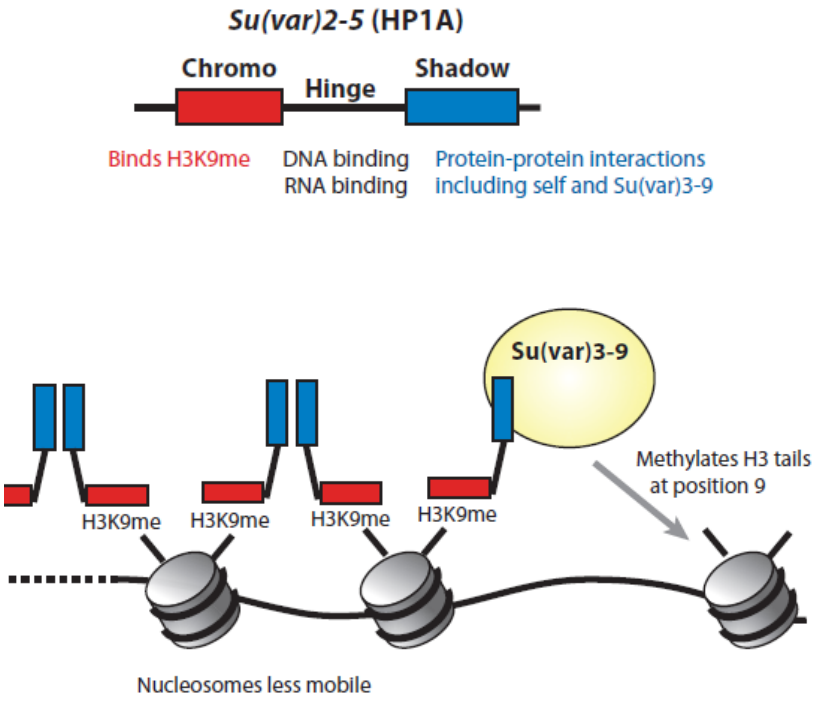


Figure 1-8: A simple model of spreading heterochromatin and a schematic representation of HP1α protein expressed by Su (var) 2-5 protein from *Drosophila melanogaster.* (Adapted from (Vermaak and Malik, 2009) Interaction of HP1 chromodomain with H3K9me3 promotes heterochromatin state, while chromoshadow domain serves to self-interlink and bind SUV39h which methylates histone tails at position 9.

Each representative of HMTases is characterized by distinct target specificity and degree of methylation (Maison et al., 2011). However, for proper initiation and efficient maintenance of HP1α heterochromatin binding, involvement of

other histone modifications is required. Recent data have demonstrated that HP1α N-terminal phosphorylation on serine residues (S11-S14) enhances the binding of HP1α to the H3K9me. Indeed, *Drosophila* studies have revealed that phosphorylated HP1α exhibits a stronger binding affinity to the heterochromatin and is involved in silencing activity (Hiragami-Hamada et al., 2011).

On the other hand, there is strong evidence that sumoylation promotes HP1α binding to DNA and thus is involved in the transcriptional repression. Recent studies showed that SUMO modification occurs in the hinge domain of the HP1α, and that the hinge domain is required for *de novo* localization of HP1α (Maison et al., 2011). In addition, alongside different types of modifications such as methylation, acetylation, phosphorylation and sumoylation, RNAs are also required for accumulation of HP1 proteins in these domains (Maison et al., 2011).

Initially, HP1 was considered as a transcriptional repressor due to its participation in the heterochromatin-mediated gene silencing. However, later it was discovered that HP1 also contributed to the transcriptional elongation, centromeric sister chromatid cohesion, telomere maintenance and DNA repair. Moreover, recent studies demonstrated that HP1α has a dual role in DNA damage response (Zeng et al., 2010).

1.5 DNA damage signalling pathway

The cellular environment is continuously being challenged by the impact of endogenous factors, such as products of normal metabolism, as well as during DNA replication, transcription, and recombination, and exogenous or

environmental factors, such as exposure to UV radiation, ionizing radiation, and treatment by various chemical agents (Wood, 1996, Sancar et al., 2004). All these factors often lead to the DNA lesions that might contribute to the various outcomes. Firstly, DNA damage might initiate malignant process; secondly, it is used to cure cancer and, thirdly, it can contribute to side effects of cancer treatment (Kurz and Lees-Miller, 2004).

Depending on the challenge, different types of DNA damage such as DNA base damage, single stranded DNA (ssDNA), interstand crosslinking of DNA and DNA double-strand breaks (DSBs) can occur. The most dangerous DNA lesion is DNA double-strand-breaks (DSB) (Kurz and Lees-Miller, 2004, Murray et al.). The failure of DSB lesion repair can lead to translocations, inversions, deletions and chromosomal abnormal rearrangements. All these alterations might lead to accumulation of the vitally dangerous mutations or promote the process of tumorigenesis.

Induced DNA damage initiates subsequent activation of the signaling pathway known as the DNA damage response (DDR) that represents a multistep process involving a network of DNA damage response protein substrates (Goodarzi et al., 2008). Once DSB occurs, the sensor substrates recognize and detect the DNA damage site with further transmission of the DNA damage signal to the transducers, proteins that promote activation of various protective pathways starting with initiation of cell-cycle checkpoints, mechanisms that arrest the cell-cycle division, followed by cell cycle arrest, DNA repair or apoptotic programs via downstream effectors (Lee and Paull, 2007).

DDR is generated by trimetric highly conserved MRN (MRE11-RAD50-NBS1) protein complex that is involved in both modes of DSB repair, non-homologous end joining (NHEJ) and homologous repair (HR) that requires the undamaged homologues DNA template to restore the original DNA sequence, and consequently restricted at S phase and G2 when the sister chromatid is available. The initial stage of implication of MRN complex in DSB happens due to nuclease activity and DNA binding capability that belong to the MRE11 and is partially determined by MRE11 and Rad interaction (Lee and Paull, 2007). Nbs1 protein is responsible for nuclear localization and placement of the complex at the DSB site via its direct interaction with protein histone variant H2AX. Furthermore, the enrichment of MRN complex at the DSB ends promotes the recruitment and activation of central DDR signaling protein kinase Ataxia Telangiectasia Mutated (ATM) (Goodarzi et al., 2008).

ATM and related kinases ATR (ATM and Rad3-related) and DNA-PK (DNA-dependent protein kinase) refer to phosphorylatidylinositol 3-kinase–like (PIKK) family of serine/threonine protein kinases, and all are implicated in DNA DSB response pathways (Goodarzi et al., 2008). The members of PIKK family possess noticeable similarities in the architectural structure and share sequence homology, particularly in the following domains such as C-terminal domain, flanking FAT (FRAP–ATM–TRRAP) and FATC (FAT C-terminal) domains (Keith & Schreiber, 1995, Bosotti et al., 2000) **(Figure 1-9)** known to be involved in the regulation of kinase activity. The N-terminal presents poorly conserved region among PIKK family members and contributes to the protein-protein interaction with various substrates (Fernandes et al., 2005).

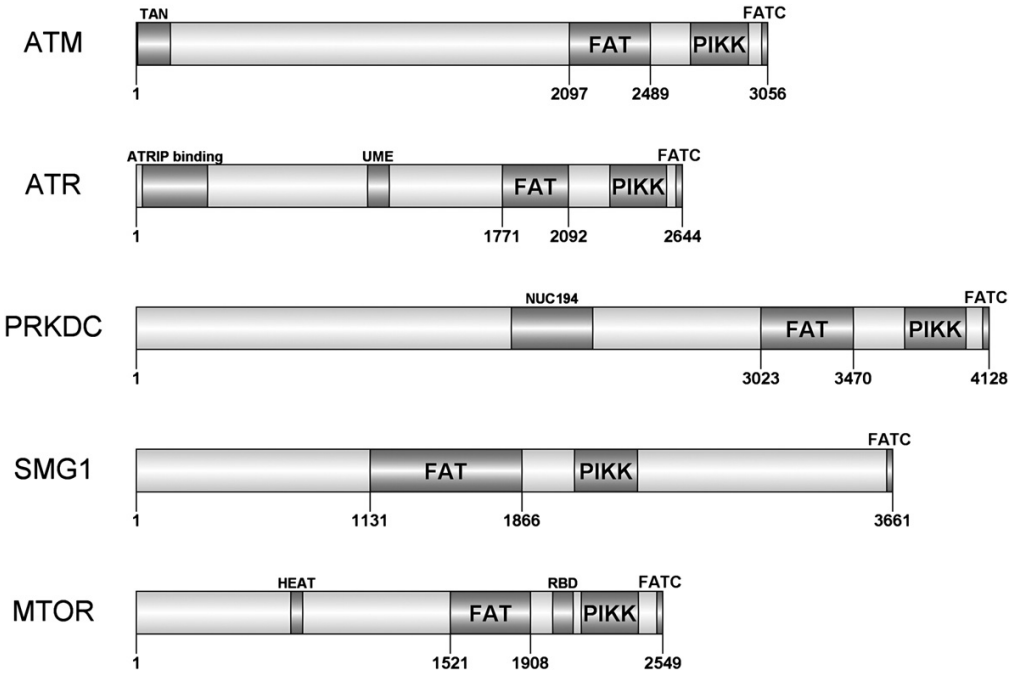


Figure 1-9: Schematic presentation of domain architecture of PIKK family members. Displayed proteins are: ATM (ataxia-telangiectasia mutated), ATR (ataxia–telangiectasia and Rad3 related), PRKDC (DNA-dependent protein kinase catalytic subunit; DNA-PKcs), SMG1 (suppressor of morphogenesis in genitalia), MTOR (mammalian target of rapamycin). Conserved domains are: FAT (FRAP–ATM–TRRAP domain), FATC (FAT C-terminal domain), PIKK (phosphatidylinositol 3-kinase-related kinase domain), TAN (Tel1/ATM N-terminal motif), ATRIP (ATR interacting protein),UME (UVSB PI3 kinase,MEI-41 and ESR1 domain), NUC194 (domain B in the catalytic subunit of DNA-dependent protein kinase), RBD (rapamycin binding domain), HEAT (Huntingtin, elongation factor 3, protein phosphatase 2A, and the yeast kinase TOR1-like repeat) [(Adapted from (Weber and Ryan, 2014)].

Ataxia Telangiectasia Mutated (ATM) is one of the central kinases that activated by formation of DNA DSBs. ATM molecule transforms from inactive dimer into an active monomer by autophosphorylation on Ser1981 as a result of DNA DSBs (Bakkenist and Kastan, 2003, Lee and Paull, 2005, Shiloh and Ziv, 2013). The

recruitment of activated ATM at sites of DNA DSBs occurs through its binding to C-terminus of NBS1 of MRN complex (Lee and Paull, 2005). This interaction promotes further kinase activity of ATM (You et al., 2005). Following its recruitment at sites of DNA DSBs, activated ATM protein kinase rapidly phosphorylates the histone variant H2AX on Serine 139 (noted as γH2AX) (Burma et al., 2001).

Alteration of histone dynamics in DNA repair is one of the crucial moments in DDR. DSBs induce not only histone modifications but also lead to the histone variants involvement in the DNA repair process. Thus, generation of γH2AX foci amplifies the DNA damage signal and promotes further recruitment of DDR proteins at the breakage sites. Accumulation of γH2AX foci in the regions flanking the lesion serves as an indicator of DSB presence and a marker for DDR activation (Soria et al., 2012). This suggests that ATM kinase initiates a cascade of DDR factors to provide effective DNA damage repair (Lim et al., 2000, Di Virgilio et al., 2009, Gatei et al., 2011). Moreover, activated form of ATM exposes protective properties through regulation of cell cycle. Thus, in response to the induction of DNA DSBs ATM triggers activation of the G1/S cell cycle checkpoint and thus restrains cells with damaged DNA from entering the S-phase. This defensive mechanism is initially mediated through direct phosphorylation of p53 on serine 15 by ATM kinase. Tumour suppressor protein p53 was reported as one of the first downstream substrates targeted by ATM kinase (Kastan et al., 1992, Siliciano et al., 1997, Banin et al., 1998, Canman et al., 1998). Additionally, stabilisation of p53 can be achieved via phosphorylation of p53 on serine 20 by checkpoint kinase (CHK2), another key target substrate of ATM (Chehab et al., 1999). This phosphorylation prevents p53 from Mdm2-

mediated ubiquitination and degradation (Haupt et al., 1997; Chehab et al., 1999; Marine and Lozano, 2010). Furthermore, ATM rescues p53 from degradation by direct phosphorylation of Mdm2 (Khosravi et al., 1999). The activated form of p53 accumulates in the nucleus and acts as a transcription factor. As a result of this function, p53 stimulates the expression of genes implicated in cell cycle activity as well as several genes contributing to cell apoptosis (Sullivan et al., 2012).

Further contribution of ATM kinase to prevent the synthesis of damaged DNA is fulfilled through its S-phase checkpoint functions. Thus, phosphorylated by ATM CHK2 kinase lead to ubiquitination and degradation of the S-phase-promoting phosphatase Cdc25A which in adequate cellular microenvironment promotes S-phase progression via activation of the cyclin-dependent kinase 2 (Cdk2) that is required for DNA synthesis (Falck et al., 2001).

Alongside ATM, the ATR signaling pathway also takes part in enforcement of the intra-S-phase checkpoint in the presence of impaired replication fork. The pathway is governed primarily by ATR, and may involve members of the Rad family of checkpoint proteins as damage sensors and as scaffolds for the assembly of checkpoint signaling complexes. The regulation of this pathway prevents mitotic catastrophe that results from incomplete or inaccurate DNA replication, and orchestrates high-fidelity DNA repair through homologous recombination (Abraham, 2001).

Similar to ATM, ATR refers to central kinases implicated in DDR. However, unlike ATM, activation of ATR kinase is provoked by single strand DNA (ssDNA) damage that occurs, for instance, at stalled replication forks (Wold, 1997; Byun et al., 2005). Thus, interaction of ATRIP (ATR-interacting protein)

and the N-terminus of ATR induce activation and localization of ATR kinase to damage sites (Zou & Elledge, 2003). Once activated, ATR exerts its DNA repair properties via recruitment of target substrates (Chen, 2000, Tibbetts et al., 2000, Sorensen et al., 2003, Xiao et al., 2003, Cimprich and Cortez, 2008, Dai and Grant, 2010, Errico and Costanzo, 2012). Many of ATR functions are achieved through CHK1 kinase, the specific ATR downstream substrate. Through CHK1-mediated degradation of Cdc25A phosphatase ATR inhibits progression of DNA replication thus ensuring sufficient time to resolve the stress condition (Sorensen et al., 2003, Xiao et al., 2003, Bartek et al., 2004). Moreover, ATR also regulates G2/M cell cycle checkpoint by preventing mitotic entry in response to DNA damage (Zhao et al., 2002, Xiao et al., 2003).

Despite the differences in the activation of ATM and ATR signaling pathways, they share the plethora of downstream target substrates. Both kinases possess similar substrate specificity and phosphorylate their target substrates on serine or threonine residues that precede glutamine residues, termed as SQ/TQ-motifs (Kim et al., 1999, Matsuoka et al., 2007). It was reported, that more than 700 ATM/ATR putative target substrates have been identified as a result of a large-scale proteomic study (Matsuoka et al., 2007). Therefore, the cellular functions of these protein kinases partially overlap, and the failure of one pathway might be compensated by other pathway (Helt et al., 2005).

ATM and ATR confer a range of biological functions including cell survival, proliferation, differentiation, metabolism and motility. Moreover, a significant body of research suggests PIKK family members are linked to tumorigenesis and refers these kinases as attractive putative targets for cancer therapy. A functional interplay between ATM and ATR contribute to the maintenance of genomic

stability after DNA damage by regulating cell cycle progression and DNA repair (Abraham, 2001, Shiloh, 2003, Cimprich and Cortez, 2008). Thus, ATM as a known tumour suppressor gene is found mutated in a wide range of human cancers such as breast, lung, colorectal and hematopoietic cancers (Landau and Wu, 2013).

Initially, ATM was identified as a gene defective in the autosomal recessive human hereditary disorder ataxia–telangiectasia (A–T) (Savitsky et al., 1995). This multisystem condition, caused by a defect in ATM function, is characterized by oculocutaneous telangiectasia, progressive cerebellar ataxia, immunodeficiency, radio-sensitivity and predisposition to malignancies (Taylor et al., 1975; Lavin, 2008).

ATR-deficiency impedes the viability of multicellular organisms (Ruzankina et al., 2007). Furthermore, it was reported that ATR depletion in adult mice manifested in the defect of tissue homeostasis as a result of restricted proliferation, whereas ATR activity is essential to maintain the proper DNA replication for all proliferating cells and thus to ensure genomic stability (Brown and Baltimore, 2000).

ATM and ATR-mediated DNA damage pathways encompass detection of DNA lesions, repair mechanisms, cell-cycle check point induction and apoptosis. However, for fulfilment the above mentioned functions it is important to consider the complexity of chromatin structure. It is noteworthy, that sensitivity of DNA to damage and the kinetics of repair can be determined by chromatin density (Cann and Dellaire, 2011).

1.5.1 Impact of chromatin structure on DNA damage response

DNA double-strand break (DNA DSB) refers to one of the most deleterious types of DNA lesions with destruction of both strands of DNA molecule. The failure in proper DSBs recovery can lead to the development of cancer via accumulation of mutations. Thus, the genomic DNA of mammalian cells evolved a robust genome surveillance system to maintain DNA integrity through activation of alternative cell fate pathways (Wood, 1996, Sancar et al., 2004, Cann and Hicks, 2007). As genomic material is presented by nucleo-protein complex, consequently DNA template and proteins involved in its compaction process are implicated in DNA damage response pathways (Cann and Dellaire, 2011). The interest in the correlation between DNA DSB induction and alterations in chromatin structure was observed throughout the decades (Groth et al., 2007). Topological organization of chromatin has impact on all nuclear processes, including DNA damage response. Thus, the difference in chromatin compaction in euchromatin and heterochromatin reflects on the both damage sensitivity and repair. Heterochromatin decondensation is crucial for inducement of DNA damage signal amplification as well as for provision of access for DNA repair proteins to the breakage sites (Campos and Reinberg, 2009). Thus, manipulation of chromatin structure dictated by ATP-dependent chromatin remodeling complexes and histone-modifying enzymes is involved in any DNA repair process to allow access to DNA (Ataian and Krebs, 2006, Costelloe et al., 2006, Campos and Reinberg, 2009, Misteli and Soutoglou, 2009).

Heterochromatin condensation impedes the DNA repair, and as a result heterochromatic double strand breaks (DSBs) recover with slower kinetics and less efficiency compare with euchromatic DSBs (Slijepcevic and Natarajan

1994, Goodarzi et al. 2008). It was demonstrated that hetero-chromatization is the principal criteria of ATM involvement, and implication of ATM in DNA damage response is determined by chromatin complexity rather than by damage complexity. Thus ≤25% of DSBs require ATM-signaling for repair where ATM kinase facilitates DSB repair by affecting the heterochromatin–building components such as KAP-1, HP1α, and/or Tip60 **(Figure 1-10)** (Kurz and Lees-Miller, 2004).

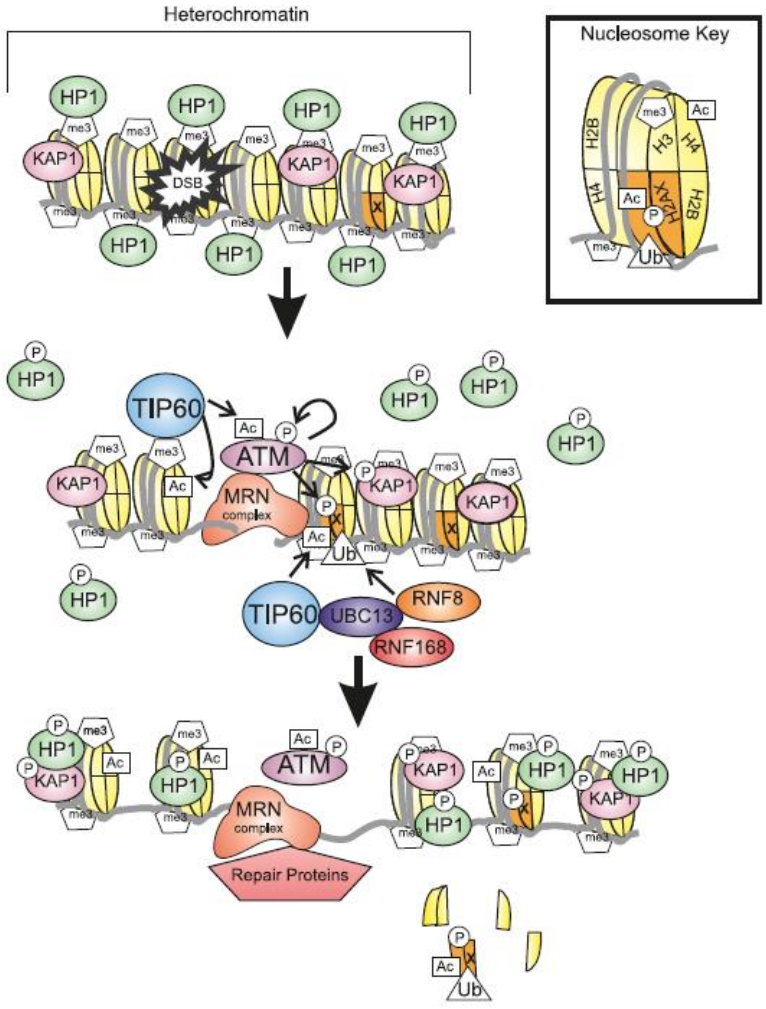


Figure 1-10: Alterations in heterochromatin architecture as a result of DNA DSBs. Triplicate MRN complex recognizes and accumulates at the DNA DSBs sites with further recruitment of ATM protein kinase. As a result of HP1α release from H3K9me3 the vacant place is occupied by Tip60 and ATM complex that promotes the involvement repair proteins. Acetylation of ATM by Tip60 leads to

the ubiquitination of ATM by RNF8 and RNF168 ubiquitin kinases and thus contributes to the amplification of DNA damage signal [(Adapted from (Cann and Dellaire, 2011)].

Recent studies demonstrate that HP1α has a dual role in DDR. Thus, phosphorylated HP1α by casein kinase 2 (CK2) temporarily removes HP1α from H3K9me3 leading to the heterochromatin de-condensation and providing access to DNA repair proteins (Cann and Dellaire, 2011). As a result of HP1α release from heterochromatin, the space vacated by H3K9me3 is occupied by complex of Tip60 and ATM that gains activation and initiates DDR by further phosphorylation of downstream substrates (Cann and Dellaire, 2011). Alternatively, it was reported that chromo-shadow domain determines the recruitment of HP1α to the DSBs sites and provides accumulation of HP1α at the sites of heterochromatic perturbation by amplifying DNA damage signal whereas chromodomain and H3K9me3 participates in the disassociation of HP1α and promotes the chromatin decondensation (Cann and Dellaire, 2011). Moreover, enrichment of HP1α at pericentric heterochromatin provides stabilization and integrity of sister chromatids as well serves as recognition site for mediators of the DNA damage response pathway. Thus, bimodal behavior of HP1α at the DNA DSBs sites is recognized as a crucial mediator of chromatin relaxation and at the same time participates in the maintenance of genomic stability and is important factor for the completion of DNA repair (Cann and Dellaire, 2011).

Experimental evidence demonstrated that chromatin relaxation is partially determined by ATM-mediated phosphorylation of transcriptional repressor

KAP1 (KRAB-associated protein; TIF1b; TRIM28). KAP1 is an abundant nuclear protein that binds in a sequence-dependent manner to KRAB domains to contribute to the heterochromatin construction through association with heterochromatin-building factors such as HP1, histone deacetylases (HDACs), SET-domain histone methyltransferases, and ATP-dependent chromatin remodelers (Goodarzi et al., 2008). ATM-KAP1 association for chromatin decondensation is required during G2 phase as well as G0/G1 cells for efficient DSB repair. However, heterochromatic DSB repair during DNA replication was demonstrated to be ATR-dependent. Therefore, the phosphorylation of KAP1 during this phase of cell cycle is mediated by ATR kinase. More recently, it was reported that mutation or deletion of heterochromatin-related factors (KAP-1, HP1, HDAC1/2, and Suv39H1/2) impedes the function of ATM kinase in DNA repair (Goodarzi et al., 2008). This data demonstrates the specificity of ATM to induce chromatin relaxation within heterochromatic DSBs (Goodarzi et al., 2008).

Alongside the contribution to the enhanced DNA damage signalling and more efficient repair, the role of heterochromatin proteins is also directed on reestablishment of chromatin structure following DNA damage. According to the recent reports, the deletion of KAP1 led to the increased DNA sensitivity thus highlighting the function of the protein in the maintenance of the genomic stability (Ziv et al., 2006, Goodarzi et al., 2008). Hence, through regulation of the access of the transcriptional machinery to the DNA strands and modulation of dynamic chromatin architecture, chromatin-associated proteins orchestrate a range of critical cellular events including DNA repair and a promotion of malignant transformation and progression (Cann and Dellaire, 2011).

1.6 Heterochromatin protein 1 binding protein 3 (HP1BP3, also known as HP1BP74)

Heterochromatin protein 1 binding protein 3 (HP1BP3) is a novel chromatin interacting protein that originally was recognised as a binding partner of HP1 molecule (Hayashihara et. al., 2011). According to Hayashihara et. al., HP1BP3 was identified as result of salt stripping of isolated and highly purified human metaphase chromosomes that were isolated from HeLa S3 cells **(Figure 1-11)**.

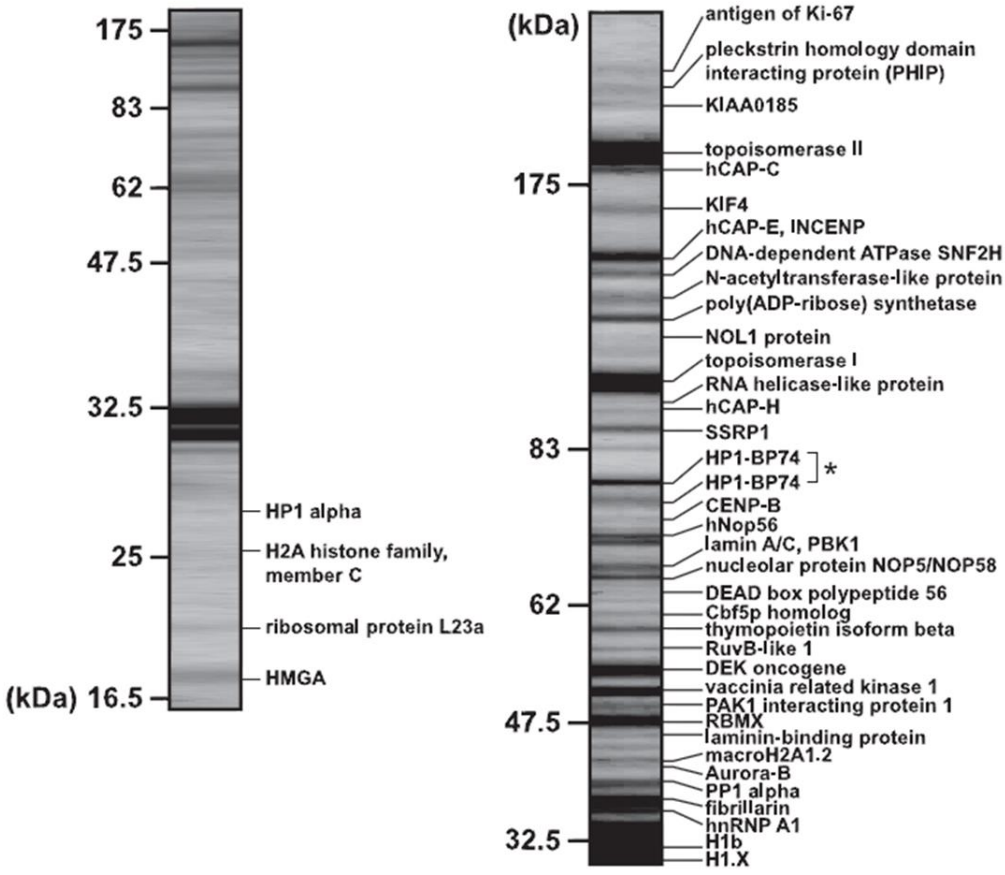


Figure 1-11: The schematic composition of human proteins involved in the formation and/or maintenance of metaphase chromosomes [(Adapted from

(Hayashihara et. al., 2011)]. Dissociation and identification of proteins was performed by application of 0.4M NaCL and mass spectrometry, respectively. HP1BP3 (HP1BP74) is expressed by two separate bands, as demonstrated.

HP1BP3 encodes a highly conserved protein found in mammals with a high degree of structural and functional similarity between human and murine (Garfinkel et al., 2015). In humans, the *HP1BP3* gene is mapped to chromosome 1 (chromosomal position: 1p36.12) and comprises 13 exons while the mouse *Hp1bp3* gene is encoded in chromosome 4 (chromosomal position: 4 D3; 4) and composed of 12 exons. Moreover, both human *HP1BP3* and mouse *Hp1bp3* encode two endogenously expressed bands corresponding to the long isoform, designated as HP1BP3a, and short isoform, designated as HP1BP3b (Hayashihara et. al., 2011, Garfinkel et al., 2015). It was reported that a short product of HP1BP3 arises as a result of alternative splicing by skipping exon 2 and starting the translation from exon 3. Thus, the splice variant lacks the first 38 amino acids located at N-terminal (Garfinkel et al., 2015). Human longer and shorter HP1BP3 protein substrates consist of 553 and 402 amino acids, respectively, whereas mouse Hp1bp3 protein produces splice variants of 500 and 462 amino acids. Both human and mouse alignment analysis of HP1BP3 transcript sequences revealed more than 84% of homology between long and short isoforms of two species. The expression of both the mRNA and protein products of HP1BP3 splice variants are reported in the majority of human and mouse tissues (Garfinkel et al., 2015). Interestingly, at least one of the HP1BP3 isoforms was expressed in all studied samples (Garfinkel et al., 2015).

1.6.1 HP1BP3 protein structure and localisation

HP1BP3 is a novel nuclear protein comprising different domains involved in distinct interactions (Hayashihara et. al., 2011, Garfinkel et al., 2015). Recent

reports demonstrated that HP1BP3 is a ubiquitously expressed protein exhibiting evolutionary and structural resemblance with histone H1 family, the most abundant family among the nucleosome-binding proteins (Garfinkel et al., 2015). Linker histone H1 variants are tightly involved in the modulation of chromatin structure and contribute to the high-order chromatin organisation through interaction with nucleosomal DNA (Happel and Doenecke, 2009). It was previously discovered that the middle part of HP1BP3 (K97-K274) contains a globular domain (M153-T237) that bears a sequence identical to the linker histone H1 and associates with linker DNA at entry/exit site of nucleosomal DNA (Hayashihara et. al., 2011). Indeed, further structural studies showed that HP1BP3 encompasses three functional motifs possessing a high sequence similarity with globular domains of H1 family members (Garfinkel et al., 2015). Thus, three consecutive globular domains, termed GD1, GD2 and GD3 were determined downstream of a glutamine rich unstructured N-terminal domain (NTD) consisting of 100 amino acids. Following GD3 there is a 20 amino acid poly aspartate/glutamate tract (DE) that neighbours with a highly positively charged C-terminal domain (CTD). The sequence conservation of triple globular region between the murine and human is very prominent (98% identity). Similar to H1 gene family, both N- and C-terminal domains are required for the chromatin binding properties of HP1BP3 which are dependent on cell cycle and post-translational modifications (Garfinkel et al., 2015). Indeed, recent experimental evidence showed that deletion of basic C-terminal tail dramatically diminished the interaction of HP1BP3 with chromatin (Garfinkel et al., 2015). Furthermore, it was shown that deletion of N-terminal extension also affected on the affinity of HP1BP3 for chromatin by reducing it (Garfinkel et al., 2015).

Moreover, it resulted in nuclear redistribution of HP1BP3 protein with accumulation in the nucleoli. Therefore, this data suggest that a triple globular region along with C- and N-terminal domains exert the cooperative function towards the proper chromatin binding of HP1BP3 (Garfinkel et al., 2015).

Along with similarities, HP1BP3 possesses structural characteristics distinct from H1 family members. Thus, it was previously reported that HP1BP3 interacts with chromoshadow domain of HP1α through a canonical HP1 binding motif, PQVKL, positioned at residues 255-259 between the first globular domains (Hayashihara et. al., 2011, Garfinkel et al., 2015). Site-directed mutagenesis with substitution of central valine (V257) to glutamate resulted in the complete abolishment of HP1BP3 interaction with heterochromatin, thus depicting an HP1-dependent heterochromatin enrichment of HP1BP3 (Garfinkel et al., 2015). In addition, a 20 amino acid poly aspartate/glutamate stretch, termed as DE and located between the third GD and CTD regions, is a unique structural property of HP1BP3. However, in spite of absence of DE region within H1 family members, it is observed in a range of distinct chaperons. The role of DE acidic tract is directed on interaction with core histones and regulation of DNA binding dynamics. The deletion of DE sequence markedly increased the duration of HP1BP3 occupation on chromatin (Garfinkel et al., 2015).

Structural characteristics of chromatin-interacting protein HP1BP3 determine its cellular localization. Thus, exhibition of "histone-H1-like" domains confer DNA binding properties of HP1BP3, whereas HP1 binding motif stabilizes its interaction with chromatin. Together, these dictate the intra-nuclear localization of HP1BP3. Indeed, according to recent evidences, the expression of HP1BP3 in all investigated cells and tissues was strictly nuclear (Garfinkel et al., 2015).

HP1BP3 is ubiquitously present in all vertebrates (Garfinkel et al., 2015). However, the tissue distribution of HP1BP3 varies with cell type. Thus, in brain the quantity of expressed HP1BP3 was 10-fold higher compared to the rest of observed tissues. Interestingly, HP1BP3 was not detected in germ cells. The high amount of HP1BP3 protein was observed in embryonic tissue but excluding trophoblast placental regions. Moreover, HP1BP3 showed variable level of expression within the same tissue. Thus, proximal tubules of kidney displayed strong signal of HP1BP3 expression compared to distal ones, thus implying the higher content of HP1BP3 within these regions. Also, HP1BP3 exhibited the distinct intra-nuclear pattern of expression depending on cell type. It was shown that the expression of HP1BP3 in the cells of Purkinje was presented by enrichment in the perinucleolar heterochromatic foci, whereas neurons of the cerebellum displayed the diffuse distribution of HP1BP3 (Garfinkel et al., 2015).

1.6.2 HP1BP3 functions

Several studies were conducted to investigate the role of HP1BP3 in chromatin-, cellular-, and patho-biology (Dutta et al., 2014a, Dutta et al., 2014b, Garfinkel et al., 2015). Since HP1BP3 initially was identified as a novel heterochromatin associated protein (Hayashihara et. al., 2011), further research was directed at how HP1BP3 impacts on heterochromatin structure. Emerging evidence showed that depletion of HP1BP3 led to unfolding of the chromatin thus altering heterochromatin architecture (Dutta et al., 2014a). Hence, these data revealed a novel regulatory role for HP1BP3 in the maintenance of heterochromatin integrity and higher order chromatin structure. Moreover, recent experimental evidences showed the involvement of HP1BP3 in chromatome dynamics (Dutta et al., 2014a). The chromatin-associated proteome (chromatome) presents a

dynamic association of DNA molecule, histone variants and non-histone chromatin proteins. Thus, applied proteomic approaches uncovered the dynamic association of HP1BP3 molecule with chromatin throughout different stages of cell cycle progression (Dutta et al., 2014a). Cell cycle is the basic biological process required for cell division and maintenance of the original cell's genome. All fundamental DNA-related processes *in-vivo* like replication, DNA repair and recombination, transcription, chromatin segregation, and genome packaging occur during cell cycle, and maintenance of dynamic status of chromatin structure throughout cell cycle is crucial for fulfilment of the genetic events. A typical eukaryotic cell cycle comprises two basic parts: mitosis (nuclear division) and interphase (distribution of doubled genomic material into daughter cells) (Cooper, 2000). The interphase-period between mitoses, takes approximately 95% of cell cycle and encompasses G1 phase (gap between mitosis and initiation of DNA replication), S phase (occurrence of DNA replication) followed by G2 (cell growth and preparation for mitosis) (Alberts et al., 2002). It was shown that chromatin interaction of HP1BP3 steadily increased during G1-S phase progression (Dutta et al., 2014 a). Furthermore, the synchronized in G1/S phase by double thymidine treatment and released from G1/S arrest in HP1BP3-depleted cells displayed faster G1/S transit and shortening the total cycle time in comparison to mock-depleted cells (Dutta et al., 2014 a). Proliferation and cell cycle kinetics are dependent on the rate of cell division and the fraction of cells participating in proliferation. Cell cycle progression and accelerated rate of proliferation are controlled by cell-cycle regulators and checkpoints regulators. The length of S, G2 and M phases of mammalian cell cycle are relatively similar but G1 phase is highly variable

(Andreeff and Pardee, 2000). According to the recent evidences, G1 and G1/S phases of cell cycle play pivotal role in the regulation of cell proliferative capacity (Weinberg, 1995, Johnson and Walker, 1999, Novak et al., 2001). The depletion of HP1BP3 in A431 epidermoid carcinoma cell line showed a high rate of cell proliferation (by 39% increase) thus highlighting the impact of HP1BP3 on G1 phase duration by regulating G1/S transition (Dutta et al., 2014 a). However, HP1BP3 knockout mouse displayed partial post-natal lethality and adult dwarfism thus underlying the physiological importance of HP1BP3 in growth and vitality (Garfinkel et al., 2015).

Furthermore, it was reported that the lack of HP1BP3 in the cells led to reduction of chromatin compaction and increased susceptibility of DNA to MNase digestion (Dutta et al., 2014a). This data presents HP1BP3 as a key switch modulator of chromatin structure by inter-converting euchromatin and heterochromatin and therefore as regulator of gene transcription through maintenance of heterochromatin integrity (Dutta et al., 2014a). However, the different group reported that HP1BP3 does not impact on global chromatin composition and no difference was observed in the sensitivity of chromatin followed MNase treatment (Garfinkel et al., 2015). But despite this disagreement, both groups showed that ablation of HP1BP3 caused alteration in protein profile expression (Dutta et al., 2014a, Garfinkel et al., 2015). Any changes in the dynamic compaction of chromatin influence the transcriptional machinery thus leading to modulation of cellular events. Alteration in transcriptional level leads to changes in protein expression level. Based on quantitative proteomic analysis, 384 proteins were affected by lack of HP1BP3, where 176 of differentially expressed proteins were up-regulated and 208 were

down regulated (Dutta et al., 2014a). Thus, presented experimental observations and evidences suggest that HP1BP3 not only plays an architectural role in the stability of heterochromatin structure but is also responsible for regulation of protein expression through governing gene transcription (Dutta et al., 2014a).

The dynamic balance of chromatin structure throughout cell cycle progression is critical for fulfilment of the basic cellular events (Uttam et al., 2013). The maintenance of chromatin integrity is supported by chromatin-protein interaction which regulate the important biological and pathological cellular functions that occur during interphase (Probst et al., 2009, Liu and Gong, 2011). Interphase consists of two constantly interchanged states of chromatin: euchromatin which provides the rapid access of the transcriptional factors to DNA template for realization normal cellular functions whereas heterochromatin prevents aberrant DNA-related events. Thus, a highly dynamic state of chromatin is crucial for efficient transfer of genetic and epigenetic material into daughter cells (Pombo, 2007). Dysregulation of chromatin-associated system might trigger disorder in cell cycle and promote carcinogenesis (Jespersen et al., 2012, Di Paola et al., 2012). Since HP1BP3 impacts on chromatin integrity by inter-converting euchromatin and heterochromatin, it might present a key driving force in tumorogenesis through deregulation of cell cycle that leads to uncontrolled cell growth, the hallmark of cancer (Dutta et al., 2014a, Dutta et al., 2014b).

Recent experimental evidences showed that chromatin association of HP1BP3 was enhanced during hypoxia-caused stress conditions altering gene expression (Dutta et al., 2014b). Hypoxia is one of the main determinants of oncogenesis and also contributes to the acquisition of therapeutic resistance (Nordsmark et

al., 1996, Brizel et al., 1999, Ghattass et al., 2013). Hypoxia-induced changes in chromatin-related processes represent key driving factors in tumour biology. The effect of HP1BP3 deficiency in hypoxia stress environment was observed *in vitro* and *in vivo* (Dutta et al., 2014b). The biological role of HP1BP3 in cancer growth and malignancy was evaluated by using a xenograft animal model of tumour growth. The results revealed that subcutaneous injection of HP1BP3-depleted cells gave rise to tumour only in three of six mice, whereas mock-depleted A431 cells manifested tumours in all six mice (Dutta et al., 2014b). The experimental observation showed that the hypoxia-dependent HP1BP3 mediated heterochromatinization led to the increased cancer cell survivability thus implying HP1BP3 as a regulator of cancer progression.

Hypoxia-induced HP1BP3-heterochromatinization caused genetic reprograming of cancer cells influencing the response to radio- and chemo-therapy. Hypoxia impedes the cancer treatment through induction of resistance against radio- and chemo-treatment (Ghattass et al., 2013). HP1BP3 contributes significantly to cell survivability during hypoxia affecting the radio- and chemo-sensitivity of cells. Thus, ablation of HP1BP3 reduced the cell viability by 18% after exposure to 10Gy of ionizing radiation; whereas the IC50 value of doxorubicin was reduced from 670.2±62ng/ml to 503.2±36ng/ml in HP1BP3-knockout cells compared to control cell line (Dutta et al., 2014b). This data suggests that depletion of HP1BP3 contributes to the increased radio-and chemo-sensitivity.

The biological findings suggest that HP1BP3 plays a key role in cancer progression and presents a potential target for new cancer therapy.

1.7 Rational and objectives of this study

1.7.1 Rational

Genomic integrity is constantly exposed to the products of metabolic activities and environmental processes that can induce DNA damage (Ciccia and Elledge, 2010). A well-organized network of signaling cascade, designated as DNA damage response (DDR), encompasses systems of damage detection, cell-cycle check-point activation and repair mechanisms (Jackson and Bartek, 2009, Ciccia and Elledge, 2010, Giglia-Mari et al., 2011). The DNA damage pathways involve not only naked DNA strands but also higher-order chromatin components, such as histone variants and heterochromatin proteins (Probst et al., 2009). However, most of studies mainly focused on the core histones, whereas the heterochromatin proteins and their partners' identity remained unknown.

Recently studies in Dr Nateri's laboratory identified the HP1BP3 as one of the FBXW7 interacting protein for degradation, using a modified yeast 2-hybrid reverse Ras-recruitment system (rRRS) (Nateri et al., 2004, Kohler and Muller, 2003, Abuzinadah et al., submitted). Our laboratory recent analysis also indicate that HP1BP3 degradation by the E3 ubiquitin ligase Fbxw7 regulates mouse hematopoietic stem cell (HSC) cycle entry and the transcriptional "signature" that is associated with the quiescent, self-renewing of HSC phenotype and leukemic status (Abuzinadah et al., submitted for publication). HP1BP3 also functions in cellular growth control and neoplasia of human colorectal cancer cells in association with HP1α and consequent epigenetically modifications (Kattan et al., submitted). To this end, our laboratory preliminary data suggests

that the modulation of HP1BP3 by the E3 ubiquitin ligase FBXW7 may determine which biological events occur in normal and cancer cells.

To further investigate the molecular mechanisms underpinning HP1BP3 protein activity regulation that signal into biological response, we investigated structural features of the HP1BP3 protein using of web-based computational analysis programs. Thus, to detect nuclear and nucleolar signaling sequences within HP1BP3 molecule, NLStradamus programme and Nucleolar localization sequence Detector (NoD) were applied in this study, respectively.

Moreover, this study determined the distribution of 3-clusters of amino acid residues surrounding the DNA damage-regulated phospho-SQ (S: Ser & Q: Gln), a consensus ATM and ATR phosphorylation motif on the HP1BP3, while this is consistent with the notion that E (Glu) or D (Asp) is often found around SQ or TQ sequence phosphorylated by ATM or ATR kinases *in vitro* (Kim et al., 1999).

We have therefore hypothesized that activation of ATM/ATR kinases in response to DNA damage caused by ultraviolet (UV) light, ionizing radiation and chemotherapeutic drugs could subsequently phosphorylate HP1BP3 protein. Phosphorylation of ATM-dependent HP1BP3 through binding to HP1α/tri-methylated H3 (H3K9me3) complex may regulate the nature of euchromatin-heterochromatin transition and result in cell cycle progression. Deregulation of these processes may cause malignant growth by disturbing DNA repair activities, and affecting transcription of DNA damage response genes. To this end our study together may lead to a conclusion that “HP1BP3 may protect cells from genome instability”.

1.7.2 Objectives & Aims

However, when I started my PhD, apart of the work in our laboratory, there was only a single published article regarding HP1BP3 protein and, in particular, there was no any experimental evidence presenting HP1BP3 as a potential ATM/ATR downstream substrate protein, their crosstalk and their potential role in CRC biology. Therefore, my project was focused on investigation the role of HP1BP3 in DNA damage response in fibroblasts and CRC cells.

Hence, my study was initially aimed on:

- Determination of HP1BP3 protein cellular distribution by generating mutated HP1BP3 proteins and testing their localisation by Immunofluorescent (IF) analyses in human fibroblast and CRC cell lines.
- Exploring the HP1BP3 protein behavior in response to DNA-damaging agents, including ultraviolet (UV) radiation, γ-Irradiation (IR) and chemotherapy drug (Oxaliplatin) in human fibroblast and CRC cell lines.
- Generating stably expressing HP1BP3 cell lines to investigate the molecular mechanisms underpinning HP1BP3 protein activity regulation signaling into biological response.
- Using site-directed mutagenesis to study the HP1BP3-phosphorylation by ATM/ATR kinases in cellular processes.
- Applying CRISPR/Cas9 System to generate HP1BP3-deficient cell lines with aim to elucidate the functional characterization of HP1BP3 *in vitro* and *in vivo.*

CHAPTER 2

General Materials and Methods

2.1 Materials

This section provides a brief introduction of all applied reagents and chemicals for biochemical, molecular and cellular purposes of the current research.

2.1.1 Cell lines

The following immortalized human cell lines were used: 1) HEK293T (Human Embryonic Kidney, clone 293) was originally purchased from ATTC, 2) Human colorectal cancer epithelial cell lines including the HCT116$^{FBXW7+/+}$ expressing both alleles of FBXW7 and HCT116$^{FBXW7-/-}$, lacking FBXW7, were a kind gift from Professors A. Balmain and B. Vogelstein (Rajagopalan et al., 2004, Babaei-Jadidi et al., 2011) and extensively used in Dr Nateri's laboratory, 3) the human embryonic skin fibroblasts (called TIGER cells) (Nateri et al., 2008) was a kind gift from Professor Gordon Peters: Molecular Oncology Lab, CRUK- London Research Institute and extensively used in Dr Nateri's laboratory including this project.

2.1.2 DNA Plasmids

All plasmids used in this study are listed in **(Table 2-1).** These plasmids were previously fully validated and used in Dr Nateri's laboratory. Chapters 3 and 4 contain the construction and identification of some recombinant plasmids generated in this study.

Table 2-1: List of DNA plasmids used throughout the thesis

Plasmid	Supplier	Cat. No.	Backbone vector	Bacterial selection
pEGFP-C2	Clontech	6083-1	NA	Kanamycin
pEGFP-C2-HP1BP3-Short	Dr.Nateri's lab	NA	pEGFP-C2	Kanamycin
pLVX-EGFP	Dr.Nateri's lab	NA	pLVX-Puro	Ampicillin
pSpCas9(BB)-2A-Puro	Addgene	48139	PX459	Ampicillin
V3LHS_339502	GE Healthcare	RHS4430-200278496	pGIPZ	Ampicillin

2.1.3 Antibodies

A list of primary and secondary antibodies applied for Western blotting and immunostaining is presented in **(Table 2-2)**.

Table 2-2: List of primary and secondary antibodies used for Western blotting and immunostaining analysis. The specificity of many of these antibodies was previously evaluated in our laboratory.

Antibody	Supplier	Cat. No	Host/Source	Dilution Factor	Purpose
Anti-GFP	In house CRUK	3E1	Mouse	1:1000	WB
Anti-ATM	Cell Signalling	sc-23291	Mouse	1:100 1:500	IF WB
Anti-pATM	Cell Signalling	sc-47739	Mouse	1:500	WB
Anti-Actin	Abcam	Ab6276	Mouse	1:10000	WB
Anti-HP1BP3	Sigma-Aldrich	HPA028215	Rabbit	1:200 1:1000	IF WB
Anti- phospho-Ser/Thr-Pro	Millipore	05-918	Mouse	1:1000	WB
Anti-p53	Leica	6015675	Mouse	1:100 1:500	IF WB
Anti-H2AX	Cell Signalling	5438	Rabbit	1:150 1:1000	IF WB
Alexa Fluor® 488 anti-rabbit	Invitrogen	A21206	Donkey	1:500	IF
Alexa Fluor® 594 anti-mouse	Invitrogen	A21206	Donkey	1:500	IF
Anti-mouse-HRP	Santa-Cruz	sc-2005	Goat	1:5000	WB
Anti-rabbit-HRP	Santa-Cruz	sc-2005	Goat	1:5000	WB

2.2 General Methods

2.2.1 Tissue culture techniques

A regular cell culture procedure for human HCT116, HEK293T and human fibroblasts (Tiger cells) as outlined above, were used for Western Blotting Assay (WB) and Immunostaining analysis (IF). Cell cultures were performed in a tissue culture room under aseptic conditions in a class II cabinet hood.

2.2.1.1 Recovering the cells

To recover the cells from a frozen stock, the cells were tasken from liquid nitrogen and defrosted in a water bath at 37°C with further placement in the volume of 10 ml pre-warmed complete medium RPMI-1640 (Sigma, R0883) that was supplemented with 10% Fetal bovine serum (FBS) (Sigma, F7524), 1% L-glutamine (2.0 mmol/L) (Invitrogen, 25030-081) and 1% penicillin/streptomycin (100 units/ml) (Invitrogen, 15140-122). Then the cells were pelleted in the bench-top Centrifuge 5702(Eppendorf) at 1500rpm for 5 min and the cell pellet was resuspended in 10 ml of fresh medium, plated in T75 flask (Costar) and incubated at 37^{o}C in a 5% CO_2 humidified incubator (Sanyo).

2.2.1.2 Culturing and splitting the cells

All cell lines (HCT116, HEK293 and Tiger cells) were grown in T75 flasks containing complete medium and maintained in a 37^{o}C incubator. Cell monolayer confluency and the medium colour were taken into consideration as indicators of cell growth. When the cell confluency was less than 60%, the old medium of the T75 flask was replaced by fresh complete growth medium to maintain further cell growth. However, in the case of high level of cell

confluency the T75 flask was sub-cultured. To detach cells, the old medium was aspirated from T75 flask and the surface of the flask was rinsed with 2 ml of sterile phosphate buffered saline (PBS) (Sigma, D8537). Then 1-2 ml of 1X Trypsin/EDTA

(Ethylenediaminetetraacetic acid) (Sigma, T3924) was added per T75 flask with further incubation period of 5-10 min at 37^{o}C in the CO_2 incubator. To prevent further trypsinization, 10 ml RPMI medium was added to the cells and cells were then pelleted by centrifugation for 5 min at 1500rpm. The cell pellet was resuspended in 10 ml of fresh medium and 3 ml of the resuspended cells were transferred into the T75 flask containing 10 ml of fresh complete growing medium. Depending on the cell type, confluency of the culture and forthcoming experiment, the trypsinized cells were diluted to a targeted concentration in complete RPMI medium and sub-cultured into sterile tissue culture plates.

2.2.1.3 Counting the cells

Neubauer haemocytometer (MARIENFELD, Germany) was applied to measure the cell number. Trypan blue (Sigma T8154) was used to stain non-viable cells. Following the thoroughly mixing by pipetting of trypsinized cells, 10 µl of cell suspension was transferred to a new Eppendorf tube containing 90 µl of fresh RPMI (dilution factor is 10). 10µl of the well-mixed stained solution was loaded onto a haemocytometer slide and the number of cells in each of the four large corner squares was counted under the microscope using the 10X objective lens as shown in **(Figure 2-1)**. Volume of fluid in a large square is 0.1 µl. The haemocytometer is designed so that the total cell concentration per 1 ml is equivalent to the average number of cells counted in four big squares multiplied

by10^4/ml. The dilution of the cells in the stain and the volume of the suspension also were taken into account.

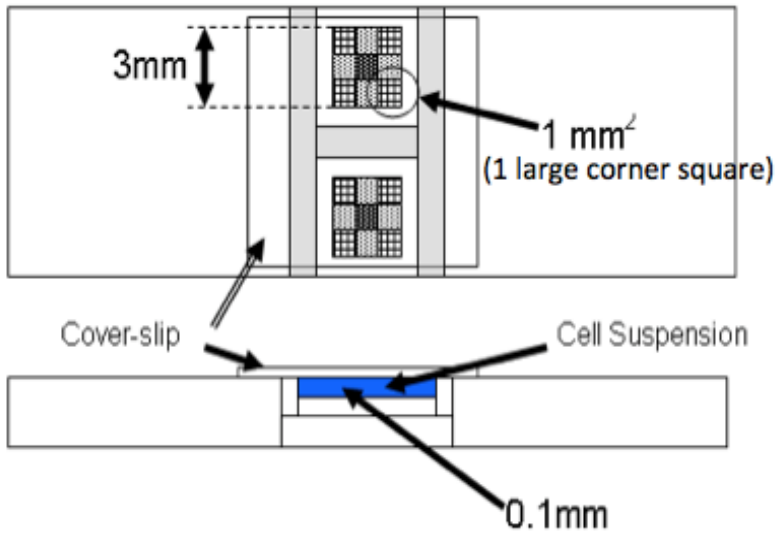


Figure 2-1: Top and side views of haemocytometer and its dimensions.
Adapted from Public Health England, 2013

2.2.1.4 Transient transfection

Transient transfection of mammalian cell lines by introducing the nucleic acids for a limited period of time provides short-term study of gene and gene products. In this study, delivery of DNA plasmids into the cells for transient expression was achieved by using Polyethylenimine (PEI) transfection reagent according to the manufacturer's instructions. Briefly, depending on the purpose of the experiment, the appropriate number of cells was seeded either in 6-well or 10 cm^2 plates and incubated overnight in a complete growth medium at 37^{o}C to

reach 60-70% confluency. Next day, 6 µg of plasmid DNA were diluted in 250 µl of Opti-MEM® I Reduced Serum Medium (Invitrogen, 31985-047) and at the same time in another set of eppendorf tubes was prepared the mixture of 6 µl of PEI and 250 µl of Opti-MEM® I. Further, the contents of the first set of eppendorf tubes were added to the second one, mixed gently together and incubated for 15 min at RT. Meanwhile, the complete growth medium of the cultured cells was aspirated and the cells were rinsed with Opti-MEM to remove any remaining medium. Then, the whole transfection mixture of each eppendorf tube was placed in the wells according to the labelling with plated cells and was kept at 37^0C incubator with incubation period of 6-7 h. After replacement of OPTI-MEM with fresh complete medium the 6-well plate was incubated for another 36-37 h and employed for downstream experiments.

2.2.1.5 Establishment of stable cell lines that constitutively express GFP-HP1BP3

Several stable cell lines were generated throughout this study. Permanent integration of HP1BP3 gene into cell genome was achieved by utilizing pLVX-HP1BP3-EGFP lentivirus particles expressing Puromycin resistant gene to produce HCT116$^{FBXW7+/+}$ cell line stably expressing HP1BP3. Lentiviral-based gene delivery system (Chaudhary et al., 2012, Lai et al., 2013, Büssow, 2015) by employing pLVX-EGFP-HP1BP3-Long plasmid was applied to produce stable expression of HP1BP3 in human fibroblasts (*Chapter 4, section 4.2.2*). Also, alongside with HP1BP3 overexpressed stable cell lines, stable long-term knockdown of the candidate protein in HCT116 CRC cell lines harbouring and lacking FBXW7 by applying shRNA based knockdown approach (C*hapter 5, section 5.2.6.1*) as well as HP1BP3 knockout in both HCT116 cell lines by using

CRISPR/Cas9 technology (Cong et al., 2013, Mali et al., 2013, Jinek et al., 2013, Cho et al., 2013, Garneau et al., 2010) (C*hapter 6, section 6.2.1*) was achieved.

As the detailed information for generation of each stable cell line is provided in appropriate chapters, therefore this section will be focused only on two main steps for Lentiviral-Based Gene Delivery system such as the Lentiviral production and the cell transduction as previously described (Chaudhary et al., 2012, Lai et al., 2013, Büssow, 2015) and detailed below.

2.2.1.5.1 Lentivirus production

Adherent HEK293-T cells were used for production of the lentiviral soap. To achieve that, HEK293-T cells were seeded in T75 flask in total 15ml lentivirus production media [DMEM high glucose (sigma# D5796), 1mM sodium pyruvate (Sigma# S8636), 1% v/v L-glutamine (Invitrogen# 25030-081), 1% v/v penicillin/streptomycin (100units/ml) (Invitrogen# 15140-122) and 10% v/v foetal bovine serum (FBS) (Sigma# F7524)], in triplicate, and grown until reached 80-90% confluency. Furthermore, the cells were co-transfected with a mixture composed of 9 µg of pLVX-Puro plasmid encoding the gene of interest and 6 µg pCMV delta R8.74 and 3 µg pMDG2 packaging plasmids was prepared in 250 µl Opti-MEM. Moreover, 43 µl of FuGENE was diluted in 650µl Opti-MEM. Following 5 mins incubation at RT, the DNA mixture and FuGENE were combined, mixed and incubated for 15 mins at RT, to form the DNA/FuGENE complex. On the day of transfection, the HEK293-T growth medium was replaced with 9 ml Opti-MEM. After the 15 mins incubation, the whole transfection mixture was transferred slowly to the cell surface and following a gentle agitation for 20 min at RT the cells were incubated overnight at 37°C.

Approximately 16 hours after lentivirus transfection, old Opti-MEM medium containing the transfection mixture was discarded and replaced by 11 ml complete culture medium. The supernatant collected from the second day after transfection for three respective days was considered as a viral soap. The transfected cells were re-fed with 11 ml fresh complete RPMI medium following each collection of culture medium containing viral particles (viral soap). The harvested viral soap was stored at 4°C until the last collection was made. The viral soap gathered from the three collections was centrifuged at 4000 rpm at 4°C for 10 mins and then filtered through 0.45 μm pore size filter to remove the contaminants from the soap. By using a pasture pipette, the purified viral soap was evenly distributed (9ml) into specific centrifuge tubes containing 1 ml of 20% Sucrose solution. Due to presence of 20% Sucrose solution, the content of each tube was divided into two layers: top (viral soap) and bottom (20% Sucrose solution). The lentiviral particles were precipitated by ultracentrifugation at 40000 rpm for 2 h at 4°C using BECKMAN L8-60M. Following aspiration of the supernatant, the viral pellet was resuspended with 30-40 μl of PBS and incubated overnight at 4°C. The viral particles were aliquoted into eppendorf tubes and stored at -80°C until the time of use.

2.2.1.5.2 Mammalian cell transduction

The produced lentiviral stock was used to promote stable gene deliver and permanent expression of the gene of interest through permanent integration of lentiviral vector into the genome of host cells. Thus, to generate stable cell lines, cells were subcultured in 24-well plate, in duplicates, and maintained in DMEM medium. After reaching 70-80% confluency, the cells were infected with 30-40 μl of the concentrated viral particles diluted in 400 μl complete DMEM medium

containing Hexadimethrine bromide (Sigma, H9268) at a final concentration of 8 µg/ml. Twenty microliters of the infection mixture was added directly into each well with constant rotation of the plate to distribute the mixture equally on the surface of the cells. Following 24 h post incubation period, the transfected cells were selected on the basis of acquired resistance to puromycin and sustained over two weeks in culture by maintaining the selective pressure. The infected cells were selected with 10-15 µg/ml Puromycin (Sigma, P8833). Furthermore, the puromycin selected cells were screened for GFP expression of the alternative protein. The GFP tag allowed for direct protein quantification by fluorescence microscopy during cell line development. Finally, the cells were expanded in puromycin-free medium and examined for the expression of the exogenously overexpressed gene through Western blotting analysis.

2.2.2 Gene cloning techniques

Following methods such as Polymerase Chain Reaction (PCR), enzymatic digestion and CRISPR/Cas9 technology were applied for genetic engineering and genome editing in the current research.

2.2.2.1 Standard Polymerase Chain Reaction (PCR)

Standard Polymerase Chain Reaction enables to produce millions of copies of a specific DNA sequence within 2 h. The reaction was performed using Veriti® Thermal Cycler machine (Applied Biosystems). Applied in this study primers are listed in the **(Table 2-3)**. In general, for a 100 µl reaction, 100-500 ng of DNA template was mixed with 1X reaction buffer (NEW ENGLAND Biolabs (NEB), #B0202S), 1 µl of each of the forward and reverse primers (final concentration 1 µM), 1 µl of 0.25mM dNTPs (Qiagen, 201913) and 1 µl Taq

polymerase enzyme (5U/µl) (Qiagen, 201205). Then the total volume was completed to 100 µl with Sigma water (W1754 Sigma). All processing steps of PCR, performed under established cycling conditions, are presented below in the **(Table 2-3)**.

Table 2-3: General cycling parameters and conditions used for standard PCR reaction

Cycle step	Temperature (°C)	Duration	No. of cycles
Initialization	94	3-5 min	1
Denaturation	94	40 sec	35-40
Annealing	55	45 sec	
Extension	72	60 sec	
Final elongation	72	10 min	1
Final hold	4	∞	-

2.2.2.2 Primer design

All oligonucleotides were designed, either manually or using the primer3 web based primer design tool (Version 0.4.0) available at http://frodo.wi.mit.edu/primer3/. Generally, primers were designed so that a pair of primers for a specific gene of interest was selected in two different exons and the size of the amplicon was limited to between 100-200 base pairs. All primers were supplied by Sigma and upon arrival they were spun down and resuspended in appropriate volume of Sigma distilled water to give a final concentration of 100 micromolars (µM) as a stock. Primers were diluted to their desired working concentrations in Sigma water and stored at -20°C until use.

2.2.2.3 Restriction enzyme digestion

Restriction endonucleases are bacterial proteins able to cleave DNA sequence at specific sites. The sequence-specific DNA cleavage activity of restriction enzymes is widely adopted in various areas of biological research. In this study, restriction endonucleases were used for gene manipulations.

All restriction enzymes were purchased from NEB, and were used according to the manufacturer's instructions with appropriate buffers at the required optimal temperature. In general, to digest DNA, the enzymatic mixture composed of the following components such as 0.5-5 µg of DNA, 10% of 10X NEB buffer and 0.5-2 µl of the restriction enzyme was prepared with total volume of 20 µl completed with Sigma water. Furthermore, the digested DNA samples were run in ethidium-bromide (EtBr)-staining gel to isolate the appropriate DNA bands for downstream experiments.

2.2.2.4 Agarose gel electrophoresis

This technique provides the visualisation of possible DNA bands and estimation of correct deletions by determination the expected size of digested DNA. For this purpose, 1% [w/v] agarose gel, which is commonly used for DNA gel electrophoresis in this study, was prepared of 1g agarose powder (Eurogenetic, EP-0010-05) and 100 ml of 1X Tris Actate EDTA (TAE) buffer Sigma (T9650). The mixture was heated up in a microwave for 1-2 min. For detection of DNA bands in the gel, approximately 10 µl EtBr (Sigma, E1385) (final concentration is 0.05 µg/µl), the intercalating agent, which binds to the DNA strands and emits fluorescence while exposed to UV light, was added to the cooled mixture (40-50^{0}C). The gel was transferred into the fixed gel casting tray with inserted

appropriate comb to build the wells for the samples. DNA samples containing 1-2 µl of 10X gel loading buffer (final concentration is 1X) (30% glycerol and 0.25% bromophenol blue in dH_2O) were loaded into appropriate wells of the gel. Bio-Rad power supply was used for realisation of the gel electrophoresis, and the program of the power source was set to 90-120 Volts for 50 min applying 1X TAE buffer as a Running Buffer. When the process was completed, the gel slide was viewed in the Ultraviolet Transilluminator Unit (UVidoc).

2.2.2.5 DNA extraction from agarose gel and soluble reactions

Detected by UV light DNA bands of interest were excised out of the agarose gel and placed in the set of micro centrifuge tubes according to the labelling. The purification process of the samples from TAE agarose gel was performed by using the QIAGEN Gel extraction kit. Below in the **(Table 2-4)** is the brief representation of the main steps of the applied extraction protocol. In addition, the same protocol was used for the purification of PCR products from PCR reactions with only difference in volume of capture buffer (500 µl). To isolate the DNA samples from agarose gel slide, 10 µl of Capture Buffer was added to each 10 µg of agarose gel that was heated up until complete dissolving. Further, the capture-buffer-sample mixture was placed in the Microspin column inserted into the Collection tube with incubation period of 1 min at RT. To obtain the pellet, the mixture was centrifuged at 14000rpm for 30 sec and afterwards was rinsed with 500 µl of Washing Buffer. To dry the pellet, it was centrifuged again at 14000rpm for 30 sec and incubated for 1 min at RT. To cleanse the left-over proteins and to lubricate the DNA sample 30-50 µl of Elution Buffer was added into the column and incubated for 1 min at RT. The concentration and purity of extracted DNA was measured by Nanodrop (*section 2.2.3.5*).

Table 2-4: Brief outline of the processing steps of the extraction protocol

Steps of the DNA Extraction Process	Description
1.Sample capture	• Calculate weight of DNA containing agarose gel slice • Add 10 µl of Capture buffer for each 10 µg of agarose gel • Heat the gel until it completely dissolved
2.Sample binding	• Transfer 600 µl of capture buffer-sample mixture into Microspin column inserted in the Collection tube • Incubate for 1 min at RT • Centrifuge at 14000 rpm for 30 sec
3.Wash and dry	• Wash the pellet with Washing buffer • Centrifuge at 14000 rpm for 30 sec • Incubate for 1 min at RT
4. Elution	• Add 30-50 µl of Elution buffer to the column • Incubate for 1 min at RT

2.2.2.6 DNA ligation

Freshly isolated from agarose gel DNA samples presented by linearized vector and insert of new recombinant DNA construct were ligated with T4-DNA ligase enzyme (NEB, M0202S) by an overnight incubation. The cohesive ends ligation was the commonly used ligation strategy throughout this study. To perform ligation reaction one volume of pre-digested plasmid backbone vector was added to seven volumes of the inserted DNA and mixed with 1X T4 DNA ligase buffer (NEB, # B0202S) and 2µl T4 DNA ligase enzyme (NEB, # M0202S). Nuclease-free water was added to the reaction mixture to reach the final volume of 20 µl

and was left at 4°C with overnight incubation period. Further, the ligated DNA was transformed into bacteria to amplify the new recombinant plasmid DNAs for the digestion and sequencing verification and eventually supplying in downstream experiments.

2.2.3 DNA preparation and manipulation

2.2.3.1 Bacterial transformation

The manipulations described above in the (*section 2.2.2*) allow creating novel recombinant DNA molecules. The next step in a gene cloning experiment is to introduce these molecules into living bacterial cells to produce numerous identical copies of not only DNA plasmid but also of the gene of interest which DNA carries. In this study, chemically prepared DH5α competent cells (*section 2.2.3.2*) underwent transformation by newly constructed DNA plasmid variants. Approximately 100-500 ng of DNA plasmid of each sample separately was mixed with 50 µl of competent cells, and incubated on ice for 30 min. In order to enhance the abilities of bacterial cells to uptake DNA plasmids efficiently, *E. coli* DH5α cells underwent to a set of chemical treatment methods, and as result acquired competent properties. The mixture was subjected to heat shock at 42^0C for 45 sec, and re-incubated on ice for another 5 min. Then, 500 µl of Luria Broth (LB) medium **(Table 2-5)** was added to the mixture and incubated at 37^0C for 1 h with shaking at 230 rpm. Following this step, 10-15 µl of the mixture was plated on a LB agar plate containing antibiotic Kanamycin (30µg/ml), and incubated overnight at 37^0C bacterial incubator. Next morning, raised single colonies were picked, cultured in 5 ml of LB medium containing Kanamycin and

re-incubated overnight at shaking incubator. Initially, the DNA was extracted by Miniprep kit (*section 2.2.3.3*). Following validation by enzymatic digestion and further DNA nucleotide sequencing analysis (using the sequencing facility at the School of Biomedical Sciences, UoN), the right DNA plasmids were isolated by Midiprep kit (*section 2.2.3.4*).

For preparation of agar plates, 1g of bacteriological agar (Sigma, #A5306) was added to 100 ml of LB medium and microwaved until it was completely dissolved. Further, Kanamycin was resuspended in homogenised agar when its temperature decreased to 50-60^{0}C. Then, this mixture was poured into 10 cm^2 petri-dishes (15 ml each) and left to solidify at RT. After solidification, agar plates immediately were used for bacterial culture or stored for 2-3 weeks at 4^{0}C until the time of use. The culture medium provided essential nutrients at the necessary concentrations to allow the bacteria to grow and divide efficiently.

Table 2-5: Composition of common solutions and buffers applied in this study

Material	Composition	Experiment	Stock con.	Working con.	Storage temp.
LB Medium	10 g Trypton, 5 g yeast extract and 10 g NaCl dissolved in 1 L distilled water (dH2O) and autoclave before usage	Bacterial transformation	1X	1X	4°C
RF1 buffer	12 g Rubidium-chloride, 9 g Manganese-chloride x 2H2O, 2.94 g Potassium acetate, 1.5 g Calcium-chloride x 2H2O, 150 g Glycerol in 900 ml dH2O, adjust pH to 5.8, then complete to 1 L with dH2O	Competent cell preparation	1X	1X	4°C
RF2 buffer	2.09 g MOPS, 1.2 g Rubidium-chloride, 11 g Calcium-chloride x 2H2O, 150 g Glycerol in 900 ml dH2O, adjust pH to 6.8, in 1 L dH2O		1X	1X	4°C
RIPA buffer	150 mM NaCl, 25 mM Tris-HCl, 1% Triton X-100, 1% Sodium deoxycholate, 1% NP-40 , 0.1% SDS in dH2O	Protein extraction	1X	1X	4°C
5X loading buffer	0.2 M Tris-HCl pH 6.8, 10% w/v sodium dodecyl sulfate, 20% glycerol 0.05% bromophenol blue, 10 mM beta-mercaptoethanol, in dH2O	Western blotting	5X	1X	-20°C
Semi-dry Transfer buffer	30.3 g Tris HCL, 14.4 g glysine, 200 ml methanol in 1 L dH2O		1X	1X	RT
TBS buffer	20 mM Tris, 13.7 mM NaCl in dH2O, pH was adjusted to 7.6		10X	1X	RT

2.2.3.2 Chemical preparation of bacterial competent cells

To prepare the chemical competent cells, 5 µl of DH1α bacterial cells was primarily cultured in 5 ml LB medium with further overnight at 37°C in a shaking incubator. Following day, 2 ml of this pre-culture was transferred to 500 ml of antibiotic-free LB medium and placed at 37°C with shacking at 230 rpm for 2-3 h. The optical density (OD) of the culture was monitored regularly by spectrophotometer (Scientific Laboratory Supplies) until the OD reading reached 0.5-0.6. Once the OD reading reached 0.5-0.6, the culture was divided into 2 sterile centrifuge bottles and incubated on ice for 30 mins with further centrifugation at 2500 rpm for 12 mins. After discarding the supernatant, the pellet of each bottle was resuspended in 20 ml RF1 buffer **(Table 2-5)**, incubated on ice for 15 mins and followed by centrifugation for 9 mins at 2500 rpm. Finally, each bacterial cell pellet was resuspended in 7 ml of RF2 buffer **(Table 2-5)**, then immediately aliquoted into sterile eppendorf tubes and stored at -80°C.

2.2.3.3 DNA isolation by Miniprep

In order to prepare cell extract, the bacteria was harvested by spinning 5 ml of culture in the bench-top Centrifuge 5424 at 3800rpm for 10 min. For extraction of DNA plasmids from bacterial transformed cells GenEluteTM plasmid miniprep kit (Sigma, #PLN350-1KT) was used according to the manufacturer's instructions. In brief, bacterial membrane was disrupted by chemical methods to release the cell components. For this purpose, the bacterial pellet was resuspended in 100 µl of chilled resuspension solution supplemented with RNase enzyme. Further, the tubes were vortexed until the cell suspension became

homogenized. The resuspended pellets were lysed with 200 µl of alkaline lysis solution and the tubes were mixed gently by inverting 5-6 times and then set for ≤ 5 min on ice to clear. Durable alkaline lysis lasting more than 5 min is undesirable as could lead to a permanent denaturation of the plasmid which may affect the subsequent applications. To prevent further lysis, the alkaline pH of the solution was neutralised by adding 150 µl of chilled neutralization buffer and the tubes were inverted 5-6 times to mix with further incubation period for 3-5 min on ice. The next step compromises the purification of DNA from cell debris. In addition to DNA, a bacterial cell extract encompasses other components, such as protein and RNA, moreover in significant quantities. To remove these contaminants, cell debris was precipitated by centrifuging the tubes at 13000rpm for 10 min. To precipitate nucleic acids 2 volumes of ethanol was added to the aqueous solution and mixed by vortex with further incubation period of 2 min. Then the mixture was centrifuged to 13000rpm for 1 min. After removal of supernatant, pellets were left to dry at room temperature (RT) for 10-15 min. A further 70% ethanol was added to pellet and the closed tube was inverted several times. Following centrifugation at 13000rpm for 1 min and discarding the supernatant, pellets were dried at RT for 10-15 min and eluted in a new collection tube with 100 µl DNase/RNase free H_2O and stored at -20°C.

Below **(Figure 2-2)** is the schematic illustration of applied MiniPrep steps:

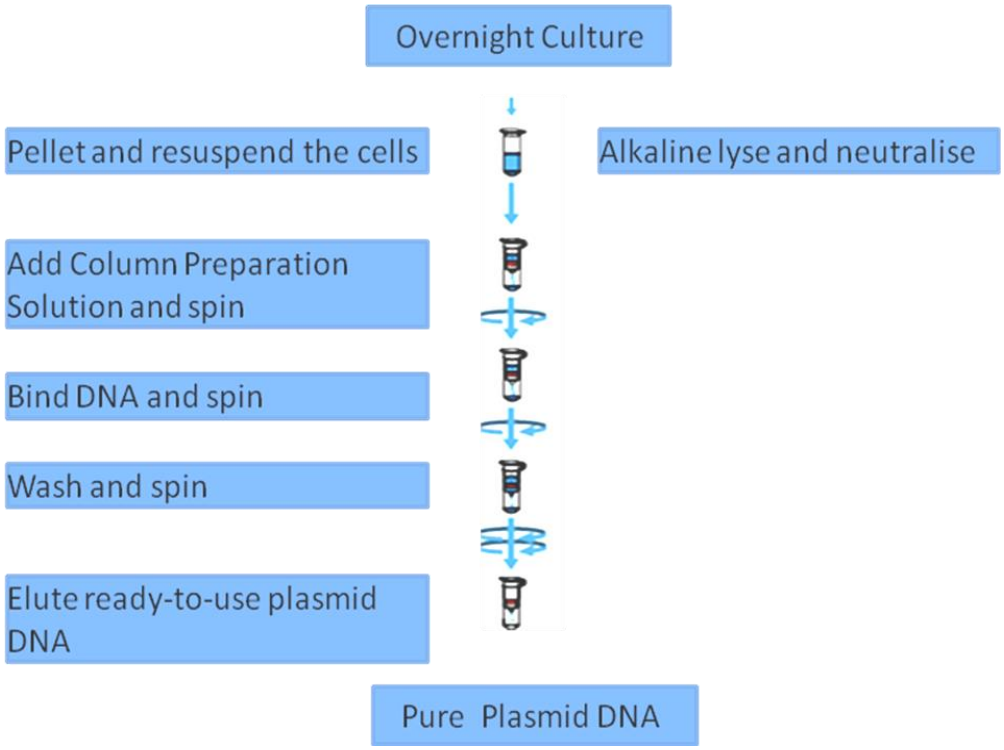


Figure 2-2: The proceeding steps of MiniPrep Protocol. All procedures were performed at RT.

2.2.3.4 DNA isolation by Midiprep

Digestion analysis of extracted DNA confirms that yielded DNA presents the correct DNA plasmid with expected gene modifications. Therefore, enzymatic digestion of DNA plasmids estimates the fidelity of selected bacterial colonies. After digestive validation, the tube with bacterial culture containing the correct DNA plasmid confirmed by agarose gel electrophoresis was used for Midiprep to yield a large quantities of DNA plasmids.

Thus, the rest of competent cells comprising the digestively confirmed DNA plasmid (approximately 1.5 ml) were pre-cultured in 5 ml of antibiotic-containing LB medium for 2-3 h at 37^0C. The pre-culture was transferred to a

big volume of LB medium with appropriate antibiotic (30ml of LB + 30µl of kanamycin) and incubated overnight at 37^0C in a shaking incubator. Next morning, Genopure Plasmid Midi Kit (Roche, 03143414001) was used to extract large amounts of DNA (100-200 µg) following the manufacturer's recommendations. All applied steps to harvest DNA plasmid are shown in **(Figure 2-3)**. The Beckman Floor Model J-2-21 Centrifuge was used in this experiment.

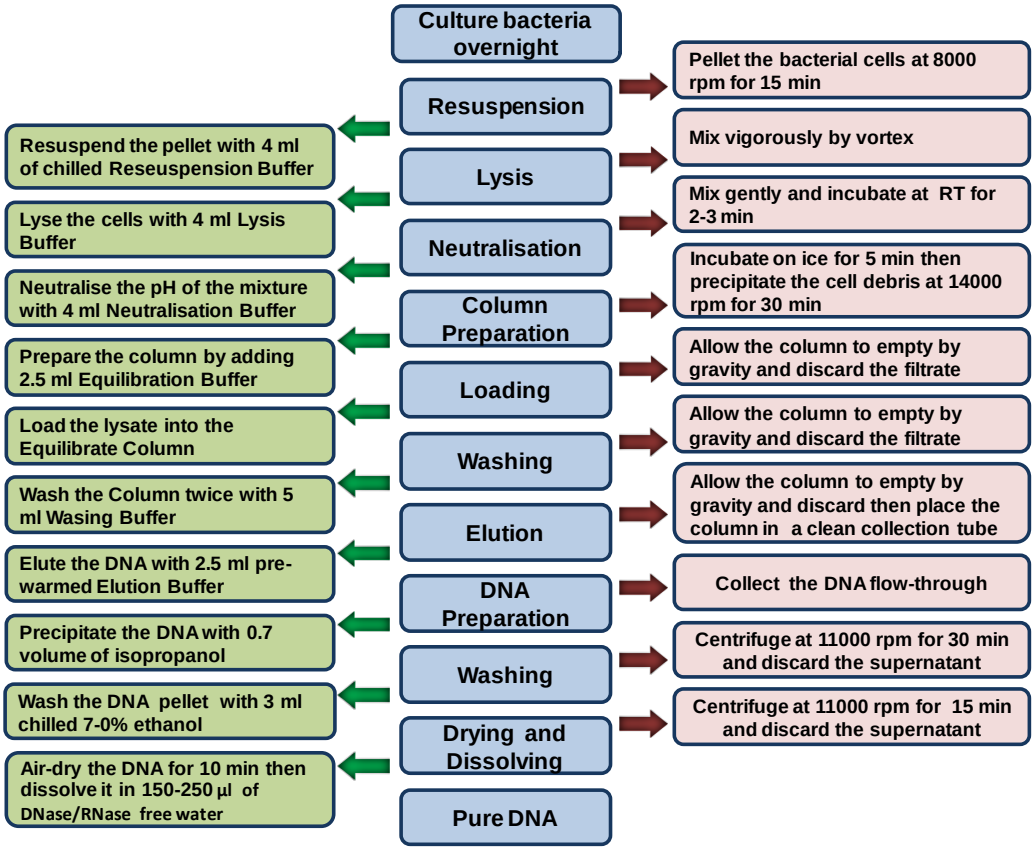


Figure 2-3: Extraction of high copy number of recombinant DNA, carrying the gene of interest from bacterial culture using Midiprep Kit. The process of centrifugation in all steps was maintained at 4^0C.

2.2.3.5 DNA quantification

A Nanodrop ND-1000 UV-Vis spectrophotometer (LabTech International Ltd, Ringmer, UK) was employed to measure the concentration and assess the purity of isolated DNA. Examination of sample spectra is the best indicator of functionality of extracted DNA in further applications. Generally, the absorbance of the extracted nucleic acid and its contaminants ranges between 230 nm and 320 nm. Therefore, the Nanodrop measures the absorbance at 230 nm, 260 nm and 280 nm. DNA has a peak absorbance at 260 nm (A260) and each one A260 unit equals to 50 μg DNA /ml H2O. The ratio A260/A280 was measured to assess the purity of the nucleic acid and ratio of > 1.8 is considered as indication of pure DNA. A lower A260/A280 ratio may depict on the presence of protein or other aromatic contaminants such as phenol. Similarly, the detection of the A260/A230 ratio is another recommended assessment for quality control check of nucleic acid. Usually it is higher than the A260/A280 value (ranges from 1.8-2.2). A lower A260/A230 ratio may indicate the presence of co-purified impurities.

To initiate the measurement of nucleic acid, initially Nanodrop blanked with 1-2 μl of the elution buffer used during the DNA preparation. Furthermore, 1.5-2 μl of the DNA was pipetted onto the pedestal of Nanodrop to calculate the concentration and evaluate the purity of nucleic acid.

2.2.4 Protein extraction and analysis

2.2.4.1 Protein extraction and quantification

RIPA (Radio immunoprecipitation assay) buffer **(Table 2-5)** supplemented with 1X protease inhibitor cocktail (Sigma, P8340) was used to lyse the cells and extract the whole cell protein. Initially, the surface of the cells was rinsed with PBS before adding 250-300 µl of RIPA buffer and afterwards a plate was maintained in constant agitation for 20 min at 4^0C. Further the lysate was collected into fresh and sterile eppendorf tubes and centrifuged using a bench-top centrifuge with maximum speed 13000rpm for 10 min at 4°C. The supernatant (protein extract) was aspirated and placed in the set of new tubes kept on ice.

Total protein concentration was measured using a Bradford Assay Kit for Protein Quantification (Sigma #B-6916) followed manufacturer's instructions. In a new set of eppendorf tubes all available samples were diluted in dH_2O (dilution factor is 1:10). 20 µl of each diluted sample were placed separately into a triplet of wells of 96-well microplate (Scientific Laboratory Supplies). A series of protein standards was prepared using bovine serum albumin (BSA) (Sigma, 4503) diluted with dH_2O according to the targeted concentrations of 0 (used as a blank), 100, 300, 500, 800 and 1000 µg/ml. 20 µl of each BSA standard solution was also distributed per a well of the microplate. Afterwards, 200 µl of the diluted Bradford solution (dilution factor is 1:5) was added per each single well both with samples and protein standards. Following up and down mixing of the

samples by pipetting, the microplate was incubated for 5 min at RT before measuring the protein concentration.

The spectrophotometer was adjusted to the microplate reader (Bio-Rad) to measure the absorbance of the standard solutions and the unknown samples at wavelength of 595 nm. The average concentration of protein extract per each sample was automatically calculated by the machine's software (Microplate Manager, version 5.2.1 Build 106) and all isolated proteins were stored at -80 prior to use.

2.2.4.2 SDS-PAGE electrophoresis and Western blotting analysis

SDS - polyacrylamide gel (SDS-PAGE) comprises upper resolving gel and lower stacking gel. The reagents required for composition of the gels are listed in the **(Tables 2-6 & 2-7)**. According to the available guidelines presented in the **(Table 2-6)**, appropriate resolving gel depending on the molecular weight of a loaded protein was prepared. SDS-PAGE was cast in between two pieces of 20 x 20 cm glass plates placed in a gel-casting frame and was incubated for 20-30 min to solidify. Meanwhile 50-100µg of total protein extracted from the samples was mixed with 5X loading buffer containing sodium dodecyl sulphate (SDS) and denatured at 95°C for 4 min. Eppendorf tubes containing denatured proteins were incubated on ice for 5 min to cool down and further were loaded into the SDS-PAGE wells created by teeth of Teflon comb. For detection the molecular weight of protein bands 5-8 µl of ColorPlus Pre-stained Protein Ladder, Broad Range (NEB #P7711S) was also applied. The electrophoresis was carried out at power source set to 140 volts for 2 h in 1X Tris/glycine/SDS (TGS) running buffer (Bio-Rad, 161-0772) to allow proteins to move through SDS-PAGE gels.

Based on the molecular size of the protein of interest, less concentrated SDS-PAGE (e.g. 6%) and wet transfer with overnight running time (up to 12-14 hours) with lower voltage (up to 15) at 4^0C (cold room) was also used in some occasions. After completing the SDS-PAGE, the gel was carefully stripped of the glass plates and placed in a Semi-Dry Electrophoretic Transfer Cell (Bio-Rad) at 15 volt for 75 min where the electrophoretically separated proteins were transferred to a Polyvinylidene Difluoride (PVDF) membrane (GE Healthcare, RPN303F) using a semi-dry transfer buffer. Then the membrane was removed and blocked with 3% dried milk (GE Healthcare, CPK1075) dissolved in Tris-Buffered Saline (TBS) containing 0.1% Tween-20 (Sigma, 1379) (TBS-T) for 1 hour at RT by following incubation with the primary antibody at the recommended concentration overnight at 4°C. Next day the membrane was washed with 5 ml of TBS-T buffer three times, 7 min each, and incubated with the secondary antibody for 1 hour at RT. β-actin was used as a loading control in all performed experiments.

Table 2-6: Solutions for preparing 6-10% resolving gels for SDS-PAGE

Solution components	Component volumes per gel mold volume of				Cat. No
	10ml	15ml	20ml	25ml	
6%					
Distilled H2O	5.3	7.9	10.6	13.2	-
30% acrylamide mix	2.0	3.0	4.0	5.0	A3699
1.5 M Tris, pH 8.8	2.5	3.8	5.0	6.3	T9650
10% SDS	0.1	0.15	0.2	0.25	L3771

10% Ammonium persulfate	0.1	0.15	0.2	0.25	A9164
TEMED	0.008	0.012	0.016	0.02	T7024
10%					
Distilled H2O	4	5.9	7.9	9.9	-
30% acrylamide mix	3.3	5.0	6.7	8.3	A3699
1.5 M Tris, pH 8.8	2.5	3.8	5.0	6.3	T9650
10% SDS	0.1	0.15	0.2	0.25	L3771
10% Ammonium persulfate	0.1	0.15	0.2	0.25	A9164
TEMED	0.004	0.006	0.008	0.01	T7024

Table 2-7: Solution for preparing 5% Stacking Gels for Tris-glycine SDS-PAGE

Solution components	**Component volumes per gel mold volume of**			
	4ml	**5ml**	**6ml**	**8ml**
Distilled H2O	2.7	3.4	4.1	5.5
30% acrylamide mix	0.67	0.83	1.0	1.3
1.0 M Tris, pH 6.8	0.5	0.63	0.75	1.0
10% SDS	0.04	0.05	0.06	0.08
10% Ammonium persulfate	0.04	0.05	0.06	0.08
TEMED	0.004	0.005	0.006	0.008

2.2.4.3 Immunoprecipitation analysis

Immunoprecipitation (IP) is the method designed to purify proteins on the basis of their binding affinity to specific antibody. IP is widely adopted technique in

many proteomics workflows. In the current study, it was employed to detect the possible interacting protein partners. Pure proteome protein A and protein G Magnetic beads (Merck Millipore) were used to pull down the endogenous proteins as described below. Briefly, bead suspension was mixed gently, and then 50 µl of the homogenized beads were transferred to 1.5ml microcentrifuge tube and placed on the Dynal MPC magnetic stand (Life Technologies) to allow the beads to migrate to the magnet. After aspirating the storage buffer, the beads were washed in 500 µl PBS/Tween-20. The buffer was removed with pipette and washed beads were resuspended 100 µl PBS/Tween-20 containing required concentration of a primary antibody of interest. Tubes were incubated with continuous rotation for 30 minutes at room temperature to couple an antibody with magnetic microspheres anti-mouse IgG and IgA.

Furthermore, supernatant was removed from the tube while beads-Ab complex was fixed by magnetic force. The beads-Ab complex was washed twice in 500 µl PBS/Tween-20 solution by gentle pipetting. The magnet stand allowed separating the supernatant from the beads between each wash. 400 µg of protein lysate was added into the beads-Ab complex and incubated at 4°C for overnight under gentle agitation of these beads. Purified antigen(s) obtained by IP was examined by Western blotting analysis.

2.2.5 Immunofluorescence (IF)

In this study IF was applied to detect and visualise the localisation and relative expression levels of overexpressed recombinant proteins HP1BP3 within the cell compartments and to observe the co-localisation of exogenous HP1BP3 mutant

clones with endogenous HP1BP3. The main principle of the technique is to visualise the antigen-antibody complex where antibodies are tagged with fluorescent dye which is detected by ultra-violet microscope. According to the IF protocol, a primary antibody specific to the protein of interest was applied and followed by immunostaining with a fluorescent dye-labelled secondary antibody directed towards the immunoglobulins of the host species in which primary antibody was initially raised. IF staining protocol comprises several steps which are presented below.

2.2.5.1 Cell preparation

The T75 cm flask containing HCT116 cells was trypsinized and after counting the required number of cells (≈ 500.000/well) was cultured on coverslips with further overnight incubation period at 37^0C incubator. Beforehand the coverslips were sterilized from both sides with 70% ethanol followed by washing twice with PBS and incubated with 1 ml of 10% Poly-L-lysine (Sigma, P8920) for 1h at RT. Afterwards, the Poly-L-lysine was discarded and the coverslips were rinsed with PBS again and subsequently with complete growth medium before seeding the cells in the 6-well plate. This step was followed by performing of transient transfection of the cells when required.

2.2.5.2 Fixation and permeabilization

The growth medium was discarded, the cells were rinsed twice in PBS and fixed with cross-linking agent 4% paraformaldehyde (PFA) (Avocado, 043368) (diluted from a 16% stock solution with PBS) for 30 min at RT to prevent further degradation of the cells and make proteins intact. The PFA was removed by washing the cells twice with PBS for 5 min each. Next, the cells were incubated

in permeabilization solution (0.1% Triton X-100 diluted in PBS) for 30 min to provide the access to intracellular and intraorganellar antigens with following washing step with PBS repeated twice for 5 min each.

2.2.5.3 Blocking and immunostaining

To prevent non-specific interactions of the antibody and to lessen the background affinity, the permeabilized cells were blocked with 3-8% serum blocking buffer for 1 h. Then cells were washed once with PBS for 5 min and incubated with the primary antibody at the recommended dilution (in 2% serum) overnight at 4ºC. The negative control (with no primary antibody added) was incubated with 2% serum. Next day, the cells were washed four times with washing buffer (1% serum and 0.1% Tween-20 in PBS) for 10 min each and incubated with the secondary antibody (diluted in 2% serum) for 1 hour at RT. The incubation with the secondary antibody and following procedures were performed in the dark place as the secondary antibodies are light sensitive, and immediately after completing every step 6-well plate was wrapped by aluminium foil. The stained cells were then washed five times with the washing buffer for 10 min each. Afterwards, the coverslips were removed gently from the 6-well plate by forceps and placed on a clean slide in an upside down position containing small amount (~25 µl) of ProLong® Gold antifade reagent with DAPI (Invitrogen, P-36931), sealed with nail varnish and incubated at RT overnight. The proteins of interest were visualized by using Leica DMI3000 B inverted microscope (Leica Microsystems). The images were captured at the required magnifications.

CHAPTER 3

Identification & Characterization of Functional Regions for Nuclear Localization of HP1BP3 protein

3.1 BRIEF INTRODUCTION

The inner architecture of eukaryotic cells is organised into distinct membrane-isolated compartments in order to maintain the balance of transport mechanisms between the nucleus and cytoplasm. Nucleocytoplasmic translocation is an orderly arranged process in the cell presented by recognition of nuclear targeting signal within cargo proteins by transporter receptors with further transportation of the protein substrates into the nucleus via regulated pores of the nuclear envelope (McLane and Corbett, 2009, Stewart, 2007). The presence of nuclear localization signal (NLS) sequence serves as a docking site for transport receptors and other regulatory proteins. Protein translocation is an essential element in normal cell function that enables proteins to exert their specific functions at the required destinations within the cell environment (Chacinska et al., 2009, Hung and Link, 2011). The impediment of the protein transportation might lead to deleterious consequences to the cell and might be involved in the pathogenesis of a range human diseases as well as in tumourigenesis (Laurila and Vihinen, 2009, McLane and Corbett, 2009).

Defining the subcellular localization of a protein is a significant initial step toward understanding its function (Hung and Link, 2011). Here, we described the HP1BP3 molecule as a not fully characterized nuclear protein. More recently published studies demonstrated HP1-dependent enrichment of HP1BP3 in heterochromatin and revealed a novel regulatory role of this molecule in the maintenance of chromatin integrity (Hayashihara et al., 2010, Garfinkel et al., 2015). However, there was no experimental evidence on how the nuclear

localization of HP1BP3 is regulated. Our initial sequence analysis revealed two putative classical nuclear localization signals (NLS) (Kalderon et al., 1984, Robbins et al., 1991, Dingwall and Laskey, 1991, Lange et al., 2007, Chelsky et al., 1989) "***KKVKK"*** and "***KKTR***", located at the positions 127-131 and 507-510, respectively in the N-terminus and C-terminus of human HP1BP3. Furthermore, by applying the NLStradamus programme (http://www.moseslab.csb.utoronto.ca/NLStradamus/), a Markov model for NLS prediction (Ba et al., 2009), we showed an additional NLS spanning amino acids ***RKTPQKSRNRKN*** in the middle region (235-246) of HP1BP3 **(Figure 3-1, A & B)**.

Thus, in order to identify the functional NLSs in HP1BP3, we constructed several of EGFP fused HP1BP3 mutants with deletions in regions of putative NLSs. The protein expression and the subcellular localization of HP1BP3 recombinant constructs were validated through both Western blotting (WB) and fluorescent microscopy assays while overexpressed in three human cell lines such as the human embryonic kidney cells (HEK-293T), human skin fibroblasts and human colorectal cell line (HCT116). These analyses showed that the expression of an EGFP-tagged N-terminal deletion construct is exclusively cytoplasmic, whereas the remaining recombinant constructs encompassing either middle region or C-terminus domain are enriched in the nucleolus. The data revealed that all available NLSs are functional for the nuclear localization of wildtype HP1BP3. Therefore, HP1BP3 contains multiple conserved NLSs, which show both middle and C-terminus NLSs function to mediate nuclear import.

A

MATDTSQGELVHPKALPLIVGAQLIHADKLGEKVEDSTMPIRRTVNSTRETPPKSKLAEGEEEKPEPDISSEE
SVSTVEEQENETPPATSSEAEQPKGEPENEEKEENKSSEETKKDEKDQSKEKEKKVKKTIPSWATLSASQL
ARAQKQTPMASSPRPKMDAILTEAIKACFQKSGASVVAIRKYIIHKYPSLELERRGYLLKQALKRELNRGVIKQ
VKGKGASGSFVVVQKSRKTPQKSRNRKNRSSAVDPEPQVKLEDVLPLAFTRLCEPKEASYSLIRKYVSQYY
PKLRVDIRPQLLKNALQRAVERGQLEQITGKGASGTFQLKKSGEKPLLGGSLMEYAILSAIAAMNEPKTCSTT
ALKKYVLENHPGTNSNYQMHLLKKTLQKCEKNGWMEQISGKGFSGTFQLCFPYYPSPGVLFPKKEPDDSR
DEDEDEDESSEEDSEDEEPPPKRRLQKKTPAKSPGKAASVKQRGSKPAPKVSAAQRGKARPLPKKAPPKA
KTPAKKKTRPSSTVIKKPSGGSSKKPATSARKEVKLPGKGKSTMKKSFRVKK

B

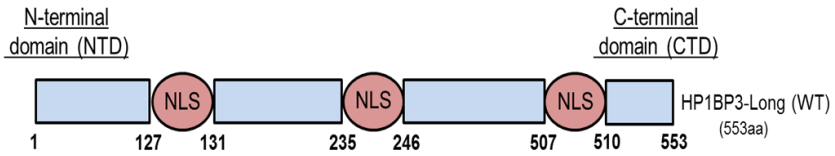


Figure 3-1: Schematic representation of human HP1BP3 domains and defined NLS sequences. **(A)** Shows the amino acid sequence of full-length human HP1BP3. The predicted NLS motifs are highlighted in red and boxed. **(B)** A diagram shows the presence of three NLS motifs distributed within the HP1BP3 structure with amino acid start and stop numbers.

3.2 RESULTS

3.2.1 Cloning of EGFP-fused HP1BP3 and its mutant constructs

3.2.1.1 Cloning of D1, D2 and D4 mutants using HP1BP3 short isoform cDNA construct

To map NLS motifs of HP1BP3 protein, pEGFP-C2-HP1BP3 short isoform (*HP1BP3-Short*), previously constructed in our lab (Abuzinadah et al., unpublished) **(Figure 3-2)** and representing a truncated mutant of long isoform HP1BP3, was initially employed to generate four deletion mutant clones of *HP1BP3* cDNA as outlined below.

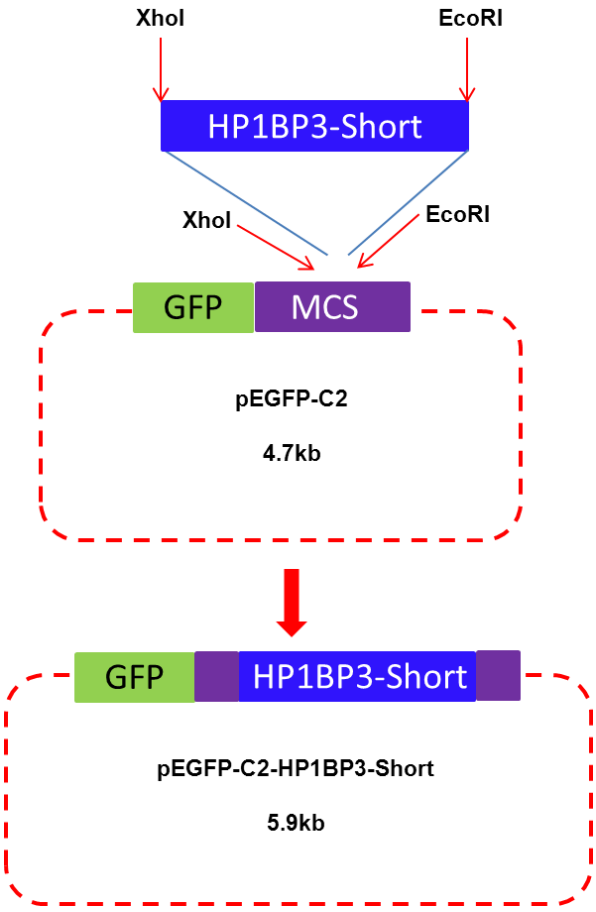


Figure 3-2: Schematic representation of *HP1BP3-Short* construction. The amplified PCR product (*HP1BP3-Short*) and the plasmid backbone vector (pEGFP-C2) were linearized using *XhoI* and *EcoRI* restriction enzymes to create cohesive compatible ends to construct pEGFP-C2-HP1BP3-Short isoform that was used for downstream cloning manipulations.

As a result of enzymatic digestion, using *Hind III*, *Pst I* and *Bgl II* restrictions enzymes, *HP1BP3-Short* cDNA gave rise to the following recombinant plasmids: pEGFP-C2-HP1BP3-D1 (*HP1BP3-D1*), pEGFP-C2-HP1BP3-D2 (*HP1BP3-D2*), and pEGFP-C2-HP1BP3-D4 (*HP1BP3-D4*), respectively. Cutting site(s), number and size of released DNA fragments resulted from each restriction enzyme digestion are listed in the **(Table 3-1)**.

Table 3-1: List of the restriction enzymes used for digestion and cloning of *HP1BP3* recombinant constructs. The cut position (s), number and size of DNA fragments resulted from each restriction enzyme digestion are indicated.

Original cDNA	Enzyme	Cut Position(s)	Produced Fragments	Size(bp)	Recombinant cDNA
HP1BP3-Short	*Hind III*	368 & 415 within *HP1BP3* coding region	2	47 + 5,894	*HP1BP3-D1*
HP1BP3-Short	*Pst I*	294, 461 & 710 within *HP1BP3* coding region and 1370 within multiple cloning site	4	167 + 250 + 520 + 5647	*HP1BP3-D2*
HP1BP3-Short	*Bgl II*	740 within *HP1BP3* coding region and 1345 within multiple cloning site	2	740 + 5201	*HP1BP3-D4*

In brief, the digested DNAs were run on a 1% agarose gel **(Figure 3-3)**, and then the required larger bands on top of the gel were excised from the gel, purified and ligated by T4-DNA ligase enzyme as described in (*Chapter 2, section 2.2.2.6*). The ligated products were then transformed into bacterial competent cells XL1Blue and plated on Kanamycin-LB agar plates (*Chapter 2, section 2.2.3.1*). Kanamycin selection marker was determined by a backbone mammalian expression vector pEGFP-C2 that contains kanamycin resistance gene. A successful clone was initially confirmed by restriction enzyme digestion analysis using the same enzymes that were used for cloning. The wild type clone (*HP1BP3-Short*) was used as a control to compare the size of DNA fragments of mutant clones.

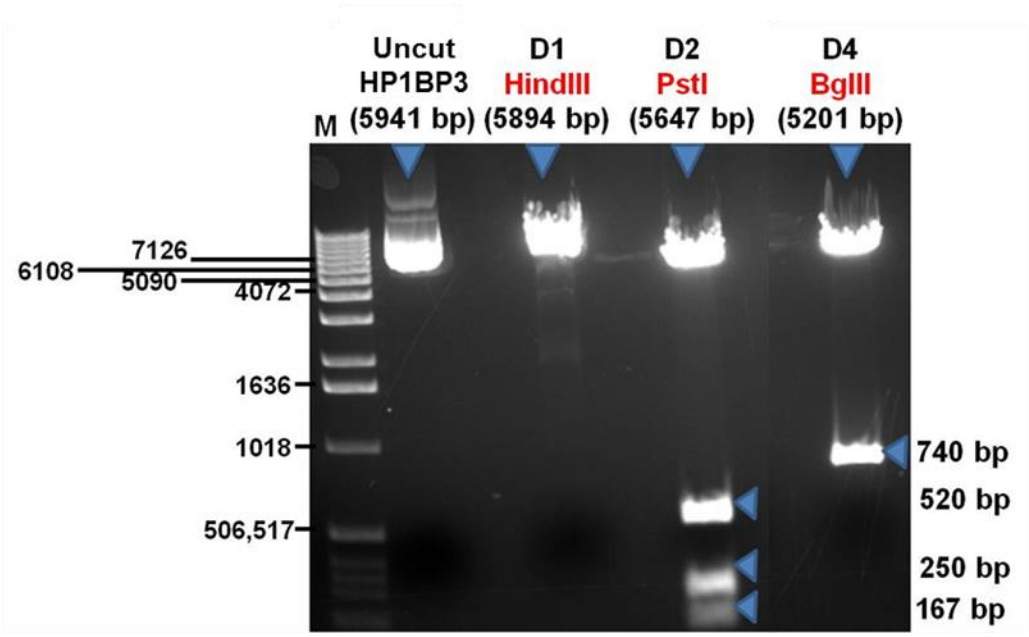


Figure 3-3: Visualization of the *HP1BP3* deletion mutant constructs on a 1% agarose gel. Relevant restriction enzymes were applied to digest *HP1BP3-Short* isoform and generate various *HP1BP3* mutant constructs. Agarose gel

demonstrates digested DNA fragments per each *HP1BP3* clones. Uncut *HP1BP3-Short* was used as the control in the experiment. M: Marker, 1Kb-DNA Ladder in bp (Invitrogen).

As shown in **(Figure 3-4)**, the DNA fragment of each *HP1BP3* deletion mutant was linearized by the enzyme used for cloning.

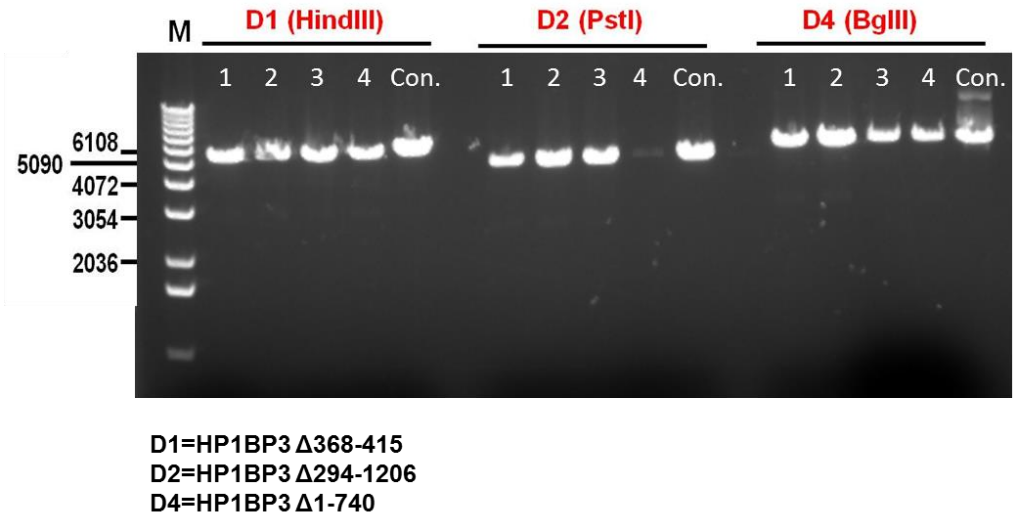
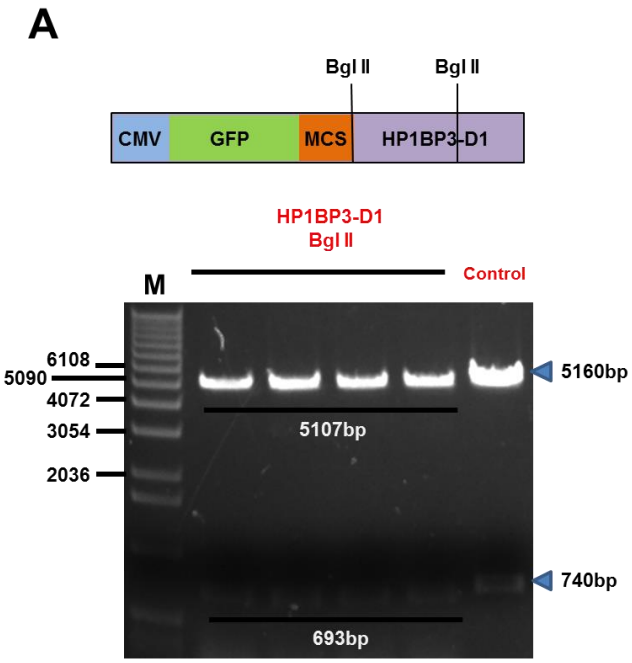


Figure 3-4: Validation of *HP1BP3* mutant clones through restriction enzyme digestion analysis. Confirmation of the successful ligation of distinct pEGFP-C2-HP1BP3 DNA plasmids was performed by restriction enzyme digestion by using previously applied for cloning restriction enzymes. *HP1BP3-Short* was used as the positive control per each construct separately in this experiment and was digested with the relevant restriction enzyme. M: Marker, 1Kb-DNA Ladder in bp (Invitrogen).

HP1BP3 deletions were also confirmed by additional enzymatic digestion with distinct restriction enzymes. Enzymatic digestion of HP1BP3-D1 by *Bgl II* showed release of two fragments as expected, 5201bp and 693bp, whereas for the control, 5201bp and 740bp were released. For *HP1BP3-D2* and *HP1BP3-D4* recombinant DNAs two single cutter enzymes were used together, such as *SnaBI* and *SacII*. *SnaBI* digests the plasmids within the human cytomegalovirus (CMV) immediate early promoter, whereas *SacII* digests at multi cloning site (MCS). Two expected fragments were released from both plasmids **(Figure 3-5)**. These data further confirmed the successful cloning of all EGFP-tagged *HP1BP3* cDNA mutants.



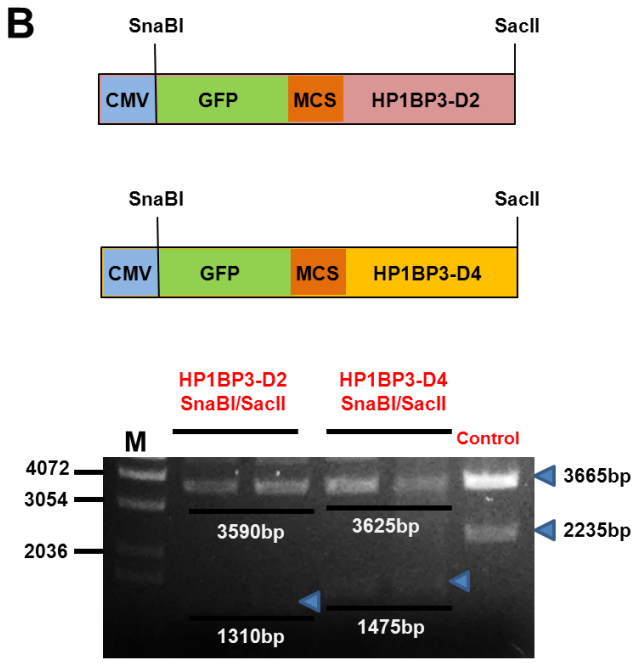


Figure 3-5: Further confirmation of *HP1BP3* recombinant DNAs derived from HP1BP3-short isoform by distinct restriction enzymes. (A) Illustrations demonstrate enzymatic digestion of *HP1BP3-D1* by *BglII*, and **(B)** enzymatic digestion of *HP1BP3-D2* and *HP1BP3-D4* by *SnaBI/SacII* restriction enzymes. *HP1BP3-Short* isoform was used as the positive control per each construct separately in this experiment and was digested with the relevant enzyme. M: Marker, 1Kb-DNA Ladder in bp (Invitrogen).

The final composition of the plasmid clones are illustrated in **(Figure 3-6)**.

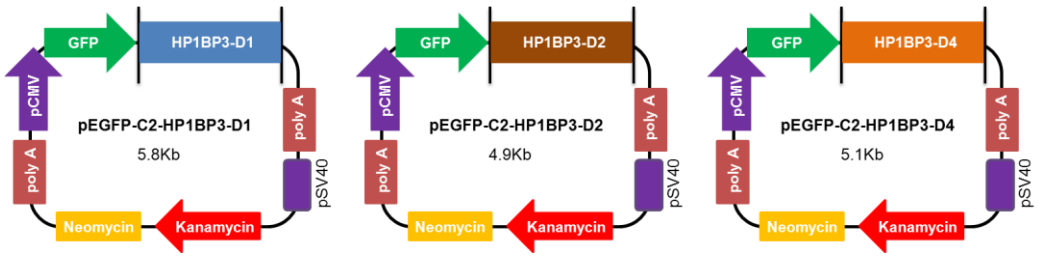


Figure 3-6: The plasmid map of successfully generated recombinant EGFP-tagged HP1BP3 clones. A diagram shows the map of *EGFP-HP1BP3-D1*, *EGFP-HP1BP3-D2* and *EGFP-HP1BP3-D4* plasmid clones with EGFP-tagged mutated human *HP1BP3* cDNAs expressed under *CMV*-promoter.

3.2.1.2 Cloning of *HP1BP3-D0* and *HP1BP3-Long* recombinant constructs

In order to further dissect the cellular localization of HP1BP3 in mammalian cell culture, the construction of two more *HP1BP3* DNA plasmids: pEGFP-C2-HP1BP3-D0 (***HP1BP3-D0***) and pEGFP-C2-HP1BP3-Long (***HP1BP3-Long***) was carried out. Two distinct DNA sequences were amplified by reverse-transcription polymerase chain reaction (RT-PCR) method using cDNA synthesised from RNA isolated from HCT116 cells lines as a template (*Chapter 2, section 2.2.2.1*), using specific primers **(Table 3-2)** to fabricate the sequences of interest **(Figure 3-7)**.

Table 3-2: Primers used to amplify EGFP-fusion compatible fragments of human *HP1BP3* cDNA. Restriction enzyme sites within primers are underlined. The core primer sequences are highlighted in grey.

Primer Use	Primer Sequence 5'-3'	Restriction Site
pEGFP-C2-HP1BP3-D0	Forward AT CTCGAG C ATGGCGACTGATACGTC	*XhoI*
	Reverse AA CTGCAG TTACGGTGTTTGTTTCTGGGCCCTG	*PstI*
pEGFP-C2-HP1BP3-Long	Forward AT CTCGAG C ATGGCGACTGATACGTC	*XhoI*
	Reverse GTATTTTCGAATAGCAACCACTGA	*BstXI**

***The restriction site for *BstXI* is located within the *HP1BP3* cDNA sequence (518nt and 529nt) and presented by CCAGAAGAGTGG.**

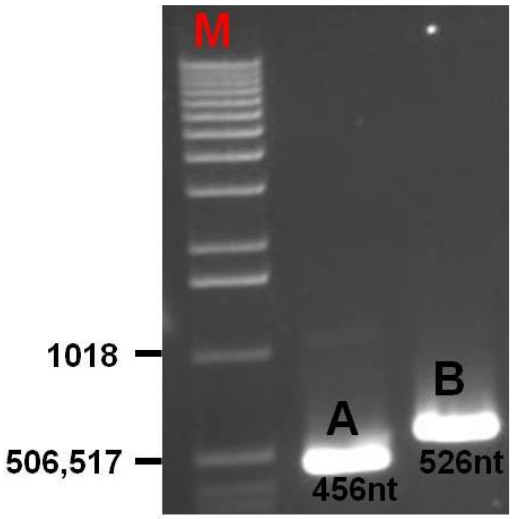


Figure 3-7: Validation of generated RT-PCR products by gel electrophoresis. Agarose gel shows amplified DNA fragments A and B from the genomic DNA extract of HCT116 (cDNA) with further application of these PCR products to construct *HP1BP3-D0* and *HP1BP3-Long*, respectively. M: Marker, 1Kb-DNA Ladder in bp (Invitrogen).

Suitable restriction enzyme sites were engineered to the primers to facilitate the cloning process as described below. The *XhoI* restriction site was added to the 5'-end of the forward primer and one extra nucleotide (C) was also added to keep an in-frame open reading frame (ORF) through the nucleotide sequences of the multiple cloning site (MCS) of the plasmid vector (pEGFP-C2). The same forward primer was used to generate both mutant *HP1BP3* cDNAs; however distinct reverse primers with *PstI* and *BstXI* restriction sites were designed for *HP1BP3-D0* and *HP1BP3-Long*, respectively **(Table 3-2)**. The aforementioned primers were used to amplify the deletion mutants of *HP1BP3* by standard PCR technique. Following gel extraction, PCR product A (for *HP1BP3-D0*) was digested with *PstI/XhoI* restriction enzymes and subsequently inserted into the multiple cloning site of pEGFP-C2 mammalian expression vector. PCR insert B (for *HP1BP3-Long*) and backbone plasmid *HP1BP3-Short* underwent enzymatic digestion with *BstxI/XhoI* restriction enzymes **(Table 3-3)** in order to create compatible cohesive ends and to construct pEGFP-C2-HP1BP3 DNA plasmids **(Figure 3-8)**.

Table 3-3: Applied restriction enzymes for generation of *HP1BP3-D0* and *HP1BP3-Long* isoform from PCR products

DNA-Insert	Backbone Vector	Restriction Enzyme N0 1	Restriction Enzyme N0 2	Recombinant cDNA
PCR-A	p-EGFP-C2	*XhoI*	*PstI*	*HP1BP3-D0*
PCR-B	HP1BP3-Short	*XhoI*	*BstxI*	*HP1BP3-Long*

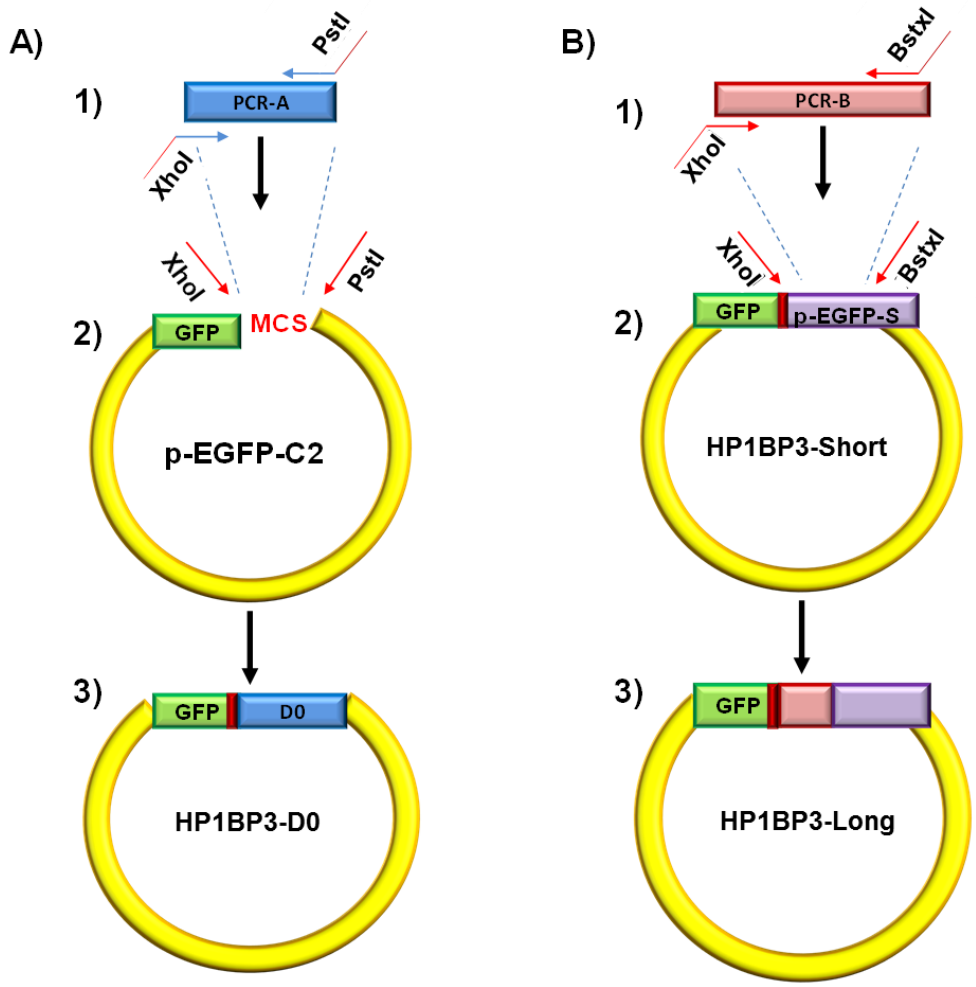


Figure 3-8: An overview of *HP1BP3* constructs cloning strategy. Diagrams **(A)** and **(B)** demonstrate the cloning steps for construction *HP1BP3-D0* and *HP1BP3-Long* isoforms.

To validate these clones, the plasmid DNA molecules were recovered from several transformed bacterial colonies and examined by the restriction enzyme digestion method. Double digestion by using *XhoI*/*BglI* was applied for *HP1BP3-D0* isoform. *XhoI* represents unique restriction site of *pEGFP-C2-HP1BP3-D0* plasmid at the position 1350bp, whereas *BglI* cuts backbone vector pEGFP-C2 at multiple sites (90bp, 215bp, 280bp and 2535bp). As shown in the **(Figure 3-9)**, five expected bands of DNA were released (65bp, 125bp, 1070bp, 1185bp and 2445bp) as result of digestive reaction. However, only the three top fragments are clearly distinguishable depending on percentage of gel. Small DNA fragments (65bp and125bp) are presented as a smear at the bottom of the agarose gel **(Figure 3-9)**.

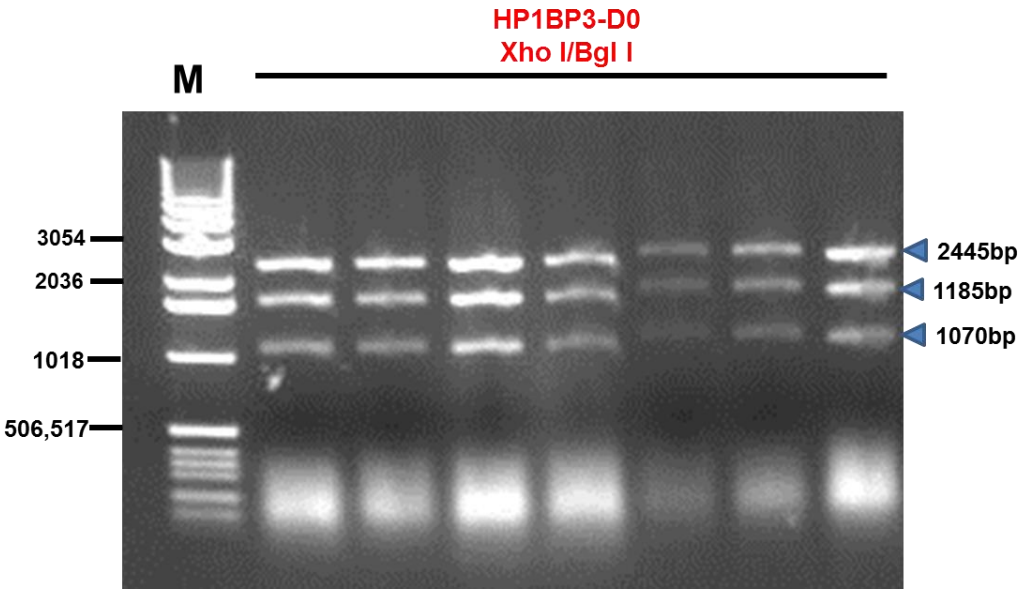


Figure 3-9: The restriction enzyme digestion analysis of HP1BP3-D0 clones. The isolated DNA from selected colonies was digested with *XhoI*/*BglI* and run on a 1% agarose gel with further visualization. Agarose gel demonstrates the release of the expected bands as indicated. Letter M, denotes a 1Kb DNA ladder in bp (Invitrogen).

HP1BP3-Long isoform was digested with *BglII* that cuts at 740bp within *HP1BP3* coding region and at MCS of backbone vector with release of two corresponding bands ~740bp and ~5620bp **(Figure 3-10)**. The data indicate the successful cloning of HP1BP3 cDNAs into pEGFP-C2 mammalian expression vector.

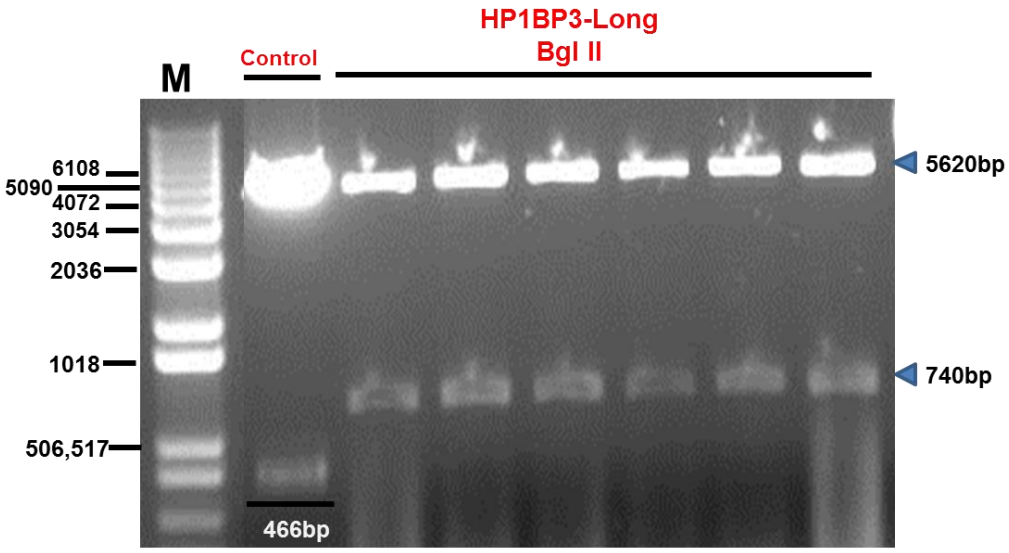


Figure 3-10: The restriction enzyme digestion analysis of HP1BP3-Long clones. An illustration shows the digested with *BglII* DNA fragments of selected colonies that were run on a 1% agarose gel and visualized as indicated. *HP1BP3-Short* was used as a control. Letter M, denotes a 1Kb DNA ladder in bp (Invitrogen).

3.2.2 Expression analysis of human HP1BP3 recombinant proteins in HEK-293T cells

For further confirmation of the recombinant constructs, the protein expression of EGFP-tagged *HP1BP3* clones (D0, D1, D2, D4, Short and Long) was examined by Western blotting analysis. HEK-293T cells were transiently

transfected (*Chapter 2, section 2.2.1.4*) with the above clones and the cell lysate was immunoblotted (*Chapter 2, section 2.2.4.2*) using anti-GFP antibody. As shown in **(Figure 3-11)**, the results of the Western blot confirmed that all constructs with EGFP-tagged *HP1BP3* cDNAs (D0, D2, D4, Short and Long) except D1 express proteins with the relevant molecular weight, indicating the successful cloning and in-frame tagging of these clones with EGFP protein.

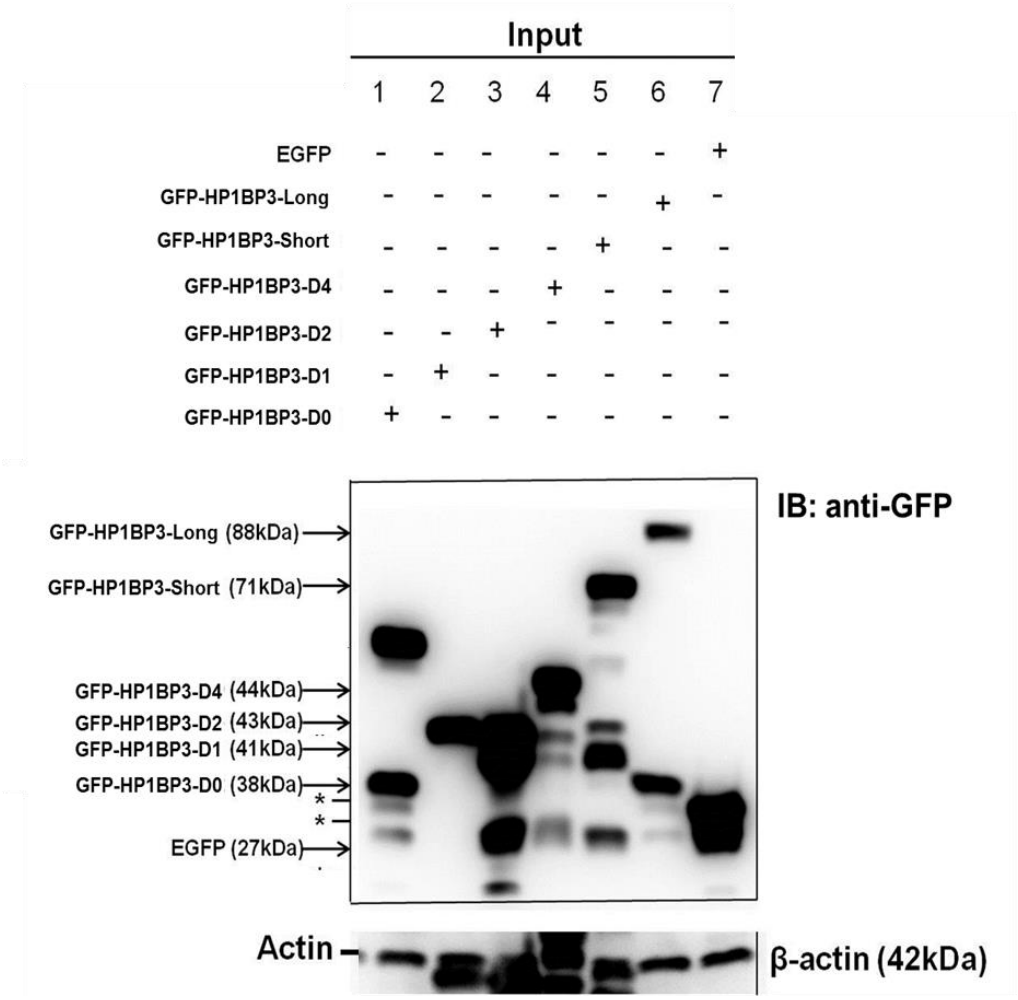


Figure 3-11: Validation assay for HP1BP3 recombinant constructs. Evaluation of EGFP-fused HP1BP3 protein expression of HP1BP3 deletions in cells was performed by Western blotting analysis. HEK-293T cells were transiently transfected with HP1BP3 mutant constructs. The protein lysates were immunoblotted against GFP antibody. Expected relevant single bands

were detected on the blot as demonstrated. The housekeeping gene β-actin (42kDa) was used as a loading control. Proteins of interest are pointed out by arrows. * indicates non-specific binding.

Interestingly, the translated protein band of *HP1BP3-D1* mutant construct was lower compared to the expected molecular weight. This fact further was explained by DNA sequencing of this particular *HP1BP3* clone **(Figure 3-12)** while all sequences of the other mutations were as expected (data not shown).

ATGGCTTCTTCCCCACGTCCCAAGATGGATGCAATCTTAACTGAGGCCATTAAGGCATG
CTTCCAGAAGAGTGGTGCATCAGTGGTTGCTATTCGAAAATACATCATCCATAAGTATC
CTTCTCTGGAGCTGGAGAGAAGGGGTTATCTCCTTAAACAAGCACTGAAAAGAGAATTA
AATAGAGGAGTCATCAAACAGGTTAAAGGAAAAGGTGCTTCTGGAAGTTTTGTTGTGGT
TCAGAAATCAAGAAAAACACCTCAGAAATCCAGAAACAGAAAGAATAGGAGCTCTGCA
GTGGATCCAGAACCACAAGTAAAATTGGAGGATGTCCTCCCACTGGCCTTTACTCGCC
TTTGTGAACCTAAAGAAGCTTCCTACAGTCTCATCAGGAAATATGTGTCTCAGTATTATC
CTAAGCTTTAGAGTGGACATCAGGCCTC

Figure 3-12: Frame – shift mutation led to formation of *HP1BP3-D1* truncation caused by formation of stop-codon "*TAG*". The digestion reaction by restriction enzyme *Hind III* that cuts *HP1BP3-Short* in two sites (recognition sites are marked by violet colour and boxed) revealed the stop-codon "*TAG*" (marked by red colour).

The result showed that deletion of *HP1BP3-Short* (Δ368-415) by *Hind III* caused formation of stop codon "*TAG*" and consequently led to the production of truncated protein *HP1BP3-D1* (~14kDa, based on the aa sequence). The cells transfected with plasmid were used as a control in the current experiment. The

expected molecular weights of the recombinant cDNAs and proteins encoded by *HP1BP3* deletions vary according to the size of the deleted cDNA region(s) as shown in **(Table 3-4)**.

Table 3-4: The expected molecular weight of HP1BP3-recombinant cDNAs and protein molecules. HP1BP3 constructs are fused with the EGFP gene, and therefore molecular weight of expressed EGFP fused HP1BP3 proteins are presented in the **Figure 3-11** includes the molecular weight of the reporter protein EGFP (27kDa).

HP1BP3 Constructs	DNA size (bp)	Protein size (kDa)
HP1BP3-D0-GFP	(~5.1 Kb)	44=17+27
HP1BP3-D1-GFP	(~5.8 Kb)	41=14+27
HP1BP3-D2-GFP	(~4.9 Kb)	38=11+27
HP1BP3-D4-GFP	(~5.1 Kb)	43=16+27
HP1BP3-S-GFP	(~5.9 Kb)	71=44+27
HP1BP3-L-GFP	(~6.3 Kb)	88=61+27

In the **Figure 3-13** there is a schematic presentation of all generated recombinant HP1BP3 proteins. The generated EGFP-HP1BP3 constructs can be broadly applied in mammalian cells for different biochemical and functional analysis.

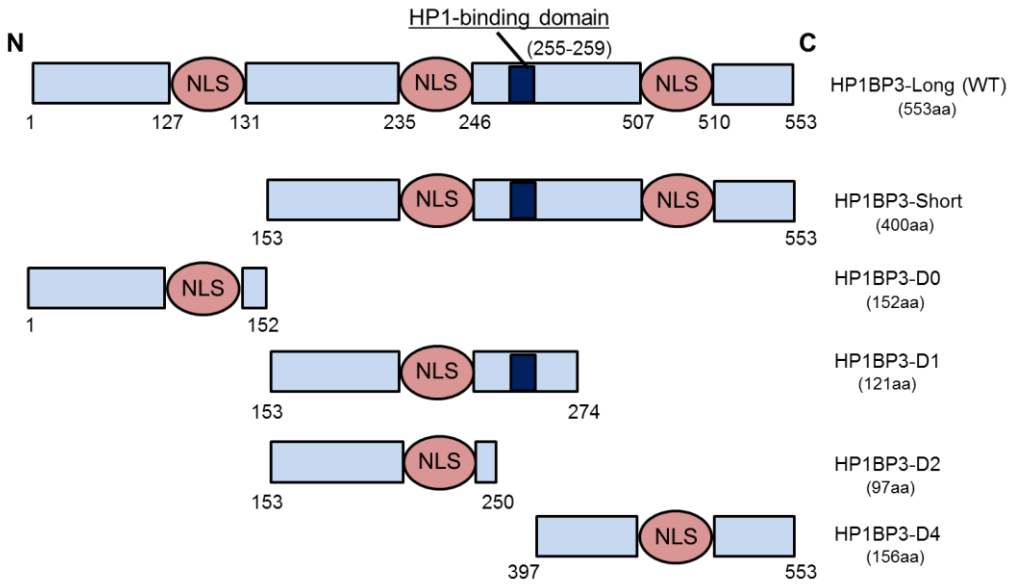


Figure 3-13: HP1BP3 constructs. Schematic representations of each HP1BP3 recombinant construct sequence with amino acid start and stop numbers.

3.2.3 Sub-cellular localization of the EGFP-tagged HP1BP3 wild-type protein and its mutants

To further examine the expression pattern and the sub-cellular allocation of HP1BP3 protein, a fluorescent microscopic analysis of overexpressed EGFP-fused HP1BP3 proteins in human CRC HCT116, HEK-293T and fibroblast cells was performed. The abovementioned cell lines were transiently transfected with EGFP-HP1BP3 clones to study the HP1BP3 expression pattern. The green fluorescent signal of the EGFP reporter gene was observed in all cases examined using a Leica DMI3000 B Inverted microscope (Leica Microsystems, UK). To detect and visualize the relative sub-cellular localization of exogenous HP1BP3 proteins, initially HP1BP3 constructs were overexpressed in HEK-293T cells. Fluorescent analysis revealed that the expression of the EGFP-fused wild type HP1BP3 (*HP1BP3-Long*) was restricted to the nucleus, whereas *HP1BP3-Short*

isoform and HP1BP3 deletions D1, D2 and D4 alongside with EGFP nuclear background displayed fractionated EGFP signal **(Figure 3-14)**. Interestingly, the green signal of the C-terminal deletion, designated of mutant D0, was diffused to the cytoplasm. Distinct EGFP-D0 nucleus is visible unless an unspecific diffusion of the high EGFP expression is detected in the cells that are highly transfected **(Figure 3-14, left, top panel)**.

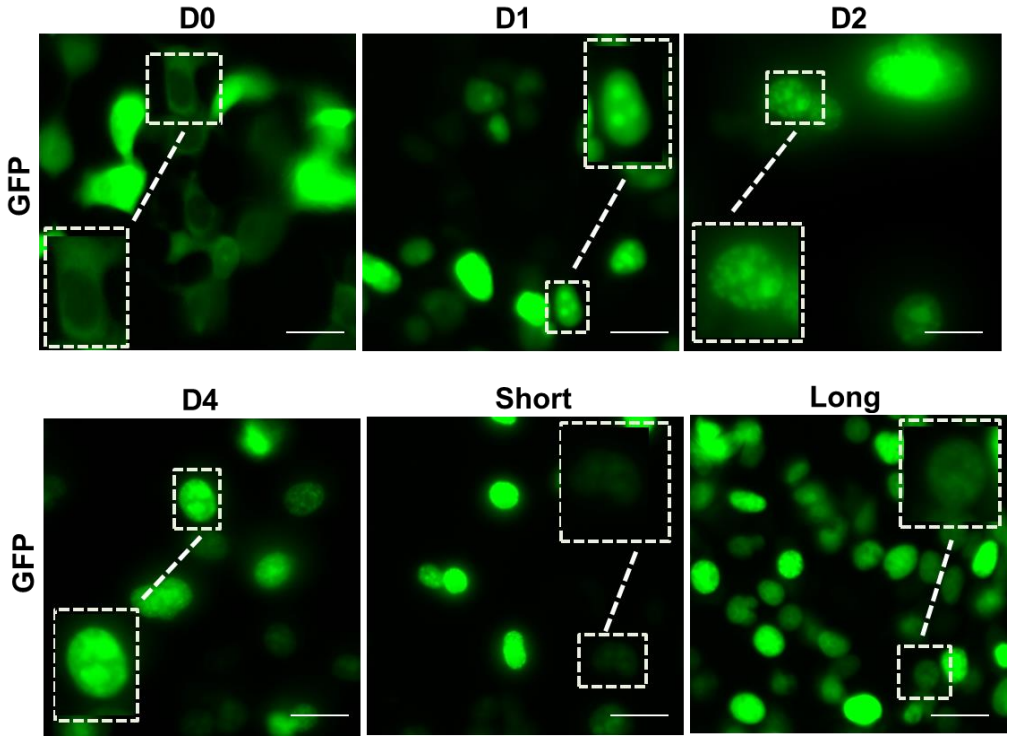


Figure 3-14: Subcellular distribution of HP1BP3 recombinant constructs in HEK-293T cells. HEK-293T cells were transiently transfected with EGFP-tagged *HP1BP3* mutant constructs. Protein expression was evaluated by fluorescent microscope analysis. HP1BP3-D0 isoform showed cytoplasmic localization whereas the rest of constructs were restricted within the borders of the nucleus. The cells with strong EGFP signal encompass a high amount of DNA plasmids, and therefore the protein expression pattern is not

distinguishable. Large white-dashed boxes present magnified views of the indicated small-white boxed regions. Scale bars, 50 μm.

To further confirm the nuclear localization of HP1BP3, the transfected HCT116 cells were stained with red fluorescent dye AlexaFluor594, conjugated secondary antibody, applied as the fluorophore marker for HP1BP3 primary antibody that recognises both endogenous and exogenous HP1BP3 proteins. As a result of exogenous HP1BP3 protein overexpression, the transfected HCT116 cells that uptake the exogenous *HP1BP3* DNA plasmids **(Figure 3-15)** detected the stronger pattern of red fluorescence emitting compared to un-transfected HCT116 cells comprising only endogenous HP1BP3 protein. DNA-binding marker, DAPI (4', 6-diamidino-2-phenylindole) (non-antibody method of fluorescent DNA-staining) was applied to visualise the nuclei of HCT116 cells. The images were captured using three different filters: DsRed (for HP1BP3 expression), DAPI (for nuclei) and green (for EGFP). As shown in **(Figure 3-15, right, bottom panel)**, the expression of EGFP-HP1BP3-Long (green) was co-localized with DAPI (blue) as well as endogenous HP1BP3 (red) confirming that HP1BP3 is expressed and localized to the nucleus. Strikingly, within the nucleus the endogenous HP1BP3 protein appears in a punctate manner spotted nuclear form **(Figure 3-15, second vertical panel)**.

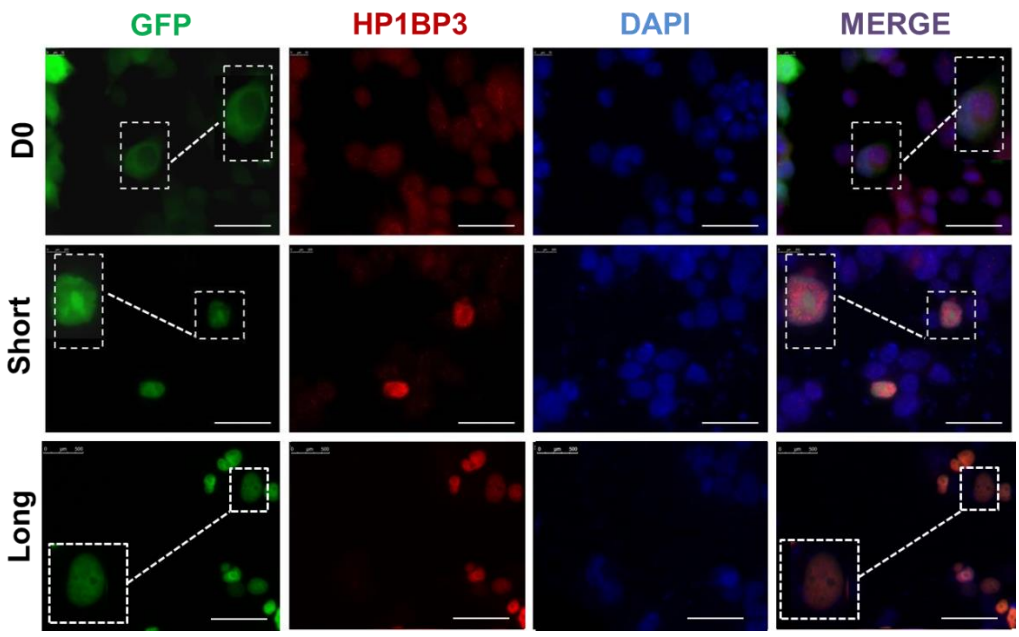


Figure 3-15: Co-localization of endogenous HP1BP3 and exogenously expressed mutant HP1BP3 proteins in HCT116 cells. HCT116 cells were transfected with HP1BP3-D0, *HP1BP3-Short* and *HP1BP3-Long* isoforms and subjected to IF assay using anti-HP1BP3 primary antibody to bind the expressed proteins of both endogenous HP1BP3 and exogenous HP1BP3 mutant clones. AlexaFluor594 secondary antibody was applied to interact with primary antibody and enable visualisation of expressed endogenous and exogenous HP1BP3 proteins. Nuclei were detected with DAPI-blue fluorescent stain. Overlaying the three images (merge) provided observation of cytoplasmic localization for HP1BP3-D0, while for the rest two isoforms is nucleolus localization. The cells exposing strong EGFP signal encompass a high amount of DNA plasmids, and therefore the protein expression pattern is not distinguishable. Large white-dashed boxes present magnified views of the indicated small-white boxed regions. Scale bars, 50 μm.

Interestingly, HP1BP3-D0 expression pattern differed in human fibroblasts **(Figure 3-16, left, top panel)** by diffusion EGFP signal throughout the whole cell with similar staining intensity in the nucleus and cytoplasm, whereas HEK-

293T and HCT116 cells demonstrated exclusively cytoplasmic expression of HP1BP3-D0. Human fibroblasts transfected by D1, D2 and D4 deletions exhibited intra-nuclear redistribution presented by nucleolar enrichment **(Figure 3-16)**. Similar observation was detected in HEK-293T cells. It is noteworthy that despite each of the HP1BP3 deletions carry NLS, movement of mutant proteins within the cellular compartments occurs and is manifested by nucleolar enrichment.

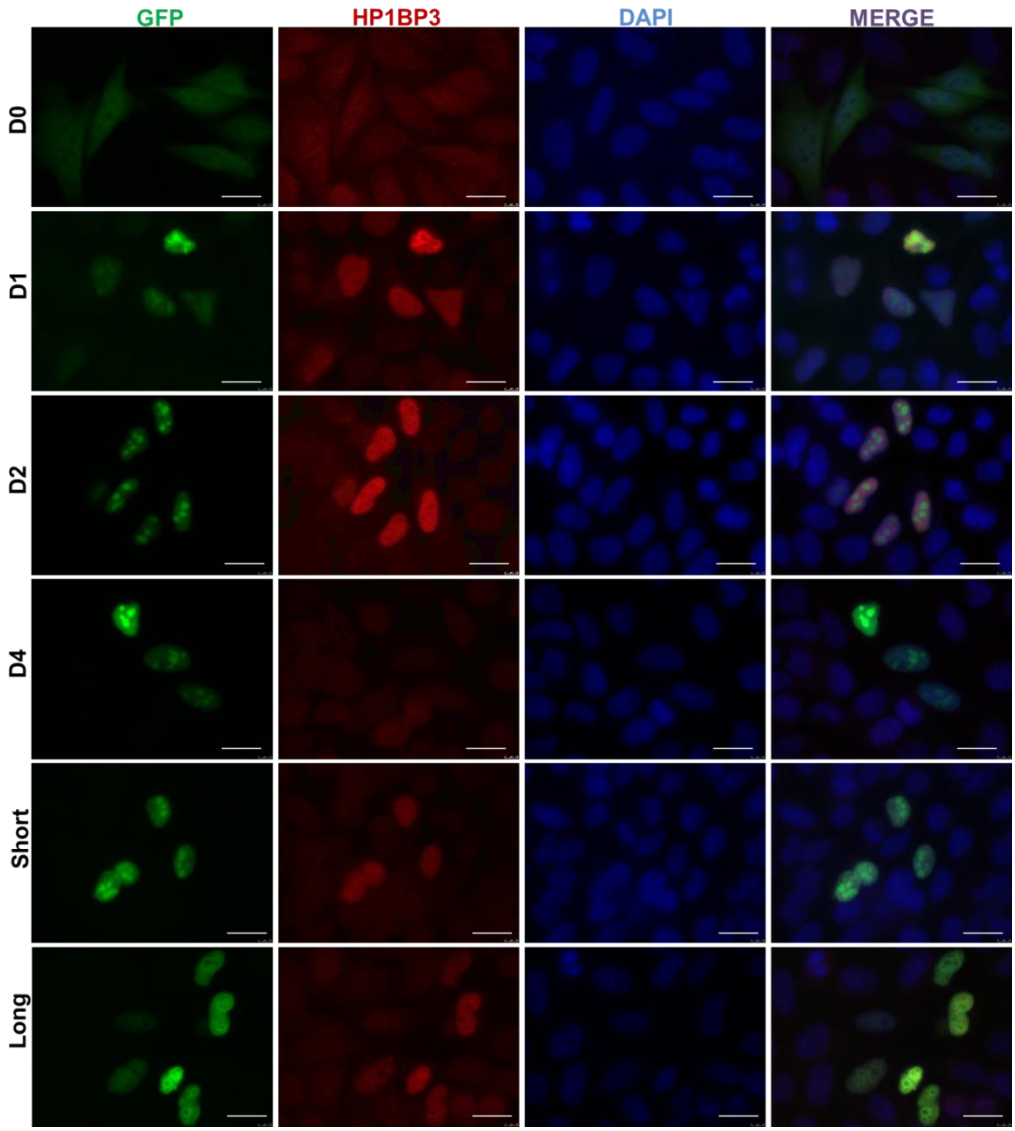


Figure 3-16: Further observation of HP1BP3 protein expression in human fibroblasts. Human fibroblasts were transiently transfected with *HP1BP3* isoforms. The transfected cells were subjected to fluorescent microscope analysis. EGFP signal in HP1BP3-D0 construct was diffused throughout whole cell encompassing both cytoplasm and nucleus. The fluorescence patterns of D1, D2, D4 and Short isoforms indicated predominant nucleolar accumulation of mutant HP1BP3 protein and the nuclear diffusion localization of HP1BP3-Long without nucleolar staining.

To further study the paradigm by which HP1BP3 recombinant proteins translocate to the nucleolus, we attempted to identify a nucleolar target sequence

(NTS) within the HP1BP3 molecule. The nucleolus is the sub-nuclear compartment lacking a membrane and therefore easy accessible for many proteins (Ahmad et al., 2009, Carmo-Fonseca et al., 2000). The functional architecture of the nucleolus is mostly related to the biogenesis of ribosomes (Scheer and Hock, 1999), although it was reported that nucleolar localization might be mediated simply through high-affinity binding to the core nucleolar components (Pederson and Tsai, 2009, Carmo-Fonseca et al., 2000). Over the last two decades several reports have emerged describing that proteins harbouring nucleolar localization sequences are sufficiently targeted to the nucleolus (Scott et al., 2011). Here, employing Nucleolar localisation sequence Detector software (NoD) (Scott et al., 2010, Scott et al., 2011) revealed the presence of four amino acid sequences encoding for NTS, two of which are located close to C-terminus **(Figure 3-17)**.

MATDTSQGELVHPKALPLIVGAQLIHADKLGEKVEDSTMPIRRTVNSTRETPPKSKLAEGEEEKPEPD
ISSEESVSTVEEQENETPPATSSEAEQPKGEPENEEKEENKSSEETKKDEKDQSKEKEKKVKKTIPSW
ATLSASQLARAQKQTPMASSPRPKMDAILTEAIKACFQKSGASVVAIRKYIIHKYPSLELERRGYLLK
QALKRELNRGVIKQVKGKGASGSFVVVQKSRKTPQKSRNRKNRSSAVDPEPQVKLEDVLPLAFTRLCE
PKEASYSLIRKYVSQYYPKLRVDIRPQLLKNALQRAVERGQLEQITGKGASGTFQLKKSGEKPLLGGS
LMEYAILSAIAAMNEPKTCSTTALKKYVLENHPGTNSNYQMHLLKKTLQKCEKNGWMEQISGKGFSGT
FQLCFPYYPSPGVLFPKKEPDDSRDEDEDEDESSEEDSEDEEPPPKRRLQKKTPAKSPGKAASVKQRG
SKPAPKVSAAQRGKARPLPKKAPPKAKTPAKKTRPSSTVIKKPSGGSSKKPATSARKEVKLPGKGKST
MKKSFRVKK

Figure 3-17: Nucleolar localization signal detection by Nucleolar localisation sequence Detector (NoD). Predicted four amino acid sequences encoding for NTS in HP1BP3 are highlighted in red colour and boxed.

Interestingly, the detected NTSs overlap with available NLSs in HP1BP3 **(Figure 3-18)**. Therefore, this finding might suggest contribution of NTS to nucleolar targeting of mutant HP1BP3 proteins.

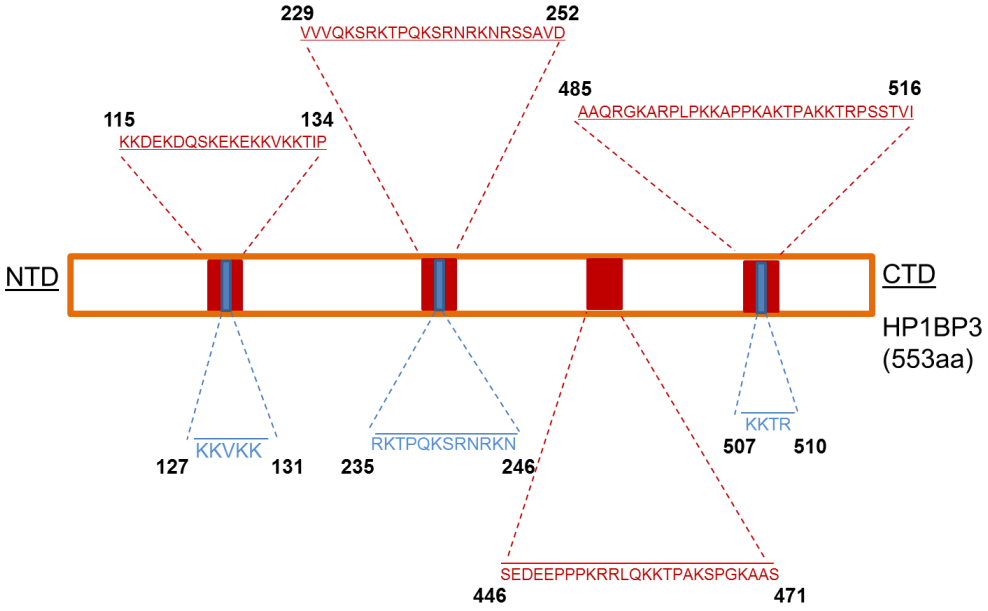


Figure 3-18: Schematic representation of joint NLS-NTS motifs of HP1BP3 protein. Amino acid sequences related to NLS are highlighted in blue and NTS in red. Start and stop amino acid numbers are shown.

As a result, the green signal of the EGFP reporter gene fused to HP1BP3-Long that represents wild type of HP1BP3 was restricted to the nucleus in all three cell lines, whereas HP1BP3-D0 showed a scattered pattern of green signal throughout the cytoplasm. Collectively, these data and previously reported results (Hayashihara et al., 2010, Garfinkel et al., 2015), strongly support HP1BP3 as a nuclear protein judged by the nuclear expression of this protein in three different human cell lines. Moreover, exclusive cytoplasmic localization

of HP1BP3-D0 in HEK-293T and HCT116 cells suggests the efficiency of C-terminal-located NLS for nuclear import of HP1BP3 protein.

3.3 DISCUSSION

The presence of sequences/motifs capable of interacting with nuclear transport machinery is a vital component for nuclear entry of most proteins. As its name denotes, HP1BP3 originally has been shown as a protein interacting with heterochromatin protein 1 (HP1), a hallmark of heterochromatin formation and propagation (Garfinkel et al., 2015, Hathaway et al., 2012, Grewal and Jia, 2007). Structural analysis revealed that HP1BP3 comprises a cluster of three predicted nuclear localization signals (NLSs) that might mediate the relocation of the protein into the cell nucleus. To test which of the available NLSs are indeed the principal sequences responsible for the nuclear homing of the HP1BP3 molecule, we applied site-directed mutagenesis by deletion of distinct regions containing the NLS sequence and monitored modulations in the subcellular distribution of the encoded HP1BP3 proteins. Designed experiments of this study determined the importance of the NLSs domains in the targeting of the HP1BP3 protein to the nucleus or the nucleolus. In agreement with previous reports, the immunofluorescent microscopy study confirms nuclear expression of wildtype HP1BP3 protein (Garfinkel et al., 2015, Hayashihara et al., 2010).

The contribution of HP1 in HP1BP3 localization was validated trough single point mutation in PQVKL, canonical HP1 binding motif (Hayashihara et al., 2010, Cheutin et al., 2003, Thiru et al., 2004, Lechner et al., 2005, Lavigne et

al., 2009). The central valine (V257) in the sequence was substituted by glutamate that led to noticeable loss of HP1BP3 accumulation in heterochromatin (Garfinkel et al., 2015). Furthermore, the chromatin binding dynamics of HP1BP3 globular domains was explored by expressing constructed EGFP-tagged deletion mutant HP1BP3 variants in HeLa cells (Garfinkel et al., 2015). Our data, however, showed the restricted localization of full length HP1BP3 within the nucleus. Interestingly, despite the remarkable abolishing of the interaction with chromatin, recombinant HP1BP3 protein lacking of both the C-terminal domain (CTD) and a 20-amino-acid poly aspartate/glutamate tract (DE region) remained within the nucleus borders.

Furthermore, in contrast to the full length, HP1BP3 mutant constructs demonstrated an altered expression pattern depending upon deletion manifested by nucleolar enrichment. The Short isoform lacking first 456 amino acids was shifted within the nucleus and migrated to the nucleolus despite containing two NLSs residues positioned in the middle and C-terminus of HP1B3, respectively. D1, D2 and D4 mutants, each encompassing the single NLS motif, displayed a similar expression pattern to HP1P3-Short by remaining within the nuclear borders with nucleolar accumulation **(Figure 3-11 & 3-13)**. Interestingly, D0 construct showed completely distinct sub-cellular localization to cytoplasm. Thus, 1-456 truncation presented by D0 construct reduced dramatically the nuclear accumulation of HP1BP3 in HEK-293T and HCT116 cells leading to cytoplasmic redistribution of the protein **(Figure 3-11 & 3-12)**. However, D0 deletion mutant expressed in fibroblasts showed a diffuse expression pattern throughout the whole cell encompassing both nucleus and cytoplasm **(Figure 3-16, left, top panel)**. These findings suggest that the actual subcellular

compartmentalization of proteins may differ in various cell types. Thus, the nuclear accumulation of D0 in human fibroblasts might be explained by possible interaction of this truncated form of HP1BP3 with other proteins expressed in the cell or regulated by post-translational modifications (Zhao, 2007, Mehta et al., 2009).

Furthermore, by analysis of the amino acid sequence motifs, we identified the presence of nucleolar targeting signals (NTS) overlapping the defined nuclear localization signals (NLS) in HP1BP3 protein. Thus, our data suggest that joint NLS-NTS motif available in HP1BP3 mutant constructs imports the protein into the nucleolus. Interestingly, despite the presence of joint NLS-NTS motif in D0, it was relatively blocked by the nuclear localization and led to cytoplasmic redistribution of the protein in HCT116 cells. Further research is required to provide evidence of possible cell signalling and/or the genomic instability contribution in HP1BP3 localisation and function presented in cancer cells.

It is noteworthy that although nuclear localization is dictated predominantly by the NLSs existence in the primary amino acid sequence, the actual nuclear homing can also be modified by possible protein-protein interactions occurring in the cell. Thus, the presence of HP1 binding motif and DNA binding regions within HP1BP3 might be contributing factors reflected in nuclear localization of the protein **(Figure 3-14)**. Although the obtained preliminary data provide valuable insight into the specific signals responsible for HP1BP3 migration into the cellular compartments, still further study is required for complete elucidation of other possible mechanisms involved in nuclear localization of HP1BP3. Thus, to test the functionality of each available NLS domain, site-directed mutagenesis

might be applied. Moreover, many studies reported regulation of nuclear localisation of proteins by post-translational modifications (Kylie et al., 2012, Poon and Jans, 2005, Zhao, 2007, Mehta et al., 2009). Interestingly, the discovery of SQ motifs (S: Serine, Q: Glutamine) in HP1BP3 molecule, which are the common phosphorylation sites of ATM/ATR protein kinases, led us to hypothesise that ATM/ATR domain might be involved in nuclear localization and/or level of HP1BP3 protein.

CHAPTER 4

DNA-Damaging Agents Modulate the HP1BP3 Protein Expression via the ATM and ATR Protein Kinases in Human Fibroblasts

4.1 BRIEF INTRODUCTION

Genomic DNA of mammalian cells is constantly challenged by the genotoxic influence of endogenous and environmental factors and, therefore has evolved a robust genome surveillance system to maintain DNA integrity through activation of alternative cell fate pathways (Wood, 1996, Sancar et al., 2004). Most of the DNA in a cell is packed by nucleosomes that together with nucleosome-associated enzymes and regulatory factors make up chromatin. Chromatin/heterochromatin modifying and remodelling molecules regulate the access of selected DNA segments in chromatin, thereby modulating transcription, DNA replication and repair. However, failure in recovery from DNA damage can lead to accumulation of mutations and development of cancer.

The maintenance of genomic stability requires not only DNA repair machineries but also signal transduction pathways that are primarily initiated by the ataxia telangiectasia mutated (ATM) and ataxia telangiectasia and Rad3-related (ATR) protein kinases (Traven and Heierhorst, 2005, Price and D'Andrea, 2013). DNA damage distribution is greatly affected by the interaction with histones and non-histone proteins in chromatin. In addition, the cellular exposure to genotoxic insults prompts the formation of ATM/ATR nuclear foci as a primary evidence of response to structural and functional alterations in DNA molecules (Tibbetts et al., 2000, Khalil et al., 2012a).

Despite the difference in stimulation, activated ATM and ATR protein kinases share the phosphorylation cascade of a plethora of downstream substrates implicated in DNA repair, DNA replication, and cell cycle transitions (Bensimon et al., 2011, Hurley and Bunz, 2007). ATM/ATR-like kinases phosphorylate

their substrates on Serine and/or Threonine residues that precede Glutamine residues, designated as SQ/TQ-motifs. The presence of a SQ/TQ domain is considered the specific characteristic feature of DNA-damage-response proteins (DDR) (Traven and Heierhorst, 2005). Nevertheless, the contribution of non-histone proteins such as HP1BP3 to control the chromatin/heterochromatin integrity in response to DNA damage is unknown.

The examination of the HP1BP3 amino acid sequence revealed the presence of hydrophobic and negatively charged amino acids immediately NH2-terminal to three putative ATM/ATR consensus phosphorylation motifs (S-Q) **(Figure 4-1)**.

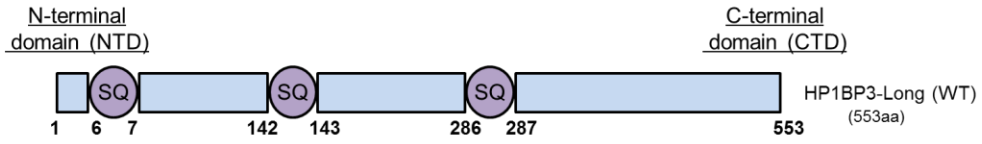


Figure 4-1: A schematic representation of the HP1BP3 protein and its putative ATM/ATR phosphorylation sites. The diagram shows the presence of three putative ATM/ATR consensus phosphorylation motifs (S-Q) with amino acid sequence position.

Hence, we investigated whether HP1BP3-dependent DNA damage response in fibroblasts is regulated by ATM/ATR protein kinases. In brief, our data suggest that a sub-lethal concentration of DNA-damaging agents, such as γ-irradiation and Oxaliplatin induces the expression of HP1BP3. Our hypothesis was further supported by the HP1BP3 foci formation in response to DNA damage. A site-directed mutagenesis SQ→AQ reaffirmed the contribution of ATM/ATR phosphorylation site on HP1BP3 protein level in the presence of DNA-damaging agent. Moreover, immunoprecipitation (IP) experiments demonstrated that

phosphorylated HP1BP3 may interact with ATM in response to DNA-damaging agents. These data suggest that upregulation of HP1BP3 via DNA-damaging agents such as UV/gamma irradiation (IR) and Oxaliplatin might be directly mediated by the ATM/ATR kinases.

4.2 RESULTS

4.2.1 UV-irradiation elicits simultaneous induction of HP1BP3 and hallmark DDR proteins (γH2AX and p53) in human fibroblasts

To study the expression level of HP1BP3 in response to ATM/ATR kinases activation, human fibroblasts were exposed to UV light. The kinetics of ATM/ATR proteins in response to DNA damage in UV-induced lesions can be ascertained by monitoring the ability of histone H2AX phosphorylation (γH2AX) to form nuclear foci and stabilisation of p53 (Kastan et al., 1991, Vrouwe et al., 2011, Tu et al., 2013, Wang et al., 2005). Therefore, the expression level of DDR proteins such as p53 and γH2AX was measured prior and following irradiation.

Initially, a fluorescent microscope technique was applied. Fibroblasts were cultured on coverslips and exposed to 50mJ/cm^2 UV irradiation (Kristin et al., 2000). The intensity of immunofluorescence was assessed in both UV-treated and UV-untreated cells. After 3 hours following UV exposure, analysis of cellular DNA content with DAPI staining showed similar intensity and location of DNA in irradiated and non-irradiated cells. Immunofluorescence double labelling revealed that UV irradiation caused the increased levels of HP1BP3 and also led to the accumulation of DDR proteins, γH2AX and p53 **(Figure 4-2**

& 4-3). High-resolution images of treated cells show the morphological difference with untreated cells, as stained with rhodamine-phalloidin for F-actin (**Figure 4-2**).

There was a significant intensity of staining of HP1BP3 in UV-treated cells versus UV-untreated cells. In the absence of UV, only DAPI staining of the DNA was observed, whereas HP1BP3 is barely visible. Following UV exposure, HP1BP3 expression was enhanced and was more intense into distinct foci **(Figure 4-3)**. Furthermore, HP1BP3 co-localized with p53 to these foci (**Figure 4-3**), suggesting that HP1BP3 localizes with ATM protein substrate in the nucleus.

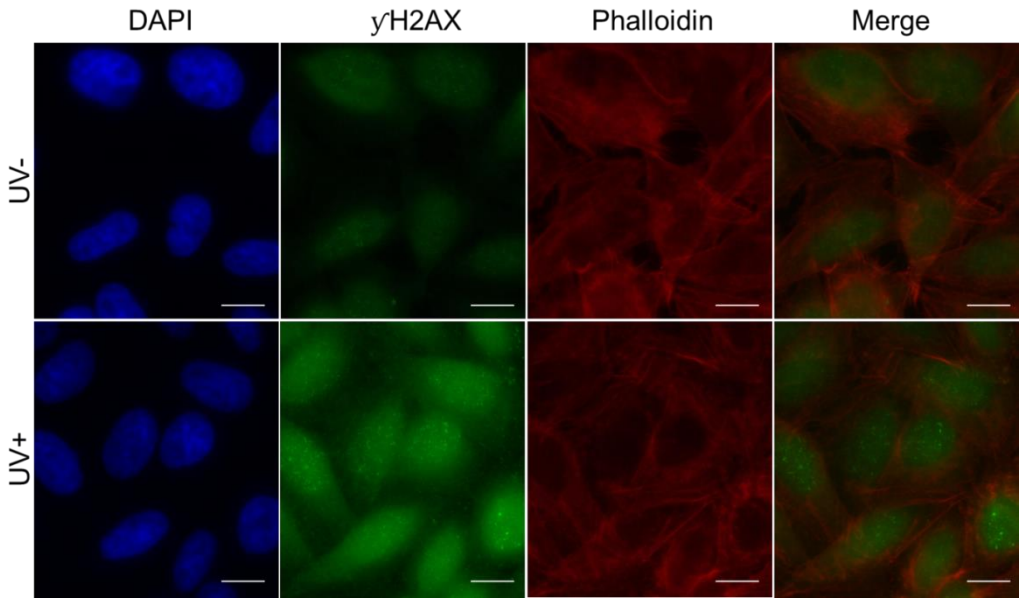


Figure 4-2: γH2AX used as a positive control for UV irradiation. Fibroblasts were exposed to 50mJ/cm^2 UV light and immunostained for γH2AX. Images demonstrate the significant elevation and spotty expression pattern of γH2AX following UV treatment. Nuclei were detected with DAPI-blue fluorescent stain. Scale bars, 50μm.

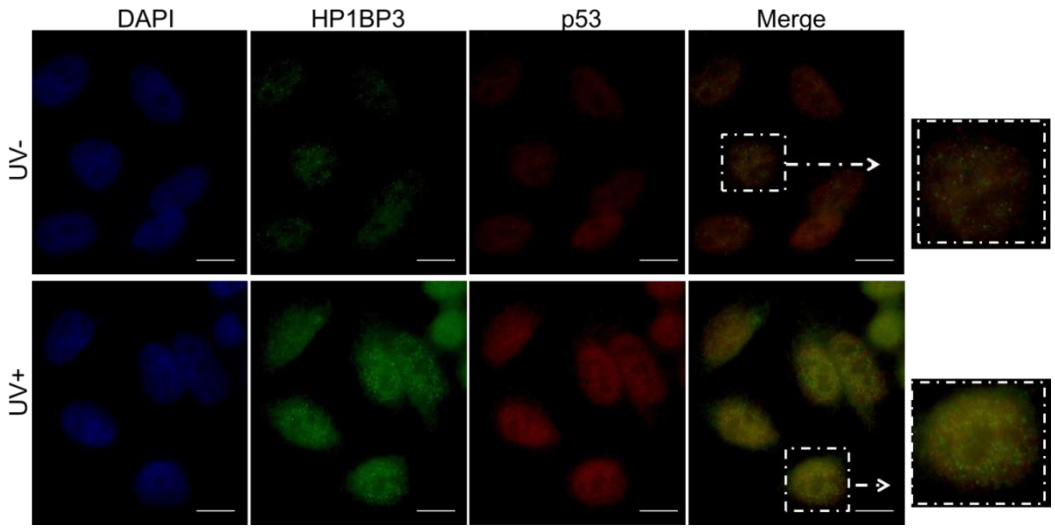


Figure 4-3: UV irradiation induced HP1BP3 expression in human fibroblasts. Fibroblasts displayed notable increase of HP1BP3 level in response to UV irradiation. HP1BP3 expression pattern appeared in a spotty format restricted within the nucleus. p53 stabilisation served as an evidence of ATM/ATR activation. Nuclei were detected with DAPI-blue fluorescent stain. Large white-dashed boxes present magnified views of the indicated small-white boxed regions. Scale bars, 50μm.

In addition to immunofluorescence assay (IF), the protein level of HP1BP3 in response to UV treatment was evaluated by Western blotting analysis. In agreement with IF data the obtained WB results showed the notable elevation of both HP1BP3 and DDR proteins after UV treatment **(Figure 4-4)**.

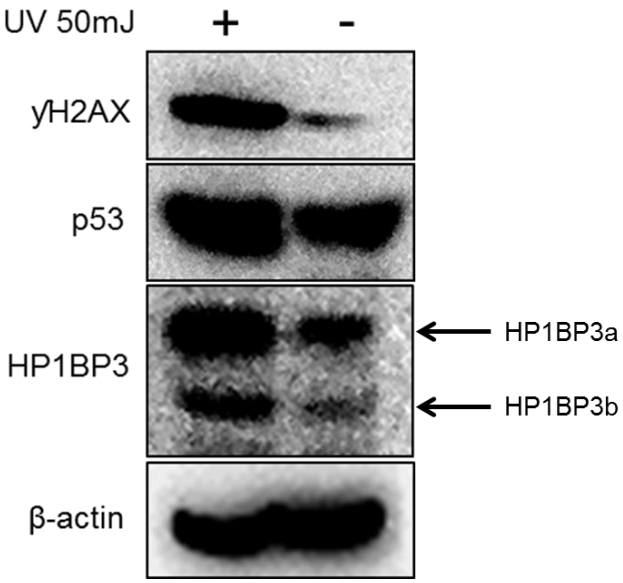


Figure 4-4: γH2AX induction (ATM/ATR activation) positively correlates with HP1BP3 expression. Protein lysates (150µg) extracted from UV-treated and UV-untreated fibroblasts were immunoblotted with γH2AX, p53 and HP1BP3 antibodies. Western blotting images demonstrate upregulation of HP1BP3 as well as DDR proteins in response to UV exposure. Arrows depict on the presence of two endogenously expressed bands of HP1BP3 named as HP1BP3a and HP1BP3b and corresponding to the long and short isoforms of HP1BP3 protein, respectively.

As it was previously reported, expression of HP1BP3 was manifested by two endogenous bands 74kDa and 70kDa, corresponding to the two distinct splice variants, and termed HP1BP3a and HP1BP3b, respectively (Hayashihara et al., 2010, Garfinkel et al., 2015). Notably, both HP1BP3 isoforms were upregulated in response to UV light. Collectively, these results indicate that the phosphorylation of HP1BP3 in human fibroblasts damaged by UV radiation may be mediated through recruitment and activation of ATM/ATR kinases (Auclair et al., 2009, Yajima et al., 2009).

UV irradiation provokes an ATR-kinase-mediated damage response initiated by stalled DNA replication and RNA transcription followed by repair (Lupardus et al., 2002, Tibbetts et al., 2000). Furthermore, stimulation of ATR kinase occurs in response to activation of the nucleotide excision repair (NER) pathway induced by UV radiation (Derheimer et al., 2007, Jiang and Sancar, 2006). NER is the only known pathway capable of removing the distortions in the DNA helix caused by cyclobutane pyrimidine dimers (CPDs) or 6-4 photoproducts (6-4PPs) from DNA in human cells (de Laat et al., 1999, Wood, 1997, Hanawalt, 2002). There is a solid evidence that ATR rather than ATM is primarily associated with H2AX phosphorylation upon DNA damage by UV(Yajima et al., 2006, Ward et al., 2004). However, the collapse of replication forks caused by UV might produce DSBs formation and therefore lead to ATM activation which in turn also contributes to phosphorylation of H2AX (Yajima et al., 2009). Thus, UV-induced DNA lesions can concomitantly activate both ATM and ATR branches of DNA damage signalling pathway (Auclair et al., 2009, Zhao et al., 2010).

4.2.2 Generation of stably-transfected human fibroblasts for the functional analysis of HP1BP3

Stable, long-term expression of a gene of interest is a powerful approach that can be achieved by well-established techniques and novel approaches (Büssow, 2015). Production of stably-transfected cell lines is employed in a wide range of applications (Lai et al., 2013, Chaudhary et al., 2012). The generation of a stable cell line is essential for studying the function and structure of recombinant proteins. Thus, we aimed to generate human fibroblasts stably expressing a long HP1BP3 protein in order to further investigate the role of this protein substrate in DNA

damage signalling pathway through activation of ATM/ATR protein kinases by applying DNA-damage triggering agents.

4.2.2.1 Cloning of *HP1BP3-Long* cDNA into pLVX-EGFP

In the current study, a Lentiviral-based gene delivery system was applied to achieve a stable expression of *EGFP-HP1BP3* gene in human fibroblasts. This approach was initiated by the cloning of HP1BP3-Long cDNA isoform into the pLVX-EGFP by employing pEGFP-C2-HP1BP3-Long plasmid. pLVX-EGFP is a modified construct produced by Dr Nateri's laboratory from the pLVX-puro vector which was reconstructed to express EGFP (Enhanced Green Fluorescence Protein) **(Figure 4-5)**.

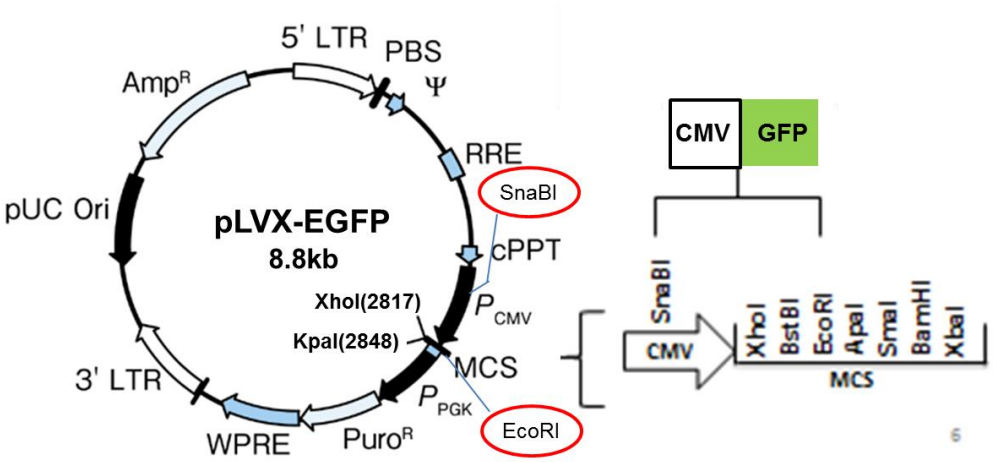


Figure 4-5: The expression plasmid pLVX-EGFP. Diagram shows the plasmid map and the approximate cut positions of *SnaBI* and *EcoRI* restriction enzymes (circled in red) in the modified Lentiviral vector (pLVX-EGFP). The indicated restriction enzymes were applied for cloning. The *CMV*-promoter drives the expression of EGFP.

pLVX-puro is an HIV-based Lentivirus expression vector. It contains a constitutively active human cytomegalovirus immediate early promoter (*P*CMV

IE) just upstream of the multiple cloning sites (MCS). The restriction digestion via "cutting and ligating strategy" was applied to excise two DNA fragments that together can produce the full-length *HP1BP3* cDNA from the pEGFP-C2-HP1BP3-Long plasmid vector. Thus, the first fragment was excised with *SnaBI* and *BstXI* restriction enzymes with a single cut position at ~341bp within the *CMV* region of the backbone vector pEGFP-C2 and at ~526bp of the HP1BP3 coding region, respectively. *EcoRI* with two recognition sites (~1362bp within *MCS* region of the backbone vector pEGFP-C2 and ~135bp of the HP1BP3 coding region) was used to cut the second fragment from pEGFP-C2-HP1BP3-Long. In parallel, the pLVX-EGFP DNA was digested with the *SnaBI/EcoRI* restriction enzymes to create compatible cohesive ends for the construction of pLVX-EGFP-HP1BP3-Long. A triple ligation of the desired DNA fragments was carried out to produce pLVX-EGFP-HP1BP3-Long. The **Figure 4-6** illustrates the schematic representation of the pLVX-EGFP-HP1BP3-Long cloning strategy.

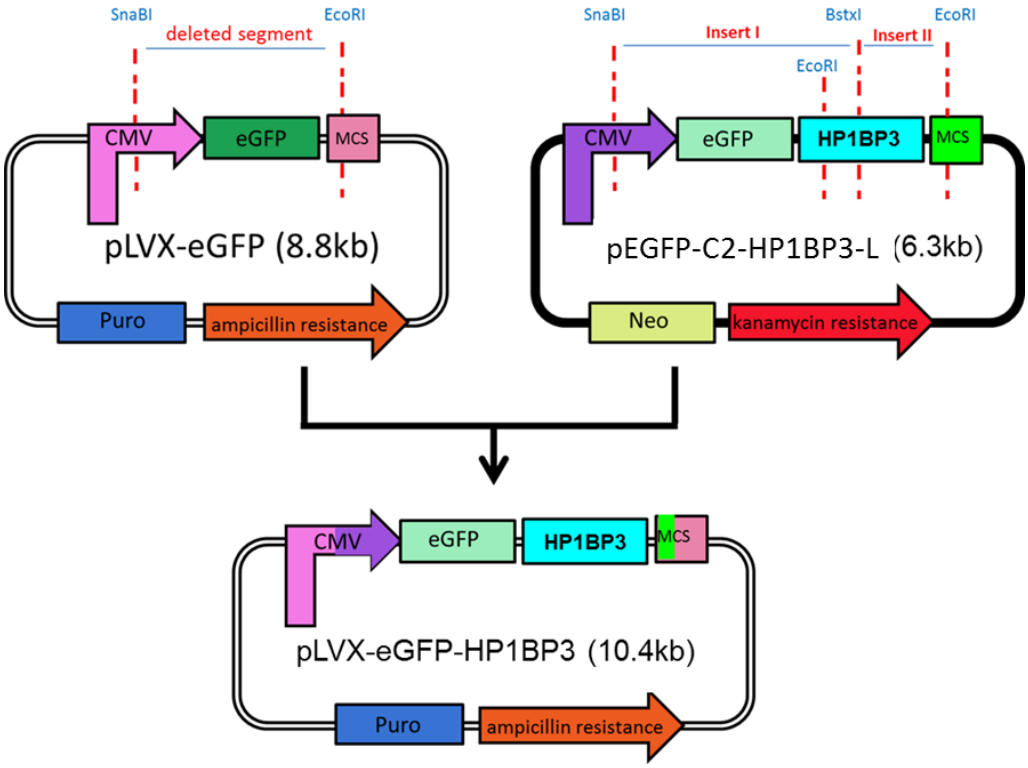


Figure 4-6: Cloning strategy for pLVX-EGFP-HP1BP3-Long DNA clone. Schematic representation of the cloning strategy of EGFP-fused *HP1BP3-Long* cDNA into the pLVX-EGFP Lentiviral vector using *SnaBI/EcoRI* restriction enzymes. The full nucleotide sequence of EGFP-tagged *HP1BP3-Long* was fused to the 3'-end of the *CMV*-promoter.

The ligated products were transformed into bacterial competent cells and plated onto the *Ampicillin* plate for pLVX-EGFP. Extracted DNA from individual bacterial colonies was validated using *EcoRI* DNA digestion. Digestion analysis indicated that 3 of 7 colonies retained the correct expected DNA bands (1.5kb and 8.9kb) **(Figure 4-7)**. However, the colony no.7 (C7) was consequently used for the subsequent Midiprep for DNA amplification and further validation analyses.

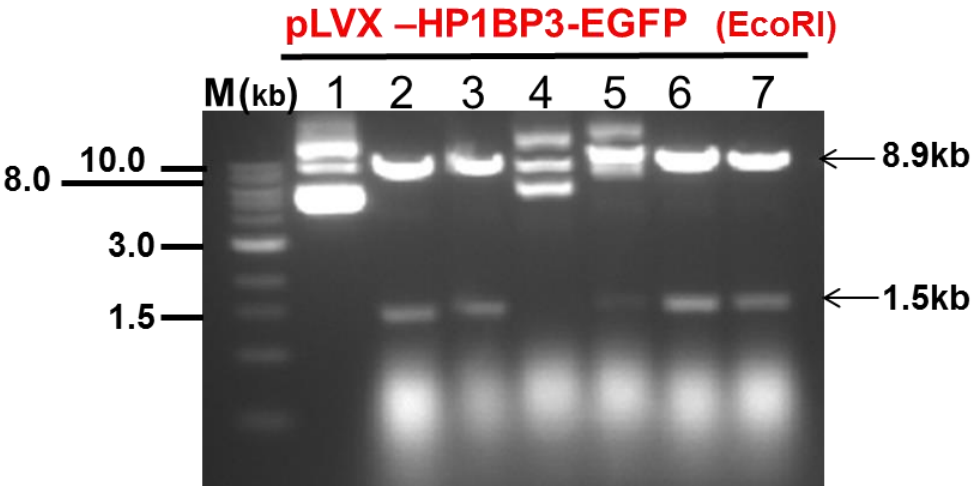


Figure 4-7: Restriction enzyme digestion analysis of pLVX-EGFP-HP1BP3-Long cDNAs. Plasmid DNA was extracted from the generated colonies and the yielded DNA construct was validated using *EcoRI* restriction enzyme digestion. Colonies C3, C6 and C7 gave the right expected bands for the recombinant pLVX-EGFP-HP1BP3-Long. Further amplification and validation was carried out for the last colony. Letter M, represents 1Kb-DNA marker in bp (BioLabs).

C7-plasmid midi-prep DNA was used for further digestion analysis using *EcoRI*. These data confirmed the successful cloning of HP1BP3-Long cDNA into the Lentiviral vector (pLVX-EGFP). As a control, the digestion of pLVX-EGFP backbone vector, with the same enzyme showed a single band of linearized DNA, as was expected **(Figure 4-8)**.

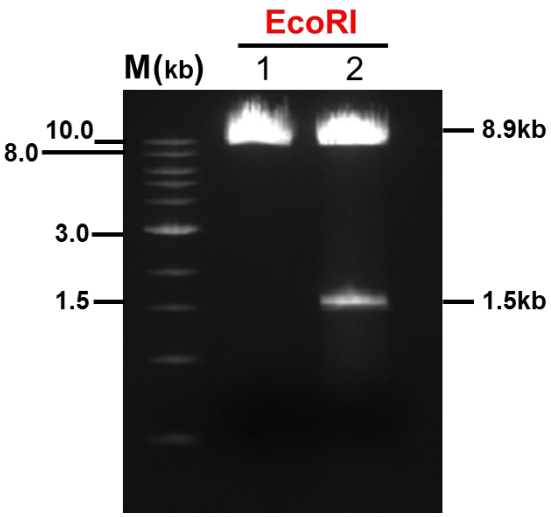


Figure 4-8: Restriction enzyme digestion analysis of Lentiviral constructs containing EGFP and EGFP-HP1BP3-Long cDNAs. Both pLVX-EGFP (lane 1) and pLVX-EGFP-HP1BP3-Long (lane 2) constructs were digested with *Eco*RI restriction enzyme. The digested DNA fragments were run on 1% agarose gel and visualized as indicated. *M* represents 1Kb-DNA marker in bp (BioLabs).

Next, a pLVX-EGFP-HP1BP3-Long plasmid was transfected into fibroblasts as described in (*Chapter 2, section 2.2.1.5*). Transfected cells were selected on the basis of acquired resistance to the Puromycin (*Chapter 2, section 2.2.1.5.2*). Untransfected cells were used as negative control and cells transfected with pLVX-EGFP plasmid as a positive control. After 48 hours transfected cells were cultured in the presence of Puromycin for the selection. Surviving cells were screened for EGFP expression of the EGFP-HP1BP3 protein. The EGFP-tag allowed for direct protein quantification by fluorescence microscopy during cell line development. Fluorescent microscopic analysis confirmed stable expression of EGFP-HP1BP3 and EGFP in colonies derived from the Puromycin resistant human fibroblasts **(Figure 4-9)**.

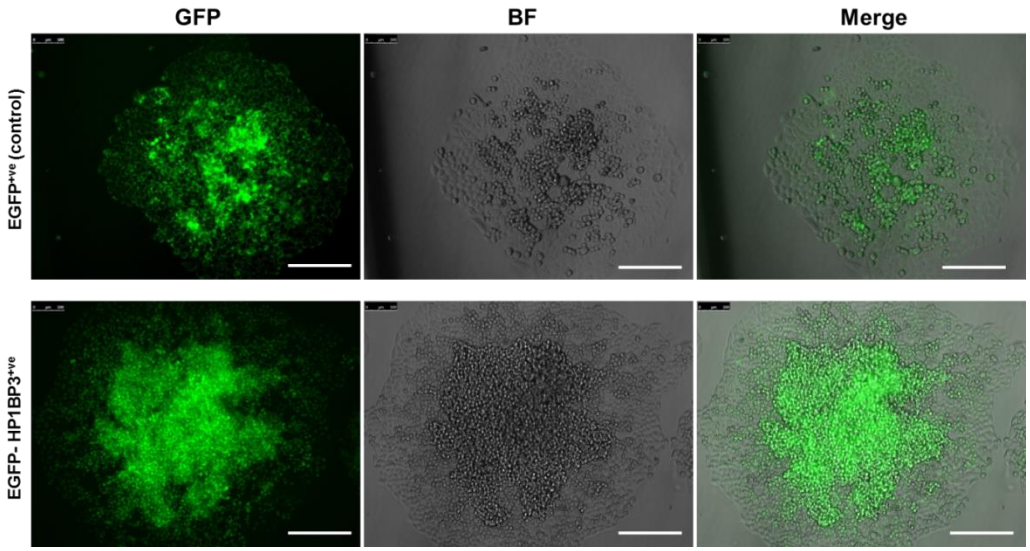


Figure 4-9: Confirmation of the stable expression of EGFP-HP1BP3 in human fibroblasts by fluorescent microscopy. Bright field and fluorescent microscopy images of the stable cell lines are generated. Merge images including both BF and EGFP-fluorescent demonstrate EGFP-HP1BP3protein production by whole population of available cells.

Notably, the stably-transfected cells exhibited the same restricted nuclear localisation of the EGFP-HP1BP3 **(Figure 4-10, D)** as reported before in (*Chapter 3, section 3.2.3*).

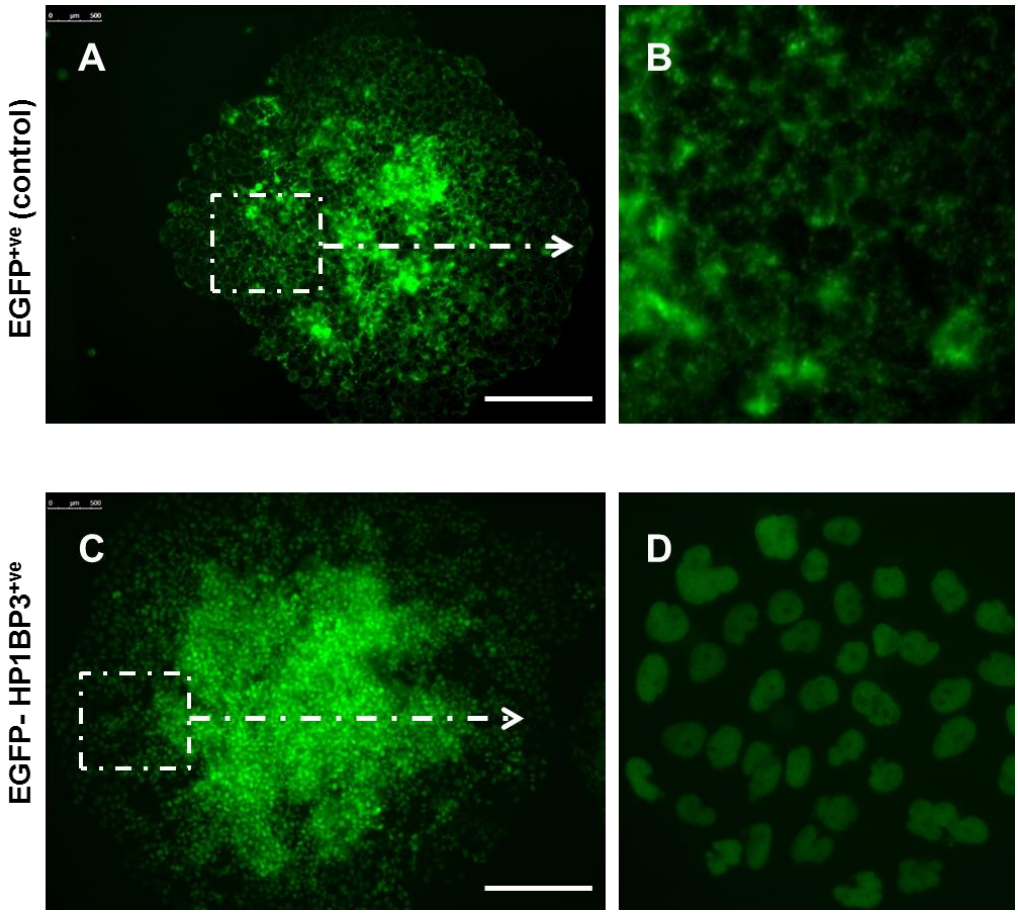


Figure 4-10: Nuclear localization pattern of stably expressed EGFP-HP1BP3. The protein expression of stably expressed EGFP **(A & B)** and EGFP-HP1BP3 **(C & D)** in human fibroblasts are shown as indicated. (**B &D)** are magnified views of the indicated white boxed areas. Scale bars, 50 μm.

In contrast, the EGFP protein alone (control cell line) was ubiquitously expressed in both nuclear and cytoplasmic compartments of fibroblasts in a spotty format **(Fig 4-10, B)**. Furthermore, after Puromycin selection, the cells were expanded and examined for the expression of the EGFP-HP1BP3 protein by immunoblotting. Western blotting analysis confirmed the ectopic expression of EGFP-HP1BP3 in stable human fibroblasts **(Figure 4-11)**.

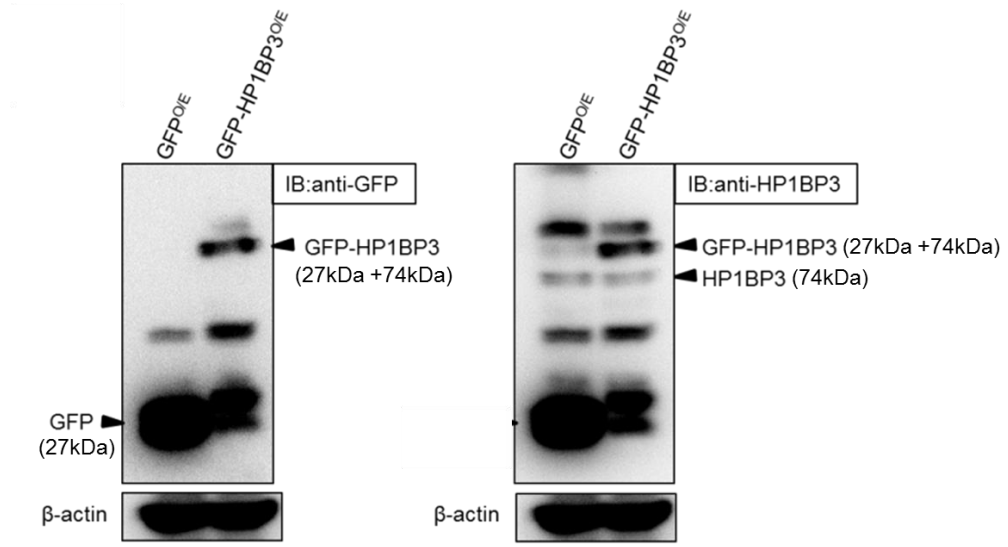


Figure 4-11: Generation of stable cell lines in human fibroblasts. Protein extracts (100 µg) from the generated cell lines were subjected to immunoblot analysis to detect the expression of EGFP-HP1BP3 and EGFP. Anti-EGFP antibody was used to detect expression of EGFP in control cells as well as the exogenous expression of EGFP-HP1BP3 in generated stable cell line. Endogenous HP1BP3 was detected using anti-HP1BP3 antibody. O/E stands for overexpression of a protein.

Collectively, these data indicate the successful genome integration of EGFP-HP1BP3 in stably-transfected human fibroblasts **(Figure 4-12)**.

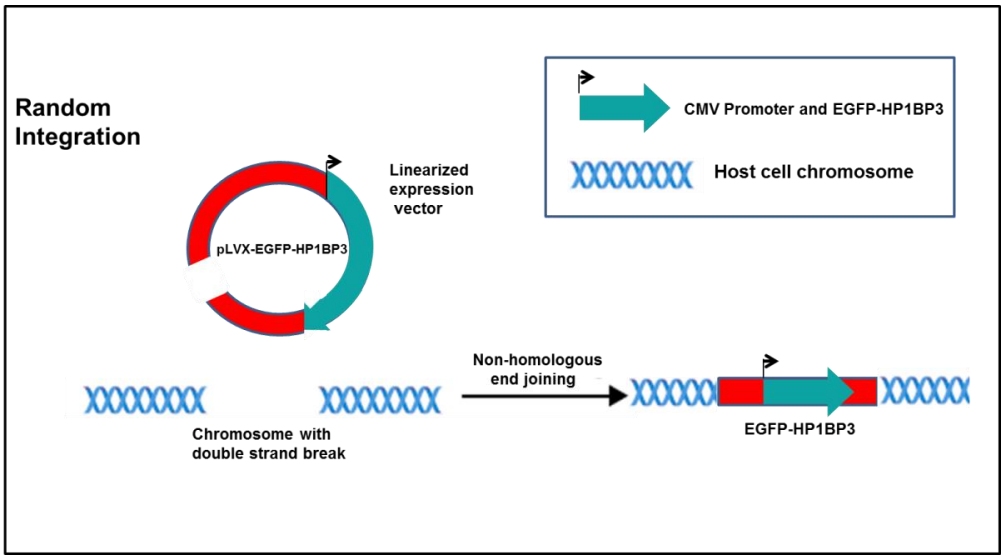


Figure 4-12: Schematic representation of possible random integration of EGFP-HP1BP3 into the genome of human fibroblasts. The linearized pLVX-EGFP-HP1BP3-Long plasmid is integrated by non-homologous end joining into the host cell genome at the position of a random chromosome break. Integration sites of introduced plasmid DNA into the nucleus of host cells are random and dictated by host cell factors(Büssow, 2015).

4.2.3 ATM/ATR-dependent induction of HP1BP3 caused by ionizing radiation

It is well known that ionizing radiation induces both single strand (ss) and double strand (ds) DNA breaks, which in turn trigger activation of ATM and ATR protein kinases. The ATM/ATR activation targets a broad range of downstream protein substrates that are involved in DNA repair, cell cycle arrest and apoptosis (Canman et al., 1998) (Falck et al., 2001, Myers and Cortez, 2006, Kastan and Bartek, 2004). Recent reports showed that over 700 proteins encompass more than 900 phosphorylation sites containing consensus ATM and ATR recognition motifs phosphorylated in response to IR (Matsuoka et al., 2007).

The detection of the three putative ATM/ATR consensus phosphorylation motifs (S-Q) within HP1BP3 suggested it was a potential candidate downstream substrate of ATM/ATR protein kinases.

Therefore, to visualize the functional consequences of ATM/ATR-dependent phosphorylation of HP1BP3, we exposed fibroblasts stably expressing EGFP-HP1BP3 (experimental cells) and fibroblasts stably expressing EGFP (control cell line) to ionizing radiation of 6Gy. Initially, we monitored the phosphorylation of H2AX as a sensitive biomarker of IR-induced DSBs (Valdiglesias et al., 2013) by Western blotting analysis using a phospho-specific antibody. The phosphorylation event at Serine 139 of histone H2AX in mammals refers to the earliest indicators of DNA DSBs and recognized as the crucial contributor in their recognition, signalling and repair (Rogakou et al., 1998). The results revealed elevation of γH2AX in both fibroblasts stably expressing EGFP-HP1BP3 as well as control irradiated cell lines approving activation of DNA damage signalling pathway. It is important to highlight here, that expression level of γH2AX was higher in fibroblasts stably expressing EGFP-HP1BP3 compared to the control cells even without application of irradiation **(Figure 4-13, B)**.

Interestingly, immunoblotting analysis showed that the level of HP1BP3 increased markedly after irradiation in cells stably expressing EGFP-HP1BP3. Induction of both endogenous (HP1BP3a & HP1BP3b) and exogenous isoforms of HP1BP3 was observed **(Figure 4-13, lane 4)**, whereas control cells showed very marginal induction of HP1BP3 isoforms **(Figure 4-13, lane 2)**. Thus, we confirmed that the HP1BP3 level increased in response to ionizing radiation by

Western blotting analysis. The band intensity of HP1BP3 protein was measured by western blot and densitometry in both cell lines prior and after ionizing radiation **(Figure 4-13, B)**, which further confirmed our above observation.

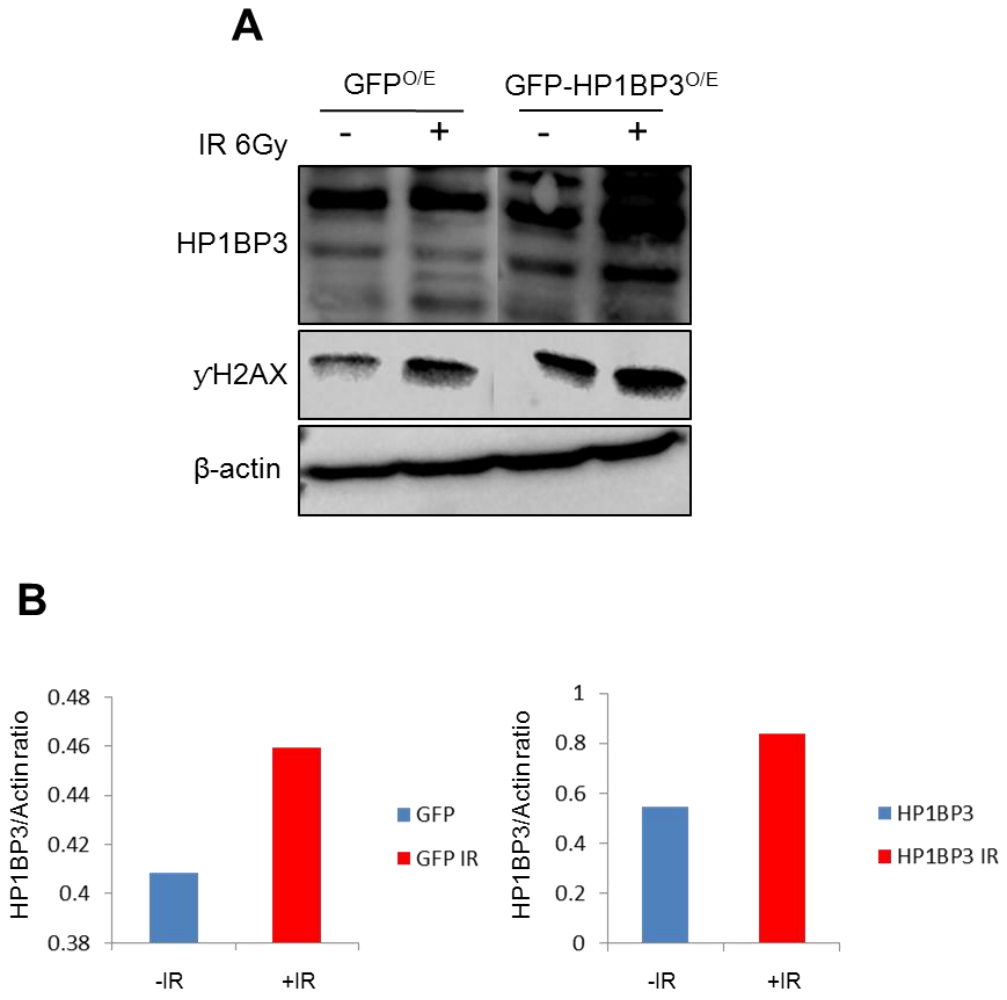


Figure 4-13: IR-induced HP1BP3 protein level in human fibroblasts stably overexpressing EGFP-HP1BP3. Western blotting analysis of protein extracts from experimental and control cell lines. Both populations underwent a single exposure to 6Gy IR. Cells were allowed to recover prior to being lysed for 1 hour post-IR. Total cell proteins (150µg) were immuno-blotted against anti-HP1BP3 and γH2AX, while β-actin was used as protein loading control. **(A, lane 2)** Very marginal alteration in HP1BP3 level was detected; however activation of γH2AX was clearly identified following IR treatment in control cells. **(A, lane 4)** IR induced significant elevation of HP1BP3 as well as γH2AX in fibroblasts overexpressing EGFP-HP1BP3. **(B)** Graphical presentation of densitometry

calculations for HP1BP3 expression versus actin loading control levels measured prior and following ionizing irradiation.

4.2.4 Oxaliplatin-induced phosphorylation of p53 positively correlated with HP1BP3 overexpression in human fibroblasts

To further elucidate ATM/ATR-dependent expression/phosphorylation of HP1BP3, we exposed fibroblasts stably expressing EGFP-HP1BP3 and control cell lines to Oxaliplatin treatment. The bulky mono-DNA adducts, intra-strand and inter-strand cross-links induced by Oxaliplatin unwind DNA double helix to different degrees with further formation of single-strand and/or double-strand DNA breaks (Mehmood, 2014). As a consequence of DNA damage, activation of ATM kinase, one of the major mediators of cell fate determination, occurs (Woynarowski et al., 2000). ATM prevents cells with damaged DNA from entering S-phase through activation of G1/S cell cycle checkpoint and governs this process primarily via the tumour suppressor protein p53 (Weber and Ryan, 2015).

To observe the HP1BP3 behaviour in response to chemotherapeutic drug fibroblasts were exposed to 1µM and 3µM of Oxaliplatin. The kinetics of Oxaliplatin-induced DNA damage was then examined by evaluation of the expression level of p53 that is activated due to Oxaliplatin-induced cell cycle arrest (Woods and Turchi, 2013). It has, however, been reported that Oxaliplatin can induce p53-independent responses in various types of tumours (Chiu, 2009). Thus, Western blotting analysis revealed that Oxaliplatin treatment did not alter the level of p53 in control cells **(Figure 4-14, A)**, however, demonstrated the concentration-dependent increase of p53 in fibroblasts stably expressing EGFP-

HP1BP3 **(Figure 4-14, B)**. Regardless of the difference in p53 expression, HP1BP3 level was induced in both cell lines, experimental and control, as a consequence of Oxaliplatin treatment **(Figure 4-14, A & B)**. Interestingly, the difference in HP1BP3 levels followed 1µM and 3µM of Oxaliplatin exposure was not distinguishable in both cell lines. Nevertheless, due to the overexpression of EGFP-HP1BP3, HP1BP3 expression level after Oxaliplatin treatment was much intensive in experimental cell line compared to the control cells **(Figure 4-14, B)**.

In summary, these data suggest that an increase of HP1BP3 in a concentration-dependent manner in control cells occurred via the p53-independent pathway. In contrast, Oxaliplatin-induced HP1BP3 protein level is accompanied by the elevation of total p53 in human fibroblasts in the presence of stably expressed HP1BP3. It was shown that HP1BP3 maintains heterochromatin integrity by involvement in transcriptional regulation. Moreover, depletion of HP1BP3 accelerated the rate of G1/S transit which leads to enhanced cell proliferation (Dutta et al., 2014a). Thus, our results propose that DNA-damage-induced lesions provoke HP1BP3 expression in order to prevent damaged DNA proceeding into S-phase. Although further investigation is required our observations imply a novel regulatory role of HP1BP3 in cell cycle progression.

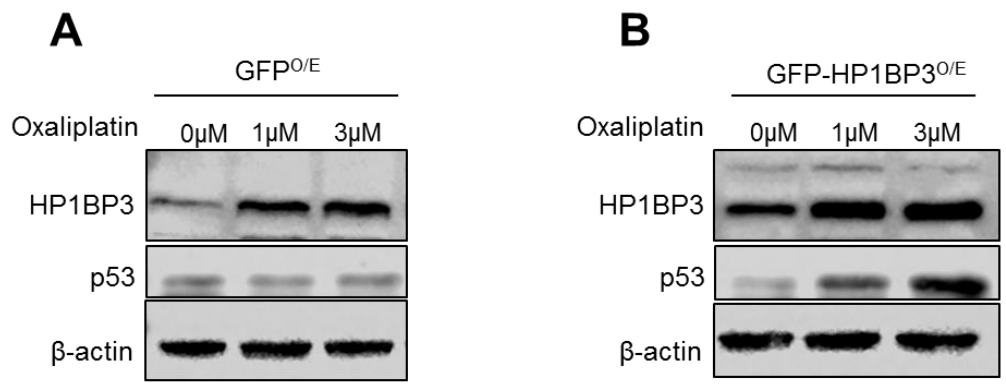


Figure 4-14: Oxaliplatin-induced HP1BP3 protein level in human fibroblasts. Images **(A)** and **(B)** show effect of Oxaliplatin on HP1BP3 expression: elevation of HP1BP3 level in both fibroblasts stably expressing EGFP-HP1BP3 and control cells after applying 1μM and 3μM of Oxaliplatin for 48 hours. Detection of p53 was used as a marker of DNA damage. 150μg of protein lysate was loaded for each cell line. Protein loading levels are monitored by probing for actin.

4.2.5 HP1BP3 is phosphorylated within S/T residues

ATM/ATR downstream substrates often comprise several closely spaced SQ/TQ motifs in their structure that have been determined as SQ/TQ cluster domains (SCDs) (Traven and Heierhorst, 2005). SCDs possess a considerable degree of diversity among proteins. They differ in the position within a protein structure, length and relative densities of SQ/TQ motifs as well as sequence composition (Matsuoka et al., 2007).

Human HP1BP3 contains three S/Q sites. Here, we, therefore, tested a possible ATM/ATR-regulation of phospho-S/Q motifs in HP1BP3 by protein-protein interaction using co-immunoprecipitation (IP) assays.

Initially, an anti-Serine/Threonine antibody was used to immunoprecipitate proteins from cell lysates isolated from fibroblasts stably expressing EGFP-

HP1BP3 and fibroblasts stably expressing EGFP (control cells). 400µg of protein lysates were briefly incubated with 50µl of beads conjugated with anti-Serine/Threonine antibody, separately, overnight (*Chapter 2, section 2.2.4.3*). For evaluation of the IP efficiency, non-immunoprecipitated protein lysates were used (Input). The standard Western blotting procedure involved the SDS-PAGE and immunoblotting (*Chapter 2, section 2.2.4.2*). Both inputs and anti-S/T-IPs samples were initially immunoblotted against anti-Serine/Threonine antibody to determine the quality of IP. As expected a wide range of potentially S/T phosphorylated proteins were detected plus the presence of IgGs specific bands in the immunoprecipitated samples **(Figure 4-15, A)**. The anti-HP1BP3 antibody was then applied on the same blot to explore the binding affinity of HP1BP3 antibody toward phospho-S/T and potentially S/Q-containing peptides. The Western blotting results revealed HP1BP3 protein expression in both HP1PB3 overexpressing and GFP control cells **(Figure 4-15, B)**. These data suggest that HP1BP3 possesses phospho-S/T domains possibly including S/Q motifs, the ATM/ATR phosphorylation consensus sequences **(Figure 4-1)**, and might undergo phosphorylation by ATM/ATR kinases in the genotoxic-stressed-caused conditions.

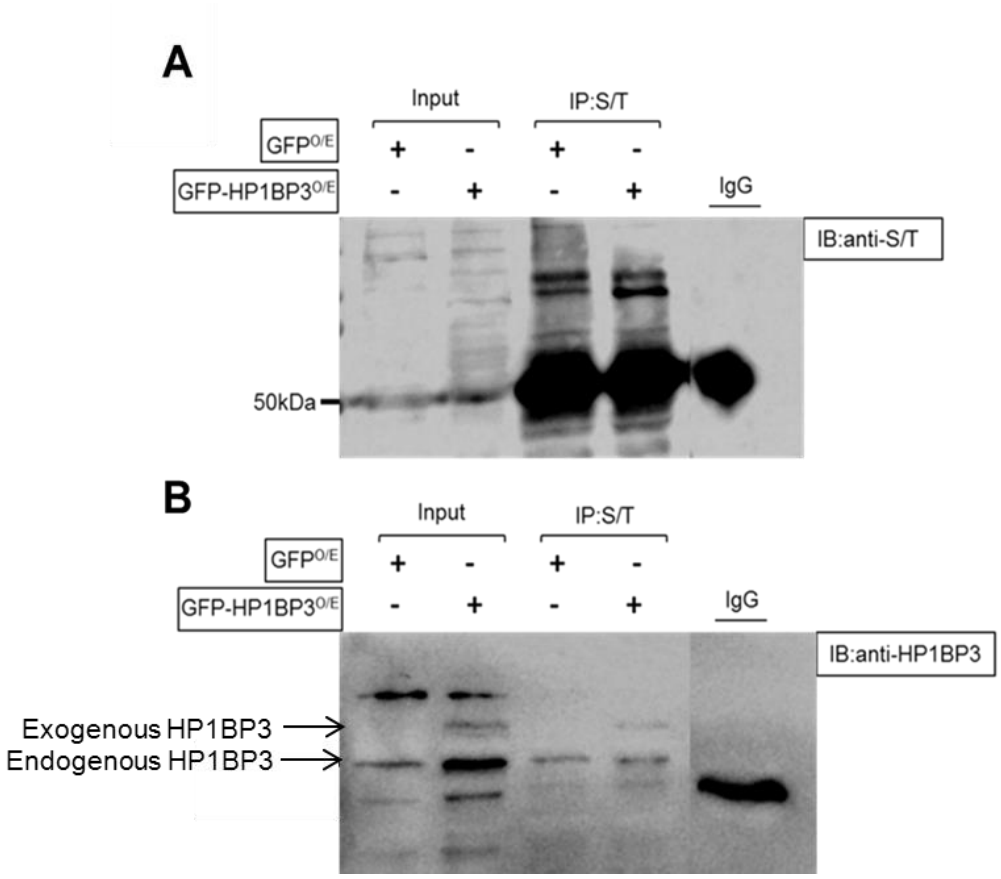


Figure 4-15: Detection of possible phospho-S/T for HP1BP3 protein by immunoprecipiation assay using anti-Serine/Threonine antibody. The protein lysates of fibroblasts stably expressing EGFP-HP1BP3 and control EGFP cell lines were immunoprecipitated with anti-Serine/Threonine antibody-conjugated magnetic beads. Both input and IP samples were immunoblotted with anti-Serine/Threonine **(A)** and anti-HP1BP3 **(B)** antibodies as indicated.

4.2.6 HP1BP3 co-localized with ATM foci in the nucleus

Therefore, due to possible phosphorylation of HP1BP3 by ATM, here we aimed to determine whether two molecules associate with the same structures by using fluorescence microscopy. To define the association between HP1BP3 foci and ATM in human fibroblasts, we applied ATM/ATR inhibitor CGK733. The

results revealed loss of ATM/HP1BP3 colocalisation in the presence of ATM/ATR kinase inhibitor **(Figure 4-16, A)** and the preservation of ATM/HP1BP3 interaction in fibroblasts in the absence of ATM/ATR kinase inhibitor **(Figure 4-16, B)**. The co-localisation was examined in several single-cells that were co-stained and was consistent; loss of colocalisation between HP1BP3 and ATM was observed in the present of inhibitor (data not shown). These data may suggest a functional relationship between ATM and the HP1BP3 within the same structure in the nucleus.

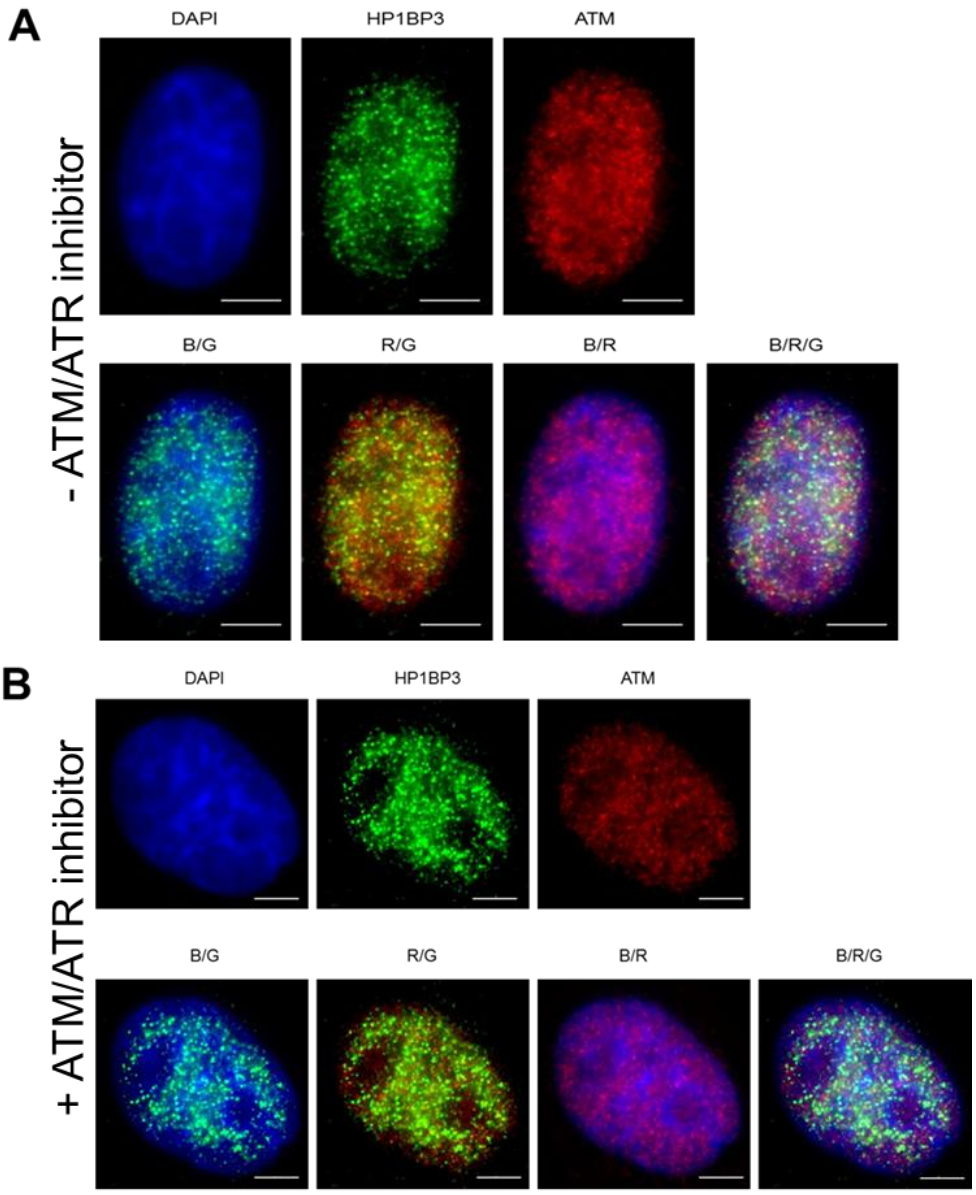


Figure 4-16: Impact of ATM/ATR kinase inhibitor on HP1BP3/ATM colocalisation. The absence of CGK733 shows the strong colocalisation of HP1BP3 and ATM presented by the yellow colour, suggesting endogenous association of these two protein substrates **(A)**.

The green signal (HP1BP3) is relatively exclusive from nucleoli of the cell. Red (ATM) staining demonstrates a similar expression pattern. Colocalisation of green and red is weak in the presence of CGK733 **(B)**.

4.2.7 A potential interaction between ATM and HP1BP3 proteins in the cells treated with Oxaliplatin

We next examined the dependence of possible HP1BP3 phosphorylation on ATM by triggering DNA damage. To explore the potential interaction between ATM protein kinase and HP1BP3, whole cell extracts from Oxaliplatin treated (1µM) and untreated cells were immunoprecipitated using either anti-ATM **(Figure 4-17; lanes 3 & 6)** or anti-HP1BP3 **(Figure 4-17; lanes 1 & 4)** antibodies followed by Western blotting analysis against anti-ATM antibody. The results clearly revealed the interaction of ATM protein in the samples immunoprecipitated using the anti-ATM antibody. More interestingly, a clear band for ATM protein appeared in the Oxaliplatin-treated fibroblasts that were immunoprecipitated using the anti-HP1BP3 antibody **(Figure 4-17, lane 4)**.

The data suggest the possible association of ATM and HP1BP3 proteins in the conditions caused by Oxaliplatin treatment. Collectively, the results further verified the possibility that HP1BP3 contains ATM/ATR phosphorylation SQ/TQ sites that are practically associated with activated form of ATM.

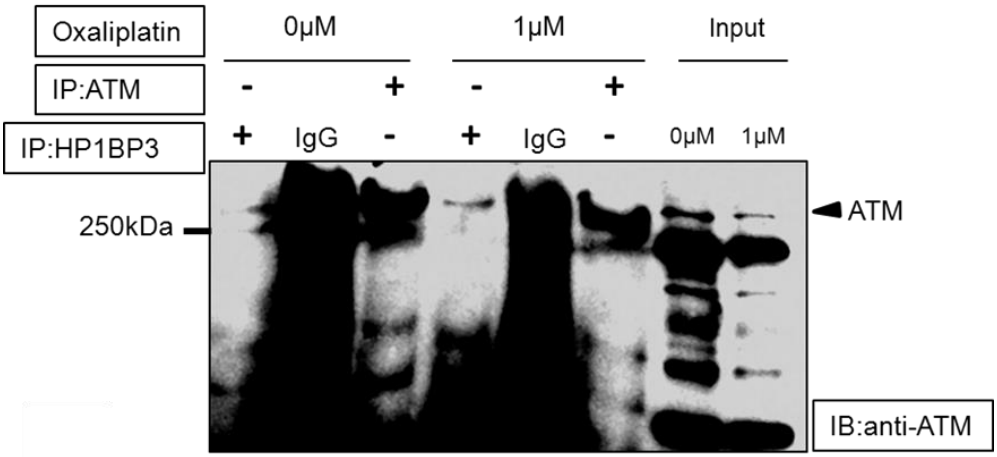


Figure 4-17: A potential interaction between ATM and HP1BP3 in Oxaliplatin treated fibroblasts. The fibroblasts stably expressing EGFP-HP1BP3 and control cell lines were exposed to 1μM of Oxaliplatin for 24 hours. The harvested protein lysates were immunoprecipitated with anti-HP1BP3 (Lanes 1, 4) and anti-ATM (Lanes 3, 6) conjugated magnetic beads, respectively, and were immunoblotted with anti-ATM antibody, as indicated.

4.2.8 Site-directed mutagenesis for replacement of Ser-Gln (SQ) with Ala-Ala (AA) in human HP1BP3 protein

HP1BP3 contains three SQ motifs **(Figure 4-1)**, potential phosphorylation sites for ATM and ATR kinases. By applying various DNA-damaging agents, we demonstrated induction of HP1BP3 in response to ATM/ATR activation. Therefore, to further verify ATM/ATR-dependent modulation of HP1BP3, substitution of SQ motif located at residues 142-143 to AA sequence was initiated. Thus, to facilitate mutation of SQ mutation in full-length HP1BP3, initially the generation of HP1BP3-D0-AA construct was planned. By using the

specifically designed primers **(Table 4-1)** and standard a PCR protocol the mutated sequence encompassing AA was produced **(Figure 4-18)**.

Table 4-1: Primer sequences used to amplify human HP1BP3-D0-AA cDNA. Restriction enzyme sites within primers are underlined. The core primer sequences are highlighted in grey. The mutated site in the reverse primer is highlighted and underlined in red.

Primer Use	Primer Sequence 5'-3'	Restriction Site
pEGFP-C2-HP1BP3-AA	Forward AT *CTCGAG* C ATGGCGACTGATACGTC	*XhoI*
	Reverse AA *GGGCCC* TGGCTAGAGCTGCGGCAGAAAGGGTAG	*ApaI*

The generated PCR product was digested with *ApaI/XhoI* restriction enzymes and subsequently cloned into the pEGFP-C2 backbone vector to produce a pEGFP-C2-HP1BP3-D0-AA construct **(Figure 4-18)**.

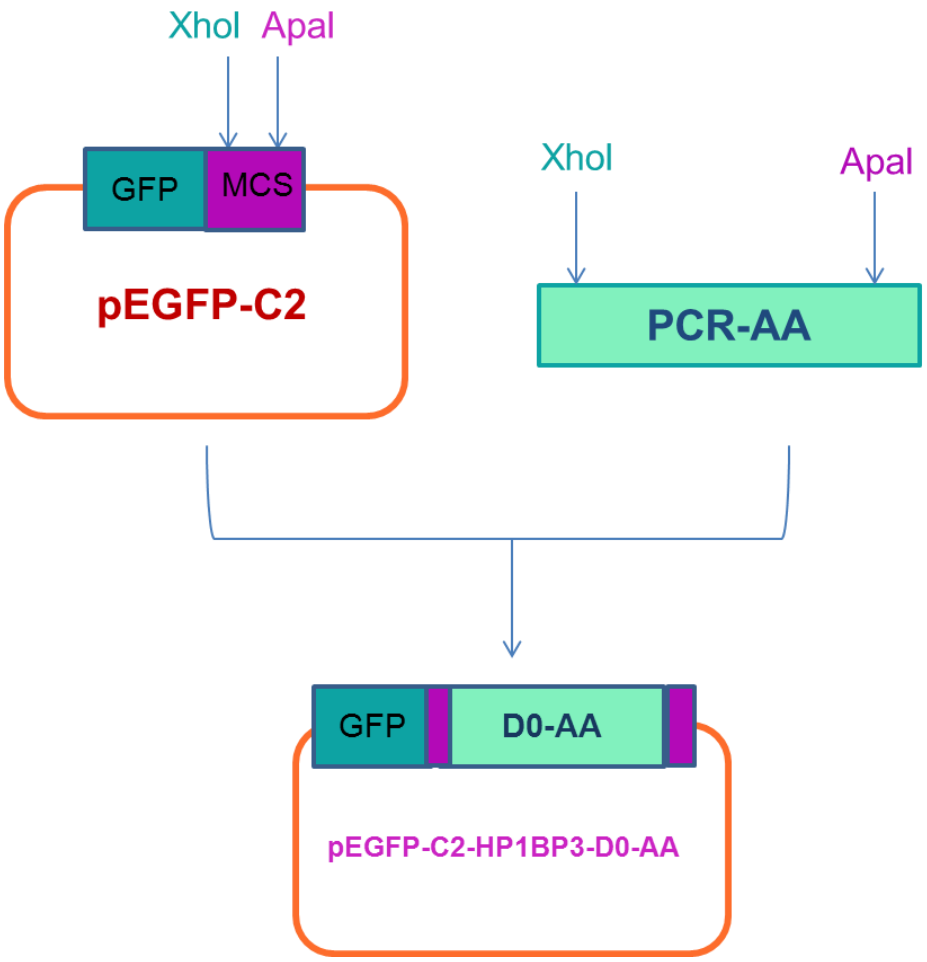


Figure 4-18: Schematic representation of cloning strategy for pEGFP-C2-HP1BP3-D0-AA plasmid. The designed PCR product of *HP1BP3-D0-AA* was ligated into a pEGFP-C2 plasmid vector to generate *pEGFP-C2-HP1BP3-D0-AA* cDNA mutated at SQ motif located at the residues 142-143.

Successful ligation of HP1BP3-D0-AA cDNA fragment was confirmed by restriction enzyme digestion analysis using *ApaI* with a single cut position at ~441bp of the *HP1BP3* coding region **(Figure 4-19)**.

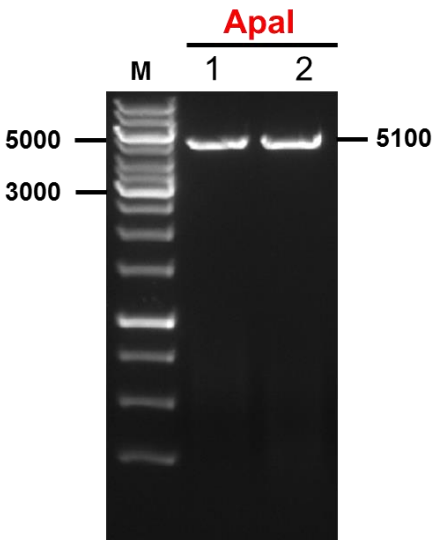


Figure 4-19: Validation of pEGFP-C2-HP1BP3-D0-AA by enzymatic digestion analysis. Both pEGFP-C2-HP1BP3-D0 (lane 1) and pEGFP-C2-HP1BP3-D0-AA (lane 2) were digested with *ApaI* restriction enzyme with a single cut at position ~441bp of the *HP1BP3* coding region. The efficiency of the digestion and linearization of the DNAs was confirmed by running 1 µl of the digested DNA on 1% agarose gel as shown. *M* denotes a 1Kb DNA Hyper ladder in bp (BioLabs).

Furthermore, DNA sequencing analysis confirmed AA point-mutation in the generated construct **(Figure 4-20)**.

```
D0-AA   TCGAGTGAGGCAGAGCAGCCAAAGGGGGAACCTGAGAATGAAGAGAAGGAAGAAAATAAG  306
D0      TCGAGTGAGGCAGAGCAGCCAAAGGGGGAACCTGAGAATGAAGAGAAGGAAGAAAATAAG  306
        ************************************************************

D0-AA   TCTTCTGAGGAAACCAAAAAGGATGAGAAAGATCAGTCTAAAGAAAAGGAGAAGAAAGTG  366
D0      TCTTCTGAGGAAACCAAAAAGGATGAGAAAGATCAGTCTAAAGAAAAGGAGAAGAAAGTG  366
        ************************************************************

D0-AA   AAAAAAACAATTCCTTCCTGGGCTACCCTTTCTGCC-GC-AGCTCTAGCCAGGGCCC    421
D0      AAAAAAACAATTCCTTCCTGGGCTACCCTTTCTGCCAGCCAGCT--AGCCAGGGCCC    421
        ***********************************************************
```

Figure 4-20: Alignment of D0 and D0-AA sequences. Boxed and red area depicts the successful mutation of SQ motif in pEGFP-C2-HP1BP3-D0-AA plasmid.

To construct full-length HP1BP3 with a mutated AA motif, the D0-AA sequence was excised from a pEGFP-C2-HP1BP3-D0-AA plasmid with *ApaI/XhoI* restriction enzymes. *ApaI/SacII* restriction enzymes were used for excising the second fragment from pEGFP-C2-HP1BP3-L **(Figure 4-21)**.

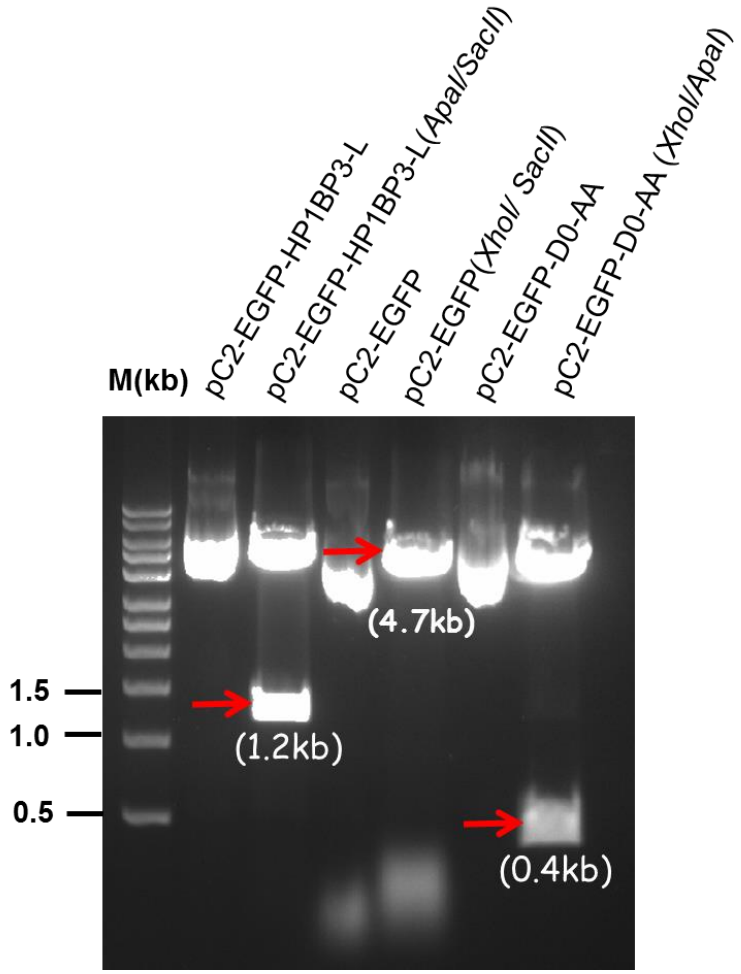


Figure 4-21: Restriction enzyme digestion to generate pEGFP-C2-HP1BP3-L-AA cDNA. pEGFP-C2-HP1BP3-L (lane 2) and pEGFP-C2-HP1BP3-D0-AA (lane 6) were digested with (*ApaI/SacII*) and (*XhoI/ApaI*) restriction enzymes, respectively. The backbone vector pEGFP-C2 was linearized with (***XhoI****/SacII).* The digested DNA fragments were run on 1% agarose gel and depicted by red arrows. Bands were cut from the gel, purified and ligated using T4 ligase. *M* denotes a 1Kb DNA ladder in kb (BioLabs).

These DNA fragments were sub-cloned into pEGFP-C2 backbone vector as illustrated **(Figure 4-22)**.

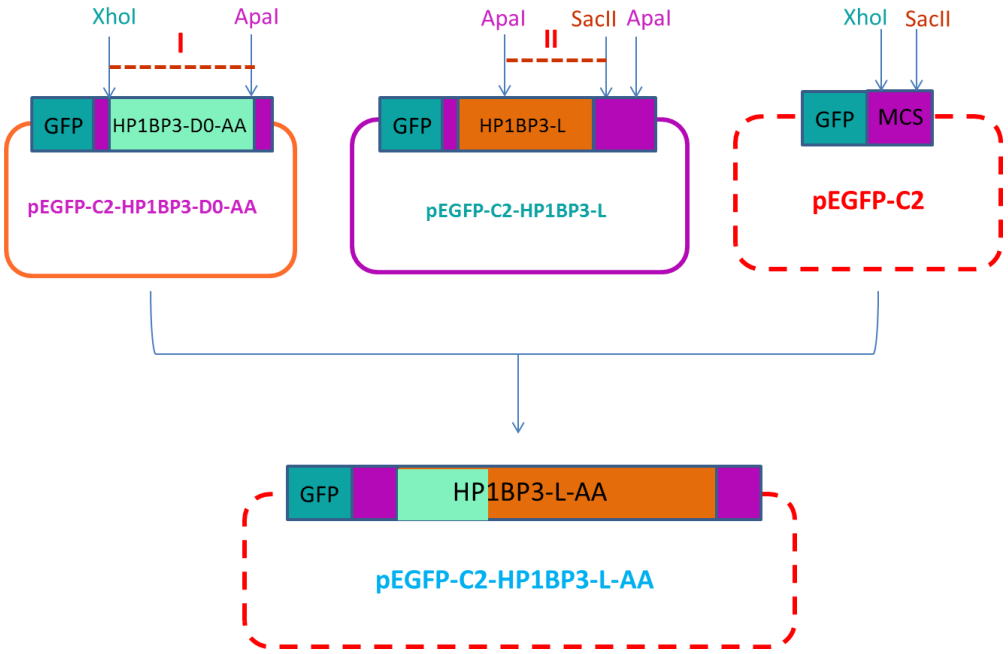


Figure 4-22: Cloning strategy for pEGFP-C2-HP1BP3-L-AA plasmid. Two different fragments were excised from pEGFP-C2-HP1BP3-D0-AA (*XhoI/ApaI*) **and** pEGFP-C2-HP1BP3-L (*ApaI/SacII*) plasmid**s, respectively, and were sub-cloned into the** pEGFP-C2 backbone vector cut by ***XhoI****/SacII* restriction enzymes to construct pEGFP-C2-HP1BP3-L-AA cDNA.

The successful construction of pEGFP-C2-HP1BP3-L-AA cDNA into the vector was examined by restriction enzyme digestion analysis using *ApaI* with restriction site located within MCS region at ~1390 bp position of the backbone vector pEGFP-C2 and at ~441 bp of the HP1BP3 coding region, respectively. Therefore, the digestion of pEGFP-C2-HP1BP3-L with *ApaI* released two DNA fragments for both pEGFP-C2-HP1BP3-L and pEGFP-C2-HP1BP3-L-AA corresponding to 5.1kb and 1.2kb as expected **(Figure 4-23)**.

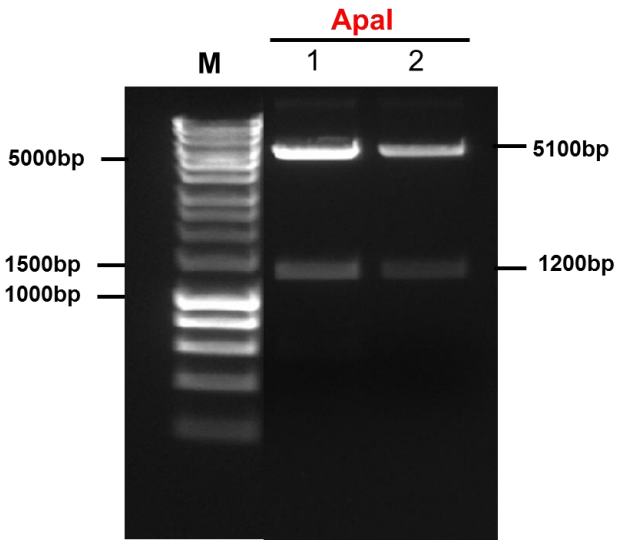


Figure 4-23: Validation of pEGFP-C2-HP1BP3-L-AA by enzymatic digestion analysis. Both pEGFP-C2-HP1BP3-L (control) (lane 1) and pEGFP-C2-HP1BP3-L-AA (lane 2) were digested with *ApaI* restriction enzyme with two recognition sites; at position ~1390 bp within MCS region of the backbone vector pEGFP-C2 and at ~441 bp of the HP1BP3 coding region, respectively. Therefore, the digestion of pEGFP-C2-HP1BP3-L with *ApaI* released two DNA fragments corresponding to 5.1kb and 1.2kb, as expected. *M* denotes a 1Kb DNA Hyper ladder in bp (BioLabs).

Furthermore, the mutation was analysed by automated DNA sequencing **(Figure 4-24)**.

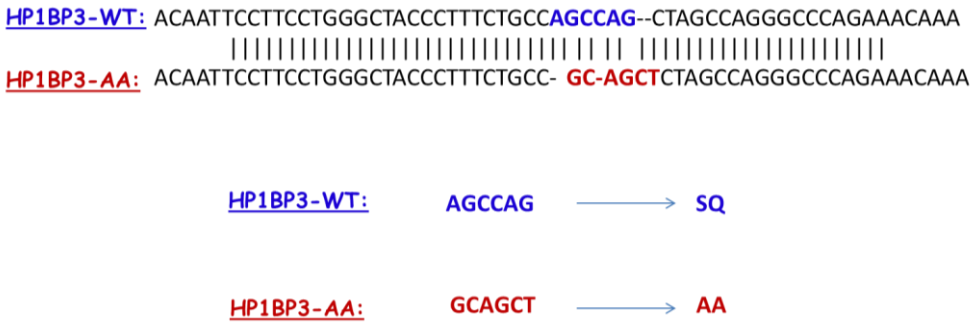


Figure 4-24: DNA sequencing result of pEGFP-C2-HP1BP3-L-AA. The original SQ sequence is shown in blue and the mutated ATM/ATR motif in red.

4.2.9 Effect of site-directed mutagenesis on functional behaviour of HP1BP3

To evaluate the significance of ATM/ATR putative motif on HP1BP3 protein response to DNA damaging agents, fibroblasts were transfected transiently with the constructed EGFP-HP1BP3-AA plasmid and exposed to 1μM of Oxaliplatin. Fibroblasts overexpressing EGFP-HP1BP3-WT were used as a control. By monitoring γH2AX, we concluded the effectiveness of the applied treatment. The level of γH2AX was elevated in both controls as well as experimental cell lines in agreement with previously reported results. Interestingly, application of chemotherapeutic drug led to slight induction of both mutated and wild-type forms of HP1BP3 **(Figure 4-25, A)**. The band intensity of HP1BP3 protein was measured by western blot and densitometry in both cell lines prior and after Oxaliplatin treatment **(Figure 4-25, B)**. These data suggest that mutation of single S→A in HP1BP3 is not sufficient to cause a change of HP1BP3 protein response to Oxaliplatin DNA-damage agent.

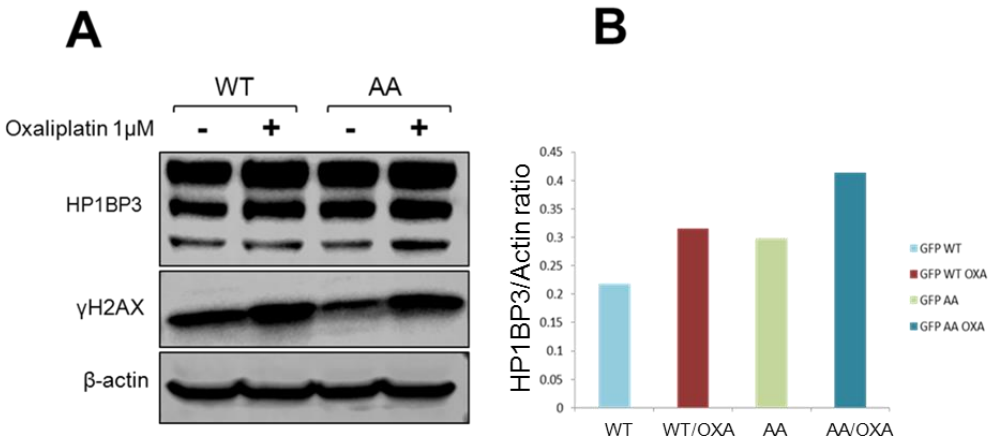


Figure 4-25: Detection of HP1BP3-AA to Oxaliplatin DNA-damage agent. (A) Human fibroblasts transfected with EGFP-HP1BP3-AA and EGFP-HP1BP3 wild-type plasmids (control) and their expression pattern is analysed in response to 1μM of Oxaliplatin. 150μg of protein lysate was loaded per each

cell line. Protein loading levels are monitored by probing for actin. **(B)** Graphical presentation of densitometry calculations for HP1BP3 expression versus actin loading control levels prior and following Oxaliplatin treatment.

4.3 DISCUSSION

HP1BP3 is a recently characterized nuclear protein that is intimately involved in chromatin dynamics. Indeed, recent studies demonstrate that HP1BP3 exerts a range of essential roles through maintenance of heterochromatin integrity (Dutta et al., 2014a). Originally discovered as a binding protein of heterochromatin protein HP1(Hayashihara et al., 2010), HP1BP3 has also been reported recently as a ubiquitous histone H1-like nuclear protein (Garfinkel et al., 2015). In addition, the results revealed the contribution of HP1BP3 in tumorigenesis and showed that HP1BP3 overexpression leads to increased tumour viability, radio- and chemo-resistance (Dutta et al., 2014b).

With regard to structural features and phosphorylation sites of the HP1BP3 protein, we determined the presence of three SQ motifs, consensus sequences of phosphorylation by ATM or ATR kinases, suggesting that HP1BP3 protein is a potential downstream substrate of AMT/ATR checkpoint kinases. However, there has not been any practical evidence that HP1BP3 can be phosphorylated in response to cellular stress responses. The presence of a consensus ATM and ATR phosphorylation motif on the HP1BP3 directed our attention and efforts to the investigation of ATM/ATR-dependent phosphorylation of HP1BP3 in stress conditions using human fibroblasts. To achieve the determined goal, we have

triggered the DNA damage signalling pathway by applying various DNA-damaging agents.

Initially, fibroblasts were exposed to UV treatment **(Figure 4-4)**. The data obtained demonstrated an elevation in the expression level of HP1BP3 in UV-treated cells as a result of ATM/ATR signalling pathway activation. Ataxia-telangiectasia mutated (ATM) plays a key role in initiating the collective response to double-strand DNA break (DSB) (Goodarzi et al., 2008, Gorgoulis et al., 2005). Thus, to reveal the functional interaction of HP1BP3 and ATM, HP1BP3 stable cell lines, alongside with control cell lines, were exposed to ionizing radiation and Oxaliplatin treatment **(Figures 4-13 & 4-14)**. The results verified that activation of ATM signalling pathway induces the expression of HP1BP3.

In order to validate the functionality of the DNA damage system, endogenous p53 and γH2AX were detected with appropriate antibodies. According to the recent evidence, phosphorylation of H2AX occurs not only in response to DNA damage but might be associated with cell cycle progression. Thus, an increase of H2AX level was observed when cells enter M phase (Tu et al., 2013). Recent study reports that HP1BP3 was identified as a novel regulator of cell cycle progression (Dutta et al., 2014a). This fact might possibly explain the induction of yH2AX in the HP1BP3 overexpressing cells; while, HP1BP3 displayed dynamic interactions with heterochromatin during interphase progression (Dutta et al., 2014a).

In addition, according to the previous studies, ATM kinase is considered a dominant physiological mediator of p53 phosphorylation (Banin et al., 1998). The activated ATM molecule contributes to the p53 stabilization primarily by

phosphorylation on Serine15. Also, ATM rescues p53 by phosphorylating MDM2 at Serine 395, thereby causing degradation of this negative regulator of p53 (Gannon et al., 2012). Moreover, through phosphorylation of checkpoint kinases Chk1 and Chk2, which in turn phosphorylate p53 at Serine20, ATM indirectly contributes for further stabilization of p53 (Shieh et al., 2000). Thus, DNA damage response initiates p53 dependent pathways and provokes cell cycle arrest at G1 and G2 phases where tumour suppressor p53 is responsible for activation of apoptosis during excessive DNA damage (Farmer et al., 2005). According to recent evidence, HP1BP3-mediated heterochromatinization leads to transcriptional reprogramming that prevents cellular growth by G0-G1 arrest during hypoxia and thus contributes to the increased cell survivability through reduction of apoptotic cell death (Dutta et al., 2014b).

Next, we examined the availability of predicted evolutionary conserved SQ motifs which are potential phosphorylation sites for ATM/ATR kinases. Thus, immunoprecipitation-coupled immunoblotting by using anti-p-S/T and anti-HP1BP3 antibodies, respectively, detected both exogenous and endogenous expression of HP1BP3 in fibroblasts stably expressing the EGFP-HP1BP3 protein (**Figure 4-15)**.

We further defined whether these SQ motifs unique to HP1BP3 are phosphorylated specifically by ATM protein kinase in response to Oxaliplatin treatment. Remarkably, immunoprecipitation assay showed the physical interaction of HP1BP3 and ATM in Oxaliplatin-stressed conditions in human fibroblasts **(Figure 4-17)**. This potentially indicates a mechanistic link between the DNA damage response pathway and induction of HP1BP3 via its SQ-

phosphorylation by ATM kinase. Using site-directed mutagenesis and PCR-based strategy, we generated and examined if SQ at site position142-143 phosphorylated by ATM would influence on ATM/HP1BP3 response to Oxaliplatin. While in mutant HP1BP3 expressing cells lower levels of γ-H2AX were detected, there was no a significant effect on HP1BP3 protein level (**Figure 4-25, A**). We concluded that, in order to achieve the complete abrogation of ATM-dependent phosphorylation of HP1BP3, the application of site-directed mutagenesis for the remaining two SQ motifs in HP1BP3 protein is essential.

Collectively, our findings discovered the unknown functional relation between ATM/ATR and HP1BP3. ATM or ATR is required for genotoxic-stress-induced phosphorylation of HP1BP3. Although the above data provide valuable insight into the mechanisms by which HP1BP3 is involved in the DNA damage activation, further examination is required in order to investigate the ATM/ATR phosphorylation specificity of HP1BP3. Thus, the lack of phospho-specific HP1BP3 antibody restricts the direct detection of ATM/ATR activation on HP1BP3 phosphorylation. Nevertheless, these obtained discoveries may shed some light on possible implications of HP1BP3 in DNA damage signalling pathway through ATM/ATR phosphorylation and its contribution to DNA repair complexity.

Furthermore, DNA-damaging agents have a long history of use in cancer chemotherapy; therefore, ATM/HP1BP3 relationship will probably be more significant in cancer biology and therapy. Hence, we have expanded our observation to cancer cells by assessing the effects of FBXW7 deficiency on HP1BP3 modulation via ATM/ATR-dependent regulation within the following chapters.

CHAPTER 5

FBXW7-Mediated Degradation of HP1BP3 is antagonized by ATM/ATR Activation in Human HCT116 Colon Carcinoma Cells

5.1 BRIEF INTRODUCTION

Protein degradation by the ubiquitin-proteasome system (UPS) orchestrates a range of basic cellular functions such as cell division, cell cycle progression, cell growth and differentiation (Ciechanover, 1998). A significant body of experimental evidence demonstrates that dysregulation of ubiquitin-dependent proteolysis results in uncontrolled cell proliferation, genetic instability, and ultimately tumorigenesis. Remarkably, the most commonly mutated UPS component in human cancers is the ubiquitin ligase FBXW7 (F-box and WD repeat domain containing 7, E3 ubiquitin protein ligase, also known Fbw7, CDC4, sel10), which exerts a suppressive role by targeting some key human oncoproteins for degradation in the normal cellular environment (Crusio et al., 2010, Welcker and Clurman, 2008). Indeed, in a wide spectrum of human tumours including human colorectal cancer (CRC), FBXW7 is functionally inactivated by altered expression, genetic mutation, and possibly other mechanisms causing in impaired regulation of target substrates, leading to increased proliferation, genetic instability, and consequently triggering tumorigenesis (Tan et al., 2008).

Recent studies in Dr Nateri's laboratory by using a modified yeast 2-hybrid reverse Ras-recruitment system (rRRS) and intestinal crypt proteomic profile assays (Li & Babaei-Jadidi, submitted for publication) identified that HP1B3 refers to one of the FBXW7 interacting proteins. Also, further work in Dr Nateri's laboratory indicated that HP1BP3 degradation by the E3 ubiquitin ligase FBXW7 regulates cellular growth and neoplasia of human colorectal cancer cells (Abuzinadah et al., submitted for publication).

As HP1BP3 is targeted by the FBXW7 tumour-suppressor gene for the ubiquitin-mediated degradation, here, we studied the complex system of interaction between FBXW7 and HP1BP3 proteins in DNA-damage signalling pathway. Recent studies have shown that genetic inactivation of FBXW7 in colorectal cell lines was associated with chromosomal instability, a hallmark of cancer (Rajagopalan et al., 2004). Furthermore, in chapter 4 we showed that the HP1BP3 level increased in response to the DNA-damaging agents via the interaction and coordination with ATM kinase in fibroblasts. In the current chapter, we examined the possibility of FBXW7 association with the HP1BP3 in response to DNA- damaging agents via ATM/ATR kinases in CRC cells. To achieve our goals, we used the human CRC HCT116 cell lines harbouring and/or lacking of FBXW7 ($HCT116^{FBXW7(+/+)}$ *vs.* $HCT116^{FBXW7(-/-)}$ cells). Interestingly, we observed that HP1BP3 and ATM/ATR coordination also occur in colon cancer $HCT116^{FBXW7(+/+)}$ cells, and FBXW7-mediated degradation of HP1BP3 is impaired during DNA damage response in the presence of FBXW7. In contrast, cells deficient for FBXW7 ($HCT116^{FBXW7(-/-)}$ cells) exhibited a reduced level of HP1BP3 protein in response to DNA-damaging agents.

5.2 RESULTS

5.2.1 Negative correlation of HP1BP3 protein expression and ATM/ATR kinase activation in the HCT116$^{FBXW7\ (-/-)}$ CRC cell line

To explore the interplay between HP1BP3 and ATM/ATR protein kinases via DNA damaging agents, in chapter 4, we applied and examined a various DNA-damaging agents on human fibroblasts. The results clearly demonstrated a positive coordination of HP1BP3 in response to activation of DNA damage signalling pathway via interaction with ATM (*Chapter 4*). Furthermore, our lab and others previously showed that HP1BP3 is targeted by FBXW7 for degradation and FBXW7 inactivation causes genomic instability in colon cancer cells (Rajagopalan et al., 2004).

Thus, in order to determine whether HP1BP3 expression is influenced by FBXW7 in ATR/ATM-phosphorylation event, initially HCT116$^{FBXW7\ (+/+)}$ and HCT116$^{FBXW7\ (-/-)}$ CRC cell lines were exposed to UV-irradiation. The phosphorylation of H2AX histone protein (γ-H2AX) was used as a biomarker for detecting a genotoxic insult caused by UV (Ibuki and Toyooka, 2015, Toyooka et al., 2011, Mistrik et al., 2009, Osipov et al., 2015). Western blotting result showed an induction of γ-H2AX in both cell lines after UV treatment **(Figure 5-1, A)**. Interestingly, the level of γ-H2AX even prior to UV exposure was detected to be higher in HCT116 cell lines with inactivated FBXW7 compared to the γ-H2AX level in wildtype HCT116 **(Figure 5-1, A)**. In agreement with recent reports, the γ-H2AX level was elevated markedly in HCT116$^{FBXW7\ (-/-)}$ compared with HCT116$^{FBXW7\ (+/+)}$ cells following UV-irradiation (Zhang et al., 2016). It was shown that FBXW7 depletion leads to the

impaired NHEJ repair. Thus, the novel role of FBXW7 in the modulation of downstream substrates through the involvement in DNA damage response was addressed (Zhang et al., 2016).

Furthermore, consistent with previous data in Dr Nateri's laboratory (Abuzinadah et al.,), Western blotting analysis revealed that expression of HP1BP3 protein was significantly increased, also in the absence of UV light, in FBXW7-deleted HCT116 cells compared to the wildtype HCT116 **(Figure 5-1, A)**. Thus, the ablation of FBXW7 led to the elevation of HP1BP3 in $HCT116^{FBXW7\ (-/-)}$. Therefore, the obtained result confirms previously reported by our lab data that HP1BP3 refers to a target substrate of FBXW7 for the degradation and that the lack of FBXW7 led to the accumulation of HP1BP3 protein level. Furthermore, according to the current results **(Figure 5-1, A)**, the induction of HP1BP3 is associated with the elevation of γ-H2AX. A similar response was observed in human fibroblasts stably expressing GFP-HP1BP3 where the level of γ-H2AX was higher compared to the control cells (*Chapter 4, section 4.2.3*).

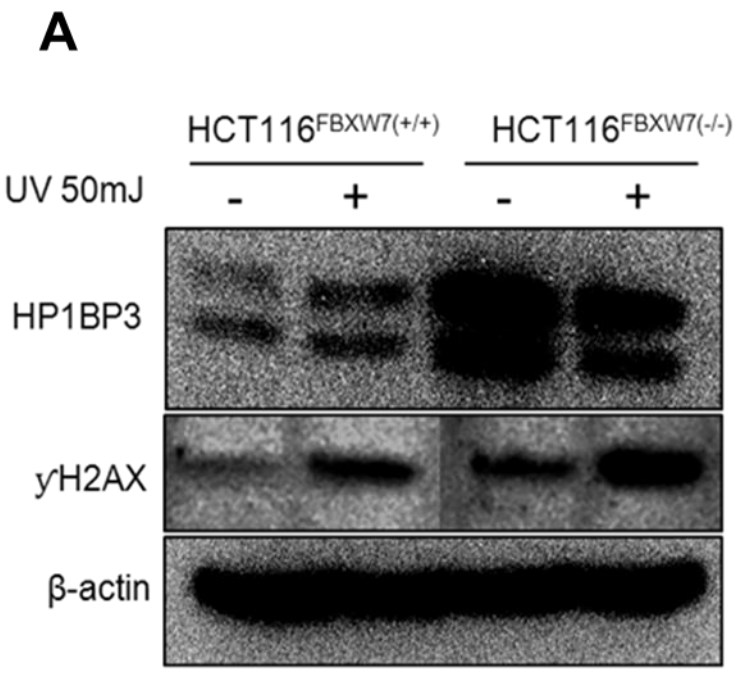
Remarkably, UV light led to the stabilisation of HP1BP3 in the HCT116 harbouring wild type of FBXW7 **(Figure 5-1, A)**, whereas, the FBXW7-deleted cells showed the substantial reduction of HP1BP3 in $HCT116^{FBXW7\ (-/-)}$ followed UV irradiation **(Figure 5-1, A)**.

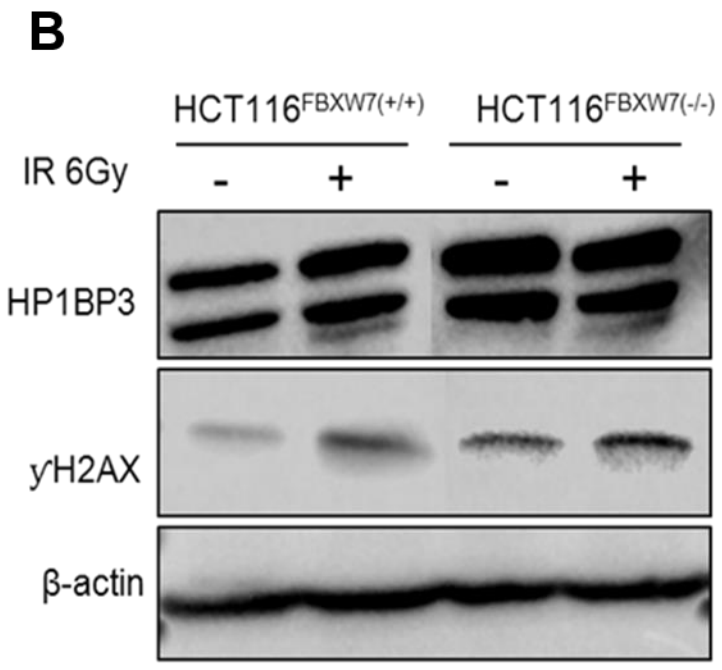
The mechanism(s) underlying the DNA-damage induced degradation of accumulated HP1BP3 in $HCT116^{FBXW7\ (-/-)}$ remains unclear and requires further studies. However, a number of recent works have found that SCF^{FBXW7} ubiquitination is regulated by other protein substrates that positively or

negatively contribute to the FBXW7 function (Min et al., 2012, Tan et al., 2008, Yeh et al., 2004). For instance, the association of a negative regulator of SCF^{FBXW7} ubiquitination, deubiquitinating enzyme USP28 (ubiquitin-specific protease 28) with c-Myc ensures ubiquitination of the protein within nucleolus and prevents the ubiquitination of c-Myc in the nucleoplasm (Popov et al., 2007b). Interestingly, UV irradiation abolished the USP28-associated ternary complex releasing FBXW7 from USP28 inhibition (Popov et al., 2007a). Thus, genotoxic stress might be considered one of the mechanisms which promote SCF^{FBXW7} ubiquitination activity.

Another possible interpretation of this result could be that HP1BP3 activity in the $HCT116^{FBXW7\ (-/-)}$ cells had already reached its maximal capacity (threshold) and therefore could not be further augmented by UV irradiation and on the contrary underwent degradation by the mechanism which needs to be elucidated.

Furthermore, ionizing radiation was applied as the next DNA damaging agent to prompt DSBs and evaluate HP1BP3 induction's dependence on FBXW7 in the presence of ATM activation in HCT116 CRC cells. Western blotting analysis also revealed that HP1BP3 protein level decreased in FBXW7-depleted $HCT116^{FBXW7\ (-/-)}$ cells after irradiation, whereas wild-type $HCT116^{FBXW7\ (+/+)}$ cells showed increased level of HP1BP3 protein in response to IR **(Figure 5-1, B)**. Nevertheless, the accumulation of γH2AX was observed in both $HCT116^{FBXW7\ (+/+)}$ and $HCT116^{FBXW7\ (-/-)}$ cell lines in response to DNA damage triggered by ionizing radiation **(Figure 5-1, B)**. The data is consistent with above results, both depicting on negative correlation of HP1BP3 and ATR/ATM activation caused by UV and ionization irradiation in $HCT116^{FBXW7\ (-/-)}$ cells.


A
HCT116FBXW7(+/+)
HCT116FBXW7(-/-)
UV 50mJ
-
+
-
+
HP1BP3
γH2AX
β-actin


B
HCT116FBXW7(+/+)
HCT116FBXW7(-/-)
IR 6Gy
-
+
-
+
HP1BP3
γH2AX
β-actin

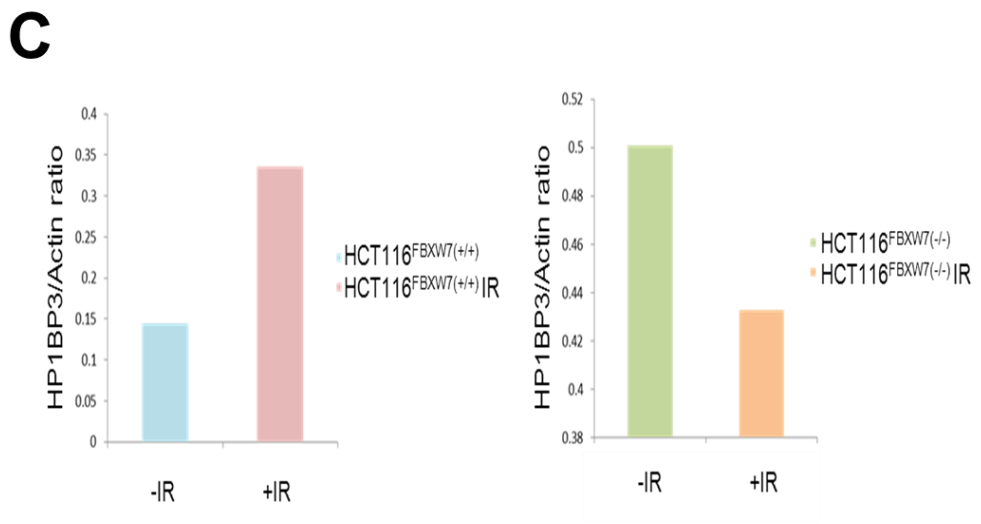


Figure 5-1: Expression of γH2AX and HP1BP3 protein levels in HCT116$^{FBXW7\ (+/+)}$ and HCT116$^{FBXW7\ (-/-)}$ cells before and after UV treatment and ionizing irradiation. (A) HCT116$^{FBXW7\ (+/+)}$ and HCT116$^{FBXW7\ (-/-)}$ cells were exposed to 50mJ of UV and harvested 3 h after treatment for Western blotting analysis. Expression of γH2AX and HP1BP3 was determined using specific antibodies as indicated. **(B)** HCT116$^{FBXW7\ (+/+)}$ and HCT116$^{FBXW7\ (-/-)}$ cells were treated with 6Gy at a low dose rate (0.5Gy/min) and after 1 h post-irradiation incubation underwent lysis for further immunoblotting. The levels of γH2AX and HP1BP3 were detected using their specific antibodies. Protein loading levels were monitored by probing for anti-actin antibody. **(C)** Graphical presentation of densitometry calculations for HP1BP3 expression versus actin loading control levels measured prior and following ionizing irradiation in HCT116$^{FBXW7(+/+)}$ and HCT116$^{FBXW7(-/-)}$ cells. Data are representative at least of two independent experiments.

5.2.2 FBXW7 deficiency induces HP1BP3 expression in HCT116 CRC cells after Oxaliplatin treatment

To further evaluate the expression of HP1BP3 in response to ATM kinase activation in the absence of FBXW7, both HCT116 cells harbouring wild-type and inactivated FBXW7 were treated with two different concentrations of

Oxaliplatin (1 μM and 3 μM), separately, for 3 consecutive days. Western blotting analysis revealed an increase of p53 in HCT116$^{FBXW7\ (-/-)}$ versus wild-type HCT116$^{FBXW7\ (+/+)}$ **(Figure 5-2, A & B)**. This data is in line with recently published data showing that FBXW7 knockout colorectal cell lines exhibit significant cell aneuploidy accompanied by an increase in p53 levels (Bailey et al., 2015). In addition, *in vivo* studies reported that mutations of FBXW7 correlate with polyploidy and aneuploidy where p53 exhibits a defense mechanism by prevention of polyploidization (Bailey et al., 2015). Thus, the excess of HCT116$^{FBXW7\ (-/-)}$ cells necessitates high basal activity of p53 to maintain a relatively typical cell cycle silhouette. Furthermore, it was demonstrated that FBXW7 deficiency does not limit the ability of p53 to respond to DNA damage (Bailey et al., 2015). Thus, activation of wild-type (wt) p53 in response to genotoxic stress caused by chemotherapeutic drug was markedly increased in FBXW7-null HCT116 cells compared to wildtype HCT116 cells **(Figure 5-2, A & B)**.

Applied Oxaliplatin treatment to HCT116 CRC harbouring wild-type FBXW7 provided induction of HP1BP3 protein expression which is consistent with data followed UV exposure and ionizing irradiation **(Figure 5-2, A)**. In contrast to wild-type HCT116$^{FBXW7\ (+/+)}$, Oxaliplatin repressed HP1BP3 protein expression in FBXW7 deficient cells in concentration-dependent manner **(Figure 5-2, B)**. The similar response was observed after UV treatment and IR that led to reduction HP1BP3 as a result of ATM/ATR activation **(Figure 5-1, A&B)**.

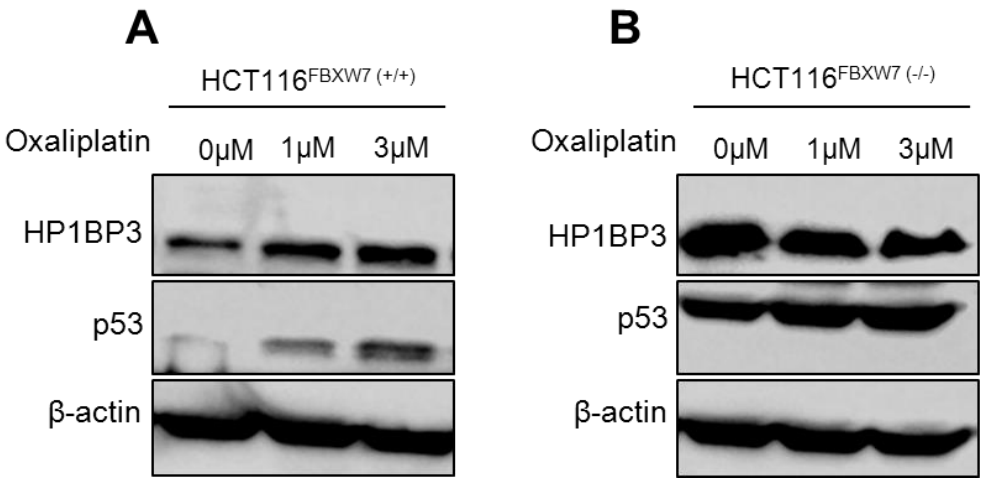


Figure 5-2: The effect of Oxaliplatin on HP1BP3 protein expression in HCT116 CRC cells with wild-type and deficient FBXW7. HCT116$^{FBXW7\ (+/+)}$ and HCT116$^{FBXW7\ (-/-)}$ cells were subjected to immunoblotting with anti-HP1BP3 and anti-p-53 antibodies. Protein loading levels were monitored by probing for actin. **(A)** Western blotting analysis revealed the induction of HP1BP3 as well as total p53 in wild type HCT116 CRC cells after applied Oxaliplatin treatment in concentration-dependent manner. **(B)** Immunoblotting result demonstrated the increase of p53 and decrease of HP1BP3 proteins after exposure of HCT116$^{FBXW7\ (-/-)}$ to Oxaliplatin treatment. Results are representative of at least three independent experiments.

Thus, here we report the direct involvement of FBXW7 in ATM/ATR-dependent regulation of HP1BP3 expression upon radiation- and chemotherapeutic drug-induced DNA damage. **Figure 5-3** demonstrates a schematic for the role of FBXW7 in the functional modulation of HP1BP3in response to ATM/ATR activation.

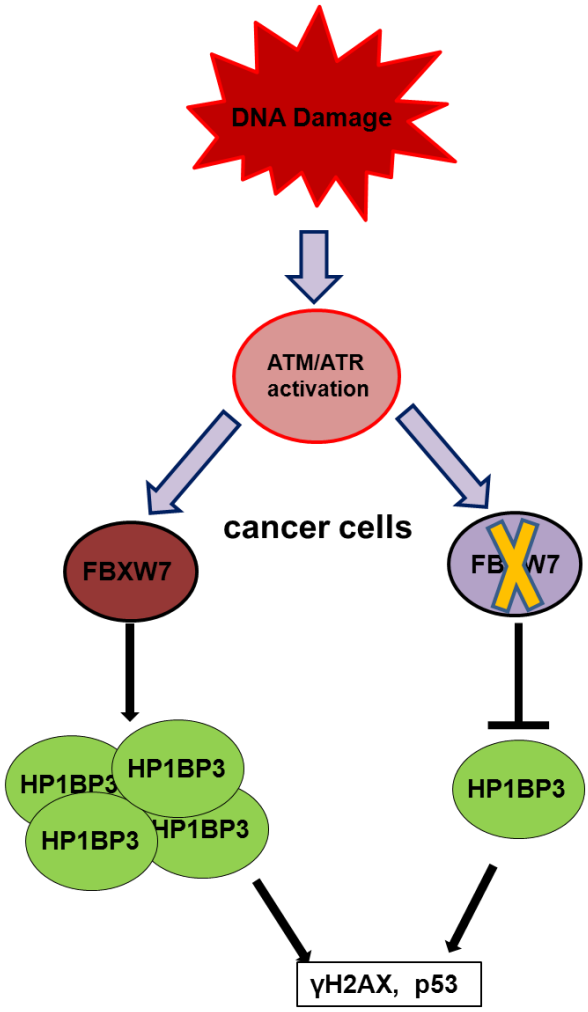


Figure 5-3: The schematic representation of FBXW-dependent recruitment of HP1BP3 in DNA damage response in HCT116 cancer cell lines. FBXW7 promotes stabilization of HP1BP3 in response to ATM/ATR activation. FBXW7 depletion caused HP1BP3 degradation following DNA damage. The recruitment of γH2AX and p53 in DNA damage response pathway occurs\d in both $HCT116^{FBXW7\ (+/+)}$ and $HCT116^{FBXW7\ (-/-)}$ cell lines.

5.2.3 ATM/ATR inhibitor induces HP1BP3 protein expression in wild type HCT116 CRC cells

In the present study we demonstrated the tight correlation of HP1BP3 repression kinetics with the presence of FBXW7 in HCT116 cell lines lacking FBXW7 through activation of DNA damage signalling pathway by applying UV light, ionizing irradiation and Oxaliplatin treatment. Thus, abrogation of FBXW7 abolished HP1BP3 induction in the presence of activated ATM/ATR kinases, proving the essential role of the FBXW7-dependent degradation of HP1BP3. The mechanism is still uncertain. Furthermore, we decided to observe the effect of FBXW7 on reponse of HP1BP3 by inhibition of ATM/ATR kinases in HCT116 CRC cells. To assess the expression level of HP1BP3 by suppression of ATM/ATR kinases, both wildtype HCT116 and FBXW7-null HCT116 cells were treated with 10μmol/L of specific ATM/ATR inhibitor CGK733 for one hour.

By monitoring p53 and γH2AX levels by Western blotting analysis, we concluded the effectiveness of applied compound concentration. ATM/ATR inhibitor CGK733 largely attenuated the H2AX phosphorylation in both experimental and control cells **(Figure 5-4)**. The presence of ATM/ATR inhibitor in both cell lines was manifested by significant reduction of p53 **(Figure 5-4)**.

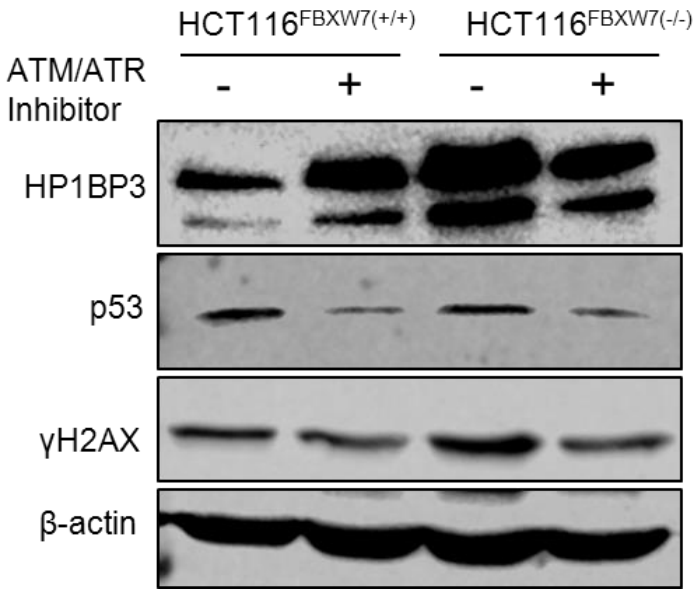


Figure 5-4: The effect of ATM/ATR inhibitor on HP1BP3 expression in HCT116 CRC cells. HCT116$^{FBXW7(+/+)}$ and HCT116$^{FBXW7(-/-)}$ cells were subjected to 10µmol/L of pharmacological ATM/ATR inhibitor for 1 h. Immunoblotting results revealed the elevation of HP1BP3 in wild type HCT116 CRC cells after drug treatment, whereas FBXW7-depleted HCT116 CRC exhibited reduction of HP1BP3 in the presence of ATM/ATR inhibitor. γH2AX protein level decreased in both HCT116$^{FBXW7(+/+)}$ and HCT116$^{FBXW7(-/-)}$ cell lines after applied inhibition of ATM/ATR kinases. Protein loading levels were monitored by probing for actin. Data are representative of at least three independent experiments.

According to the aforementioned results demonstrating induction of HP1BP3 as a result of ATM/ATR activation by triggering DNA damage signalling pathway, it was expected that inhibition of ATM/ATR protein kinases might lead to downregulation of HP1BP3. According to the recent evidence, inhibition of ATM activity by ATM kinase inhibitor KU causes induction of total ATM protein; moreover, this auto regulatory induction of ATM kinase is accompanied by a transient upregulation of p53, its key substrate, in a time-dependent manner.

It was revealed that pATM, as well as p53, showed induction at the 0.5h time point after application of ATM inhibitor followed by reduction of protein signal at 1 and 1.5h post-treatment. Levels of pATM remained lower compared with untreated cells at all time points except 0.5h. However, total ATM and total p53 levels at 1h still showed slightly higher signal in comparison to untreated controls (Khalil et al., 2012c).

In contrast to the published data, we did not observe the higher level of p53 in the treated cells compared to the controls at1h post-treatment. Western blotting analysis revealed reduction of p53 at 1h post-treatment that positively correlates with inhibition of ATM/ATR activity.

Western blotting data determined a notable elevation of HP1BP3 level in wildtype HCT116 in the presence of ATM/ATR pharmacological inhibitor **(Figure 5-4)**. Induction of HP1BP3 in HCT116 cells might be explained by involvement of other kinases in regulation of HP1BP3or ATM may have another kinase independent function, e.g. scaffold protein.

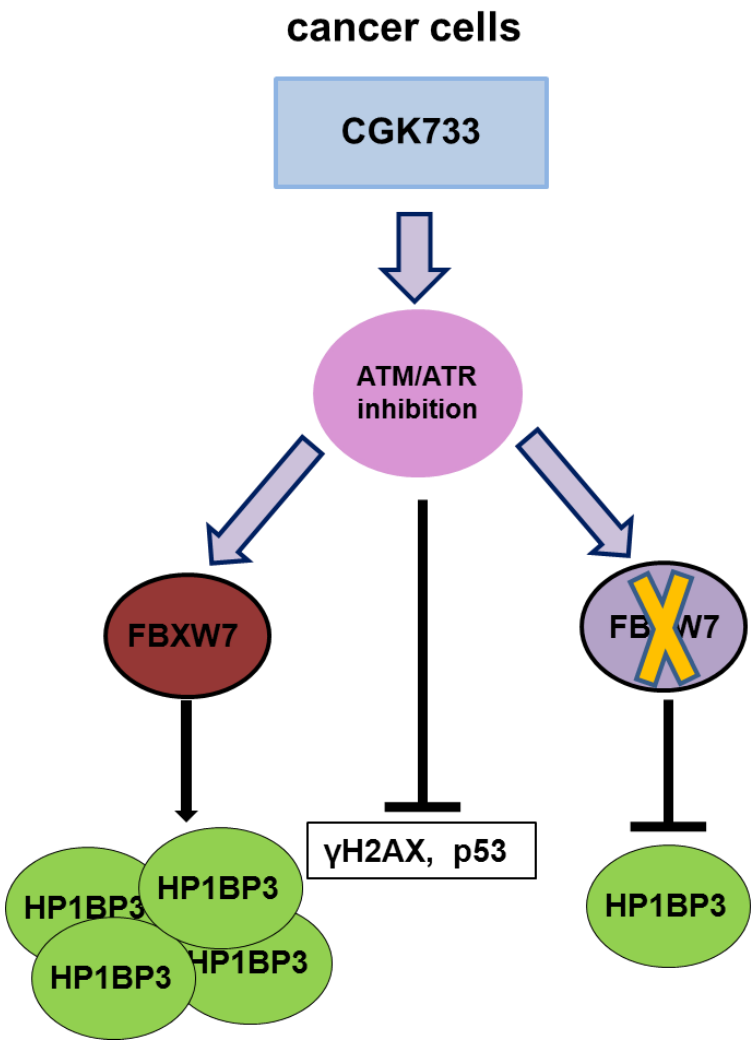


Figure 5-5: The schematic representation of HP1BP3 responses the presence of ATM/ATR pharmacological inhibitor in HCT116 cancer cell lines. Interestingly, FBXW7 promotes accumulation of HP1BP3 in response to ATM/ATR inhibition. FBXW7 depletion led to HP1BP3 reduction following application of ATM/ATR inhibitor. The levels of γH2AX and p53 were downregulated in both HCT116$^{FBXW7\ (+/+)}$ and HCT116$^{FBXW7\ (-/-)}$ cell lines while suppressing the function of ATM/ATR kinases.

Furthermore, we aimed to study formation of HP1BP3 foci by applying ATM/ATR inhibitor CGK733 in wildtype HCT116 cells. The results revealed slight loss of ATM/HP1BP3 colocalisation in the presence of ATM/ATR kinase inhibitor **(Figure 5-6, top panel)** and the conservation of ATM/HP1BP3 interaction in HCT116 in the absence of ATM/ATR kinase inhibitor **(Figure 5-6, low panel)**. This IF data confirms previously reported results obtained from fibroblasts (*Chapter 4, section 4.2.6*) treated with ATM/ATR inhibitor.

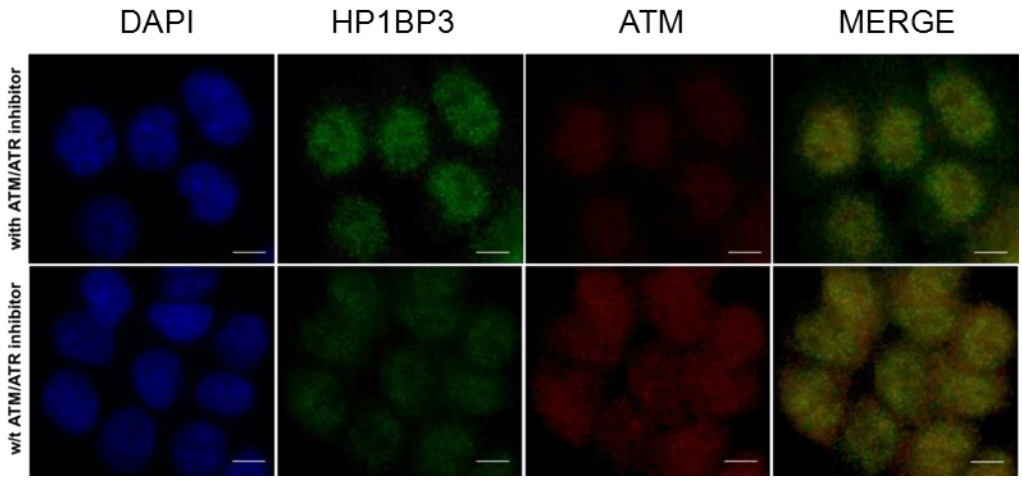


Figure 5-6: Impact of ATM/ATR kinase inhibitor on HP1BP3/ATM colocalisation in HCT116 CRC cells. HCT 116 cells were seeded on coverslips and further underwent exposure with ATM/ATR pharmacological inhibitor treatment for 1h. Co-localisation of HP1BP3 and ATM protein substrates is weak in the presence of CGK733 **(top panel)**. The absence of CGK733 shows the weak co-localisation of HP1BP3 (green) and ATM (red) expressed by slightly distinguishable yellow colour suggesting endogenous association of these two protein substrates **(low panel)**.

5.2.4 The S-Q motif position on 142-143 a.a. of HP1BP3 protein is phosphorylated by ATM *in vivo*

The presence of three putative ATM/ATR consensus phosphorylation motifs (S-Q) within HP1BP3 structure and functional alterations of HP1BP3 mediated by activation of ATM/ATR kinases suggested it was a potential DNA-damage-response protein. In chapter 4, we described the generation of SQ→AA mutant for HP1BP3 (*Chapter 4, section 4.2.8*). However due to lack phospho-specific HP1BP3 antibody it was impossible to directly verify if the S-Q is phosphorylated by ATM/ATR activation. Therefore, to explore whether this Serine is subject to ATM phosphorylation, we transiently transfected HCT116$^{FBXW7\ (+/+)}$ cells with HP1BP3-AA mutant and wild-type plasmid constructs. Thus, we aimed to gain clear interpretation of the requirement of ATM/ATR phosphorylation site (S-Q) on HP1BP3 for presumed interaction with ATM/ATR protein kinases using CRC cells. HCT116$^{FBXW7\ (+/+)}$ cells transfected with HP1BP3-WT were used as control.

Transfected cells were exposed to Oxaliplatin treatment for subsequent initiation and activation of DNA damage. Furthermore, immunoprecipitation (IP) was used to examine whether ATM protein would recognise and bind to S-Q motif on HP1BP3 protein. Thus, harvested cell extracts were immunoprecipitated against anti-ATM antibody followed by immunoblotting against anti-phospho-Serine/Threonine antibody. The results showed that ATM immunoprecipitations revealed efficient binding of wildtype HP1BP3 protein in both Oxaliplatin-containing and Oxaliplatin-free conditions **(Figure 5-7, A)**. In contrast, the interaction of ATM and HP1BP3 was abolished in the cells transfected with mutated S-Q domain **(Figure 5-7, B)**. Current data revealed that direct

association between ATM and HP1BP3 protein substrates occurs via S-Q motif located at residues 142-143 of HP1BP3. However, further study is required to test the role of the remaining two available S-Q motifs in DNA damage response and possible interaction with ATM/ATR.

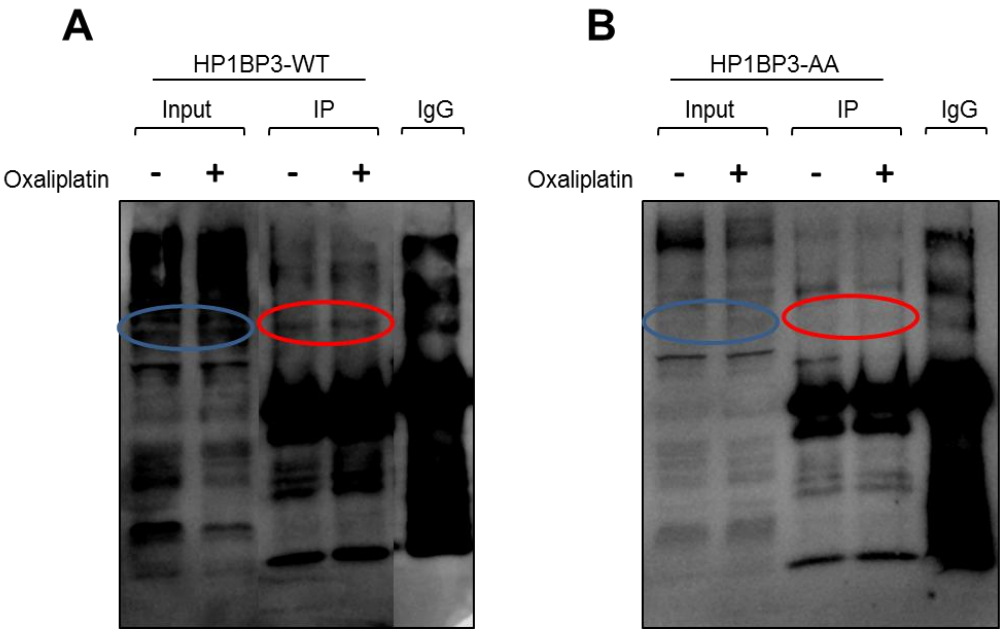


Figure 5-7: The mutated clone of HP1BP3 (AA) lost its physical interaction with ATM kinase due to lack of SQ phosphorylation. HCT116$^{FBXW7\ (+/+)}$ cells were transfected to express HP1BP3-WT and HP1BP3-AA, separately, then treated with 3 μM of Oxaliplatin for 24h. Untreated cells were used as controls. The protein lysate from both experimental and control cell lines was immunoprecipitated with anti-ATM-conjugated magnetic beads. Both input and IP samples were immunoblotted with anti-phospho-Serine/Threonine antibody as indicated. Western blot analysis revealed the interaction of wildtype HP1BP3 with ATM kinase **(A)** and failed to identify an association between these two protein substrates in the absence of S-Q domain on HP1BP3 **(B)**.

5.2.5 Impact of HP1BP3-AA mutation on ATM and p53 protein expression levels

Given previous data on the effect of HP1BP3 on p53, we next examined the level of total ATM kinase protein in both HCT116 lacking and expressing FBXW7 in the presence of mutated HP1BP3 construct. The cell lines transiently transfected with HP1BP3-AA mutant isoform were used to identify the effect of the altered S-Q phosphorylation site of HP1BP3 on expression of ATM and p53 by activation DNA damage in the presence of chemotherapeutic drug and further by diminishing ATM function by applying ATM/ATR inhibitor. The transfection efficiency was evaluated by fluorescence microscopy. $HCT116^{FBXW7\ (+/+)}$ and $HCT116^{FBXW7\ (-/-)}$ cells transfected with HP1BP3-WT were used as controls. Western blotting analysis revealed that ATM expression was slightly increased in both $HCT116^{FBXW7\ (+/+)}$ and $HCT116^{FBXW7\ (-/-)}$ cells transfected with HP1BP3-AA plasmid compared to control cells prior to Oxaliplatin treatment **(Figure 5-8, A & B)**.

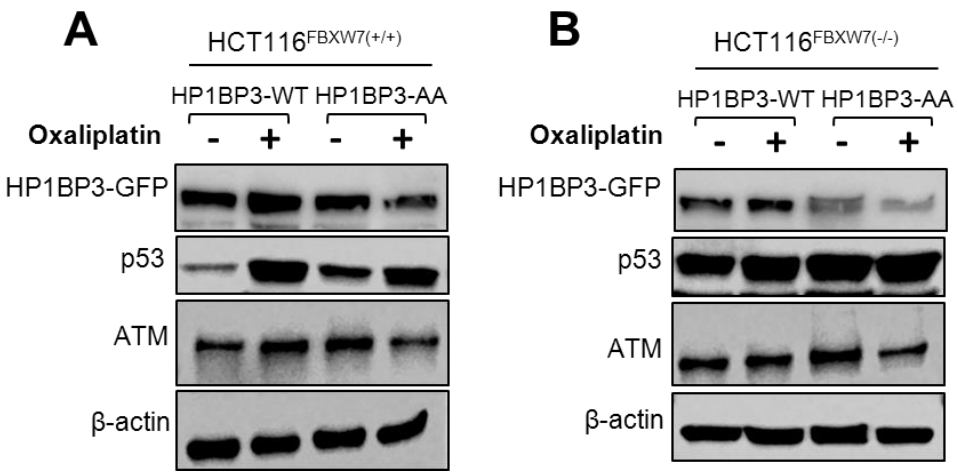


Figure 5-8: HP1BP3-AA dependent expression of ATM and p53 in HCT116 CRC cells.

$HCT116^{FBXW7\ (+/+)}$ and $HCT116^{FBXW7\ (-/-)}$ cells were transfected with HP1BP3-WT and HP1BP3-AA plasmids, separately, and were exposed to 3 μM of Oxaliplatin treatment for 24h **(A & B)**. Untreated cells were used as controls. The harvested protein lysate from both experimental and control cell lines was subjected to immunoblotting with anti-GFP, anti-p53 and anti-ATM antibodies. Protein loading levels are monitored by probing for actin. Data are representative of two independent experiments.

Interestingly, the level of total ATM remarkably decreased in both $HCT116^{FBXW7(+/+)}$ and $HCT116^{FBXW7(-/-)}$ cell lines overexpressing the mutated form of HP1BP3 followed exposure to Oxaliplatin, whereas wildtype HP1BP3 led to the induction of ATM level in response to genotoxic stress in HCT116 harbouring FBXW7 **(Figure 5-8, A)** and did not alter in HCT116 lacking FBXW7 **(Figure 5-8, B)**. **Figure 5-9** shows a schematic for the effects of S-Q phosphorylation site of HP1BP3 on p53 and ATM expression in $HCT116^{FBXW7\ (+/+)}$ and $HCT116^{FBXW7\ (-/-)}$ cell lines.

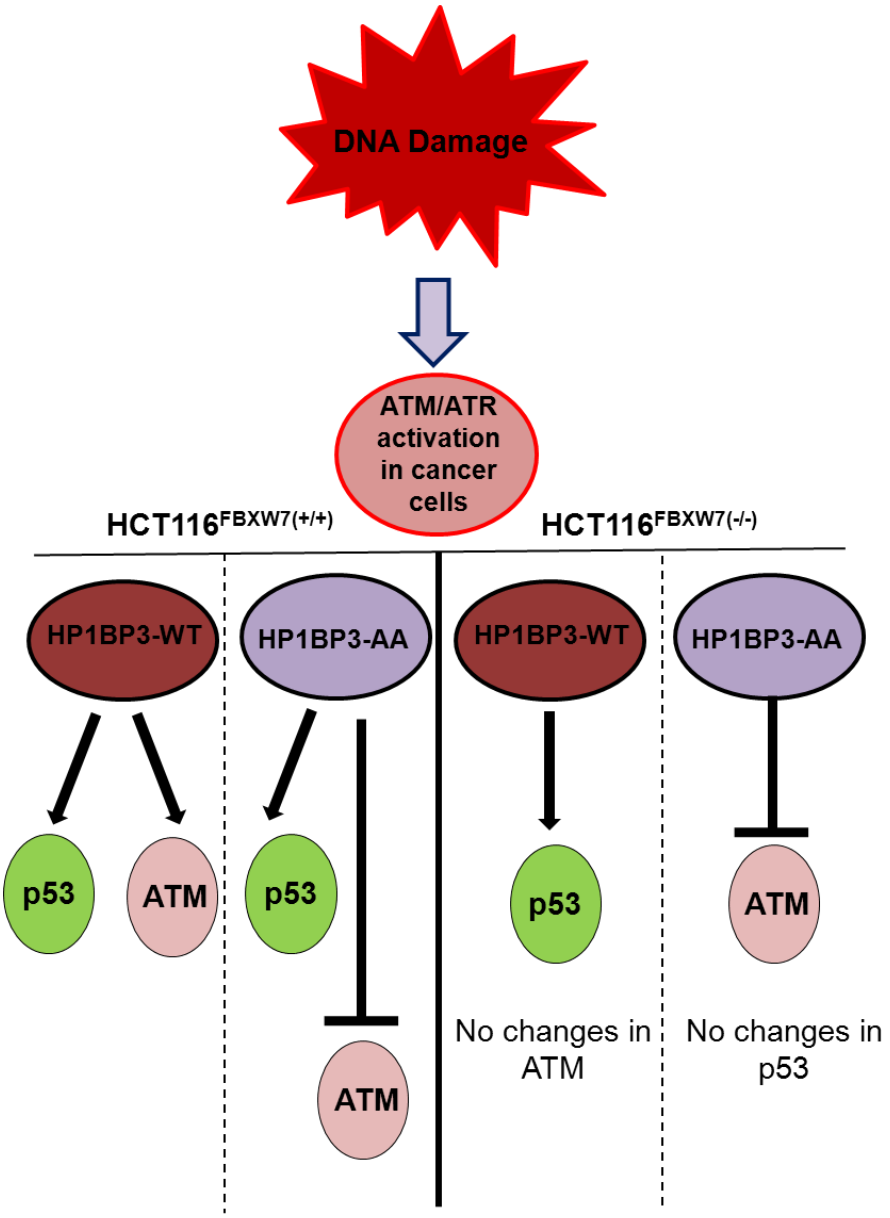


Figure 5-9: Dependence of expression levels of p53 and ATM proteins upon S-Q phosphorylation motif. HCT116$^{FBXW7\ (+/+)}$ and HCT116$^{FBXW7\ (-/-)}$ cells were transfected with HP1BP3-WT and HP1BP3-AA plasmids, separately, and were exposed to 3 μM of Oxaliplatin treatment for 24h.

These findings suggest the importance of S-Q domain in HP1BP3/ATM interplay. Strikingly, when we aimed to perform the experiment in the presence of pharmacological inhibitor of ATM, we found almost complete abolishment

of ATM expression in HCT116FBXW7 $^{(+/+)}$ encompassing HP1BP3-AA mutant construct, whereas in HCT116$^{FBXW7\ (-/-)}$ cells transfected with HP1BP3-AA plasmid no alterations in ATM expression occurred **(Figure 5-10, A&B)**.

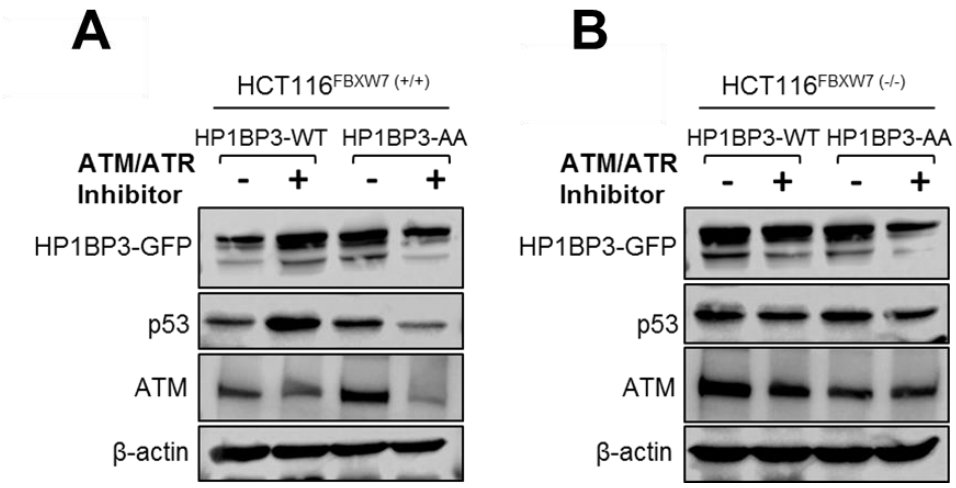


Figure 5-10: HP1BP3-AA dependent expression of ATM and p53 in HCT116 CRC cells.

HCT116$^{FBXW7\ (+/+)}$ and HCT116$^{FBXW7\ (-/-)}$ cells were transfected with HP1BP3-WT and HP1BP3-AA plasmids, separately, and were exposed to 10µmol/L of ATM/ATR inhibitor for 1h **(A & B)**. Untreated cells were used as controls. The harvested protein lysate from both experimental and control cell lines was subjected to immunoblotting with anti-GFP, anti-p53 and anti-ATM antibodies. Protein loading levels are monitored by probing for actin. Experiment was repeated on two independent occasions.

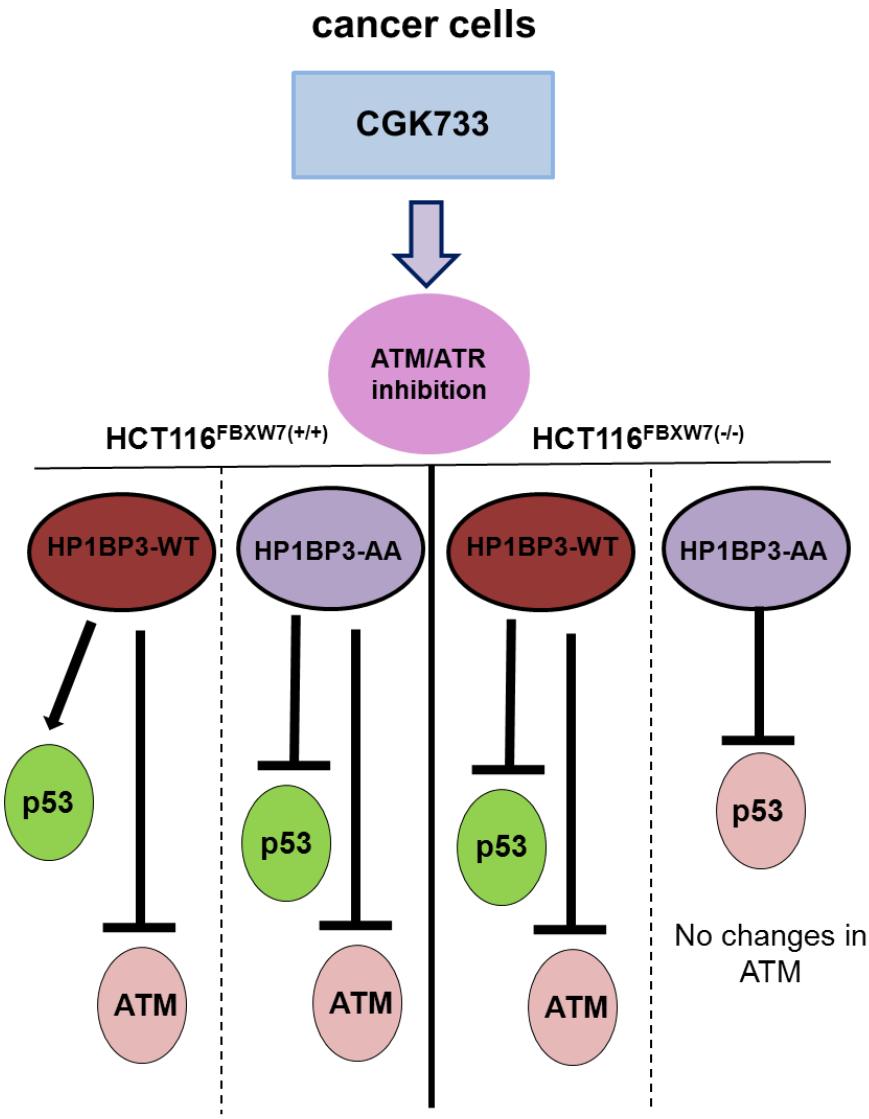


Figure 5-11: ATM and p53 expression levels in response to Inhibition of ATM/ATR in the presence of mutated S-Q phosphorylation site. HCT116$^{FBXW7\ (+/+)}$ and HCT116$^{FBXW7\ (-/-)}$ cells were transfected with HP1BP3-WT and HP1BP3-AA plasmids, separately, and were subjected to 10µmol/L of ATM/ATR inhibitor for 1h. The response of DDR proteins are indicated on the presented schematic presentation.

By studying the HP1BP3/ATM correlation, we observed p53 modulation. Remarkably, the both wildtype HCT116 and FBXW7-depleted HCT116 untreated cells transfected with HP1BP3-AA mutant construct exhibited higher expression of p53 compared to control cells prior Oxaliplatin treatment **(Figure 5-8, A & B)**. It is noteworthy that HCT116$^{FBXW7\ (-/-)}$ cells harbouring the mutant HP1BP3 demonstrated higher p53 expression in comparison to HCT116$^{FBXW7\ (+/+)}$. However, Oxaliplatin treatment significantly induced p53 level in wild type HCT116 transfected with HP1BP3-AA, whereas in the HCT116 lacking FBXW7 p53 levels remained unchanged **(Figure 5-8, B)**.

Taken together, despite the differences in p53 expression, all cell lines, except HCT116$^{FBXW7\ (-/-)}$ transfected with HP1BP3-AA, showed elevation of the p53 expression followed Oxaliplatin treatment. Interestingly, in HCT16 CRC cells harbouring FBXW7 the level of total p53 reduced in the presence of the mutated S-Q domain after treatment with the ATM/ATR inhibitor **(Figure 5-9, A & B)**, whereas wildtype displayed induction of p53 which is consistent with previously reported data. Similar to the wild type HCT116 transfected with HP1BP3-AA, mutation in HCT116$^{FBXW7\ (-/-)}$ cells exhibited downregulation of p53 in the presence of pharmacological ATM/ATR inhibitor. It is important to mention, that the higher p53 expression in drug-free conditions in the experiment with Oxaliplatin treatment compared to the study with ATM/ATR inhibitor might be explained by a serum-starvation effect. It was shown that loss of growth factors resulted in accumulation of p53 in ATM-dependent manner (Hasan et al., 1999, Shi et al., 2012). Indeed, serum starvation-induced p53 activation was observed in human colorectal cancer HCT116 cells lacking FBXW7 **(Figure 5-8, B)**.

5.2.6 Effect of HP1BP3 inhibition on p53 protein expression

5.2.6.1 Successful shRNA-mediated knockdown of HP1BP3 in HCT116$^{FBXW7\ (+/+)}$ and HCT116$^{FBXW7\ (-/-)}$ cell lines

To further explore the HP1BP3 functional behaviour in DNA damage response, we applied small hairpin RNA (shRNA) cloned into pGIPZ lentiviral vector **(Figure 5-12, A)** to perform knockdown experiments. The shRNA based knockdown approach was adopted to generate stable long-term knockdown of the candidate protein in HCT116 CRC cell lines harbouring and lacking FBXW7. Both HCT116$^{FBXW7(+/+)}$ and HCT116$^{FBXW7(-/-)}$ cell lines were transfected with HP1BP3 specific plasmid (**HP1BP3 shRNA V3LHS_339498**) **(Figure 5-12, B)**.

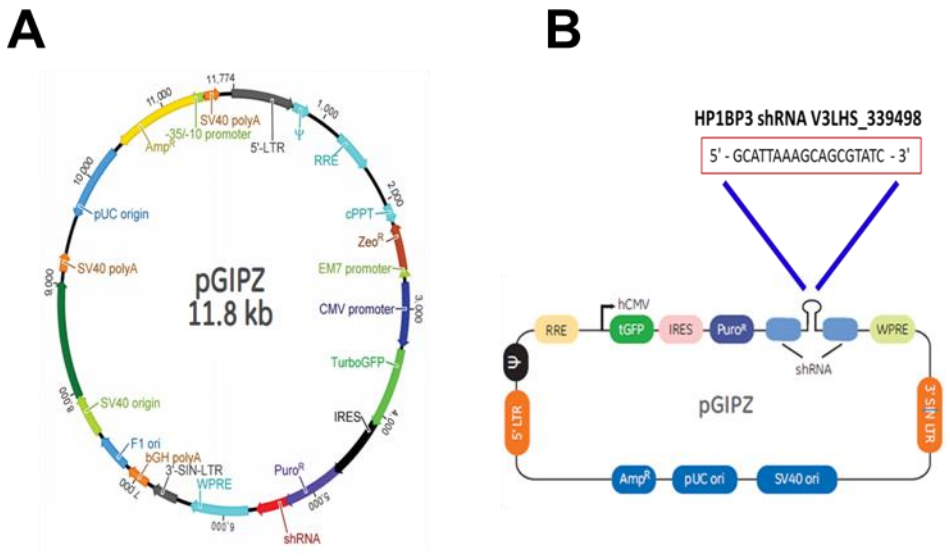


Figure 5-12: Schematic presentation of pGIPZ backbone vector (A) and inserted HP1BP3 shRNA into pGIPZ plasmid (B). The target sequence is encompassed in red box.

The hairpin is cloned downstream to GFP in pGIPZ lentiviral plasmid that contains the selectable marker puromycin. The transfected cells were incubated for 48 hours prior to puromycin drug selection. Transfected cells were selected on the basis of acquired resistance to the puromycin and sustained over 2-3 days in culture by maintaining the selective pressure. The selection was terminated in two weeks. As anticipated, the surviving cells expressed GFP, distributed homogenously throughout the nucleus. Furthermore, the selected cells were amplified and examined for the expression of HP1BP3. Western blotting results showed remarkable reduction of both HP1B3 isoforms in both HP1BP3 knockdown HCT116$^{FBXW7\ (+/+)}$ and HCT116$^{FBXW7\ (-/-)}$ cell lines **(Figure 5-13, A & B)**.

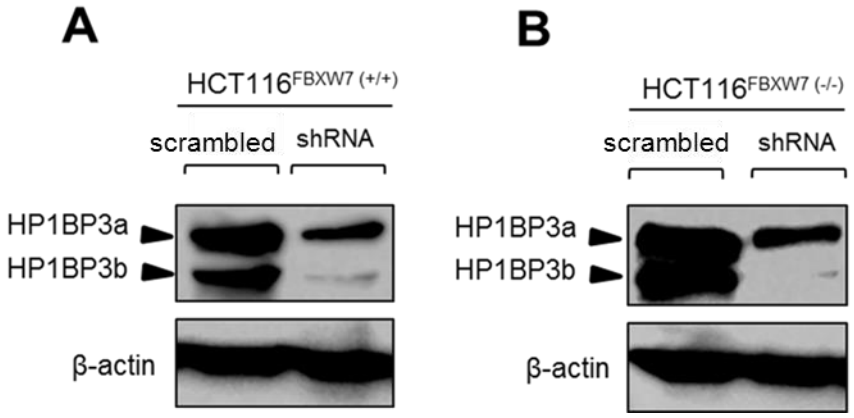


Figure 5-13: Successful shRNA-mediated knockdown of HP1BP3 in HCT116 CRC cells. (A & B) HCT116$^{FBXW7\ (+/+)}$ and HCT116$^{FBXW7\ (-/-)}$ cells were transfected with **HP1BP3 shRNA V3LHS_339498** with following puromycin selection process prolonged for two weeks. Selected cells were expanded, amplified and harvested for detection of HP1BP3 using a specific anti-HP1BP3

antibody. Immunoblot results for endogenous expression of HP1BP3 knockdown HCT116$^{FBXW7(+/+)}$ and HCT116$^{FBXW7(-/-)}$cells show significant reduction of HP1BP3 expression compared to scrambled GFP expressing HCT116 cell lines, respectively.

5.2.6.2 Loss of HP1BP3 led to accumulation of total p53 in HCT116 CRC cells after ionizing irradiation

We further investigated FBXW7-dependent response of HP1BP3 and DNA damage related proteins in the generated HP1BP3 knockdown HCT116$^{FBXW7\ (+/+)}$ and HCT116$^{FBXW7\ (-/-)}$ cell lines by activation of ATM protein kinase. DNA damage was induced by exposing HCT116 CRC cells to 6Gy of ionizing irradiation and total cellular γH2AX formation was measured by immunoblotting. In control cells (HCT116$^{FBXW7\ (+/+)}$ and HCT116$^{FBXW7\ (-/-)}$), IR induced phosphorylation of H2AX **(Figure 5-14, A & B)**. In contrast, we observed the opposite pattern of H2AX expression in HP1BP3 knockdown HCT116$^{FBXW7\ (+/+)}$, wherein IR reduced the level of H2AX phosphorylation. However, FBXW7-null HCT116 cells displayed a slight induction of γH2AX following IR.

In addition, we examined IR-induced response of total p53 and ATM protein substrates. Immunoblotting detected a marked increase of p53 in HP1BP3 knockdown HCT116$^{FBXW7\ (+/+)}$ followed irradiation compared to the control (HCT116$^{FBXW7\ (+/+)}$), whereas HCT116$^{FBXW7\ (-/-)}$ and HP1BP3 knockdown HCT116$^{FBXW7\ (-/-)}$ exhibited a similar pattern of p53 expression level **(Figure 5-14, A & B)**. Importantly, downregulation of HP1BP3 in HCT116$^{FBXW7\ (+/+)}$ led to higher expression of ATM compared to the control (HCT116$^{FBXW7\ (+/+)}$),

wherein HP1BP3 expression remained unchanged prior and followed irradiation **(Figure 5-14, A)**. While in HP1BP3 knockdown HCT116$^{FBXW7\ (-/-)}$ irradiation caused slightly reduction of ATM kinase **(Figure 5-14, B)**. With regard to HP1BP3, its expression in HP1BP3 knockdown HCT116$^{FBXW7\ (+/+)}$ remained without alteration **(Figure 5-14, A)**, whereas in HP1BP3 knockdown HCT116$^{FBXW7\ (-/-)}$ HP1BP3 reduced significantly followed irradiation **(Figure 5-14, B)**. **Figure 5-15** illustrates the expression levels of ATM, p53 and γH2AX proteins in the HP1BP3-knockout HCT116 cell lines.

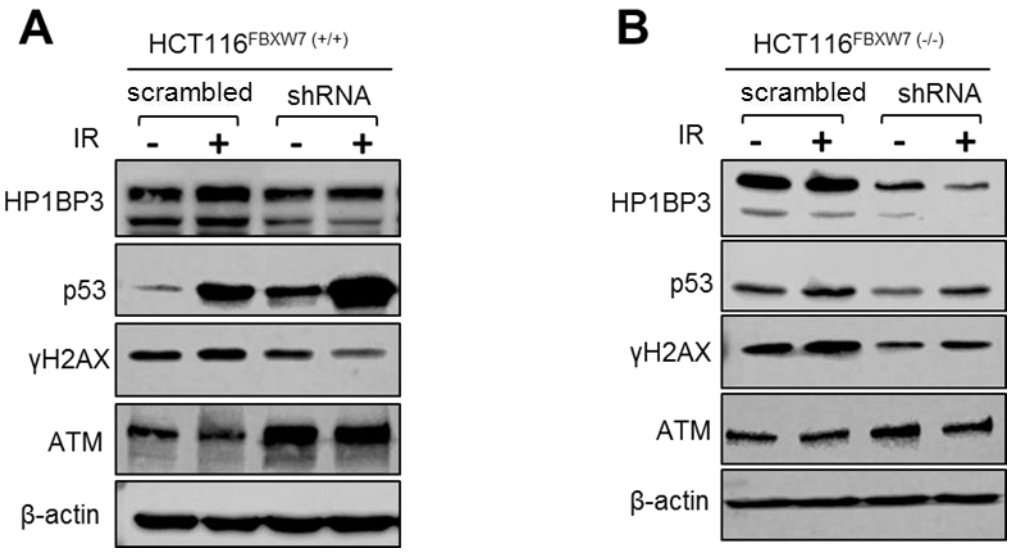


Figure 5-14: The response of HP1BP3-knockdown HCT116 CRC cells to ionizing radiation. (A & B) HCT116 CRC cells downregulated in HP1BP3 were either untreated or treated with 6Gy IR and harvested 60 min later. HCT116$^{FBXW7\ (+/+)}$ and HCT116$^{FBXW7\ (-/-)}$ cells were used as controls. The extracted cell lysates were immunoblotted with anti-HP1BP3, anti-p53, anti-γH2AX and anti-ATM antibodies. Protein loading levels are monitored by probing for actin.

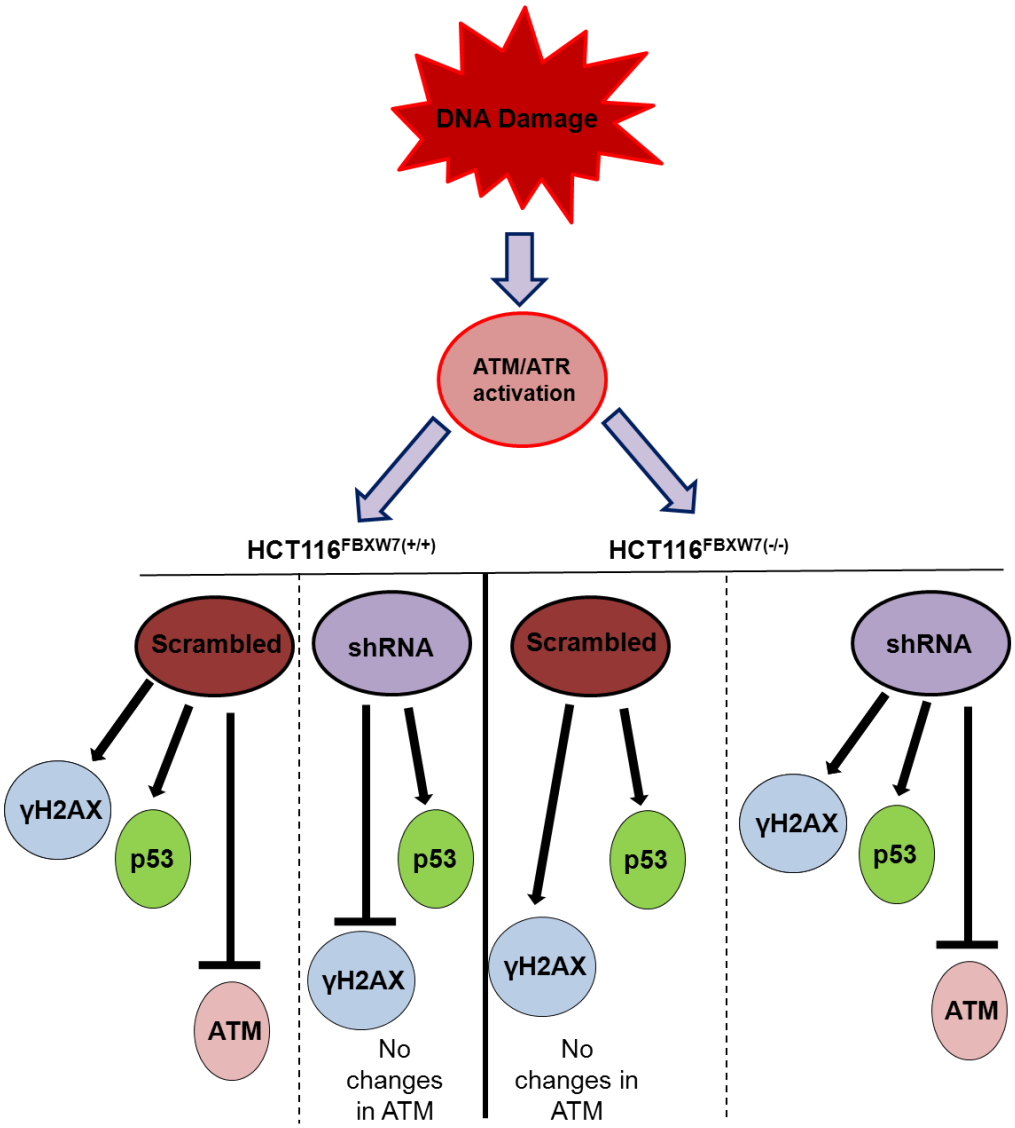


Figure 5-15: Schematic representation of the DNA damage effect on the expression levels of **ATM, p53 and γH2AX proteins in HP1BP3-knockout HCT116 cell lines**. Scrambled and HP1BP3-knockout HCT116 cell lines were exposed to 6Gy IR and aforementioned proteins were monitored, as demonstrated.

5.2.6.3 Downregulation of HP1BP3 reduced the level of total p53 in HCT116 CRC lacking FBXW7 following Oxaliplatin treatment

To evaluate the cytotoxic effect of chemotherapeutic drug on CRC-cells with suppressed HP1BP3 expression, both HP1BP3-knockdown HCT116$^{FBXW7\ (+/+)}$ and HP1BP3-knockdown HCT116$^{FBXW7\ (-/-)}$ cells were treated with 1µM of Oxaliplatin for 3 consecutive days. HCT116$^{FBXW7\ (+/+)}$ and HCT116$^{FBXW7\ (-/-)}$ cells were used as controls. The cell lysates were harvested at the same time and the expression of ATM and p53 proteins were assessed by immunoblotting. Western blotting results showed the expression of HP1BP3 increased in HP1BP3-knockdown HCT116$^{FBXW7\ (+/+)}$ after Oxaliplatin treatment, whereas in HP1BP3-knockdown HCT116$^{FBXW7\ (-/-)}$ cells no significant changes were observed **(Figure 5-16, A & B)**. p53 expression appeared to be downregulated in both cell lines, however in HP1BP3-knockdown HCT116$^{FBXW7(-/-)}$ cells the difference is more remarkable **(Figure 5-16, B)**. Interestingly, despite the reduced level of p53 in HP1BP3-knockdown HCT116 cells, Oxaliplatin induced p53 level notably in HP1BP3-knockdown HCT116$^{FBXW7\ (+/+)}$ compared to HP1BP3-knockdown HCT116$^{FBXW7\ (-/-)}$ **(Figure 5-16, A)**.

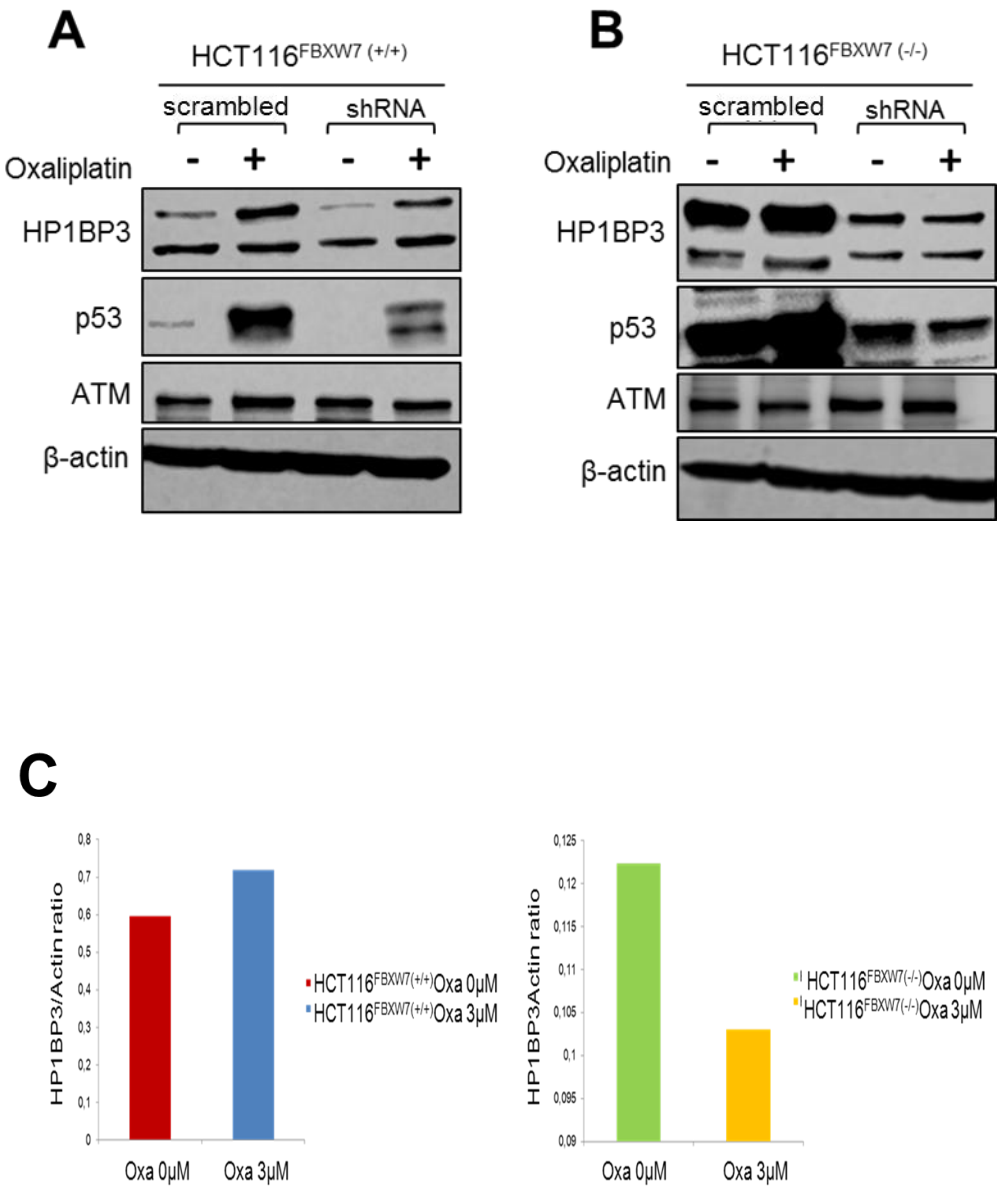


Figure 5-16: The response of HP1BP3-knockdown HCT116 CRC cells to Oxaliplatin exposure. (A & B) HP1BP3 knockdown HCT116$^{FBXW7\ (+/+)}$ and HCT116$^{FBXW7\ (-/-)}$ cells were exposed to 1 μM of Oxaliplatin and cell lysates were harvested with further immunoblotting against anti-p-53, anti-p-p53 and anti-ATM antibodies. HCT116$^{FBXW7\ (+/+)}$ and HCT116$^{FBXW7\ (-/-)}$ cells were used as controls. Protein loading levels are monitored by probing for actin. **(C)** Graphical presentation of densitometry calculations for HP1BP3 expression versus actin loading control levels in HP1BP3-knockdown HCT116$^{FBXW7\ (-/-)}$ cell lines prior

and following Oxaliplatin treatment. Experiment was repeated on three independent occasions.

5.3 DISCUSSION

FBXW7 is an evolutionarily conserved E3 ubiquitin ligase that catalyzes protein destruction by the ubiquitin-proteasome system and thus tightly governs the activity of target substrates (Welcker and Clurman, 2008, Tan et al., 2008). Some studies have suggested the regulatory role of FBXW7 in G1–S cell-cycle checkpoint via control of the cell proliferation, whereas others proposed the contribution of FBXW7 in genetic instability (Rajagopalan et al., 2004). On the other hand, evidence has emerged emphasizing the importance of DNA repair mechanisms in the maintenance of genomic integrity via correction of DNA lesions (Ziv et al., 2006, Goodarzi et al., 2008).

Genomic instability can impede normal cell cycle progression or even cause cycle arrest (Aguilera and Gómez-González, 2008). Hence in order to repair DNA damage and maintain appropriate progression of the cell cycle, several distinct repair mechanisms are implicated at different stages of the cell cycle (Kastan and Bartek, 2004). The requirement of the proteins associated with specific DNA repair mechanism to repair DNA lesions is dictated by the type of DNA lesion and chromatin-dependent genetic events (Zhou and Elledge, 2000). Therefore, HP1BP3, as a novel chromatin associated protein, may play a key role to link the DNA lesion and chromatin-dependent genetic events.

On the basis of HP1BP3 structure, the determination of several closely spaced SQ motifs, a classical hallmark of DNA-damage-response-proteins (Traven and Heierhorst, 2005, Abraham, 2001), suggests that HP1BP3 is a potential downstream target substrate of ATM/ATR protein kinases. Additionally, recent work of our group reported that phosphorylated HP1BP3 is degraded by FBXW7.

Here, we initiated our study by exposing HCT116$^{FBXW7\ (+/+)}$ and HCT116$^{FBXW7\ (-/-)}$ cells to various DNA-damaging agents and observed the distinctive responses of HP1BP3 depending upon the FBXW7 availability in HCT116 CRC cells. Wild type HCT116 exhibited consistent HP1BP3 induction and HP1BP3 positive correlation in response to ATM/ATR activation. Moreover, accumulation of wild type p53 and phosphorylation of H2AX, fundamental DNA-damage-related events, were monitored throughout the study. By contrast to wild type HCT116, noticeable differences in HP1BP3 expression were observed in FBXW7-deleted HCT116 cells. Both UV light and ionizing irradiation reduced HP1BP3 expression whereas Oxaliplatin treatment increased HP1BP3 level. Despite the diversity of HP1BP3 response, the level of p53 and γH2AX were upregulated in response to ATM/ATR activation. Interestingly, suppression of ATM/ATR led to induction of HP1BP3 in wild type HCT116 and reduction in FBXW7-deleted HCT116 cells.

These findings demonstrated significant HP1BP3 reduction in the absence of FBXW7 and a diminished level of ATM/ATR kinases. The mechanisms underlying such response still need to be elucidated. Furthermore, by using the HP1BP3 stable knockdown HCT116 generated cell lines it was interesting to

observe the change in p53 and ATM level compared to control cell lines. Previous experimental data demonstrated p53 expression level was increased in A431 cells lacking HP1BP3 (Dutta et al., 2014). Indeed, HP1BP3–depleted HCT116 cells exhibited higher p53 expression levels, particularly HP1BP3–depleted HCT116$^{FBXW7\ (-/-)}$ cells where p53 expression was significant compare with control cells (HCT116$^{FBXW7\ (-/-)}$). Interestingly, HP1BP3-knockdown in HCT116 lacking FBXW7 demonstrated completely the opposite result by reducing p53 expression level compared to control HCT116$^{FBXW7\ (-/-)}$ cells. Whereas expression level of p53 was similar in both HP1BP3-depleted and HP1BP3-knockdown HCT116$^{FBXW7\ (+/+)}$ cells.

Based on our results, further work to investigate the molecular mechanisms implicated in the FBXW7/HP1BP3 binding to ATM/ATR during DNA repair are required to provide more insight into cellular response to DNA-damaging agents.

CHAPTER 6

Generation of HP1BP3-Deficient CRC Cell Lines by Using the CRISPR/Cas9 Technology

6.1 BRIEF INTRODUCTION

The classical approach in the field of genetics to elucidate a gene function is achieved either by deletion or by overexpressing it in living organisms, which previously presented an obstacle in terms of complexity and time duration (Banga and Boyd, 1992, Gloor et al., 1991, Rong and Golic, 2000, Gong and Golic, 2003). In recent years, novel strategies of the genome editing have emerged, including the zinc-finger nucleases (ZFNs) (Porteus and Baltimore, 2003, Miller et al., 2007, Sander et al., 2011, Wood et al., 2011), transcription activator–like effector nucleases (TALENs) (Wood et al., 2011, Christian et al., 2010, Zhang et al., 2011, Hockemeyer et al., 2011, Reyon et al., 2012) and the RNA-guided CRISPR/Cas9 nuclease system (Cong et al., 2013, Mali et al., 2013, Jinek et al., 2013, Cho et al., 2013, Garneau et al., 2010).

All the technologies listed above are based on engineered, programmable and highly specific nucleases, which are applied to facilitate precise editing in the genomes of cellular organisms through targeted deletions, insertions, and specific sequence changes. Cas9 promotes genome editing by stimulating a double stranded break (DSB) at a target genomic locus, in similar way to ZFNs and TALENs.

Distinct from ZFNs and TALENs, there are several advantages for CRISPR/Cas9. ZFNs and TALENs are popular genome editing platforms constructed on protein guided DNA cleavage, whereas CRISPR/Cas9 only requires a short programmable gRNA for DNA targeting (Ran et al., 2013,

Zhang et al., 2014). Upon cleavage by Cas9, the target genomic locus usually undergoes repair through one of two major pathways. More recent reports suggested that CRISPR/Cas9 system provides a robust and highly-accessible genome editing tool widely adopted by researchers for precise manipulation of genome sequence and functional elucidation of target genes in biology and human diseases.

In the current study, CRISPR/Cas9 technology has been applied to obtain stable and genomic specific HP1BP3-knockout in FBXW7-wildtype and FBXW7-deficient HCT116 CRC cells. The successful HP1BP3 depletion in HCT116 cell lines was validated through isolating, expanding single cell clones and Western blotting analysis **(Figure 6-1)**.

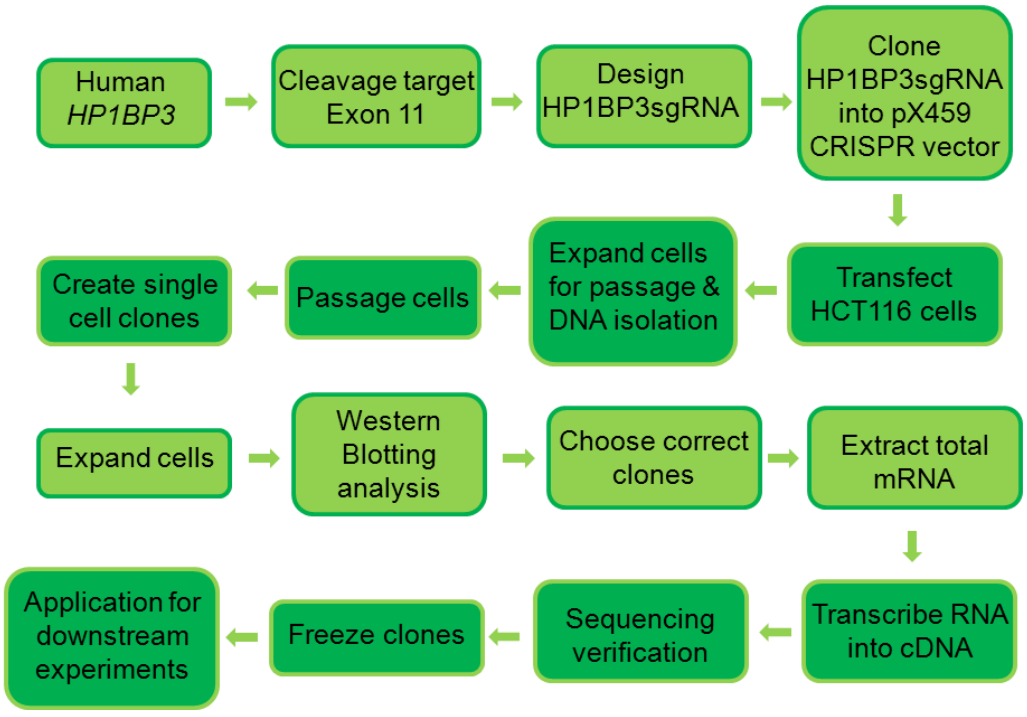


Figure 6-1: The schematic design for generation HP1BP3-knockout HCT116 CRC cell lines by application CRISPR/Cas9 technology. Brief overview of experimental plans in the shape of flow chart demonstrating the

subsequent steps to produce HP1BP3-depleted cells by using a novel genome editing technique.

6.2 RESULTS

6.2.1 Cloning of HP1BP3 sgRNA into pX459 expression plasmid

This piece of work was focused on generation of HP1BP3 knockout HCT116 CRC cells by utilizing CRISPR/Cas9 methodology, an advanced technology in genome engineering (Torres-Ruiz and Rodriguez-Perales, 2015, Laufer and Singh, 2015, Hilton and Gersbach, 2015, Sánchez-Rivera and Jacks, 2015). The technique allows efficient creation of site-specific genomic deletions and presents an easily applicable approach for effective loss-of-function studies of genes and genetic elements in mammalian cell lines (Bauer et al., 2015).

The applied CRISPR/Cas9 strategy was based on plasmid delivery expressing Cas9 and with a pair of chimeric single guide RNAs (sgRNAs) specifying a 20-nt targeting sequence for the HP1BP3 locus. Upon cleavage by Cas9, the target locus undergoes two double-stranded DNA breaks (DSBs) at target sites with further cleavage of the intervening DNA segment, followed by non-homologous end joining (NHEJ) repair.

Here, we exploited pSpCas9 (BB)-2A-Puro (pX459) (Addgene plasmid ID 48139) backbone vector **(Figure 6-2)** to deliver appropriate sgRNA into mammalian cells. It was reported that application of plasmid-based sgRNA delivery frequently achieves higher cleavage efficiency compared to PCR-generated U6-sgRNA expression cassette (Ran et al., 2013).The PX459

construct allows for the simultaneous expression of desired sgRNA and Cas9 nuclease, moreover it contains puromycin as a selectable marker (Ran et al., 2013). CRISPR protocol initiates with design of a pair of ~20-bp-long oligos which can be achieved either manually or by employing freely available online tools (http://tools.genome-engineering.org) (Ran et al., 2013). Two key points such as the 5′-NGG PAM for *S. pyogenes* Cas9 and the minimization of off-target activity have to be taken into consideration while generating 20-nt guide sequence (Hsu et al., 2013, Fu et al., 2013). It is noteworthy that the location of PAM is required to be proximately downstream of the target sequence to mediate Cas9 cleavage at ~3 bp upstream of the PAM, besides it is exclusive from the 20-nt guide sequence of the sgRNA (Jinek et al., 2012). In addition, the presence of a G is preferable at 5' position, corresponding to the first base of the 20-bp target site, to facilitate the efficient U6 transcription of sgRNA (Ran et al., 2013).

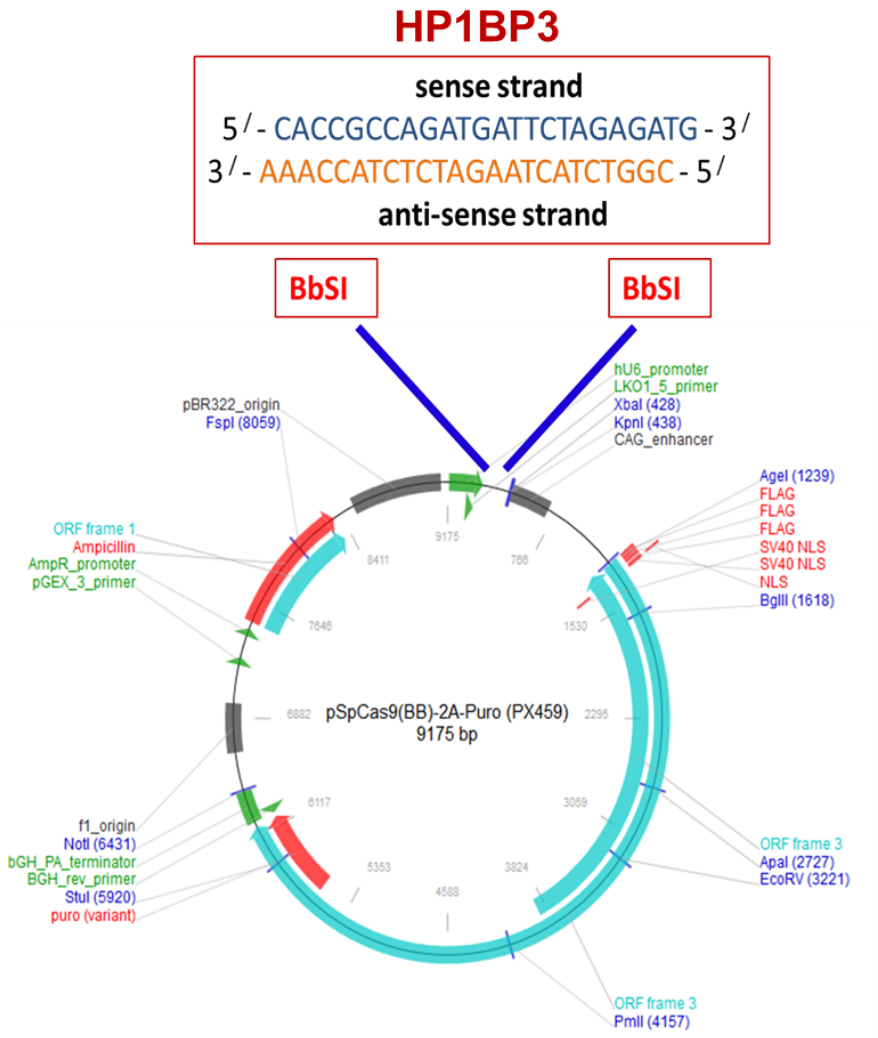


Figure 6-2: The construction of pX459 expression plasmid for HP1BP3sgRNA. The schematic shows the insertion of the pair annealed HP1BP3sgRNA into pX459 backbone vector digested by *BbsI* restriction enzyme.

To generate a pX459 expression plasmid for HP1BP3sgRNA, two pairs of manually designed and annealed sgRNAs **(Table 6-1)** were cloned into the pX459 backbone vector separately, both targeting the human HP1BP3 locus. It is recommended to design more than one sgRNAs due to possibility of DNA cleavage failure by sgRNA (Ran et al., 2013).

Table 6-1: Two sets of guide sequence oligos used to engineer pX459 expression plasmids for HP1BP3sgRNA. Restriction enzyme sites for *BbsI* within primers are underlined. The core primer sequences are highlighted in grey. The first pair of guide oligos failed to produce a HP1BP3 deletion, therefore only the second set of primers was employed for downstream experiments.

Primer Use	Primer Sequence 5'-3'	Restriction Site
HP1BP3-CRISPR (first set)	Forward (top) *CACC* GCGGACAAGTTAGGTGAG GT	*BbsI*
	Reverse (bottom) *AAACA* CCTCACCTAACTTGTCCGC	*BbsI*
HP1BP3-CRISPR (second set)	Forward (top) *CACC* GCCAGATGATTCTAGAGATG	*BbsI*
	Reverse (bottom) *AAAC* CATCTCTAGAATCATCTGGC	*BbsI*

Thus, two sets of guide oligos targeting the sequences located within first and eleventh exons of HP1BP3 gene, respectively, were designed. In the current experiment we encountered inefficiency of first set of HP1BP3 sgRNAs for mediating DSBs, and therefore the application of these sgRNAs was terminated. Single stranded and phosphorylated DNA oligos corresponding to individual 20-bp human HP1BP3 encompass overhanging *BbsI* sequences to produce compatible cohesive ends for subsequent cloning into pX459 backbone vector. We initially validated the vector by successfully *BbsI* enzymatic digestion as presented in **(Figure 6-3)**.

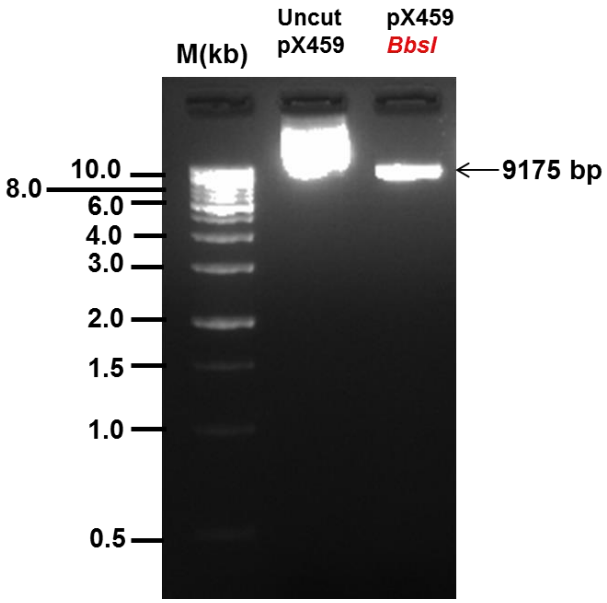


Figure 6-3: The restriction enzyme digestion analysis of pX459 expression plasmid. Agarose gel shows linearization of pX459 backbone vector by *BbsI* restriction enzyme (second panel). Uncut pX459 was used as the negative control in the experiment (first panel). M: Marker, 1Kb DNA Ladder in kb (New England BioLabs).

Next, the oligo pairs encoding the 20-nt guide sequence of HP1BP3 were annealed according to the *Nature protocol* (Ran et al., 2013) **(Table 6-2)** and then inserted into the digested *BbsI* pX459 plasmid bearing both Cas9 nuclease and the remainder of the sgRNA as an invariant scaffold immediately following the oligo cloning site **(Figure 6-4)**.

Table 6-2: Preparation of the HP1BP3 sgRNA oligos inserts. The following components were utilised to produce the mixture as indicated in the table below. Phosphorylation and annealing of sgRNA oligos (top and bottom strands) was performed in thermocycler by applying following strategy: 37 °C for 30 min; 95 °C for 5 min; ramp down from 25 °C and hold at 5 °C.

Component	Amount (µl)
sgRNA (top) (100µM)	1
sgRNA (bottom) (100µM)	1
T4 ligation buffer, 10x	1
T4 PNK	1
ddH2O	6
Total Volume	10

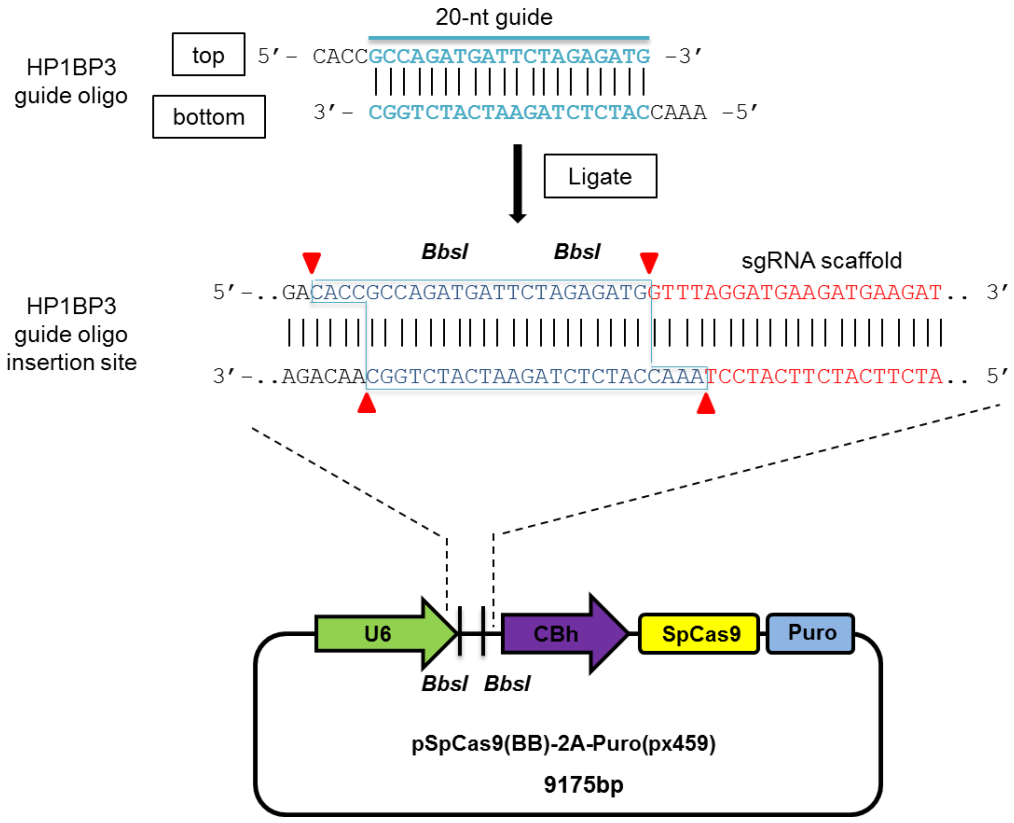


Figure 6-4: Schematic representation for cloning steps of the guide sequence oligos into a plasmid containing Cas9 and the sgRNA scaffold (pSpCas9 (BB)). Both guide oligos and pX459 expression plasmid contain overhangs for ligation presented by *BbsI* sites. PX459 backbone vector encompasses a puromycin resistance gene to aid the selection of transfected cells.

The ligated products were transformed into bacterial competent cells and plated into the Ampicillin plate for pX459. Competent cells transformed with empty pX459 backbone vector were used as a negative control. The number of bacterial colonies in the experimental plate was 5-6 times higher compared to the control. Approximately eight individual bacterial colonies were picked from the experimental agar plate; the plasmid DNA was extracted manually and underwent validation using PCR technique **(Table 6-3)**.

Table 6-3: Set up of PCR mixture for further validation. The following components were used to prepare the PCR mixture for extracted DNA from each individual colony.

Component	Amount (µl)
Extracted DNA	0.5
PCR buffer, 10x	2.5
dNTPs	0.25
Reverse oligo primer (100µM)	0.25
Reverse primer (plasmid)	0.25
Sequencing primer	0.25
Taq polymerase	0.25
ddH2O	20.75
Total Volume	25

Agarose gel showed the right expected two bands for all isolated clones **(Figure 6-5).**

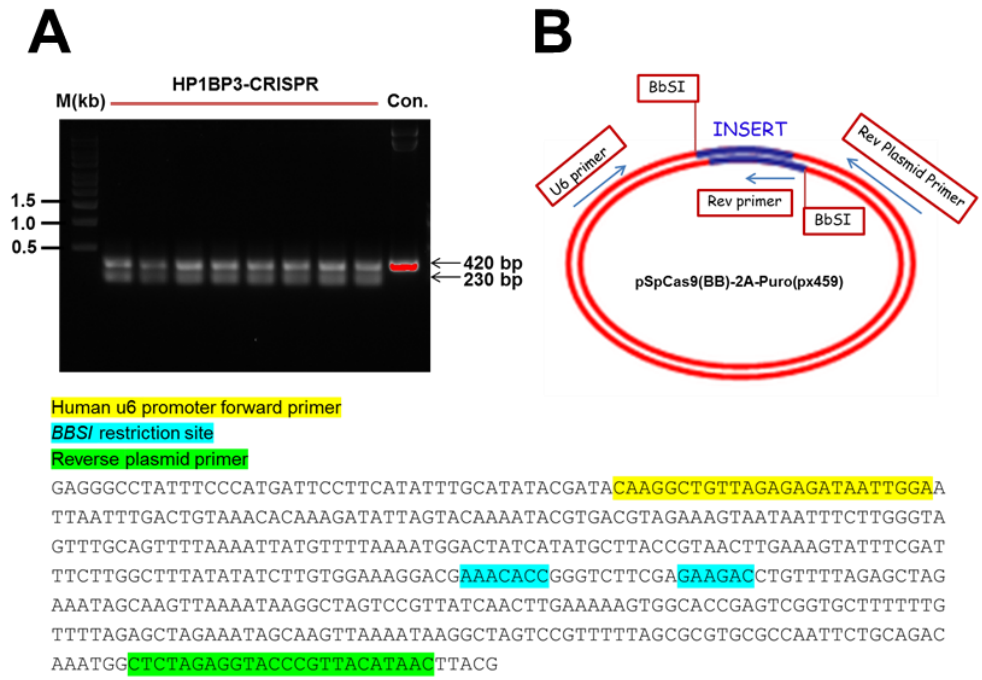


Figure 6-5: Validation of successful cloning of annealed HP1BP3 sgRNA into px459 expression vector by agarose gel electrophoresis. (A) 5µl of PCR product was run on 3% agarose gel to check for size of the products for the presence or absence of sgRNA insertion. Isolated HP1BP3-CRISPR clones show two bands as was anticipated. PCR mixture composed of the same components (Table 6-3) but with difference in DNA template presented by empty px459 backbone vector was used as the negative control in this experiment. As a result of the absence of sgRNA insertion, control sample showed one band as was expected. **(B)** Schematic and presented nucleotide sequence allows understanding the presented data on agarose gel. M: Marker, 1Kb DNA Ladder in kb (New England BioLabs).

Harvested by Midiprep DNA from selected clone was further verified through automated DNA sequencing (Sequencing Facilities, Queen's Medical Centre, Nottingham University) **(Figure 6-6)**.

HP1BP3/CRISPR

AGTAGGCGAAAAATGATATCGATTCTTGGCTTAATATCTTGTGGAAGGACGAAA**CACCGCCAGA**
TGATTCTAGAGATGGTTTTAGAGCTAGAAATAGCAAGTTAAAATAAGGCTAGTCCGTTATCAAC
TTGAAAAAGTGGCACCGAGTCGGTGCTTTTTTGTTTTAGAGCTAGAAATAGCAAGTTAAAATAA
GGCTAGTCCGTTTTTAGCGCGTGCGCCAATTCTGCAGACAAATGGCTCTAGAGGTACCCGTTAC
ATAACTTACGGTAAATGGCCCGCCTGGCTGACCGCCCAACGACCCCCGCCCATTGACGTCAATA
GTAACGCCAATAGGGACTTTCCATTGACGTCAATGGGTGGAGTATTTACGGTAAACTGCCCACT
TGGCAGTACATCAAGTGTATCATAT

HP1BP3 Forward genotyping primer : CACCGCCAGATGATTCTAGAGATG

Figure 6-6: DNA sequencing result for the generated HP1BP3/CRISPR plasmid. Sequence shows the successful cloning of HP1BP3 sgRNA (highlighted in red) into px459 backbone vector.

The next phase of CRISPR/Cas9 protocol is the delivery of complete and sequence-verified pX459 plasmid expressing Cas9 nuclease and HP1BP3 sgRNA that was performed through transfection of HCT116 CRC cell lines harbouring and lacking of FBXW7 gene. Forty eight hours post-transfection, the cells were selected on the basis of acquired resistance to puromycin and sustained over 2 days in culture by maintaining the selective pressure. The working puromycin concentration for HCT116 CRC cells ranges from 3-5ug/ml. The puromycin selected cell lines were expanded and amplified. Previous reports suggest that clonal isolation is a preferable step in generation of cell lines with specific modifications (Ran et al., 2013). Thus, serial dilution with single cell isolation was applied in the current study for the generated of HP1BP3

knockout HCT116 cell lines with a further clonal expansion period to produce a new clonal cell line. The ability of the introduced px459 plasmid bearing Cas9 and HP1BP3 sgRNA to mediate target cleavage in HCT116 cells was tested by expression analysis. The protein lysate was extracted from the novel generated cell lines, run on a SDS-PAGE gel, and immunoblotted with anti-HP1BP3 antibody as outlined in (*Chapter 2, section 2.2.4.2*). Western blotting results of all plasmid clones are presented in **(Figure 6-5)**. According to the obtained data, clones 1 and 4 **(Figure 6-7A, red-dashed box, lanes 1&4)** for wildtype HCT116 and clones 5 and 6 **(Figure 6-7B, red-dashed box, lanes 5&6)** for FBXW7-deleted HCT116 cells showed depletion of both HP1BP3 isoforms.

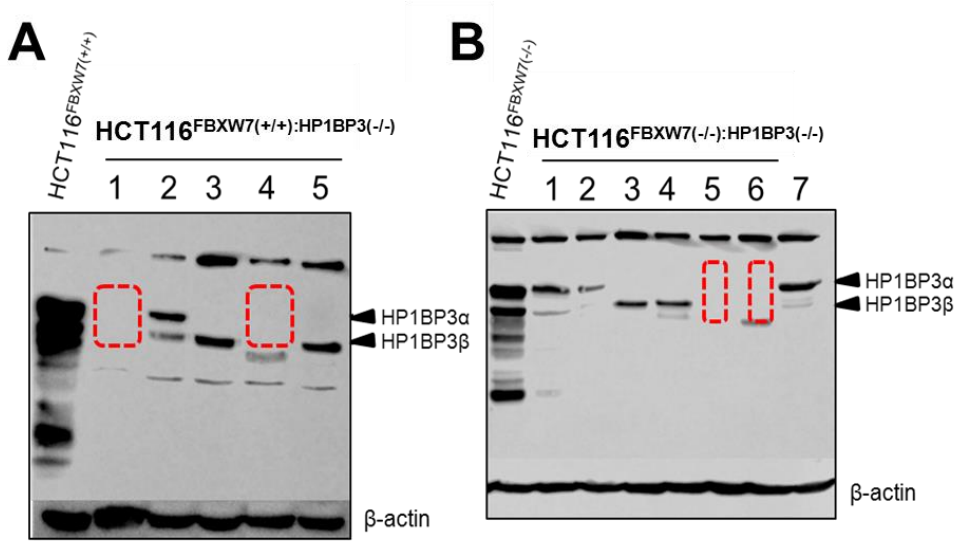


Figure 6-7: Protein expression analysis of isolated clones derived from HCT116$^{FBXW7\ (+/+):HP1BP3\ (-/-)}$ and HCT116$^{FBXW7\ (-/-):HP1BP3\ (-/-)}$ cell pool. Initially, the selection of stable clones from both wildtype HCT116 and FBXW7-deleted HCT116 cell lines was performed in order to detect the knockout of HP1BP3 in the generated HCT116 CRC cells. Isolated stable clones were expanded to enlarge cultivation and furthermore screened by Western blotting analysis. Screening of clonal cell lines confirmed the ablation of both isoforms HP1BP3a

and HP1BP3b in 1st and 4th clones for HCT116$^{FBXW7\ (+/+)}$/CRISPR **(A)** and 5th and 6th for HCT116$^{FBXW7\ (-/-)}$/CRISPR **(B)** cell lines.

To further evaluate the above observations, Western blotting data was supported by DNA sequencing analysis of CRISPR/Cas9-derived HCT116 cell lines as outlined in the following section.

6.2.2 DNA sequence analysis of genomic PCR products illustrates alterations of HP1BP3 gene sequence in HCT116 cell lines

For further validation of HP1BP3 knock-out in HCT116 cells a genomic PCR and DNA sequencing analysis were performed. Total RNA was extracted from CRISPR/Cas9-applied HCT116$^{FBXW7\ (+/+)}$ (samples 1&4) and HCT116$^{FBXW7(-/-)}$ (samples 5&6) alongside control cell lines (HCT116$^{FBXW7(+/+)}$ and HCT116$^{FBXW7(-/-)}$, accordingly) using RNeasy Mini Kit as described in (*Chapter 2, section 2.2.3.3*). Following total RNA isolation, the extracted RNA was measured by Nanodrop. Total RNA was then reverse transcribed into cDNA using TAKARA kit (Takara-Clontech Laboratories) according to the manufacture's recommendations. Two reaction mixtures with and without retro transcriptase per each experimental as well as control cell lines were prepared for cDNA synthesis **(Table 6-4)** and were incubated under conditions presented in the **(Table 6-5)**.

Table 6-4: Set up of the mixture for cDNA production. The following components were used to perform retro transcription from extracted RNA to cDNA.

Component	Amount (µl)
Extracted RNA	1
Prime Script Buffer, 5x	4
Prime Script RT Enzyme MixI	1
Oligo dt Primer (50µM)	1
Random 6 mers (100µM)	1
ddH2O	12
Total Volume	20

Table 6-5: Conditions required for process of reverse transcription.

Condition	Outcome
37^0C 15 min	Reverse transcription
85^0C 5 sec	Inactivation of Reverse transcription with heat

The standard PCR protocol (*Chapter 2, section 2.2.2.1*) was used to amplify the genome-depleted HP1BP3 region from resulted genomic DNA extract per each sample using specific primers **(Table 6-6)**.

Table 6-6: Primers used to amplify HP1BP3-deleted clones

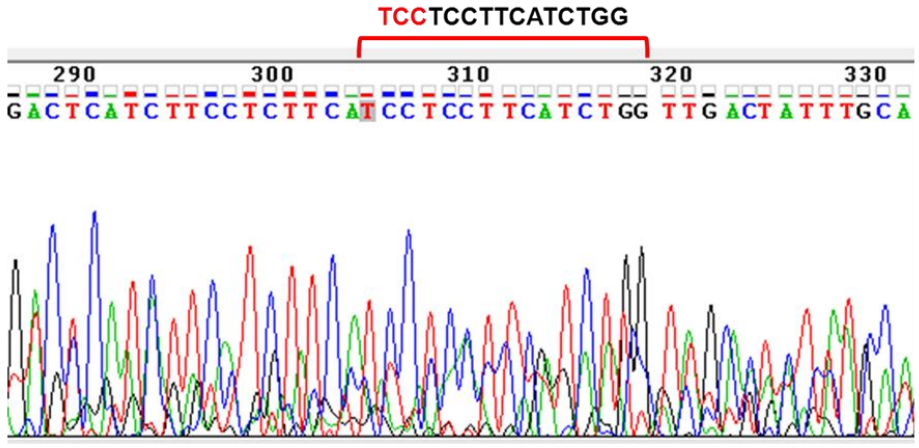
Primer Use	Primer Sequence 5'-3'
HP1BP3-Fwd	GACTGATACGTCTCAGGTG
HP1BP3-Rev	GACTTCTTCATGGTGGATTTTG

A forward primer (HP1BP3-Fwd) and a reverse primer (HP1BP3-Rev) inside the HP1BP3 coding sequence were used to amplify a full-length HP1BP3 gene from the extracted genomic DNA of CRISPR/Cas9-applied HCT116$^{FBXW7\ (+/+)}$ and HCT116$^{FBXW7\ (-/-)}$ as well as control cell lines. The expected size of the amplified DNA fragment by the above described primers is 1.6 Kb. To examine possible genomic alterations in CRISPR/Cas9-modified HCT116 cell lines, PCR products derived from the genomic DNA of above mentioned cells were extracted and subjected to automated DNA sequencing. HP1BP3-Rev primer was used for DNA sequence analysis of the submitted samples. The obtained results were reversed into 5'-3' DNA sequence by using online tool *Reverse Complement*. The sequencing results were then aligned to the previously approved nucleotide sequence of human *HP1BP3* [provided by the NCBI gene bank (Gene ID: 50809)]. As shown in **(Figures 6-8, 6-9, 6-10 & 6-11)**, the alignment data revealed various outcomes of the submitted samples as a result

of CRISPR/Cas9 application. Thus, CRISPR/Cas9/HCT116$^{FBXW7\ (+/+)}$ (sample1) showed partial deletion of the targeted DNA sequence, whereas the sequence of the PCR amplified DNA in sample 4 lost the fragment of interest. Moreover, its DNA sequence underwent mutation prior to the deleted part. CRISPR/Cas9/HCT116$^{FBXW7\ (-/-)}$ (sample5) also demonstrated complete deletion of the targeted sequence as well as the mutated fragment that precede the deleted part. Similar to the sample 1 of CRISPR/Cas9/HCT116$^{FBXW7\ (+/+)}$, sample 6 of CRISPR/Cas9/HCT116$^{FBXW7\ (-/-)}$ showed the partial deletion of the DNA sequence located within exon 11 of *HP1BP3* gene.

Thus, based on this observation, despite of isolating single cell clones, presence of heterogeneous population of cells harbouring different modified/mutated sequences of HP1BP3 in HCT116 cell lines was determined. This could be a result of cross-contamination of single cell isolation procedure carried on through generation of single cell clones. Although all these mutations resulted to HP1BP3 protein deficient expression, further single cell clone isolation will be required for subsequent single-cell analysis.

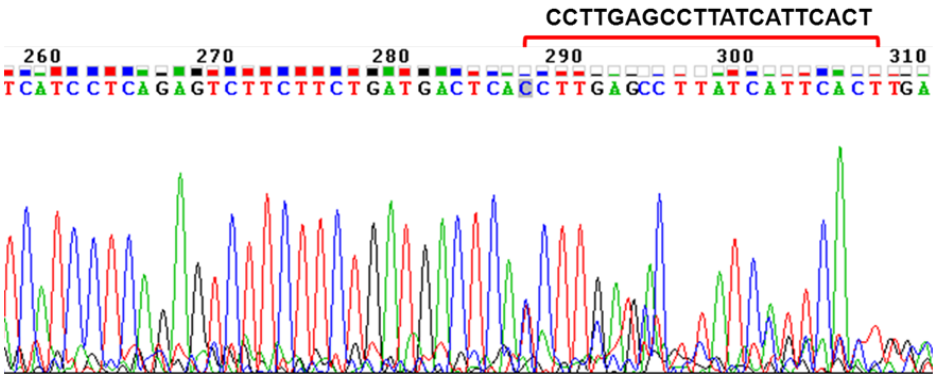
HCT116$^{FBXW7(+/+):HP1BP3(-/-)}$ sample N1 DNA sequencing result



AGTTCTTCTAGCAGCCAAGACTATGACCGATCAGTCTATAGCAATTAGAATATG
AACTGAGACGAATCATATACGTTGCTCGAGTATGCATTGCTGCATGCCAGAGTA
GGCAGTCACCAGAAGCTAAACCCAGATGTCTCCATGCCACTGCGGTTCCATGA
TCGGTAGCAATCTAGTAGACGGATACTGCGTCATGCCTTCAGACAGAGTGGTG
CATCAGTGATGTTACTCGAAAACTGCATCATCCATAAGTGCCTTTCGTCTCGTG
CTGCAGAGATGGTGTTATCTCATTAAACAAGCACTGAAAAGAGAATTGACAGA
GGAGTCCTCAATCAGGGCTAAAGAAAAAGTCGTTCTCGTAGATGTGTTGTGGT
TCAGAAATCGAGCTAAACACCTCTGACATCCAGAAACAGAAAGAATAGGAGC
TCAGCAGTGGATCCAGCACCACAAGGAAAACTGGAGGATGTCCTCCCAGAGG
CCTTTACTGACCACTGTGAAGCTAAAGAGAGCTTCCTACAGTCTCATCAGAAA
ATATGTGTGTCAGTATTATCCTGAGGACAGAGTGGACATCAGGCTTCAGGTGT
TGAAGCACGCTGTGCAGAGTGCTGTAGACAGGGGCCAGTTTCAACAAAAAA
GAGGCAAAGGGTATTCGGAGACATTCCAGGAGAAGAAATCTGAAGAATAAC
GTCTCAAGGGGCGGAAAGTCTCTCGTCCCTGTCATGCCATTAGTAAGTAATGT
TCAGAAACAGCGGTTCCTGGAACATTCCAATAGGTTGTCGTGCTTTCTAAGGC
ACCATCACCCATAGTCCGATCTCTGTTATCACACCCGGACAGGAACACTCAGGT
GCAAATAGTCAACCAGATGAAGGAGGATGAAGAGGAAGATGAGTCATCAGA
AGAAGGCTCTGAGGATGAAGAGCCGCCACGTCA

Figure 6-8: The DNA sequencing result for sample 1 of HCT116$^{FBXW7 (+/+):HP1BP3 (-/-)}$. CACCGCCAGATGATTCTAGAGATG sequence that has to be deleted by application of CRISPR/Cas9 technique, but the result revealed the sequence highlighted by blue color was deleted in the sample N1; however the green part is remained.

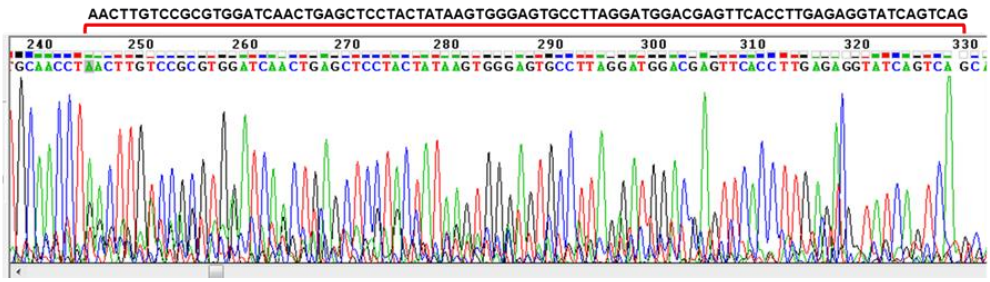
HCT116$^{FBXW7(+/+):HP1BP3(-/-)}$ sample N4 DNA sequencing result



GCAACATGAGCTATGAAGCACTATTTCATGAAAACAGGAGACCGGA
GCCTTTGGCACAGTGAGGTGGATTGTTGTCCGGAGAGATTACCGC
TGTAAAATCAGGGGAGAAAGTTCTGCTTGGTGGAATAGGGGTGGA
GGAGGCAATGAATGTGACCTCTGGAGGAGTACTAGACCATGTGAC
TGATACGTCTCAAGGTGTCTATCAAAATGATGTAGGGGGTATCTTAA
ACTGTCCAAGGCAATCATGCATGGATGTTTAGTCTTAAGCAGAGGA
AAATCTCTCCTCGCAGATATAACAGCTAAACTTTATTTTCAGAAGCA
GAGGTTGCAGGACCAGTGAGTTATTTTCTCTTGTTTTCTTTTCAGGA
TCTTAATAAGGGAAGAAAGTTCCTCCTAAGTCTAGGGAGAGATATTT
AAGAGAAGGAATGATCCACTCAAGTGAATGATAAGGCTCAAGGTGA
GTCATCAGAAGAAGACTCTGAGGATGAAGAGCCGCCACCTAAGAG
AAGGTTGCAGAAGAAAACCCCAGCCAAGTCCCCAGGGAAGGCCGC
ATCTGTGAAGCAGAGAGGGTCCAAGCCTCAAGGAAAGTATCACATG
CCCAGCGGGGGAAACATAGATGACTGAAACGTCTCAAGGTGCCAA
GGATGTTCCACCTAGCAAGTAGGCCTGACAGTTGTCACACACTCAA
CACAAGCCGAGCGGGGCTCCCAAAGAACCCTGCACACAGGCAACC
AAGAAGAATTGC

Figure 6-9: The DNA sequencing result for sample 4 of HCT116$^{FBXW7\ (+/+):\ HP1BP3\ (-/-)}$. CACCGCCAGATGATTCTAGAGATG sequence that has to be deleted by application of CRISPR/Cas9 technique, and the result showed complete deletion of this sequence. The blue highlighted sequence was mutated before deleted part of HP1BP3.

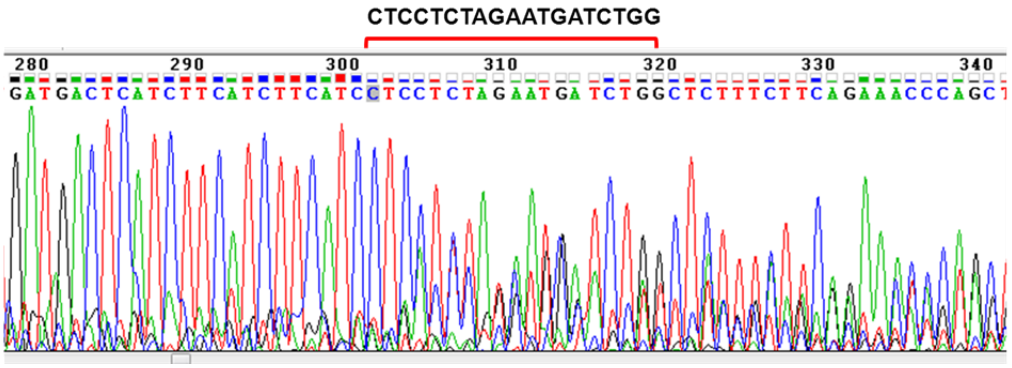
HCT116$^{FBXW7(-/-):HP1BP3(-/-)}$ sample N5 DNA sequencing result



AAGCACTGAAAAAGAGAATTAAAATAGAGGAGTCATCAAACAGGT
TAAAAGGAAAAAGGTGCTTCTGGAAGTTTTGTTGTGGTTCAGAAA
TCAAGAAAAACACCTCAGAAATCCAGAAACAGAAAGAATAGGAGC
TCTGCAGTGGATCCAGAACCACAAGTAAAATTGGAGGATGTCCTC
CCACTGGCCTTTACTCGCCTTTGTGAACCTAAAGAAGCTTCCTAC
AGTCTCATCAGGAAATATGTGTCTCAGTATTATCCTAAGCTTAGAG
TGGACATCAGGCCTCAGCTGTTGAAGAACGCTCTGCAGAGAGCA
GTAGAGAGGGGCCAGTTAGAACAGATAACTGGCAAAGGTGCTTC
GGGGACATTCCAGCTGAAGAAATCTGGGGAGAAACCCCTGCTTG
GTGGAAGCCTGATGGAATATGCAATCTTGTCTGCCATTGCTTCCA
TGAATGAGCGGAAGACCTGCTCTTCCATTGCTTTGAAGAAGTATG
TCTTAGAGAATCACCCAGGAACCAATTCTACCTATCAAATCAATC
CCTGAAAAAGTCCGTGCTGACTGATACCTCTCAAGGTGAACTCGT
CCATCCTAAGGCACTCCCACTTATAGTAGGAGCTCAGTTGATCCA
CGCGGACAAGTTAGGTTGCAGAAGAAAACCCCAGCCAAGTCCCC
AGGGAAGGCCGCATCTGTGAAGCAGAGAGGGTCCAAACCTGCAC
CTAAAGTCTCAGCTGCCCAGCGGGGGAAAGCTAGGCCCTTGCCT
AAGAAAGCACCTCCAAGGCCAAAACGCCTGCCAAGAAGACCAGA
CCCTCATCCACAGTCATCAAGAAACCTAGTGGTGGCTCCTCAAAG
AAGCCTGCAACCAGGCAAGAAAGGAAGAAATGCGG

Figure 6-10: The DNA sequencing result for sample 5 of HCT116$^{FBXW7\ (-/-):HP1BP3\ (-/-)}$. CACCGCCAGATGATTCTAGAGATG sequence that has to be deleted by application of CRISPR/Cas9 technique and the result showed complete deletion of this sequence. The yellow highlighted sequence was mutated before deleted part of HP1BP3.

HCT116$^{FBXW7(-/-):HP1BP3(-/-)}$ sample N6 DNA sequencing result



TTTGTAAACGTAAAGTATCTGCATGCCATGTTGAAAGATTGTGTG
GTATGACTCATCGAATTAAAGATGAAGGGGTCCTTTTTAAGGTTA
GCGATGCAGCTTAAAGGGAAGAATATGATGATTGTGACTTATCCA
GGTGAAGTCGTCCTTCTTCAGGCACTGCCACTTATAGTAGGAGTA
GAGGTGAAGCTGGCGGACAAGTTAACCCAGGAGCTGGGTTTCTG
AAGAAAGAGCCAGATCATTCTAGAGGAGGATGAAGATGAAGATG
AGTCATCAGAAGAAGACTCTGAGGATGAAGAGCCGCCACCTAAG
AGAAGGTTGCAGAAGAAAACCCCAGCCAAGTCCCCAGGGAAGGC
CGCATCTGTGAAGCAGAGAGGGTCCAAACCTCAAGGAAAGTCTC
ACATGCCCAGCGGGGGAAACATAAATGACTGAAACGTCTCAAGG
TGCCAAGGATGTTCCACCTAGAAACTCGGCCTGACAGATGTCAC
ACACTCAAAGCAAGCCGGGTGGGCCTCCCAAAGAAGCCTGCAAC
CAGGCAACCAGAGGACTTTCT

Figure 6-11: The DNA sequencing result for sample 6 of HCT116$^{FBXW7\ (-/-):HP1BP3\ (-/-)}$. CACCGCCAGATGATTCTAGAGATG sequence that has to be deleted by application of CRISPR/Cas9 technique. The yellow highlighted sequence is presented in the sample N6 and the rest was mutated.

6.2.3 Loss of HP1BP3 led to accumulation of total p53 in HCT116 CRC lacking FBXW7 after ionizing irradiation

Previously obtained data (*Chapter 5*) demonstrated accumulation of total levels of p53 in HCT116 cells harbouring FBXW7 compared to FBXW7-deleted HCT116 cell lines in stress-free conditions and confirms recently published reports that FBXW7 ablation in CRC cells results in elevation of steady-state levels of p53 (wt) (Li et al., 2015). Next, we studied FBXW7/p53 correlation in the absence of HP1BP3 in $HCT116^{FBXW7\ (+/+)}$/CRISPR [$HCT116^{FBXW7\ (+/+):\ HP1BP3\ (-/-)}$] and $HCT116^{FBXW7\ (-/-)}$/CRISPR [$HCT116^{FBXW7\ (-/-):\ HP1BP3\ (-/-)}$] cell lines prior and following ionizing irradiation. Alongside p53, expression of ATM was identified in HP1BP3-depleted $HCT116^{FBXW7\ (+/+)}$ and $HCT116^{FBXW7\ (-/-)}$ cells. HP1BP3 depletion in $HCT116^{FBXW7(-/-)}$ cells promoted a remarkable accumulation of total p53 as well as a significant increase of ATM kinase compared with wildtype cell line ($HCT116^{FBXW7(+/+)}$) prior to treatment **(Figure 6-12)**. It is noteworthy, that ionizing irradiation markedly increased p53 expression in both wildtype and FBXW7-null HCT116 cells compared to untreated controls.

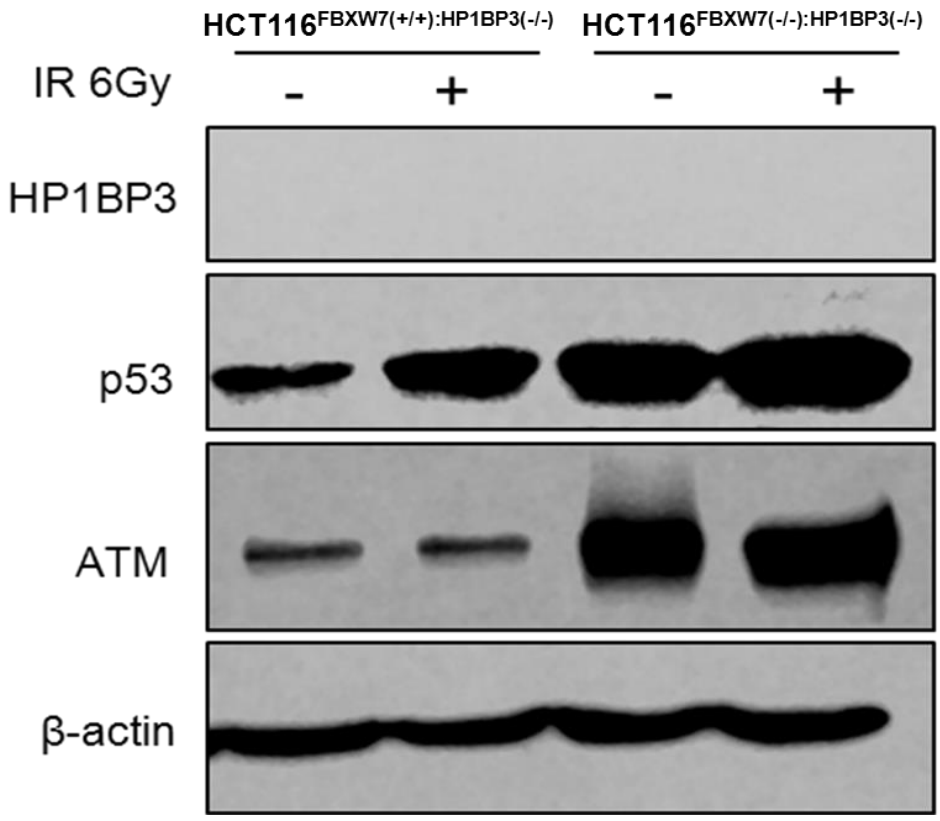


Figure 6-12: The response of HP1BP3-knockout HCT116 CRC cells; [HCT116$^{FBXW7\ (+/+):HP1BP3\ (-/-)}$] vs. [HCT116$^{FBXW7\ (-/-):HP1BP3\ (-/-)}$] **to ionizing radiation.** HCT116 CRC cells lacking HP1BP3 were exposed to 6Gy of ionizing radiation. The extracted cell lysates were immunoblotted with anti-HP1BP3, anti-p53, anti-γH2AX and anti-ATM antibodies. Protein loading levels are monitored by probing for actin.

6.3 DISCUSSION

The invention of CRISPR/Cas9 technology became an important research breakthrough in the field of genome editing. In the current work, CRISPR based gene editing was applied to produce genetically knockout in HCT116 CRC cell lines by targeting human HP1BP3 protein. Furthermore, by using stably HP1BP3 knockout HCT116 generated cell lines it was interesting to observe the

change in p53 and ATM expression level compared to the control cell lines. Previous experimental data demonstrated total level of p53 was increased in A431 cells lacking HP1BP3 (Dutta at el., 2004b). Indeed, HP1BP3–depleted HCT116 cells exhibited higher p53 expression levels, particularly HP1BP3–depleted HCT116$^{FBXW7(-/-)}$ cells where p53 expression was markedly increased compared to the control cells (HCT116$^{FBXW7(-/-)}$). Interestingly, that HP1BP3-knockdown in HCT116 lacking FBXW7 demonstrated completely opposite result by reducing p53 expression level compared to the control HCT116$^{FBXW7\ (-/-)}$ cells. Whereas expression level of p53 was similar in both HP1BP3–depleted and HP1BP3-knockdown HCT116$^{FBXW7\ (+/+)}$ cells. The result suggests possible involvement of FBXW7 in HCT116 CRC cells on p53 expression. ATM kinase response was in line with p53 protein expression. Based on our results, further work to investigate the cellular mechanisms implicated in the FBXW7/HP1BP3 phenomenon is required to provide more insight into the underlying mechanisms.

Although it was planned but due to time limitation, I was unable to carry on genotyping of HP1BP3-targeted knockout clones by Sanger sequencing analysis, as recommended by Ran et al (Ran et al., 2013).

CHAPTER 7

General Discussion

7.1 BRIEF INTRODUCTION

Higher order chromatin organization coordinates all nuclear activities, including promotion of the DNA damage response (DDR) that requires the modification of chromatin structure (Campos and Reinberg, 2009). Over the past several years, numerous lines of evidence showed that the compaction level in heterochromatin and euchromatin entities reflects on both damage sensitivity and repair capacity (Goodazri et al., 2008, Murray et al., 2012). The underlying complexity of heterochromatin is determined by the level of interaction of DNA molecule with histones (Kornberg, 1977) and DNA bound proteins (Probst et al., 2009, Li and Reinberg, 2011).

The condensed structure of heterochromatin provides protection for DNA molecules from damage, thus significantly contributing to the maintenance of genomic stability. Over the past decade, it has become increasingly clear that contribution of chromatin dynamics in chromatin integrity is crucial (Groth et al., 2007). From another perspective, the compacted chromatin environment also presents an impediment to DNA repair. Therefore, heterochromatin exhibits properties distinct from euchromatin dynamics in response to DNA damage. As such, repair kinetics in heterochromatin are slower compared to euchromatin and require structural changes in surrounding chromatin (Goodazri et al., 2008).

Reorganization of heterochromatin structure upon DNA damage ensures the acceptability of damaged sites to DNA repair components. Rearrangement of nucleosomes, the chief protein components of chromatin, represents the initial stage of chromatin manipulation in response to DNA damage (Ura et al., 2001).

The non-histone chromosomal proteins present an additional layer of complexity in tightly compacted nature of the heterochromatin architecture. The involvement of heterochromatin proteins in the DNA damage signaling cascade within heterochromatin regions is just emerging issue. The focus is directed to study the interplay between DDR and chromatin dynamics, where higher-order chromatin components actively and positively contribute to efficient repair (Soria et al., 2012).

HP1BP3 originally was discovered as a novel chromatin binding protein (Hayashihara et. al., 2011). Recent evidence reported a regulatory role of this molecule in the maintenance of chromatin structural integrity and transcriptional regulation (Dutta et al., 2014a). Moreover, recent studies in Dr Nateri's laboratory identified HP1B3 as one of the FBXW7 interacting proteins by using a modified yeast 2-hybrid reverse Ras-recruitment system (rRRS) (Nateri et al., 2004, Kohler and Muller, 2003); Abuzinadah et al., submitted).

In this thesis, my study was focused on defining HP1BP3 as a potential ATM/ATR-related protein substrate and to study its expression, the regulation and the biological function in response to DNA-damaging agents in the fibroblasts and CRC cells.

Thus, the current work provided evidence that:

1. HP1BP3 is a strictly nuclear protein.
2. HP1BP3 is upregulated in response to DNA-damaging agents in human fibroblasts and CRC cells.
3. HP1BP3 is a direct binding substrate of ATM protein kinase.
4. HP1BP3 expression is dependent upon FBXW7 in response to ATM and possibly ATR activation.

7.2 HP1BP3 expression in fibroblasts and CRC cell lines

We and others have provided experimental evidence that HP1BP3 is a strictly nuclear protein (Garfinkel et al., 2015). Several structural characteristics suggest nuclear localization of HP1BP3. The interaction of HP1BP3 with heterochromatin protein 1 (HP1) through PQVKL motif and the association of the protein with entry/exit site of nucleosomal DNA via its globular domain determine the nuclear occupation of HP1BP3 (Garfinkel et al., 2015, Hayashihara et al., 2010). Moreover, by applying web based programs, such as NLStradamus programme (http://www.moseslab.csb.utoronto.ca/NLStradamus/), a Markov model for NLS prediction (Ba et al., 2009) and nucleolar localization sequence Detector software (NoD) (Scott et al., 2010, Scott et al., 2011) we have discovered a cluster of three predicted nuclear localization signals (NLSs), overlapping with nucleolar targeting signals (NTS) within HP1BP3 structure.

To determine subcellular localization of HP1BP3, several GFP- tagged plasmids containing different lengths of HP1BP3 cDNA were constructed by applying site-directed mutagenesis. Using fluorescence microscopy we observed the cellular localization pattern of exogenous and endogenous expression of HP1BP3 in fibroblasts and CRC cells. The expression of wild-type HP1BP3 was restricted within nuclear borders as previously reported (Garfinkel et al., 2015, Hayashihara et al., 2010), whereas HP1BP3 mutant constructs displayed distinct cellular localization pattern expressed by nucleolar enrichment. Despite

differences in nuclear redistribution, all HP1BP3 mutant variants exhibited similar pattern of cellular expression in both fibroblasts and CRC cell lines.

Interestingly, the expression pattern of the D0 construct was cell-specific **(Figures 3-11, 3-12 & 3-16)**. Thus, HP1BP3-D0 was manifested by cytoplasmic redistribution in HCT116 cells, whereas in fibroblasts it showed a diffused expression pattern throughout the whole cell encompassing both the nucleus and cytoplasm. Many studies have demonstrated that post-translational modifications (PTMs) play critical role in nuclear localization of proteins. These modifications include phosphorylation, acetylation, methylation, sumoylation, ubiquitylation, and glycosylation (Wagstaff et al., 2012, Poon and Jans, 2005, Zhao, 2007). Thus, the presence of SQ motifs (S: Serine, Q: Glutamine) in HP1BP3 molecule, which are the common phosphorylation sites of ATM/ATR protein kinases, might be involved in nuclear localization and/or level of the HP1BP3 protein. It has been shown that phosphorylation contributes to substrate activity, stability, interaction with other proteins and subcellular localization and is often involved in subsequent additional PTMs (Shiloh and Ziv, 2013).

Thus, the precise mechanisms that underlying nuclear expression of HP1BP3 is not clear. Therefore, further research is required to study possible critical determinants that might have an affect on the actual nuclear homing of HP1BP3.

7.3 HP1BP3 is a potential substrate of ATM/ATR kinases

There is no available experimental data demonstrating a possible involvement of HP1BP3 molecule in DNA damage complex. For the first time, we have identified HP1BP3 as a potential ATM/ATR substrate. The structural analysis of HP1BP3 discovered the three SQ motifs, consensus sequences of phosphorylation by ATM /ATR kinases. Therefore, we have applied our efforts on the investigation of ATM/ATR-dependent phosphorylation of HP1BP3 in DNA-damaging stress conditions using human fibroblasts and CRC cells. Several DNA-damaging agents such as UV light, ionizing radiation and chemotherapeutic drugs were applied in order to activate ATM/ATR protein kinases, apical kinases that are able to mobilise an extensive DNA damage signalling pathway **(Figures 4-4, 4-13, 4-14, 5-1 & 5-2)**.

The expression of DDR proteins such as p53 and γH2AX was monitored prior and following applied treatment. The elevation of both proteins in response to ATM/ATR activation was observed, as expected, in both fibroblasts and CRC cell lines. Interestingly, the level of HP1BP3 was also upregulated in response to DNA damage **(Figures 4-4, 4-13, 4-14, 5-1 & 5-2).**

According to the recent publication, HP1BP3 exerts a novel role during hypoxia by altering chromatin compaction that leads to increased tumour cell viability and enhanced radio-resistant and chemo-resistant phenotypes. This observation presents HP1BP3 as a key contributor in tumour biology. HP1BP3-mediated heterochromatization, caused by hypoxia stress, drives tumour progression and determines the acquisition of therapy-resistant properties in cancer cells (Dutta

et al., 2014b). On another hand, it was shown that hypoxia sparks activation of ATM (Hammond and Giaccia, 2004), a central controller of genomic stability. Thus, the cytoplasmic distribution of ATM protein suggests on a role of ATM in response to oxidative stress (Watters et al., 1999, Li et al., 2009). Therefore, based on our experimental observations and evidence, we suggest that ATM activation induces HP1BP3. However, the impact of ATM-dependent H1BP3 modulation on heterochromatin structure and therefore transcriptional role of HP1BP3 is still to be elucidated.

Furthermore, in order to test the direct interaction of HP1BP3 with ATM/ATR kinases, immunoprecipitation-coupled immunoblotting by using anti-p-S/T and anti-HP1BP3 antibodies in fibroblasts was performed. The results revealed expression of both exogenous and endogenous bands of HP1BP3 in fibroblasts stably expressing the EGFP-HP1BP3 protein. Moreover, to identify the specificity of SQ phosphorylation site, Oxaliplatin-treated fibroblasts were immunoprecipitated against anti-HP1BP3 and anti-ATM antibodies. Interestingly, the direct association of the two molecules was observed in Oxaliplatin-stressed conditions. These discoveries indicate potential phosphorylation of HP1BP3 by ATM kinase, and thus recognizing HP1BP3 as one of the downstream substrates of ATM. Further research is required to elucidate the functional relation between ATM/ATR and HP1BP3 substrates.

7.4 The interplay between HP1BP3 and FBXW7

Despite the clear evidence that mutated FBXW7 (also known hCDC4, Ago, Sel10, Fbw7) is a major contributor to oncogenesis (Babaei-Jadidi et al., 2011, Moberg et al., 2001, Spruck et al., 2002, Strohmaier et al., 2001), its mechanism of action is yet undetermined. This is partly because it is an E3-ubiquitin ligase, critically regulating proteasome degradation, the biology of which has yet to be revealed.

By applying the yeast two-hybrid reverse Ras Recruitment System (rRRS) (Nateri et al., 2004) and 2D-MALDI-MS assays via intestinal crypt isolation it was aimed to determine phosphorylation-dependent interactions of FBXW7 substrate(s) (Li N et al., in publication). The obtained data suggested a direct binding of FBXW7 to phosphorylated HP1BP3 for degradation, a new FBXW7-associated protein which encodes a heterochromatin protein binding protein.

HP1BP3 as a chromosomal protein that provides a potential route for FBXW7 regulating the entry/exit site of nucleosomal DNA through binding to HP1 (heterochromatin protein 1). Furthermore, we aimed to determine if ATM and ATR phosphorylation putative motifs on HP1BP3 mediated modulation of DNA damage/repair signaling pathways, and subsequently, how alterations in the properties of HP1BP3 determined molecular mechanism(s) within the euchromatin-heterochromatin transition, underlying tumorigenic activities of colorectal cancer cells through the presence of mutated-FBXW7.

Thus, by using HCT116$^{FBXW7\ (+/+)}$ and HCT116$^{FBXW7\ (-/-)}$ cells and applying various DNA-damaging agents, we observed the HP1BP3 behavior in correlation with or without FBXW7. Wild type HCT116 exhibited consistent HP1BP3 induction and HP1BP3 positive correlation in response to ATM/ATR activation, whereas FBXW7-deleted HCT116 cells displayed HP1BP3 reduction **(Figures 5-1 & 5-2)**. Interestingly, the level of DDR proteins such as p53 and γH2AX was upregulated in both cell lines following DNA damage induction **(Figures 5-1 & 5-2)**. **Figure 7-13** presents a brief overview of our current observations, although there is no experimental evidence to suggest a direct correlation between ATM/ATR and FBXW7. Hence, the detailed mechanisms underlying such a response still need to be elucidated.

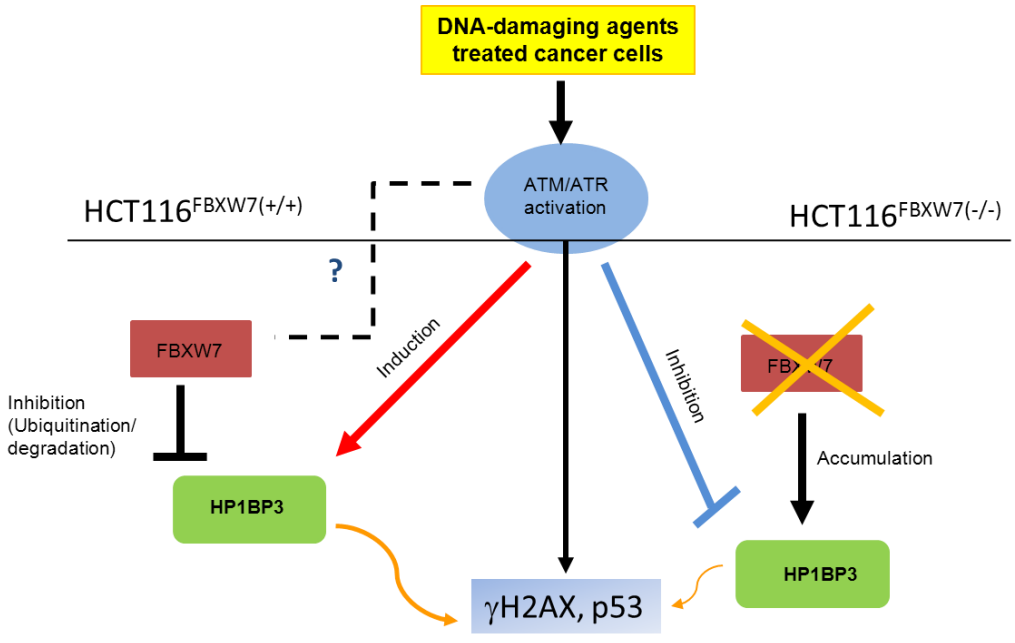


Figure 7-1: Schematic presentation of FBXW7-dependent expression of HP1BP3 in response to ATM/ATR activation in HCT116 CRC cell line with and without FBXW7 mutation. The image illustrates accumulation of HP1BP3

in the presence of FBXW7 and reduction of HP1BP3 in the absence of FBXW7 in response to DNA damage. The elevation of DDR proteins in response to DNA damage is independent of FBXW7.

7.5 Experimental Limitations

To achieve the determined goals of the current research a wide range of experimental plans has been adjusted. However, several experimental limitations have been encountered on the path of study, such as:

1- The absence of anti-phospho-Ser/Thr HP1BP3 antibodies that could recognize the endogenous expression level of phosphor-HP1BP3 in response to DNA damage. It would be helpful to precisely define the phospho-HP1BP3 status as the direct binding partner of activated ATM/ATR protein kinases to chemotherapeutics.

2- Further investigation is required to explore how ATM/ATR activity may modulate the degradation of HP1BP3 by the FBXW7 E3 ligase. This would shed light on HP1BP3 functions in genome and epigenome stability, and therefore tumour biology.

3- Due to time limitation we could not complete the validation of the remaining HP1BP3 phosphorylation sites by site-directed mutagenesis and to determine their significances in drug response, cell cycle and cancer biology.

4- Due to time limitation we could not provide further validation and characterization of HP1BP3 knockout HCT116 cell lines generated by CRISPR/Cas9 technique. It would accomplish studies of

HP1BP3/FBXW7 interplay in response to the activation of DNA damage signaling pathway.

5- Absence of xenograft studies, animal models also present one of the limitations. Such approaches are necessary to explore and validate functional characteristics of HP1BP3 *in vivo* and in associations with the mutated forms of FBXW7 in CRC cells.

7.5 Conclusions & Perspectives

In conclusion**,** we have uncovered the potential involvement of HP1BP3 in DNA damage response. It was achieved by applying various DNA-damaging agents that usually trigger the activation of ATM/ATR kinases. Hence, our data may support the hypothesis that HP1BP3 might be one of the downstream substrates of ATM/ATR proteins. From another perspective, regulation of HP1BP3/FBXW7 by ATM/ATR would act as a dynamic assembly implicated in damage signaling and response activities through chromatin modulation. In the longer term, the interactions and functions of HP1BP3 would help understand the role of HP1BP3 in the tumour microenvironment that could be critical in future targeted therapeutics.

Several key points that need to be taken into further consideration:

- Producing a specific anti-phospho-Ser/Thr HP1BP3 antibody that could detect phosphorylation form of HP1BP3 protein
- Further study of FBXW7/ATM/HP1BP3 interplay in cancer biology
- *In vivo* animal studies such as xenograft and knockout mice to investigate tumourigenic properties and characteristics of HP1BP3

- Studies are also need to be directed at identification of possible regulatory mechanisms that control the expression and/or activity of HP1BP3 such as post-transcriptional and/or other type of post-translational modifications and their significance in cell biology.
- A further study could be considered on the chromatin changes in response to DNA damage and in association with ATM/HP1BP3 **(Figure 7-2)**, using the genetically modified HP1BP3 cells generated. For example, examining the level of H3K9 methylation, acetylation, methyl transferases, HP1α.

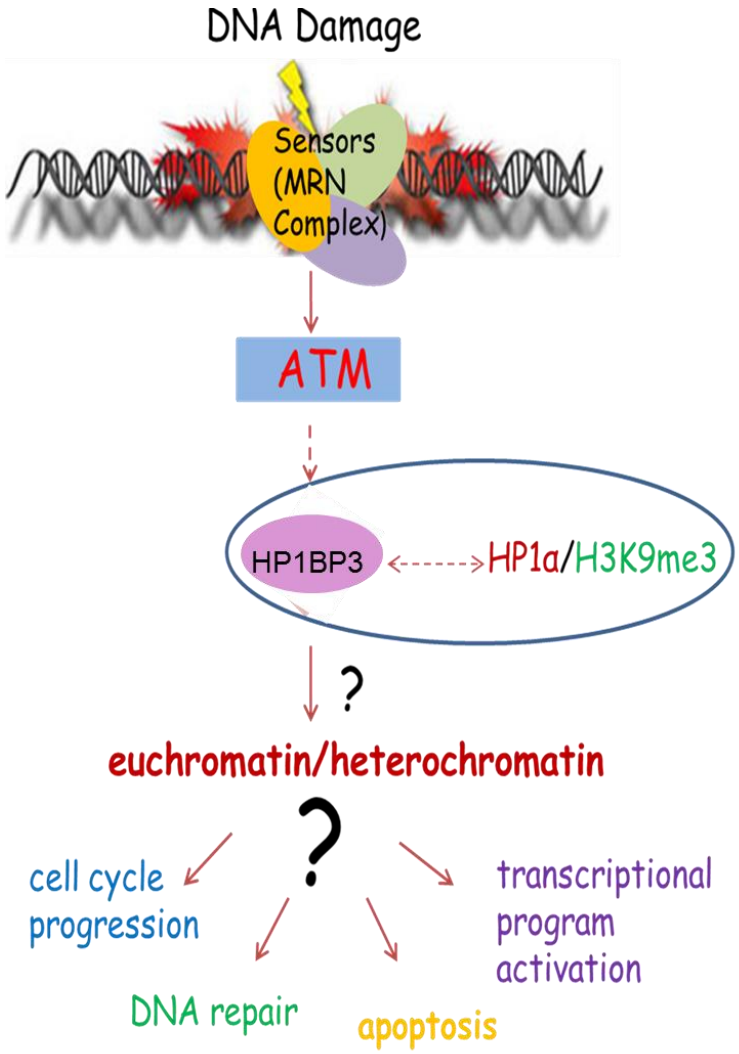


Figure 7-2: Schematic presentation of possible cellular outcomes of HP1BP3-dependent chromatin modulation. Further research is required to elucidate the possible impacts of ATM-dependent HP1BP3 phosphorylation on chromatin functions through involvement in HP1α/H3K9me3 complex.

References

ABRAHAM, R. T. 2001. Cell cycle checkpoint signaling through the ATM and ATR kinases. *Genes & development,* 15**,** 2177-2196.

AGUILERA, A. & GÓMEZ-GONZÁLEZ, B. 2008. Genome instability: a mechanistic view of its causes and consequences. *Nature Reviews Genetics,* 9**,** 204-217.

AHMAD, Y., BOISVERT, F.-M., GREGOR, P., COBLEY, A. & LAMOND, A. I. 2009. NOPdb: nucleolar proteome database—2008 update. *Nucleic acids research,* 37**,** D181-D184.

AL-TASSAN, N., CHMIEL, N. H., MAYNARD, J., FLEMING, N., LIVINGSTON, A. L., WILLIAMS, G. T., HODGES, A. K., DAVIES, D. R., DAVID, S. S., SAMPSON, J. R. & CHEADLE, J. R. 2002. Inherited variants of MYH associated with somatic G : C -> T : A mutations in colorectal tumors. *Nature Genetics,* 30**,** 227-232.

ANDREEFF, M. G.D. & PARDEE, A.B. 2000. Cell proliferation, differentiation, and apoptosis. *Holland-Frei Cancer Medicine.* 5th edition ed. Hamilton (ON): BC Decker.

ARENTS, G. & MOUDRIANAKIS, E. N. 1993. TOPOGRAPHY OF THE HISTONE OCTAMER SURFACE - REPEATING STRUCTURAL MOTIFS UTILIZED IN THE DOCKING OF NUCLEOSOMAL DNA. *Proceedings of the National Academy of Sciences of the United States of America,* 90.

AUCLAIR, Y., ROUGET, R. & DROBETSKY, E. A. 2009. ATR kinase as master regulator of nucleotide excision repair during S phase of the cell cycle. *Cell Cycle,* 8**,** 1865-1871.

BA, A. N. N., POGOUTSE, A., PROVART, N. & MOSES, A. M. 2009. NLStradamus: a simple Hidden Markov Model for nuclear localization signal prediction. *BMC bioinformatics,* 10**,** 202.

BABAEI-JADIDI, R., LI, N., SAADEDDIN, A., SPENCER-DENE, B., JANDKE, A., MUHAMMAD, B., IBRAHIM, E. E., MURALEEDHARAN, R., ABUZINADAH, M., DAVIS, H., LEWIS, A., WATSON, S., BEHRENS, A., TOMLINSON, I. & NATERI, A. S. 2011. FBXW7 influences murine intestinal homeostasis and cancer, targeting Notch, Jun, and DEK for degradation. *Journal of Experimental Medicine,* 208**,** 295-312.

BAILEY, M. L., SINGH, T., MERO, P., MOFFAT, J. & HIETER, P. 2015. Dependence of Human Colorectal Cells Lacking the FBW7 Tumor Suppressor on the Spindle Assembly Checkpoint. *Genetics,* 201**,** 885-895.

BAILIS, J. M. & FORSBURG, S. L. 2003. It's all in the timing: linking S phase to chromatin structure and chromosome dynamics. *Cell cycle.* 2, 303–306.

BAKKENIST, C. J. & KASTAN, M. B. 2003. DNA damage activates ATM through intermolecular autophosphorylation and dimer dissociation. *Nature,* 421, 499–506.

BANGA, S. S. & BOYD, J. B. 1992. Oligonucleotide-directed site-specific mutagenesis in Drosophila melanogaster. *Proceedings of the National Academy of Sciences,* 89**,** 1735-1739.
BANIN, S., MOYAL, L., SHIEH, S. -Y., TAYA, Y., ANDERSON, C. W., CHESSA, L., SMORODINSKY, N.I., PRIVES, C., REISS, Y., SHILOH, Y. & ZIV, Y. 1998. Enhanced phosphorylation of p53 by ATM in response to DNA damage. *Science,* 281, 1674–1677.
BANNISTER, A. J., ZEGERMAN, P., PARTRIDGE, J. F., MISKA, E. A., THOMAS, J. O., ALLSHIRE, R. C. & KOUZARIDES, T. 2001. Selective recognition of methylated lysine 9 on histone H3 by the HP1 chromo domain. *Nature,* 410.
BARTEK, J., LUKAS, C. & LUKAS, J. 2004. Checking on DNA damage in S phase. *Nat Rev Mol Cell Biol,* 5, 792–804.
BAUER, D. E., CANVER, M. C. & ORKIN, S. H. 2015. Generation of Genomic Deletions in Mammalian Cell Lines via CRISPR/Cas9. *Journal of visualized experiments: JoVE*.
BENSIMON, A., AEBERSOLD, R. & SHILOH, Y. 2011. Beyond ATM: the protein kinase landscape of the DNA damage response. *FEBS letters,* 585**,** 1625-1639.
BOND, G. L., HU, W. & LEVINE, A. J. 2005. MDM2 is a central node in the p53 pathway: 12 years and counting. *Current cancer drug targets,* 5**,** 3-8.
BOSOTTI, R., ISACCHI, A. & SONNHAMMER, E. L. 2000. FAT: A novel domain in PIK-related kinases. *Trends Biochem Sci*, 25, 225–227
BRIZEL, D.M., DODGE, R.K., CLOUGH, R.W. & DEWHIRST, M.W. 1999. Oxygenation of head and neck cancer: changes during radiotherapy and impact on treatment outcome. *Radiotherapy and Oncology,* 53, 113-117.
BROWN, E. J. & BALTIMORE, D. 2000. ATR disruption leads to chromosomal fragmentation and early embryonic lethality. *Genes Dev,* 14, 397–402.
BURMA, S., CHEN, B. P., MURPHY, M., KURIMASA, A. & CHEN, D. J. 2001. ATM phosphorylates histone H2AX in response to DNA double-strand breaks. *Journal of Biological Chemistry,* 276**,** 42462-42467.
BÜSSOW, K. 2015. Stable mammalian producer cell lines for structural biology. *Current opinion in structural biology,* 32**,** 81-90.
CAMPOS, E.I. & REINBERG, D. 2009. Histones: annotating chromatin. *Annu. Rev. Genet*. 43, 559–599.
CANMAN, C. E., LIM, D.-S., CIMPRICH, K. A., TAYA, Y., TAMAI, K., SAKAGUCHI, K., APPELLA, E., KASTAN, M. B. & SILICIANO, J. D. 1998. Activation of the ATM kinase by ionizing radiation and phosphorylation of p53. *Science,* 281**,** 1677-1679.
CANN, K. L. & DELLAIRE, G. Heterochromatin and the DNA damage response: the need to relax. *Biochemistry and Cell Biology-Biochimie Et Biologie Cellulaire,* 89**,** 45-60.
CARMO-FONSECA, M., MENDES-SOARES, L. & CAMPOS, I. 2000. To be or not to be in the nucleolus. *Nature cell biology,* 2**,** E107-E112.
CARPENTER, A. J. & PORTER, A. C. G. 2004. Construction, characterization, and complementation of a conditional-lethal DNA

topoisomerase II alpha mutant human cell line. *Molecular Biology of the Cell,* 15.

CHACINSKA, A., KOEHLER, C. M., MILENKOVIC, D., LITHGOW, T. & PFANNER, N. 2009. Importing mitochondrial proteins: machineries and mechanisms. *Cell,* 138**,** 628-644.

CHANG, C. J., GOULDING, S., EARNSHAW, W. C. & CARMENA, M. 2003. RNAi analysis reveals an unexpected role for topoisomerase II in chromosome arm congression to a metaphase plate. *Journal of Cell Science,* 116.

CHAO, C., SAITO, S. I., ANDERSON, C. W., APPELLA, E. & XU, Y. 2000. Phosphorylation of murine p53 at ser-18 regulates the p53 responses to DNA damage. *Proceedings of the National Academy of Sciences,* 97**,** 11936-11941.

CHAUDHARY, S., PAK, J. E., GRUSWITZ, F., SHARMA, V. & STROUD, R. M. 2012. Overexpressing human membrane proteins in stably transfected and clonal human embryonic kidney 293S cells. *nature protocols,* 7**,** 453-466.

CHEHAB, N. H., MALIKZAY, A., STAVRIDI, E. S. & HALAZONETIS, T. D. 1999. Phosphorylation of Ser-20 mediates stabilization of human p53 in response to DNA damage. *Proc Natl Acad Sci U S A,* 96, 13777–13782.

CHELSKY, D., RALPH, R. & JONAK, G. 1989. Sequence requirements for synthetic peptide-mediated translocation to the nucleus. *Molecular and cellular biology,* 9**,** 2487-2492.

CHEN, J. 2000. Ataxia telangiectasia-related protein is involved in the phosphorylation of BRCA1 following deoxyribonucleic acid damage. *Cancer Res,* 60, 5037–5039.

CHENG, Y. & LI, G. 2012. Role of the ubiquitin ligase Fbw7 in cancer progression. *Cancer and Metastasis Reviews,* 31.

CHEUTIN, T., MCNAIRN, A. J., JENUWEIN, T., GILBERT, D. M., SINGH, P. B. & MISTELI, T. 2003. Maintenance of stable heterochromatin domains by dynamic HP1 binding. *Science,* 299**,** 721-725.

CHEVILLARD, C., REIK, W., MCDERMOTT, M., FONTES, M., MATTEI, M. G. & SINGH, P. B. 1993. Chromosomal localization of human homologs of the drosophila heterochromatin protein-1 (hp1) gene. *Mammalian Genome,* 4.

CHIU, S. J., LEE, Y. J., HSU, T. S. & CHEN. W.S. 2009. Oxaliplatin-induced gamma-H2AX activation via both p53-dependent and-independent pathways but is not associated with cell cycle arrest in human colorectal cancer cells. *Chemico-Biological Interactions,* 182, 173-183.

CHO, S. W., KIM, S., KIM, J. M. & KIM, J.-S. 2013. Targeted genome engineering in human cells with the Cas9 RNA-guided endonuclease. *Nature biotechnology,* 31**,** 230-232.

CHRISTIAN, M., CERMAK, T., DOYLE, E. L., SCHMIDT, C., ZHANG, F., HUMMEL, A., BOGDANOVE, A. J. & VOYTAS, D. F. 2010. Targeting DNA double-strand breaks with TAL effector nucleases. *Genetics,* 186**,** 757-761.

CICCIA, A. & ELLEDGE, S.J. 2010. The DNA damage response: making it safe to play with knives. *Mol. Cell,* 40, 179–204.

CIECHANOVER, A. 1998. The ubiquitin–proteasome pathway: on protein death and cell life. *The EMBO journal,* 17**,** 7151-7160.
CIMPRICH, K. & CORTEZ, D. 2008. ATR: An essential regulator of genome integrity. *Nat Rev Mol Cell Biol,* 9, 616–627.
CONG, L., RAN, F. A., COX, D., LIN, S., BARRETTO, R., HABIB, N., HSU, P. D., WU, X., JIANG, W. & MARRAFFINI, L. A. 2013. Multiplex genome engineering using CRISPR/Cas systems. *Science,* 339**,** 819-823.
COOPER G.M. 2000. The eukaryotic cell cycle. The cell: a molecular approach. 2nd edition ed. Sunderland (MA): Sinauer Associates.
CRUSIO, K., KING, B., REAVIE, L. & AIFANTIS, I. 2010. The ubiquitous nature of cancer: the role of the SCFFbw7 complex in development and transformation. *Oncogene,* 29**,** 4865-4873.
DAI, Y. & GRANT, S. 201). New insights into checkpoint kinase 1 in the DNA damage response signaling network. *Clin Cancer Res,* 16, 376–383.
DAVIS, R. J., WELCKER, M. & CLURMAN, B. E. 2014. Tumor suppression by the Fbw7 ubiquitin ligase: mechanisms and opportunities. *Cancer cell,* 26**,** 455-464.
DAVIES, R. J., MILLER, R. & COLEMAN, N. 2005. Colorectal cancer screening: Prospects for molecular stool analysis. *Nature Reviews Cancer,* 5**,** 199-209.
DAWSON, M. A. & KOUZARIDES, T. 2012. Cancer Epigenetics: From Mechanism to Therapy. *Cell,* 150.
DE LAAT, W. L., JASPERS, N. G. & HOEIJMAKERS, J. H. 1999. Molecular mechanism of nucleotide excision repair. *Genes & development,* 13**,** 768-785.
DERHEIMER, F. A., O'HAGAN, H. M., KRUEGER, H. M., HANASOGE, S., PAULSEN, M. T. & LJUNGMAN, M. 2007. RPA and ATR link transcriptional stress to p53. *Proceedings of the National Academy of Sciences,* 104**,** 12778-12783.
DHALLUIN, C., CARLSON, J. E., ZENG, L., HE, C., AGGARWAL, A. K. & ZHOU, M. M. 1999. Structure and ligand of a histone acetyltransferase bromodomain. *Nature,* 399.
DI VIRGILIO, M., YING, C. Y. & GAUTIER, J. 2009. PIKK-dependent phosphorylation of Mre11 induces MRN complex inactivation by disassembly from chromatin. *DNA Repair,* 8, 1311–1320.
DILLON, N. & FESTENSTEIN, R. 2002. Unravelling heterochromatin: competition between positive and negative factors regulates accessibility. *Trends in Genetics,* 18.
DINGWALL, C. & LASKEY, R. A. 1991. Nuclear targeting sequences—a consensus? *Trends in biochemical sciences,* 16**,** 478-481.
DOUGLAS, E. J., FIEGLER, H., ROWAN, A., HALFORD, S., BICKNELL, D. C., BODMER, W., TOMLINSON, I. P. M. & CARTER, N. P. 2004. Array comparative genomic hybridization analysis of colorectal cancer cell lines and primary carcinomas. *Cancer Research,* 64.
DUTTA, B., REN, Y., HAO, P., SIM, K. H., CHEOW, E., ADAV, S., TAM, J. P. & SZE, S. K. 2014a. Profiling of the chromatin-associated proteome identifies HP1BP3 as a novel regulator of cell cycle progression. *Molecular & Cellular Proteomics,* 13**,** 2183-2197.

DUTTA, B., YAN, R., LIM, S. K., TAM, J. P. & SZE, S. K. 2014b. Quantitative profiling of chromatome dynamics reveals a novel role for HP1BP3 in hypoxia-induced oncogenesis. *Molecular & Cellular Proteomics,* 13**,** 3236-3249.

EISSENBERG, J. C. & ELGIN, S. C. R. 2000. The HP1 protein family: getting a grip on chromatin. *Current Opinion in Genetics & Development,* 10.

ENROTH, S., RADA-IGLESISAS, A., ANDERSSON, R., WALLERMAN, O., WANDERS, A., PAHLMAN, L., KOMOROWSKI, J. & WADELIUS, C. 2011. Cancer associated epigenetic transitions identified by genome-wide histone methylation binding profiles in human colorectal cancer samples and paired normal mucosa. *Bmc Cancer,* 11.

ERRICO, A. & COSTANZO, V. 2012. Mechanisms of replication fork protection: A safeguard for genome stability. *Crit Rev Biochem Mol Biol,* 47, 222–235.

ESTELLER, M. 2006. Epigenetics provides a new generation of oncogenes and tumour-suppressor genes. *British Journal of Cancer,* 94.

FALCK, J., MAILAND, N., SYLJUÅSEN, R. G., BARTEK, J. & LUKAS, J. 2001. The ATM–Chk2–Cdc25A checkpoint pathway guards against radioresistant DNA synthesis. *Nature,* 410**,** 842-847.

FANTI, L., BERLOCO, M., PIACENTINI, L. & PIMPINELLI, S. 2003. Chromosomal distribution of Heterochromatin Protein 1 (HP1) in Drosophila: a cytological map of euchromatic HP1 binding sites. *Genetica,* 117.

FARMER, H., McCABE, N., LORD, C. J., TUTT, A. N., JOHNSON, D.A., RICHARDSON, T. B., SANTAROSA, M., DILLON, K. J., HICKSON, I., KNIGHTS, C., MARTIN, N. M., JACKSON, S. P., SMITH, G. C. & ASHWORTH, A. 2005. Targeting the DNA repair defect in BRCA mutant cells as a therapeutic strategy. *Nature,* 434, 917-921.

FEINBERG, A. P., GEHRKE, C. W., KUO, K. C. & EHRLICH, M. 1988. REDUCED GENOMIC 5-METHYLCYTOSINE CONTENT IN HUMAN COLONIC NEOPLASIA. *Cancer Research,* 48.

FERNANDES, N., SUN, Y., CHEN, S., PAUL, P., SHAW, R. J., CANTLEY, L.C. & PRICE, B.D. 2005. DNA damage-induced association of ATM with its target proteins requires a protein interaction domain in the N terminus of ATM. *J Biol Chem*, 280, 15158–15164.

FISHEL, R., LESCOE, M. K., RAO, M. R. S., COPELAND, N. G., JENKINS, N. A., GARBER, J., KANE, M. & KOLODNER, R. 1993. THE HUMAN MUTATOR GENE HOMOLOG MSH2 AND ITS ASSOCIATION WITH HEREDITARY NONPOLYPOSIS COLON-CANCER. *Cell,* 75**,** 1027-1038.

FU, Y., FODEN, J. A., KHAYTER, C., MAEDER, M. L., REYON, D., JOUNG, J. K. & SANDER, J. D. 2013. High-frequency off-target mutagenesis induced by CRISPR-Cas nucleases in human cells. *Nature biotechnology,* 31**,** 822-826.

FULDA, S. 2012. Histone deacetylase (HDAC) inhibitors and regulation of TRAIL-induced apoptosis. *Experimental Cell Research,* 318.

GANNON, H. S., WODA, B. A. & JONES, S. N. 2012. ATM phosphorylation of Mdm2 Ser394 regulates the amplitude and duration of the DNA damage response in mice. *Cancer cell,* 21**,** 668-679.
GARFINKEL, B. P., MELAMED-BOOK, N., ANUKA, E., BUSTIN, M. & ORLY, J. 2015. HP1BP3 is a novel histone H1 related protein with essential roles in viability and growth. *Nucleic acids research,* gkv089.
GARNEAU, J. E., DUPUIS, M.-È., VILLION, M., ROMERO, D. A., BARRANGOU, R., BOYAVAL, P., FREMAUX, C., HORVATH, P., MAGADÁN, A. H. & MOINEAU, S. 2010. The CRISPR/Cas bacterial immune system cleaves bacteriophage and plasmid DNA. *Nature,* 468**,** 67-71.
GLOOR, G. B., NASSIF, N. A., JOHNSON-SCHLITZ, D. M., PRESTON, C. R. & ENGELS, W. R. 1991. Targeted gene replacement in Drosophila via P element-induced gap repair. *Science,* 253**,** 1110-1117.
GONG, W. J. & GOLIC, K. G. 2003. Ends-out, or replacement, gene targeting in Drosophila. *Proceedings of the National Academy of Sciences,* 100**,** 2556-2561.
GOODARZI, A. A., NOON, A. T., DECKBAR, D., ZIV, Y., SHILOH, Y., LÖBRICH, M. & JEGGO, P. A. 2008. ATM signaling facilitates repair of DNA double-strand breaks associated with heterochromatin. *Molecular cell,* 31**,** 167-177.
GORGOULIS, V. G., VASSILIOU, L.-V. F., KARAKAIDOS, P., ZACHARATOS, P., KOTSINAS, A., LILOGLOU, T., VENERE, M., DITULLIO, R. A., KASTRINAKIS, N. G. & LEVY, B. 2005. Activation of the DNA damage checkpoint and genomic instability in human precancerous lesions. *Nature,* 434**,** 907-913.
GARFINKEL, B. P., MELAMED-BOOK, N., ANUKA, E., BUSTIN, M. & ORLY, J. 2015. HP1BP3 is a novel histone H1 related protein with essential roles in viability and growth. *Nucleic acids research,* gkv089.
GATEI, M., JAKOB, B., CHEN, P., KIJAS, A. W., BECHEREL, O. J., GUEVEN, N.,BIRREL, G., LEE, J.H., PAULL, T. T., LERENTHAL, Y., FAZRY, S., TAUCHER-SCHOLZ, G., KALB, R., SCHINDLER, D., WALTES, R., DORK, T. & LAVIN, M.F. 2011. ATM protein-dependent phosphorylation of Rad50 protein regulates DNA repair and cell cycle control. *J Biol Chem,* 286, 31542–31556.
GHATTASS, K., ASSAH, R., EL-SABBAN, M. & GALI-MUHTASIB, H. 2013. Targeting hypoxia for sensitization of tumors to radio-and chemo-therapy. *Current cancer drug targets,* 13, 670-685.
GIGLIA-MARI, G., ZOTTER, A. & VERMEULEN, W. 2011. DNA damage response. *Cold Spring Harb Perspect Biol,* 3, a000745.
GOODARZI, A. A., NOON, A. T., DECKBAR, D., ZIV, Y., SHILOH, Y., LOEBRICH, M. & JEGGO, P. A. 2008. ATM signaling facilitates repair of DNA double-strand breaks associated with heterochromatin. *Molecular Cell,* 31**,** 167-177.
GRADY, W. M. & CARETHERS, J. M. 2008. Genomic and epigenetic instability in colorectal cancer pathogenesis. *Gastroenterology,* 135.
GREWAL, S. I. S. & ELGIN, S. C. 2002. Heterochromatin: new possibilities for the inheritance of structure. *Current Opinion in Genetics & Development,* 12.

GREWAL, S. I. & JIA, S. 2007. Heterochromatin revisited. *Nature Reviews Genetics,* 8**,** 35-46.

GROTH, A., ROCHA, W., VERREAULT, A. & ALMOUZNI, G. 2007. Chromatin challenges during DNA replication and repair. *Cell,* 128, 721–733.

GUENATRI, M., BAILLY, D., MAISON, C. & ALMOUZNI, G. 2004. Mouse centric and pericentric satellite repeats form distinct functional heterochromatin. *Journal of Cell Biology,* 166.

HAMMOND, E.M. & GIACCIA, A.J. 2004. The role of ATM and ATR in the cellular response to hypoxia and reoxygenation. *DNA Repair (Amst),* 3, 1117–22.

HANAWALT, P. C. 2002. Subpathways of nucleotide excision repair and their regulation. *oncogene,* 21**,** 8949-8956.

HAPPEL, N. & DOENECKE, D. 2009. Histone H1 and its isoforms: contribution to chromatin structure and function. *Gene,* 431, 1–12.

HASAN, N. M., ADAMS, G. E. & JOINER, M. C. 1999. Effect of serum starvation on expression and phosphorylation of PKC-α and p53 in V79 cells: Implications for cell death. *International journal of cancer,* 80**,** 400-405.

HATHAWAY, N. A., BELL, O., HODGES, C., MILLER, E. L., NEEL, D. S. & CRABTREE, G. R. 2012. Dynamics and memory of heterochromatin in living cells. *Cell,* 149**,** 1447-1460.

HAUPT, Y., MAYA, R., KAZAZ, A. & OREN, M. 1997. Mdm2 promotes the rapid degradation of p53. *Nature,* 387, 296–299.

HAYASHIHARA, K., UCHIYAMA, S., SHIMAMOTO, S., KOBAYASHI, S., TOMSCHIK, M., WAKAMATSU, H., NO, D., SUGAHARA, H., HORI, N., NODA, M., OHKUBO, T., ZLATANOVA, J., MATSUNAGA, S. & FUKUI, K. 2010. The Middle Region of an HP1-binding Protein, HP1-BP74, Associates with Linker DNA at the Entry/Exit Site of Nucleosomal DNA. *Journal of Biological Chemistry,* 285.

HEDIGER, F. & GASSER, S. M. 2006. Heterochromatin protein 1: don't judge the book by its cover! *Current Opinion in Genetics & Development,* 16.

HENIKOFF, S., AHMAD, K. & MALIK, H. S. 2001. The centromere paradox: Stable inheritance with rapidly evolving DNA. *Science,* 293.

HERMSEN, M., POSTMA, C., BAAK, J., WEISS, M., RAPALLO, A., SCIUTTO, A., ROEMEN, G., ARENDS, J. W., WILLIAMS, R., GIARETTI, W., DE GOEIJ, A. & MEIJER, G. 2002. Colorectal adenoma to carcinoma progression follows multiple pathways of chromosomal instability. *Gastroenterology,* 123.

HILTON, I. B. & GERSBACH, C. A. 2015. Enabling functional genomics with genome engineering. *Genome research,* 25**,** 1442-1455.

HIRAGAMI-HAMADA, K., SHINMYOZU, K., HAMADA, D., TATSU, Y., UEGAKI, K., FUJIWARA, S. & NAKAYAMA, J.-I. 2011. N-Terminal Phosphorylation of HP1 alpha Promotes Its Chromatin Binding. *Molecular and Cellular Biology,* 31.

HIRANO, T. & MITCHISON, T. J. 1994. A HETERODIMERIC COILED-COIL PROTEIN REQUIRED FOR MITOTIC CHROMOSOME CONDENSATION IN-VITRO. *Cell,* 79.

HOCKEMEYER, D., WANG, H., KIANI, S., LAI, C. S., GAO, Q., CASSADY, J. P., COST, G. J., ZHANG, L., SANTIAGO, Y. & MILLER, J. C. 2011. Genetic engineering of human pluripotent cells using TALE nucleases. *Nature biotechnology,* 29**,** 731-734.

HSU, P. D., SCOTT, D. A., WEINSTEIN, J. A., RAN, F. A., KONERMANN, S., AGARWALA, V., LI, Y., FINE, E. J., WU, X. & SHALEM, O. 2013. DNA targeting specificity of RNA-guided Cas9 nucleases. *Nature biotechnology,* 31**,** 827-832.

HUDSON, D. F., VAGNARELLI, P., GASSMANN, R. & EARNSHAW, W. C. 2003. Condensin is required for nonhistone protein assembly and structural integrity of vertebrate mitotic chromosomes. *Developmental Cell,* 5.

HUNG, M.-C. & LINK, W. 2011. Protein localization in disease and therapy. *Journal of cell science,* 124**,** 3381-3392.

HURLEY, P. J. & BUNZ, F. 2007. ATM and ATR: components of an integrated circuit. *Cell cycle,* 6**,** 414-417.

IBUKI, Y. & TOYOOKA, T. 2015. Evaluation of chemical phototoxicity, focusing on phosphorylated histone H2AX. *Journal of radiation research,* 56**,** 220-228.

JACKSON, S.P. & BARTEK, J. 2009. The DNA-damage response in human biology and disease. *Nature,* 461, 1071–1078.

JAMES, T. C., EISSENBERG, J. C., CRAIG, C., DIETRICH, V., HOBSON, A. & ELGIN, S. C. R. 1989. DISTRIBUTION PATTERNS OF HP1, A HETEROCHROMATIN-ASSOCIATED NONHISTONE CHROMOSOMAL PROTEIN OF DROSOPHILA. *European Journal of Cell Biology,* 50.

JENUWEIN, T. & ALLIS, C. D. 2001. Translating the histone code. *Science,* 293.

JIANG, G. & SANCAR, A. 2006. Recruitment of DNA damage checkpoint proteins to damage in transcribed and nontranscribed sequences. *Molecular and cellular biology,* 26**,** 39-49.

JINEK, M., CHYLINSKI, K., FONFARA, I., HAUER, M., DOUDNA, J. A. & CHARPENTIER, E. 2012. A programmable dual-RNA–guided DNA endonuclease in adaptive bacterial immunity. *Science,* 337**,** 816-821.

JINEK, M., EAST, A., CHENG, A., LIN, S., MA, E. & DOUDNA, J. 2013. RNA-programmed genome editing in human cells. *Elife,* 2**,** e00471.

JONKER, D. J., SPITHOFF, K. & MAROUN, J. 2011. Adjuvant Systemic Chemotherapy for Stage II and III Colon Cancer after Complete Resection: An Updated Practice Guideline. *Clinical Oncology,* 23**,** 314-322.

JOHNSON, D.G. & WALKER, C.L. 1999. Cyclins and cell cycle checkpoints. *Annual review of pharmacology and toxicology*. 39: 295-312.

KALDERON, D., RICHARDSON, W. D., MARKHAM, A. F. & SMITH, A. E. 1984. Sequence requirements for nuclear location of simian virus 40 large-T antigen.

KASTAN, M. B., ZHAN, Q., EL-DEIRY, W. S., CARRIER, F., JACKS, T., WALSH, W. V., PLUNKETT, B. S., VOGELSTEIN, B. & FORNACE. JR. A. J. 1992. A mammalian cell cycle checkpoint

pathway utilizing p53 and GADD45 is defective in ataxia–telangiectasia. *Cell,* 71, 587–597.
KASTAN, M. B. & BARTEK, J. 2004. Cell-cycle checkpoints and cancer. *Nature,* 432**,** 316-323.
KASTAN, M. B., ONYEKWERE, O., SIDRANSKY, D., VOGELSTEIN, B. & CRAIG, R. W. 1991. Participation of p53 protein in the cellular response to DNA damage. *Cancer research,* 51**,** 6304-6311.
KHALIL, H., TUMMALA, H. & ZHELEV, N. 2012a. ATM in focus: A damage sensor and cancer target. *Biodiscovery,* 5.
KHALIL, H. S., TUMMALA, H., CHAKAROV, S., ZHELEV, N. & LANE, D. P. 2012b. Targeting ATM pathway for therapeutic intervention in cancer. *Biodiscovery,* 1.
KHALIL, H. S., TUMMALA, H., HUPP, T. R. & ZHELEV, N. 2012c. Pharmacological inhibition of ATM by KU55933 stimulates ATM transcription. *Experimental Biology and Medicine,* 237**,** 622-634.
KEITH, C. T. & SCHREIBER, S. L. 1995. PIK-related kinases: DNA repair, recombination, and cell cycle checkpoints. *Science,* 270, 50–51.
KHOSRAVI, R., MAYA, R., GOTTLIEB, T., OREN, M., SHILOH, Y. & SHKEDY, D. 1999. Rapid ATM dependent phosphorylation of MDM2 precedes p53 accumulation in response to DNA damage. *Proc Natl Acad Sci U S A,* 96, 14973–14977.
KIM, S. T., LIM, D. S., CANMAN, C. E. & KASTAN, M. B. 1999. Substrate specificities and identification of putative substrates of ATM kinase family members. *Journal of Biological Chemistry,* 274**,** 37538-37543.
KOHLER, F. & MULLER, K. M. 2003. Adaptation of the Ras-recruitment system to the analysis of interactions between membrane-associated proteins. *Nucleic Acids Research,* 31.
KORNBERG, R.D. 1977. Structure of chromatin. *Annu. Rev. Biochem,* 46, 931–954.
KOUZARIDES, T. 2007. Chromatin modifications and their function. *Cell,* 128.
KURZ, E. U. & LEES-MILLER, S. P. 2004. DNA damage-induced activation of ATM and ATM-dependent signaling pathways. *DNA Repair,* 3**,** 889-900.
KYLIE, M. W., HARAN, S., STEVEN, M. H., DAVID, H. & DAVID, A. J. 2012. Ivermectin is a specific inhibitor of importin alpha/beta-mediated nuclear import able to inhibit replication of HIV-1 and dengue virus. *Biochemical Journal,* 443**,** 851-856.
LAI, T., YANG, Y. & NG, S. K. 2013. Advances in mammalian cell line development technologies for recombinant protein production. *Pharmaceuticals,* 6**,** 579-603.
LANDAU, D. A. & WU, C. J. 2013. Chronic lymphocytic leukemia: Molecular heterogeneity revealed by high-throughput genomics. *Genome Med,* 5.
LANGE, A., MILLS, R. E., LANGE, C. J., STEWART, M., DEVINE, S. E. & CORBETT, A. H. 2007. Classical nuclear localization signals: definition, function, and interaction with importin α. *Journal of Biological Chemistry,* 282**,** 5101-5105.

LAUFER, B. I. & SINGH, S. M. 2015. Strategies for precision modulation of gene expression by epigenome editing: an overview. *Epigenetics & chromatin,* 8**,** 1-12.

LAURILA, K. & VIHINEN, M. 2009. Prediction of disease-related mutations affecting protein localization. *BMC genomics,* 10**,** 122.

LAVIGNE, M., ESKELAND, R., AZEBI, S., SAINT-ANDRÉ, V., JANG, S. M., BATSCHÉ, E., FAN, H.-Y., KINGSTON, R. E., IMHOF, A. & MUCHARDT, C. 2009. Interaction of HP1 and Brg1/Brm with the globular domain of histone H3 is required for HP1-mediated repression. *PLoS Genet,* 5**,** e1000769-e1000769.

LAVIN, M. F. 2008. Ataxia–telangiectasia: From a rare disorder to a paradigm for cell signalling and cancer. *Nat Rev Mol Cell Biol,* 9, 759–769.

LECHNER, M. S., SCHULTZ, D. C., NEGOREV, D., MAUL, G. G. & RAUSCHER, F. J. 2005. The mammalian heterochromatin protein 1 binds diverse nuclear proteins through a common motif that targets the chromoshadow domain. *Biochemical and biophysical research communications,* 331**,** 929-937.

LECKER, S. H., GOLDBERG, A. L. & MITCH, W. E. 2006. Protein degradation by the ubiquitin-proteasome pathway in normal and disease states. *Journal of the American Society of Nephrology,* 17**,** 1807-1819.

LEE, J. H. & PAULL, T. T. 2005. ATM activation by DNA double-strand breaks through the Mre11–Rad50–Nbs1 complex. *Science,* 308, 551–554.

LEE, J.H. & PAULL, T. T. 2007. Activation and regulation of ATM kinase activity in response to DNA double-strand breaks. *Oncogene,* 26**,** 7741-7748.

LEROY, G., RICKARDS, B. & FLINT, S. J. 2008. The double bromodomain proteins Brd2 and Brd3 couple histone acetylation to transcription. *Molecular Cell,* 30.

LEVINE, S. S., KING, I. F. G. & KINGSTON, R. E. 2004. Division of labor in Polycomb group repression. *Trends in Biochemical Sciences,* 29.

LI, G. & REINBERG, D. 2011. Chromatin higher-order structures and gene regulation. *Curr. Opin. Genet. Dev,* 21, 175–186.

LI, J., HAN, Y.R., PLUMMER, M.R. & HERRUP, K. 2009. Cytoplasmic ATM in neurons modulates synaptic function. *Curr Biol,* 19, 2091–6.

LI, N., LORENZI, F., KALAKOUTI, E., NORMATOVA, M., BABAEI-JADIDI, R., TOMLINSON, I. & NATERI, A. S. 2015. FBXW7-mutated colorectal cancer cells exhibit aberrant expression of phosphorylated-p53 at Serine-15. *Oncotarget,* 6**,** 9240-9256.

LIEFER, K.M., KOSTER, M.I., WANG, X., YANG, A., MCKEON, F. & ROOP, D.R. 2000. Down-Regulation of p63 is required for Epidermal UV-B-induced Apoptosis. *Cancer Research,* 60, 4016–4020.

LIM, D. -S., KIM, S. -T., XU, B., MASER, R. S., LIN, J., PETRINI, J. H. J. & KASTAN, M. B. 2000. ATM phosphorylates p95/nbs1 in an S-phase checkpoint pathway. *Nature,* 404, 613–617.

LIU, Q. & GONG, Z. 2011. The coupling of epigenome replication with DNA replication. *Curr. Opin. Plant Biol.* 14, 187–194.

LOMBERK, G., WALLRATH, L. L. & URRUTIA, R. 2006. The Heterochromatin Protein 1 family. *Genome Biology,* 7.

LUGER, K., MADER, A. W., RICHMOND, R. K., SARGENT, D. F. & RICHMOND, T. J. 1997. Crystal structure of the nucleosome core particle at 2.8 angstrom resolution. *Nature,* 389.

LUPARDUS, P. J., BYUN, T., YEE, M.-C., HEKMAT-NEJAD, M. & CIMPRICH, K. A. 2002. A requirement for replication in activation of the ATR-dependent DNA damage checkpoint. *Genes & development,* 16**,** 2327-2332.

MATSUOKA, S., BALLIF, B. A., SMOGORZEWSKA, A., MCDONALD, E. R., HUROV, K. E., LUO, J., BAKALARSKI, C. E., ZHAO, Z., SOLIMINI, N. & LERENTHAL, Y. 2007. ATM and ATR substrate analysis reveals extensive protein networks responsive to DNA damage. *Science,* 316**,** 1160-1166.

MCLANE, L. M. & CORBETT, A. H. 2009. Nuclear localization signals and human disease. *IUBMB life,* 61**,** 697-706.

MCMANUS, K. J. & HENDZEL, M. J. 2005. ATM-dependent DNA damage-independent mitotic phosphorylation of H2AX in normally growing mammalian cells. *Molecular biology of the cell,* 16**,** 5013-5025.

MEHMOOD, R.K., PARKER, J., AHMED, S., QASEM, E., MOHAMMED, A. A., ZEESHAN. M. & JEHANGIR, E. 2014. Review of cisplatin and oxaliplatin in current immunogenic and monoclonal antibodies perspective. *World Journal of Oncology,* 3, 97-108.

MEHTA, T. S., LU, H., WANG, X., URVALEK, A. M., NGUYEN, K.-H. H., MONZUR, F., HAMMOND, J. D., MA, J. Q. & ZHAO, J. 2009. A unique sequence in the N-terminal regulatory region controls the nuclear localization of KLF8 by cooperating with the C-terminal zinc-fingers. *Cell research,* 19**,** 1098-1109.

MIN, S.-H., LAU, A. W., LEE, T. H., INUZUKA, H., WEI, S., HUANG, P., SHAIK, S., LEE, D. Y., FINN, G. & BALASTIK, M. 2012. Negative regulation of the stability and tumor suppressor function of Fbw7 by the Pin1 prolyl isomerase. *Molecular cell,* 46**,** 771-783.

MISTRIK, M., OPLUSTILOVA, L., LUKAS, J. & BARTEK, J. 2009. Low-dose DNA damage and replication stress responses quantified by optimized automated single-cell image analysis. *Cell Cycle,* 8**,** 2592-2599.

MYERS, J. S. & CORTEZ, D. 2006. Rapid activation of ATR by ionizing radiation requires ATM and Mre11. *Journal of Biological Chemistry,* 281**,** 9346-9350.

MAISON, C. & ALMOUZNI, G. 2004. HP1 and the dynamics of heterochromatin maintenance. *Nature Reviews Molecular Cell Biology,* 5.

MAISON, C., BAILLY, D., ROCHE, D., DE OCA, R. M., PROBST, A. V., VASSIAS, I., DINGLI, F., LOMBARD, B., LOEW, D., QUIVY, J.-P. & ALMOUZNI, G. 2011. SUMOylation promotes de novo targeting of HP1 alpha to pericentric heterochromatin. *Nature Genetics,* 43.

MALI, P., YANG, L., ESVELT, K. M., AACH, J., GUELL, M., DICARLO, J. E., NORVILLE, J. E. & CHURCH, G. M. 2013. RNA-guided human genome engineering via Cas9. *Science,* 339**,** 823-826.

MILLER, J. C., HOLMES, M. C., WANG, J., GUSCHIN, D. Y., LEE, Y.-L., RUPNIEWSKI, I., BEAUSEJOUR, C. M., WAITE, A. J., WANG, N. S. & KIM, K. A. 2007. An improved zinc-finger nuclease architecture for highly specific genome editing. *Nature biotechnology,* 25**,** 778-785.

MAO, J.-H., KIM, I.-J., WU, D., CLIMENT, J., KANG, H. C., DELROSARIO, R. & BALMAIN, A. 2008a. FBXW7 Targets mTOR for Degradation and Cooperates with PTEN in Tumor Suppression. Science, 321, 1499-1502.

MARESCA, T. J., FREEDMAN, B. S. & HEALD, R. 2005. Histone H1 is essential for mitotic chromosome architecture and segregation in Xenopus laevis egg extracts. *Journal of Cell Biology,* 169.

MARINE, J. -C. & LOZANO, G. 2010.Mdm2-mediated ubiquitylation: p53 and beyond. *Cell Death Differ,* 17, 93–102.

MARTIN, E. S., TONON, G., SINHA, R., XIAO, Y., FENG, B., KIMMELMAN, A. C., PROTOPOPOV, A., IVANOVA, E., BRENNAN, C., MONTGOMERY, K., KUCHERLAPATI, R., BAILEY, G., REDSTON, M., CHIN, L. & DEPINHO, R. A. 2007. Common and distinct genomic events in sporadic colorectal cancer and diverse cancer types. *Cancer Research,* 67.

MATEESCU, B., BOURACHOT, B., RACHEZ, C., OGRYZKO, V. & MUCHARDT, C. 2008. Regulation of an inducible promoter by an HP1 beta-HP1 gamma switch. *Embo Reports,* 9.

MATSUOKA, S., BALLIF, B. A., SMOGORZEWSKA, A., MCDONALD, E. R., HUROV, K. E., LUO, J., BAKALARSKI, CE, ZHAO, Z., SOLIMINI, N., LERENTHAL, Y., SHILOH, Y., GYGI, S.P. & ELLEDGE S.J. 2007. ATM and ATR substrate analysis reveals extensive protein networks responsive to DNA damage. *Science,* 316, 1160–1166.

MOBERG, K. H., BELL, D. W., WAHRER, D. C., HABER, D. A. & HARIHARAN, I. K. 2011. Archipelago regulates Cyclin E levels in Drosophila and is mutated in human cancer cell lines. *Nature*, 413, 311–316.

MUCHARDT, C., GUILLEME, M., SEELER, J. S., TROUCHE, D., DEJEAN, A. & YANIV, M. 2002. Coordinated methyl and RNA binding is required for heterochromatin localization of mammalian HP1 alpha. *Embo Reports,* 3.

MURRAY, J. M., STIFF, T. & JEGGO, P. A. DNA double-strand break repair within heterochromatic regions. 2012. *Biochemical Society Transactions*, 40**,** 173-178.

NATERI, A. S., RIERA-SANS, L., DA COSTA, C. & BEHRENS, A. 2004. The ubiquitin ligase SCFFbw7 antagonizes apoptotic JNK signaling. *Science*, 303**,** 1374-1378.

NATERI, A.S., SPENCER-DENE, B. & BEHRENS, A. 2005. Interaction of phosphorylated c-Jun with TCF4 regulates intestinal cancer development. *Nature*, 437, 281-285.

NORDSMARK, M., OVERGAARD, M. & OVERGAARD, J. 1996. Pretreatment oxygenation predicts radiation response in advanced squamous cell carcinoma of the head and neck. *Radiotherapy and oncology : journal of the European Society for Therapeutic Radiology and Oncology*, 41, 31-39.

NOVAK, B., SIBLE, J.C. & TYSON, J.J. 2002. Checkpoints in the Cell Cycle. *eLS*: John Wiley & Sons, Ltd.

OSIPOV, A. N., PUSTOVALOVA, M., GREKHOVA, A., EREMIN, P., VOROBYOVA, N., PULIN, A., ZHAVORONKOV, A., ROUMIANTSEV, S., KLOKOV, D. Y. & EREMIN, I. 2015. Low doses of X-rays induce prolonged and ATM-independent persistence of γH2AX foci in human gingival mesenchymal stem cells. *Oncotarget,* 6**,** 27275-27287.

OWEN, D. J., ORNAGHI, P., YANG, J. C., LOWE, N., EVANS, P. R., BALLARIO, P., NEUHAUS, D., FILETICI, P. & TRAVERS, A. A. 2000. The structural basis for the recognition of acetylated histone H4 by the bromodomain of histone acetyltransferase Gcn5p. *Embo Journal,* 19.

PAPADOPOULOS, N., NICOLAIDES, N. C., WEI, Y. F., RUBEN, S. M., CARTER, K. C., ROSEN, C. A., HASELTINE, W. A., FLEISCHMANN, R. D., FRASER, C. M., ADAMS, M. D., VENTER, J. C., HAMILTON, S. R., PETERSEN, G. M., WATSON, P., LYNCH, H. T., PELTOMAKI, P., MECKLIN, J. P., DELACHAPELLE, A., KINZLER, K. W. & VOGELSTEIN, B. 1994. MUTATION OF A MUTL HOMOLOG IN HEREDITARY COLON-CANCER. *Science,* 263**,** 1625-1629.

PEDERSON, T. & TSAI, R. Y. 2009. In search of nonribosomal nucleolar protein function and regulation. *The Journal of cell biology,* 184**,** 771-776.

PETERS, A., O'CARROLL, D., SCHERTHAN, H., MECHTLER, K., SAUER, S., SCHOFER, C., WEIPOLTSHAMMER, K., PAGANI, M., LACHNER, M., KOHLMAIER, A., OPRAVIL, S., DOYLE, M., SIBILIA, M. & JENUWEIN, T. 2001. Loss of the Suv39h histone methyltransferases impairs mammalian heterochromatin and genome stability. *Cell,* 107.

POMBO, A. 2007. Advances in imaging the interphase nucleus using thin cryosections. *Histochem.Cell Biol.* 128, 97–104.

POON, I. K. & JANS, D. A. 2005. Regulation of nuclear transport: central role in development and transformation? *Traffic,* 6**,** 173-186.

POPOV, N., HEROLD, S., LLAMAZARES, M., SCHÜLEIN, C. & EILERS, M. 2007a. Fbw7 and Usp28 regulate myc protein stability in response to DNA damage. *Cell cycle,* 6**,** 2327-2331.

POPOV, N., WANZEL, M., MADIREDJO, M., ZHANG, D., BEIJERSBERGEN, R., BERNARDS, R., MOLL, R., ELLEDGE, S. J. & EILERS, M. 2007b. The ubiquitin-specific protease USP28 is required for MYC stability. *Nature cell biology,* 9**,** 765-774.

PORTEUS, M. H. & BALTIMORE, D. 2003. Chimeric nucleases stimulate gene targeting in human cells. *Science,* 300**,** 763-763.

POWELL, S. M., ZILZ, N., BEAZERBARCLAY, Y., BRYAN, T. M., HAMILTON, S. R., THIBODEAU, S. N., VOGELSTEIN, B. & KINZLER, K. W. 1992. APC MUTATIONS OCCUR EARLY DURING COLORECTAL TUMORIGENESIS. *Nature,* 359.

PRICE, B. D. & D'ANDREA, A. D. 2013. Chromatin remodeling at DNA double-strand breaks. *Cell,* 152**,** 1344-1354.

PROBST, A. V. & ALMOUZNI, G. 2008. Pericentric heterochromatin: dynamic organization during early development in mammals. *Differentiation,* 76.
PROBST, A. V., DUNLEAVY, E. & ALMOUZNI, G. 2009. Epigenetic inheritance during the cell cycle. *Nat. Rev. Mol. Cell Biol.* 10, 192–206.
RAFF, M., ALBERTS, B., JOHNSON, A., LEWIS, J. & ROBERTS, K. 2002. An overview of the cell cycle. molecular biology of the cell. 4th edition ed. New York: Garland Science.
RAJAGOPALAN, H., JALLEPALLI, P. V., RAGO, C., VELCULESCU, V. E., KINZLER, K. W., VOGELSTEIN, B. & LENGAUER, C. 2004. Inactivation of hCDC4 can cause chromosomal instability. *Nature,* 428.
RAN, F. A., HSU, P. D., WRIGHT, J., AGARWALA, V., SCOTT, D. A. & ZHANG, F. 2013. Genome engineering using the CRISPR-Cas9 system. *Nature protocols,* 8**,** 2281-2308.
RAPPOLD, I., IWABUCHI, K., DATE, T. & CHEN, J. 2001. Tumor suppressor p53 binding protein 1 (53BP1) is involved in DNA damage–signaling pathways. *The Journal of cell biology,* 153**,** 613-620.
REYON, D., TSAI, S. Q., KHAYTER, C., FODEN, J. A., SANDER, J. D. & JOUNG, J. K. 2012. FLASH assembly of TALENs for high-throughput genome editing. *Nature biotechnology,* 30**,** 460-465.
RICCI-VITIANI, L., LOMBARDI, D. G., PILOZZI, E., BIFFONI, M., TODARO, M., PESCHLE, C. & DE MARIA, R. 2007. Identification and expansion of human colon-cancer-initiating cells. *Nature,* 445.
RICE, J. C. & ALLIS, C. D. 2001. Histone methylation versus histone acetylation: new insights into epigenetic regulation. *Current Opinion in Cell Biology,* 13.
ROBBINS, J., DILWORTHT, S. M., LASKEY, R. A. & DINGWALL, C. 1991. Two interdependent basic domains in nucleoplasmin nuclear targeting sequence: identification of a class of bipartite nuclear targeting sequence. *Cell,* 64**,** 615-623.
ROGAKOU, E. P., PILCH, D. R., ORR, A. H., IVANOVA, V. S. & BONNER, W. M. 1998. DNA double-stranded breaks induce histone H2AX phosphorylation on serine 139. *Journal of biological chemistry,* 273**,** 5858-5868.
RUZANKINA, Y., PINZON-GUZMAN, C., ASARE, A., ONG, T., PONTANO, L., COTSARELIS, G., ZEDIAK, V.P., VELEZ, M., BHANDOOLA, A. & BROWN, E.J. 2007. Deletion of the developmentally essential gene ATR in adult mice leads to age-related phenotypes and stem cell loss. *Cell Stem Cell* , 1, 113–126.
SANCAR, A., LINDSEY-BOLTZ, L. A., ÜNSAL-KAÇMAZ, K. & LINN, S. 2004. Molecular mechanisms of mammalian DNA repair and the DNA damage checkpoints. *Annual review of biochemistry,* 73**,** 39-85.
SANDER, J. D., DAHLBORG, E. J., GOODWIN, M. J., CADE, L., ZHANG, F., CIFUENTES, D., CURTIN, S. J., BLACKBURN, J. S., THIBODEAU-BEGANNY, S. & QI, Y. 2011. Selection-free zinc-finger-nuclease engineering by context-dependent assembly (CoDA). *Nature methods,* 8**,** 67-69.
SAVITSKY, K., BAR-SHIRA, A., GILAD, S., ROTMAN, G., ZIV, Y., VANAGAITE, L., TAGLE, D.A,, SMITH, S., UZIEL, T., SFEZ, S., ASHKENAZI, M., PECKER, I., FRYDMAN, M., HARNIK, R.,

PATANJALI, S.R., SIMMONS, A., CLINES, G.A., SARTIEL, A., GATTI, R.A., CHESSA, L., SANAL, O., LAVIN, M.F., JASPERS, N.G., TAYLOR, A.M., ARLETT, C.F., MIKI, T., WEISSMAN, S.M., LOVETT, M., COLLINS, F.S. & SHILOH, Y. 1995. A single ataxia telangiectasia gene with a product similar to PI-3 kinase. *Science,* 268, 1749–1753.

SCHAFER, S. & JUNG, M. 2005. Chromatin modifications as targets for new anticancer drugs. *Archiv Der Pharmazie,* 338.

SCHEER, U. & HOCK, R. 1999. Structure and function of the nucleolus. *Current opinion in cell biology,* 11**,** 385-390.

SCOTT, M. S., BOISVERT, F.-M., MCDOWALL, M. D., LAMOND, A. I. & BARTON, G. J. 2010. Characterization and prediction of protein nucleolar localization sequences. *Nucleic acids research,* 38**,** 7388-7399.

SCOTT, M. S., TROSHIN, P. V. & BARTON, G. J. 2011. NoD: a Nucleolar localization sequence detector for eukaryotic and viral proteins. *BMC bioinformatics,* 12**,** 317.

SHI, Y., FELLEY-BOSCO, E., MARTI, T. M., ORLOWSKI, K., PRUSCHY, M. & STAHEL, R. A. 2012. Starvation-induced activation of ATM/Chk2/p53 signaling sensitizes cancer cells to cisplatin. *BMC cancer,* 12**,** 571.

SHIEH, SY., AHN, J., TAMAI, K., TAYA, Y. & PRIVES, C. 2000. The human homologs of checkpoint kinases Chk1 and Cds1 (Chk2) phosphorylate p53 at multiple DNA damage-inducible sites. *Genes Dev*, 14, 289-300.

SHILOH, Y. 2003. ATM and related protein kinases: Safeguarding genome integrity. *Nat*
Rev Cancer, 3, 155–168.

SHILOH, Y. & ZIV, Y. 2013. The ATM protein kinase: Regulating the cellular response to genotoxic stress, and more. *Nat Rev Mol Cell Biol*, 14, 197–210.

SILICIANO, J. D., CANMAN, C. E., TAYA, Y., SAKAGUCHI, K., APPELLA, E. & KASTAN, M. B. 1997. DNA damage induces phosphorylation of the amino terminus of p53. *Genes Dev*, 11, 3471–3481.

SJOEBLOM, T., JONES, S., WOOD, L. D., PARSONS, D. W., LIN, J., BARBER, T. D., MANDELKER, D., LEARY, R. J., PTAK, J., SILLIMAN, N., SZABO, S., BUCKHAULTS, P., FARRELL, C., MEEH, P., MARKOWITZ, S. D., WILLIS, J., DAWSON, D., WILLSON, J. K. V., GAZDAR, A. F., HARTIGAN, J., WU, L., LIU, C., PARMIGIANI, G., PARK, B. H., BACHMAN, K. E., PAPADOPOULOS, N., VOGELSTEIN, B., KINZLER, K. W. & VELCULESCU, V. E. 2006. The consensus coding sequences of human breast and colorectal cancers. *Science,* 314.

SORENSEN, C. S., SYLJUASEN, R. G., FALCK, J., SCHROEDER, T., RONNSTRAND, L., KHANNA, K. K., ZHOU, B.B., BARTEK, J. & LUKAS, J. 2003. Chk1 regulates the S phase checkpoint by coupling the physiological turnover and ionizing radiation-induced accelerated proteolysis of Cdc25A. *Cancer Cell,* 3, 247–258.

SORIA, G., POLO, S.E. & ALMOUZNI, G. 2012.Prime, Repair, Restore: The Active Role of Chromatin in the DNA Damage Response. *Molecular Cell,* 46.

SRIVASTAVA, N., GOCHHAIT, S., DE BOER, P. & BAMEZAI, R. N. 2009. Role of H2AX in DNA damage response and human cancers. *Mutation Research/Reviews in Mutation Research,* 681**,** 180-188.

SPRUCK, C. H., STROHMAIER, H., SANGFELT, O., MÜLLER, H.M., HUBALEK, M., MÜLLER-HOLZNER, E., MARTH, C., WIDSCHWENDTER, M. & REED, S.I. 2002. hCDC4 gene mutations in endometrial cancer. *Cancer Res,* 62, 4535–453.

STEWART, M. 2007. Molecular mechanism of the nuclear protein import cycle. *Nature Reviews Molecular Cell Biology,* 8**,** 195-208.

STRAHL, B. D. & ALLIS, C. D. 2000. The language of covalent histone modifications. *Nature,* 403.

STROHMAIER, H., SPRUCK, C.H., KAISER, P., WON, K.A., SANGFELT, O. & REED, S.I. Human F-box protein hCdc4 targets cyclin E for proteolysis and is mutated in a breast cancer cell line. *Nature,* 413, 316–322.

SULLIVAN, K. D., GALLANT-BEHM, C. L., HENRY, R. E., FRAIKIN, J. -L. & ESPINOSA, J. M. 2012. The p53 circuit board. *Biochim Biophys Acta,* 1825, 229–244. SÁNCHEZ-RIVERA, F. J. & JACKS, T. 2015. Applications of the CRISPR-Cas9 system in cancer biology. *Nature Reviews Cancer*.

TAN, Y., SANGFELT, O. & SPRUCK, C. 2008. The Fbxw7/hCdc4 tumor suppressor in human cancer. *Cancer letters,* 271**,** 1-12.

TAYLOR, A.M. R., HARNDEN, D. G., ARLETT, C. F., HARCOURT, S. A., LEHMANN, A. R., STEVENS, S. & BRIDGES. A. 1975. Ataxia telangiectasia: A human mutation with abnormal radiation sensitivity. *Nature,* 258, 427–429.

THIRU, A., NIETLISPACH, D., MOTT, H. R., OKUWAKI, M., LYON, D., NIELSEN, P. R., HIRSHBERG, M., VERREAULT, A., MURZINA, N. V. & LAUE, E. D. 2004. Structural basis of HP1/PXVXL motif peptide interactions and HP1 localisation to heterochromatin. *The EMBO journal,* 23**,** 489-499.

TIBBETTS, R. S., CORTEZ, D., BRUMBAUGH, K. M., SCULLY, R., LIVINGSTON, D., ELLEDGE, S. J. & ABRAHAM, R. T. 2000. Functional interactions between BRCA1 and the checkpoint kinase ATR during genotoxic stress. *Genes & Development,* 14**,** 2989-3002.

TORRES-RUIZ, R. & RODRIGUEZ-PERALES, S. 2015. CRISPR-Cas9: A Revolutionary Tool for Cancer Modelling. *International journal of molecular sciences,* 16**,** 22151-22168.

TOYOOKA, T., ISHIHAMA, M. & IBUKI, Y. 2011. Phosphorylation of histone H2AX is a powerful tool for detecting chemical photogenotoxicity. *Journal of Investigative Dermatology,* 131**,** 1313-1321.

TRAVEN, A. & HEIERHORST, J. 2005. SQ/TQ cluster domains: concentrated ATM/ATR kinase phosphorylation site regions in DNA-damage-response proteins. *Bioessays,* 27**,** 397-407.

TU, W.-Z., LI, B., HUANG, B., WANG, Y., LIU, X.-D., GUAN, H., ZHANG, S.-M., TANG, Y., RANG, W.-Q. & ZHOU, P.-K. 2013. γH2AX foci formation in the absence of DNA damage: Mitotic H2AX

phosphorylation is mediated by the DNA-PKcs/CHK2 pathway. *FEBS letters,* 587**,** 3437-3443.

TUREK-PLEWA, J. & JAGODZINSKI, P. P. 2005. The role of mammalian DNA methyltransferases in the regulation of gene expression. *Cellular & Molecular Biology Letters,* 10.

UCHIYAMA, S., KOBAYASHI, S., TAKATA, H., ISHIHARA, T., HORI, N., HIGASHI, T., HAYASHIHARA, K., SONE, T., HIGO, D., NIRASAWA, T., TAKAO, T., MATSUNAGA, S. & FUKUI, K. 2005. Proteome analysis of human metaphase chromosomes. *Journal of Biological Chemistry,* 280.

URA, K., ARAKI, M., SAEKI, H., MASUTANI, C., ITO, T., IWAI, S., MIZUKOSHI, **T**., KANEDA, Y. & ANAOKA, F. 2001. ATP-dependent chromatin remodeling facilitates nucleotide excision repair of UV-induced DNA lesions in synthetic dinucleosomes. *EMBO J,* 20.

UTTAM, S., BISTA, R.K., STATON, K., ALEXANDROV, S., CHOI, S., BAKKENIST, C.J., HARTMAN, D. J., BRAND, R.E. & LIU. Y. 2013. Investigation of depth-resolved nanoscale structural changes in regulated cell proliferation and chromatin decondensation. *Biomedical optics express*, 4, 596-613.

VALDIGLESIAS, V., GIUNTA, S., FENECH, M., NERI, M. & BONASSI, S. 2013. γH2AX as a marker of DNA double strand breaks and genomic instability in human population studies. *Mutation Research/Reviews in Mutation Research,* 753**,** 24-40.

VAN ENGELAND, M., DERKS, S., SMITS, K. M., MEIJER, G. A. & HERMAN, J. G. 2011. Colorectal Cancer Epigenetics: Complex Simplicity. *Journal of Clinical Oncology,* 29.

VERMAAK, D., HENIKOFF, S. & MALIK, H. S. 2005. Positive selection drives the evolution of rhino, a member of the heterochromatin protein 1 family in Drosophila. *Plos Genetics,* 1.

VERMAAK, D. & MALIK, H. S. 2009. Multiple Roles for Heterochromatin Protein 1 Genes in Drosophila. *Annual Review of Genetics,* 43.

VROUWE, M. G., PINES, A., OVERMEER, R. M., HANADA, K. & MULLENDERS, L. H. F. 2011. UV-induced photolesions elicit ATR-kinase-dependent signaling in non-cycling cells through nucleotide excision repair-dependent and -independent pathways. *Journal of Cell Science,* 124**,** 435-446.

WAGSTAFF, K.M., SIVAKUMARAN, H., HEATON, S.M., HARRICH, D. & JANS, D.A. 2012. Ivermectin is a specific inhibitor of importin alpha/beta-mediated nuclear import able to inhibit replication of HIV-1 and dengue virus. *Biochem J,* 443, 851-856.

WANG, Z., INUZUKA, H., FUKUSHIMA, H., WAN, L., GAO, D., SHAIK, S., SARKAR, F. H. & WEI, W. 2012a. Emerging roles of the FBW7 tumour suppressor in stem cell differentiation. *Embo Reports,* 13**,** 36-43.

WANG, Z., INUZUKA, H., ZHONG, J., WAN, L., FUKUSHIMA, H., SARKAR, F. H. & WEI, W. 2012b. Tumor suppressor functions of FBW7 in cancer development and progression. *Febs Letters,* 586**,** 1409-1418.

WANG, Z. H., CUMMINS, J. M., SHEN, D., CAHILL, D. P., JALLEPALLI, P. V., WANG, T. L., PARSONS, D. W., TRAVERSO, G., AWAD, M.,

SILLIMAN, N., PTAK, J., SZABO, S., WILLSON, J. K. V., MARKOWITZ, S. D., GOLDBERG, M. L., KARESS, R., KINZLER, K. W., VOGELSTEIN, B., VELCULESCU, V. E. & LENGAUER, C. 2004. Three classes of genes mutated in colorectal cancers with chromosomal instability. *Cancer Research,* 64.

WANG, H., WANG, M., WANG, H., BÖCKER, W. & ILIAKIS, G. 2005. Complex H2AX phosphorylation patterns by multiple kinases including ATM and DNA-PK in human cells exposed to ionizing radiation and treated with kinase inhibitors. *Journal of cellular physiology,* 202**,** 492-502.

WARD, I. M., MINN, K. & CHEN, J. 2004. UV-induced ataxia-telangiectasia-mutated and Rad3-related (ATR) activation requires replication stress. *Journal of Biological Chemistry,* 279**,** 9677-9680.

WATTERS, D., KEDAR, P., SPRING, K., BJORKMAN, J., CHEN, P., GATEI, M., BIRRELL, G., GARRONE, B., SRINIVASA, P., CRANE, D.I. & LAVIN, M.F. 1999. Localization of a portion of extranuclear ATM to peroxisomes. *J Biol Chem*, 274, 34277–82.

WEBER, A. M. & RYAN, A. J. 2015. Atm and atr as therapeutic targets in cancer. *Pharmacology & therapeutics,* 149**,** 124-138.

WEINBERG, R.A. 1995. The retinoblastoma protein and cell cycle control. *Cell*, 81, 323-330.

WELCKER, M. & CLURMAN, B. E. 2008. FBW7 ubiquitin ligase: a tumour suppressor at the crossroads of cell division, growth and differentiation. *Nature Reviews Cancer,* 8**,** 83-93.

WONG, J. J. L., HAWKINS, N. J. & WARD, R. L. 2007. Colorectal cancer: a model for epigenetic tumorigenesis. *Gut,* 56**,** 140-148.

WOOD, L. D., PARSONS, D. W., JONES, S., LIN, J., SJOBLOM, T., LEARY, R. J., SHEN, D., BOCA, S. M., BARBER, T., PTAK, J., SILLIMAN, N., SZABO, S., DEZSO, Z., USTYANKSKY, V., NIKOLSKAYA, T., NIKOLSKY, Y., KARCHIN, R., WILSON, P. A., KAMINKER, J. S., ZHANG, Z., CROSHAW, R., WILLIS, J., DAWSON, D., SHIPITSIN, M., WILLSON, J. K. V., SUKUMAR, S., POLYAK, K., PARK, B. H., PETHIYAGODA, C. L., PANT, P. V. K., BALLINGER, D. G., SPARKS, A. B., HARTIGAN, J., SMITH, D. R., SUH, E., PAPADOPOULOS, N., BUCKHAULTS, P., MARKOWITZ, S. D., PARMIGIANI, G., KINZLER, K. W., VELCULESCU, V. E. & VOGELSTEIN, B. 2007. The genomic landscapes of human breast and colorectal cancers. *Science,* 318.

WOOD, R. D. 1996. DNA repair in eukaryotes. *Annual review of biochemistry,* 65**,** 135-167.

WOOD, R. D. 1997. Nucleotide excision repair in mammalian cells. *Journal of Biological Chemistry,* 272**,** 23465-23468.

WOOD, A. J., LO, T.-W., ZEITLER, B., PICKLE, C. S., RALSTON, E. J., LEE, A. H., AMORA, R., MILLER, J. C., LEUNG, E. & MENG, X. 2011. Targeted genome editing across species using ZFNs and TALENs. *Science,* 333**,** 307-307.

WOODS, D. & TURCHI, J. J. 2013. Chemotherapy induced DNA damage response: convergence of drugs and pathways. *Cancer biology & therapy,* 14**,** 379-389.

WOYNAROWSKI, J. M., FAIVRE, S., HERZIG, M. C., ARNETT, B., CHAPMAN, W. G., TREVINO, A. V., RAYMOND, E., CHANEY, S. G., VAISMAN, A. & VARCHENKO, M. 2000. Oxaliplatin-induced damage of cellular DNA. *Molecular pharmacology,* 58**,** 920-927.

WU, Z., EARLE, J., SAITO, S. I., ANDERSON, C. W., APPELLA, E. & XU, Y. 2002. Mutation of mouse p53 Ser23 and the response to DNA damage. *Molecular and cellular biology,* 22**,** 2441-2449.

XIAO, Z., CHEN, Z., GUNASEKERA, A. H., SOWIN, T. J., ROSENBERG, S. H., FESIK, S. & ZHANG, H. 2003. Chk1 mediates S and G2 arrests through Cdc25A degradation in response to DNA-damaging agents. *J Biol Chem,* 278, 21767–21773.

YAJIMA, H., LEE, K.-J. & CHEN, B. P. 2006. ATR-dependent phosphorylation of DNA-dependent protein kinase catalytic subunit in response to UV-induced replication stress. *Molecular and cellular biology,* 26**,** 7520-7528.

YAJIMA, H., LEE, K.-J., ZHANG, S., KOBAYASHI, J. & CHEN, B. P. 2009. DNA double-strand break formation upon UV-induced replication stress activates ATM and DNA-PKcs kinases. *Journal of molecular biology,* 385**,** 800-810.

YEH, E., CUNNINGHAM, M., ARNOLD, H., CHASSE, D., MONTEITH, T., IVALDI, G., HAHN, W. C., STUKENBERG, P. T., SHENOLIKAR, S. & UCHIDA, T. 2004. A signalling pathway controlling c-Myc degradation that impacts oncogenic transformation of human cells. *Nature cell biology,* 6**,** 308-318.

YOU, Z., CHAHWAN, C., BAILIS, J., HUNTER, T. & RUSSELL, P. 2005. ATM activation and its recruitment to damaged DNA require binding to the C terminus of Nbs1. *Mol Cell Biol,* 25, 5363–5379.

ZENG, W., BALL, A. R., JR. & YOKOMORI, K. 2010. HP1 Heterochromatin binding proteins working the genome. *Epigenetics,* 5.

ZHANG, F., CONG, L., LODATO, S., KOSURI, S., CHURCH, G. M. & ARLOTTA, P. 2011. Efficient construction of sequence-specific TAL effectors for modulating mammalian transcription. *Nature biotechnology,* 29**,** 149-153.

ZHANG, F., WEN, Y. & GUO, X. 2014. CRISPR/Cas9 for genome editing: progress, implications and challenges. *Human molecular genetics***,** ddu125.

ZHANG, Q., KARNAK, D., TAN, M., LAWRENCE, S.T., MORGAN, A.M. & SUN., Y. 2016. FBXW7 Facilitates Nonhomologous End-Joining via K63-Linked Polyubiquitylation of XRCC4. *Molecular Cell,* 61, 419-433.

ZHAO, H., WATKINS, J. L. & PIWNICA-WORMS, H. 2002. Disruption of the checkpoint kinase1/cell division cycle 25A pathway abrogates ionizing radiation-induced S and G2 checkpoints. *Proc Natl Acad Sci U S A,* 99, 14795–14800.

ZHAO, J. 2007. Sumoylation regulates diverse biological processes. *Cellular and molecular life sciences,* 64**,** 3017-3033.

ZHAO, H., TRAGANOS, F. & DARZYNKIEWICZ, Z. 2010. Kinetics of the UV-induced DNA damage response in relation to cell cycle phase. Correlation with DNA replication. *Cytometry part A,* 77**,** 285-293.

ZHOU, B.-B. S. & ELLEDGE, S. J. 2000. The DNA damage response: putting checkpoints in perspective. *Nature,* 408**,** 433-439.